Flux balance analysis to model microbial metabolism for electricity generation

---

A thesis
submitted in partial fulfilment
of the requirements for the Degree of
Doctor of Philosophy
in Computational Biology and Bioengineering

at
Lincoln University
by
Longfei Mao

Lincoln University
2013

Abstract of a thesis submitted in partial fulfilment of the
requirements for the Degree of Philosophy

Flux balance analysis to model microbial metabolism for electricity generation

by

Longfei Mao

Microbial fuel cells (MFCs) are bioelectrochemcial devices that possess a similar design to a fuel cell, with an anode and a cathode connected through an electrical circuit. Unlike fuel cells, MFCs use microorganisms as biocatalysts to convert organic matter into electrons and protons, of which a portion can be transferred to electrode to generate electricity. Since all microorganisms transfer electrons during metabolism inside the cell, there could potentially be unlimited choices of biocatalyst candidates for MFCs for various applications. However, in reality, the application of MFCs is heavily restricted by their low current outputs. As the performance of an MFC is associated with various factors, MFC research devoted to improve energy output level is a very interdisciplinary field and demands knowledge from a diverse range of scientific areas including microbiology, environmental science and chemical engineering.

Because the MFC current is fundamentally produced by the metabolic activity of the microorganisms, it would be desirable to elucidate the innate capacity of the microbial systems to sustain the energy extraction processes in MFCs, and pertinent metabolic pathways and burdens. However, due to the large number of cellular reactions (up to thousands for a eukaryote), no previous study has provided such information regarding the complete metabolic processes inside the cells during an MFC operation. Therefore, to understand the metabolic potential and behaviours at the whole-cell level and obviate the difficulties experienced in reductionist investigative methods, the present PhD thesis employed *in silico* metabolic engineering techniques to model the optimal metabolic states and flux adjustments of the four selected microbial species for electricity generation.

The first part of this thesis is the development of a framework method based on existing constraint-based methods to analyse the impact of microbial electricity generation on the metabolisms of the selected microorganisms at genome-scale. To identify the alternative equivalent solutions and avoid the disturbance of futile cycle in a network mode, we developed a method, **f**lux variability **a**nalysis with **t**arget flux **mi**nimization (FATMIN), which can characterize the metabolic strategies underlying a high current output compatible with reaction stoichiometry and realistic biological constraints.

The second part of this thesis is the application of the constraint-based methods to model the four selected microorganisms for current production. The present study mainly considered NADH as the intracellular electron source for MET mode and c-type cytochrome for DET mode. In DET mode, charge is directly transferred from the microorganism to the electrode, and in MET mode a mediator molecule performs the transfer. The results have shown that that *S. cerevisiae* was the best candidate for MFC use based on its highest potential computed for current output (5.781 for aerobic and 6.193 A/gDW for anaerobic growths) and coulombic efficiency (over 85%). *G. sulfurreducen* had a potential to achieve the second highest current, up to 2.711 A/gDW for MET mode, 3.710 A/gDW for DET mode and 3.272 A/gDW for a putative mixed MET and DET mode. On the other hand, the maximum current values of 2.368 and 0.792 A/gDW were obtained from MET mode for *C. reinhardtii* under mixotrophic conditions and from DET mode for *Synechocystis* sp. PCC 6803 under autotrophic conditions respectively. Subsequently, the present study elucidated the impact of NADH, type-c cytochrome, ferredoxin and quinol-dependent current generation on the metabolisms and possible metabolic pathways that microorganisms can use to resolve the redox disruption arising from the energy extraction. It is expected that these referential data on the four pure cultures to be a good starting point for development of other experimental MFC research.

The final part of the thesis is the employment of an optimization algorithm to test the suitability of reaction deletion strategy for improving the electron transfer rates for electricity generation. The results show that the reaction deletion strategy has improved the reducing equivalent regeneration capability for MFC current production in all the cases of *G. sulfurreducens*, *C. reinhardtii* and *Synechocystis* to different extents. Notably, the identified knockouts could effectively produce *S. cerevisiae* mutants that have elevated the lower limits of the current output to about two-third the theoretical maximum current.

Overall, this thesis is the first report of using *in silico* modelling approach to study the capability and underlying metabolisms of microbial oxidation at the anode. It is expected the knowledge extended by this thesis in the microbial processes for electricity generation will integrate with advance in electrochemical engineering to increase performance of MFCs in future.

Keywords: MFC; Microbial fuel cell; *Geobacter sulfurreducens*; *Chlamydomonas reinhardtii*; *Synechocystis* sp. PCC 6803; *Sachoromyoces cerevisiae*; bioelectricity; Flux balance analysis; Flux variability analysis; Flux minimization; FATMIN; Mathematical optimization; Metabolic model; Metabolic network analysis; Metabolic network redesign; Metabolic engineering; *In silico* simulation; Model-driven discovery.

List of Publications

Some parts of materials in this thesis have been published or accepted, and some have been submitted for publications

- Verwoerd, W. S., & Mao, L. (2014). The Problem of Futile Cycles in Metabolic Flux Modeling: Flux Space Characterisation and Practical Approaches to its Solution. In S. K. Basu & N. Kumar (Eds.), *Simulation Foundations, Methods and Applications: Modeling and Simulation Methods and Applications*: Springer (In press).

- Mao, L., & Verwoerd, W. S. (2013). Selection of organisms for systems biology study of microbial electricity generation: a review. *International Journal of Energy and Environmental Engineering*, *4*(1), 17.

- Mao, L., & Verwoerd, W. S. (2013) Model-driven elucidation of the inherent capacity of *Geobacter sulfurreducens* for electricity generation. *Journal of Biological Engineering*, 7(1), 14.

- Mao, L., & Verwoerd, W. S. Computational comparison of mediated MFC current generation capacity of *Chlamydomonas reinhardtii* in photosynthetic and respiratory growth modes. *Submitted to Molecular BioSystems*

- Mao, L., & Verwoerd, W. S. (2013) Genome-scale stoichiometry analysis to elucidate the innate capability of the cyanobacterium *Synechocystis* for electricity generation. *Journal of Industrial Microbiology & Biotechnology*, 40(10), 1161-1180.

- Mao, L., & Verwoerd, W. S. (2013). Exploration and comparison of inborn microbial capacity of aerobic and anaerobic metabolisms of *Saccharomyces cerevisiae* for current production. *Bioengineered*, 4(6), 23-22.

- Mao, L., & Verwoerd, W. S. (2013). *MFCoT - a computational toolbox to study the metabolism of MFC biocatalysts.* In *4th international microbial fuel cell conference; Cairns, Australia*. 82-83.

Acknowledgments

The production of a doctoral thesis often involves uncertainty, sacrifice, failure and aloneness. However, in addition to those stressful feelings, my PhD experience contains enjoyableness, cooperativeness, effectiveness and success. All these are possible due to two key ingredients: one is my supervisor, Dr. Wynand Verwoerd, and the other is the passion for science that he has passed on to me. Perhaps, in the multi-disciplinary laboratory of the systems biology at Lincoln, I was the most ignorant and naive of my colleagues, but with the inspiration and expertise of Dr. Verwoerd, I could push myself to the limit and learn as much as possible. For the past years, Dr. Verwoerd has been a phenomenal mentor to me, and represents an exceptional scientist who is fast, inquisitive and explorative. I truly appreciate the valuable opportunity he gives me to pursue a PhD under his mentorship. I think I am fortunate enough to know him and to be his student in this life.

I would also like to acknowledge Professor Don Kulasiri for all his good suggestions and insightful conversions about the life and philosophy during the Wednesday group meeting. As the head of Centre for Advanced Computational Solutions (C-fACS), he has provided unwavering supports over the course of this project. To the fellow students at C-fACS, I have to express my appreciation for sharing the knowledge. Besides, I am grateful to Caitriona Cameron for her useful advice in improving my acadmetic writting skills.

Furthermore, to Elizabeth Burtt, I would like to give my gratitude for providing such a perfect accommodation while I am studying at Lincoln that I can devote all my time to my research.

Finally, I dedicate this thesis to my beloved mother and father for their love and support throughout all these years. 此论文献给养育我的母亲张宝荣和父亲毛义山!

Longfei Mao

Lincoln University, New Zealand

June, 2013

Table of Contents

List of Tables

List of Figures

Abbreviations

AOS	Alternate optimal solutions
Auto	Photo-autotrophic
BG	Bromocresol green
CE-MS	Capillary electrophoresis–mass spectrometry
CE-TOFMS	Capillary electrophoresis time-of-flight mass spectrometry
COI	Coefficient of importance
DET	Direct electron transfer
EM	Elementary mode
ExPa	Extreme pathway
FBA	Flux balance analysis
Ferred	Ferredoxin
FVA	Flux variability analysis
FATMIN	Flux variability analysis with target flux minimization
GEM	Genome-scale metabolic network
GC-MS	Gas chromatography–mass spectrometry
Hetero	Heterotrophic
LC-MS	Liquid chromatography–mass spectrometry
LP	Linear programming
MALDI-MS	Matrix-assisted laser desorption/ionization -mass spectrometry
MET	Mediated electron transfer
MFC	Microbial fuel cell
MFCoT	MFC optimization toolbox
Mixo	Mixotroophic
MOMA	Minimization of metabolic adjustment
ROOM	Regulatory On/Off Minimization
NMR	Nuclear magnetic resonance
NR	Neutral red
NAD	Nicotinamide adenine dinucleotide (oxidized)
NADH	Nicotinamide adenine dinucleotide (reduced)
NADH_mfc	NADH flux shunted towards electrode for current production
NADP	Nitcotinamide adenine dinucleotide phosphate (oxidized)
NADPH	Nitcotinamide adenine dinucleotide phosphate (reduced)
Q	Quinone
QH_2	Quinol

CHAPTER 1 Introduction

1.1 Background

The technology for extracting an electrical current for use in external circuits from the metabolic processes of living microbes has been in development for more than a century [1]. The resulting devices, termed microbial fuel cells or MFCs, have several potential advantages over more prominent sustainable energy technologies such as solar or wind power. For example, they can directly convert organic waste into electricity [2] without pollution or inefficient intermediate steps that involve mechanical generators. This feature, energy recovery from solid wastes, has been exploited in proposed national strategies for many Asian countries [3]. It may be possible to achieve the same goal by inorganic catalysts or enzymes, but using living cells makes it possible to exploit their adaptability to environmental conditions and avoids the high capital cost of installation for other waste-to-energy systems reviewed by Eddine *et al.*, (2012) [4]. The whole organisms used in MFCs contain various enzymes and therefore allow different substrates (or mixed substrates) to be used. The organisms in the fuel cell system can be considered as micro-reactors and provide optimal conditions for different enzymes. Because the organisms are self-replicating, the organic matter oxidation implemented by these bio-catalysts are self-sustaining [5] and not subject to catalytic poisoning like metallic catalysts or degradation of enzyme catalysts. By selecting photosynthetic microbes, solar energy could be converted at the same time. One can envisage portable electronics powered by MFCs that are "charged " by feeding them nutrients rather than electric current; or medical implants that derive their power directly from nutrients circulating in the bloodstream. Perhaps the process can be reversed, and external electrical power supplied to an MFC converted into biomass, as a temporary storage, to overcome the intermittent nature of many other sustainable energy sources – a possibility currently under serious consideration [6-8].

However, these future possibilities are still severely hampered by the low energy yields per mass or volume that are currently achieved [9]. Generally MFC energy output is reported in milliwatts per square metre of electrode area or per cubic metre of electrolyte volume [10]. Scientific research has increased the densities of MFCs to over 1 kW m^{-3} (reactor volume) and

to 6.9 W/m^{-2} (anode area) under optimal conditions in the laboratory [11]. However, these values still cannot meet the needs of many applications, which require a power output larger than $100kW/m^2$ [12]. For this reason, large scale waste water treatment is the application closest to industrial realisation and is the domain of much current MFC research.

A variety of designs are under development to improve the efficiency and potential application of MFCs to industry. Areas under investigation include the selection of electrode materials for optimal electrochemical performance and maximising electrode surface to volume ratios; improving charge transfer between microbes and electrodes either chemically or by mechanical design, and finding and maintaining optimal living conditions for microbe colonies, efficient supply of nutrients and removal of effluent. Different configurations are being investigated for extracting current, sometimes in combination with production of hydrogen or other metabolites of further use in energy generation, and with or without exploitation of photosynthesis. The choice of process configuration and engineering design is also closely linked with the selection of the most suitable organism for a particular design or for whether overall priority is given to energy generation, waste disposal or some other objectives.

For improvement of an MFC's performance, most of the previous work focuses on engineering aspects of the device and selection of different candidate organisms, i.e., mainly prokaryotes and mixed consortia, as the 'biocatalyst'. A schematic representation of MFC research activity is shown in Figure 1-1. While there is a large volume of biochemical research literature on for example, electron transfer chains and redox processes in cell metabolism that is relevant to MFC, relatively few studies focus specifically on MFC. This is exacerbated by the fact that ongoing research continues to identify new mechanisms for electron exchange between microbes and electrodes, new design strategies to exploit these and consequently new candidate organisms. Such organisms have not necessarily been well studied experimentally before.

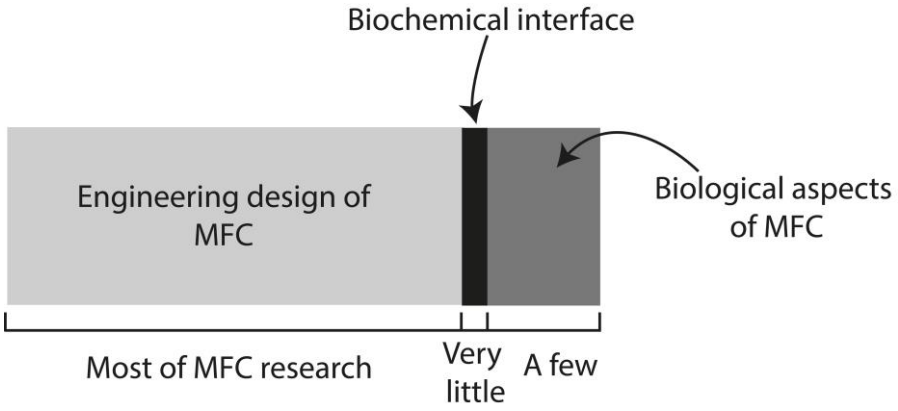

Figure 1-1: Areas covered in current microbial fuel cell (MFC) research.

In silico modelling is well suited to bridge this gap and extend knowledge in the biochemical interface between MFC biology and engineering design. Externally, electron flow (in the external circuit) and the counterflow of protons in the electrolyte make up the current that carries useful electrical power. Internally, both of these are comprehensively woven into the fabric of metabolism: electrons being transported by redox carrier molecules such as NADH that participate in a large fraction of all biochemical reactions, and protons that for example, drive ATP synthesis needed for energy transport are also ubiquitously involved in a great many reactions. This clearly calls for a systems level approach rather than the reductionist strategy of pathway-oriented, conventional biochemistry.

A few previous studies have embarked on *in silico* modelling MFCs. These studies commonly centered on description of the dynamics processes of electron transfer [13] and power generation [14, 15], or biofilm formation and species distribution within the biofilm and different microbial populations competing for biofilm space and substrate [16, 17]. However, these models above were built from engineering perspectives on chemical fuel cells, specific to certain MFC configurations, and cannot elucidate the complex metabolic processes and mechanisms underlying electricity generation at the genome-scale level, which fundamentally determines the current output of an MFC.

1.2 Knowledge gaps

Compared to technological challenges in screening for new applications and designing systems for MFCs, the microbiology of the anodic microbial catalysts and the associated mechanisms of electron transfer to the electrode are more fundamental to the power generation. In many MFC studies, the mechanisms between a microorganism and an anode, such as mediated electron transfer (MET) or direct electron transfer (DET), are fully discussed, but the complete biochemical mechanisms inside the microorganism, which underlie the electrogenic activity at the anode, have been overlooked. A recent study has explicitly stated that the intracellular exoelectrogenic process is a rate-limiting step for exoelectrogenic microorganisms in biological electricity generation [18]. This accentuates the need to examine the metabolic mechanisms of living microorganisms that determine the innate current generation potential of the bioelectrocatalytic processes in MFCs.

Even though many MFC studies have proposed that the electron transport system in the electrochemically active microbes utilizes NADH, iron/sulfur proteins such as ferredoxin and c-type cytochrome, and quinol as the electron carriers [19-24], further research is required to elucidate the detailed metabolic response consequent to the redox balance perturbations of electrons draining from these sites. For example, some recent studies thus far have focused on investigating the interspecies electron transfer mechanisms that enable biofilms to reduce the electrode [25-27], but little is known about how electron donors affect the growth and selection of metabolic pathways of individual biofilm cells. Studying these metabolic features should provide valuable knowledge of the biochemical energetics of the reaction mechanisms. Such information may facilitate the optimization of functional bioanodes and the development of better-performing strains, and reveal significant insights in the quest for higher power output MFCs.

Unfortunately, there has been no published literature that has systematically examined the metabolic processes of a biocatalyst supporting electricity generation in MFCs. This may be due to the difficulties experienced in reductionist investigative strategies for metabolic engineering of interested biotechnological processes at the whole-cell level. Although studies of bioelectrocatalysis systems based on whole-cell biocatalyst can discuss the metabolisms for supplying electrons in MFCs based on empirical knowledge of the textbook biochemical

pathways or limited experimental evidence, there is still an urgent demand for quantitative identification of the active metabolic pathways resulting from the interaction of thousands of reactions (inside an eukaryote) during MFC operation [28]. This therefore, highlights the importance to develop a method that can elucidate the inherent potential of microorganisms for electricity generation and pertinent underlying biochemical pathways. Such a method would provide a basis to rank the microorganisms' potential for MFC use and would be a high priority (and of huge benefit) to MFC research.

Furthermore, the choice of substrate has a great influence on the electricity generation of MFCs [29]. Acetate and glucose are the two commonly used substrates in MFCs [30]. Previous MFC experimental studies have speculated on the relationships between choice of substrates and the observed growth rate and current output. Nevertheless, no studies have elucidated the maximum potential of these two substrates for current output in different organisms.

1.3 Motivation of this study

Unlike the previously developed fuel cell configuration models, the present study intends to investigate the perturbation by MFC operation of metabolic mechanisms of cells and elucidate the underlying complex metabolic processes for the electric current generation. This can be done with analysis of genome-scale network (GEM) models that include all reactions that occur inside cells.

The recently developed constraint-based modelling approach can be employed to build flux models that describe the metabolic restriction and molecular mechanisms for particular electron transfer cases in MFCs. Also, genome-scale modelling can facilitate discovery of novel pathways or metabolisms related to electricity generation beyond textbook-based biochemical knowledge. The domain of this thesis is indicated in Figure 1-1. Since the capability of microbes determine the electron availability, understanding bottlenecks of metabolisms of microbes can help researchers to select the most suitable microbes for particular applications and to design reactors accordingly, in order to make the microbes able to achieve their maximum electric current.

With a genome-scale metabolic model, we can solve several bottlenecks in MFC research, 1) lack of method to model the metabolism of microorganisms for electricity generation, 2) deficient characterization of intracellular microbial mechanisms that are linked to electron transfer to electrode and 3) shortage of knowledge in microbial electron generation efficiency in different organisms, which can implicate the consequent effect of anode microbial community composition.

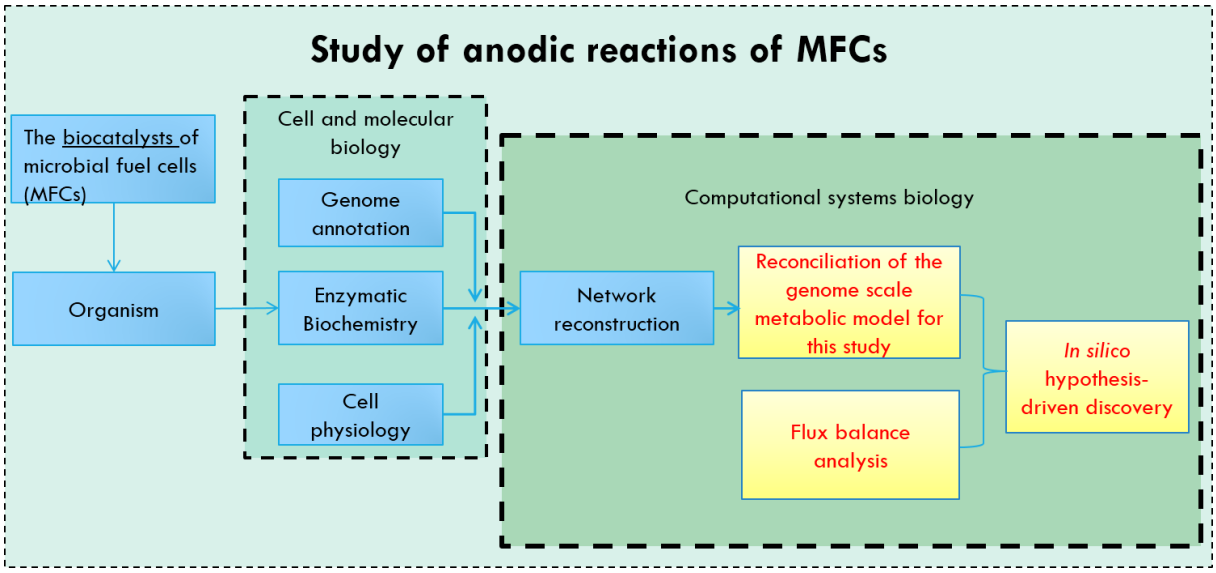

Figure 1-2: The scope of the present study.

Blue rectangles contain the knowledge that can be retrieved from literature. The words in red colour (in the yellow rectangles) indicate the tasks conducted in the present study.

In this study, metabolism of the microorganism operates under redox perturbation caused by electron generation. For modelling different MFC operation modes, different electron sites in the metabolism are targeted for electricity generation. To model the case of DET, this study considers c-type cytochrome as a redox intermediary to be linked to the electrode.

For the MET mode, this study addresses the impact of pulling electrons away from NADH on the metabolism and pertinent metabolic response. In some MFC configurations, the MET mode may involve different exogenous mediators to extract reducing energy from different intracellular (terminal) electron shuttles of various biocatalysts, but the metabolic modelling techniques developed in this thesis can easily be adapted to these case-specific MET modes for future research interests. This study mainly focus on the NADH-linked MET mode, since

NADH possesses many natural characteristics that make a suitable intracellular electron source for energy extraction.

- NADH is commonly used in reactions related to energy metabolisms [21, 31], which is different from the other chemically similar redox cofactor, NADPH, involved in biosynthesis of cellular components and defence systems against oxidative stresses [32]. A recent reporting based on computational modelling analysis has indicated that, compared with NADPH, which is necessary for biomass production, NADH is optional to maintaining a viable growth state [33]. Because NADH and NADPH are regulated independently and used by different sets of enzymes, we did not model the microorganism into a state where the turnover rates of the two reducing molecules were concurrently up-regulated. This can cost too much metabolic 'effort' in terms of energy and other valuable resources (such as amino acids). The synthesis of NADP and the enzymes that maintain its reduced state are of critical importance to the survival of cells [34]. For MFC application, it would be ideal to force the cell into a metabolic state, in which the mechanism of regenerating NADH at a fast rate is the way to sustain electricity generation.

- NADH can be considered as a 'hub' in terms of network theory [35], since it is a major electron carrier in microbial metabolism connecting many different cellular processes. For example, NADH generated in beta-oxidation, glycolysis and the TCA cycle is transferred to oxidative phosphorylation to produce ATP [31]. Therefore, study of NADH supplying electrons to mediators can elucidate the response of energy metabolism to the perturbation induced by electricity generation.

- NADH is suggested as the optimal intracellular electron source for the mediated electron generation process [36], because 1) NADH has a lower redox potential (-320 mV) than other redox compounds such as $FADH_2$ (−180 mV) and succinate (31 mV) [22]. 2) The reducing energy stored in NADH can be extracted in the form of electrons with the aid of artificial mediators with low potential, such as bromocresol green (BG) (-0.385 mV) and neutral red (NR) (-0.290 mV) [37]. Particularly, NR has been demonstrated to be an effective electron mediator for electricity production by *E. coli* cultures in MFCs, due to its redox potential close to that of NADH [36, 38, 39]. It

is suggested that NR may directly exchange electrons with NADH from metabolic steps prior to respiratory chains [40]. On the other hand, it has been proposed that the theoretical limit of MFC voltage output is the potential difference between NADH and the reaction in the cathode if microorganisms are to remain as a biological catalyst [22, 41]. Therefore, targeting NADH as the electron source in the modelling can estimate the maximum power achievable for a microorganism in MFC.

- Furthermore, the NADH is the universal electron carrier used in the catabolism of all living cells, connecting many different cellular processes. Study of this redox molecule as the electron donor can help elucidation of the difference in the current production potential among the four microorganisms of different categories. Compared with NADPH, which participates in biosynthesis, NADH acts merely as an electron shuttle and its production is more energetically favourable [42]. Because feedstock cost is the major component of the overall production cost, increases in yield directly improve the economic viability of current production. Thus, NADH should be preferred to maximize the current yield, and we hypothesize that electricity generation linked to NADH would enable the highest theoretical maximum current yield of electrons per unit of substrate consumed.

Traditional MFC anodic chambers demand anoxic conditions, because when oxygen is present in the anode chamber microorganisms oxidize the fuel with the reduction of oxygen rather than electron transfer to the anode. On the other hand, an aerobic anode chamber has recently been developed to enhance the electrochemical performance of MFCs, since the aerobic metabolisms involve higher levels of active biomass and more efficient substrate utilization [43-46]. In addition, an aerobic anode allows MFC to be applied in a more diverse region such as an air/water interface. Therefore, anaerobic conditions are not considered as a prerequisite for modelling anodic reactions of MFCs in this study.

1.4 Statement of objectives

In this study, we develop an integrative computational framework that elucidates the system-wide effect of MFC perturbations on microbial metabolism and metabolic engineering design

strategies. We focus on four microorganisms and presume extraction of electrons in thirteen cases of MET or DET mode of MFCs (Table 1-1), although any biochemical network and desired metabolic perturbation can be incorporated into our methodology. The resultant metabolic models can be used to assess the perturbation effects of exogenous electron acceptors, biological causalities and MFC output. We then identify distinctive phenotypic characteristics that differentiate innate organism-specific metabolic capabilities and evaluate which organisms are more suitable for MFCs, based on amperage per gram dry weight of cells.

In general, we expect to elucidate 1) The potential of a biological system for current output; and 2) The metabolic behaviours caused by perturbation of NADH-dependent electricity generation. In order to achieve these aims, we therefore:

1. **Develop a framework to analyse the inherent potential of microorganisms for current generation using published genome-scale network models.**

The framework also includes developing a method based on exisiting constraint-based approches for identifying the flux ranges of the cellular reactions that actually sustain microbial electricity generation (exemplified by NADH-dependent electricity generation). The framework and the methods developed for this specific objective are presented in Chapter 3.

2. **Determine metabolic states optimized for energy extraction supporting external electrical current in each case of the four microorganisms and compute the theoretical maximum current output.**

Multi-objective optimization is used to model the stressed metabolic states optimized for electron transfer from intracellular redox metabolites to an electrode. The details of this method are present in Chapter 3. The created stressed model can help understand which metabolic reactions are primarily responsible for the targeted redox metabolite regeneration, e.g., NADH, which is a step toward increasing the electron transfer in whole-cell biocatalysts. The theoretical power output of the four microorganisms and pertinent metabolic mechanisms underlying the electricity generation are obtained through case-specific modelling (Table 1-1):

i. **Determine metabolic states of *G. sulfurreducens* optimized for electricity generation using NADH-dependent MET mode and c-type cytochrome-dependent DET mode under anaerobic cultivation** - this work is presented in Chapter 4.

ii. **Determine metabolic states of *C. reinharditii* optimized for electricity generation using NADH-dependent MET mode under mixo-, photoauoto- and heterotrophic growth conditions** - this work is presented in Chapter 5.

iii. **Determine metabolic states of *Synechocystis* sp. PCC6803 optimized for electricity generation using 1) ferredoxin- and plastoquinone-targeted MET mode and c-type cytochrome-linked DET mode under photoautotrophic conditions, 2) NADH-dependent MET mode under mixo-, photoauoto- and heterotrophic growth conditions** - this work is presented in Chapter 6.

iv. **Determine metabolic states of *S. cerevisiae* optimized for electricity generation under aerobic and anaerobic condition and compute corresponding current outputs** - this work is presented in Chapter 7.

Table 1-1: Microbial species and their metabolism and electron transfer types investigated in the present metabolic modelling.

Organisms	Transfer type	Electron source (Terminal microbial electron shuttle)	Metabolic type	
G.sulfurreducens	Membrane-driven	c-type cytochrome	Anaerobic	Heterotrophic
	Mediator-driven	NADH		
	Mixed mode (Membrane-driven and Mediator-driven at the same time)	c-type cytochrome & NADH		
C. reinharditii	Mediator-driven	NADH	Aerobic	Mixotrophic
				Photoautotrophic
				Heterotrophic
Synechocystis sp. PCC 6803	Membrane-driven	Ferredoxin	Aerobic	Photoautotrophic
		Quinones/ cytochromes (*)		Photoautotrophic
	Mediator-driven	NADH		Mixotrophic
				Photoautotrophic
				Heterotrophic
S.cerevisae	Mediator-driven	NADH	Aerobic	Heterotrophic
			Anaerobic	

*. The flux model of the *Synechocystis* cannot identify the difference between these two sites for electricity generation.

3. Compare the merits of the four microorganisms with relation to electricity generation

Work related to this objective is discussed in Chapter 8.

4. Evaluate *in silico* reaction-knock strain design for increasing electricity generation

The OptGene algorithm is implemented to identify sets of reaction deletions towards the maximization of electron transfer rates in each case of the four selected microorganisms. Work related to this objective is presented in Chapter 9.

1.5 Thesis structure

This PhD thesis is separated into ten chapters. Chapter 1 presents knowledge gaps and objectives of this thesis. Chapter 2 contains a literature review of MFC operational modes, MFC research directions, microbial entities in MFCs, and important metabolic engineering and constrained-based modelling techniques. Chapter 3 presents general parameter calculations for all MFC experiments, and methodology of modelling development and mathematical rationale used in this thesis. In Chapters 4-7, a) four selected microorganisms are modelled for MFC current productions, b) pertinent analyses are conducted to quantitatively compute the desired electron transfer rates, c) the underlying metabolic mechanisms are elucidated, and d) the effects of substrate uptake rates on current performance of the cells are investigated. Chapter 8 compares the results previously obtained for the four microorganisms and analytically discusses the productivities of each microorganism. Chapter 9 demonstrates the possibility of using reaction pathway modification as a strategy to improve the current output of the microbes. In addition, the reaction knockout results of OptGene algorithms are discussed, and relevant suggestions are made. Finally, Chapter 10 concludes the thesis and indicates the future directions that are possible stemming from the present work. Figure 1-3 schematically details how the chapters are related - the logical flow of the chapters.

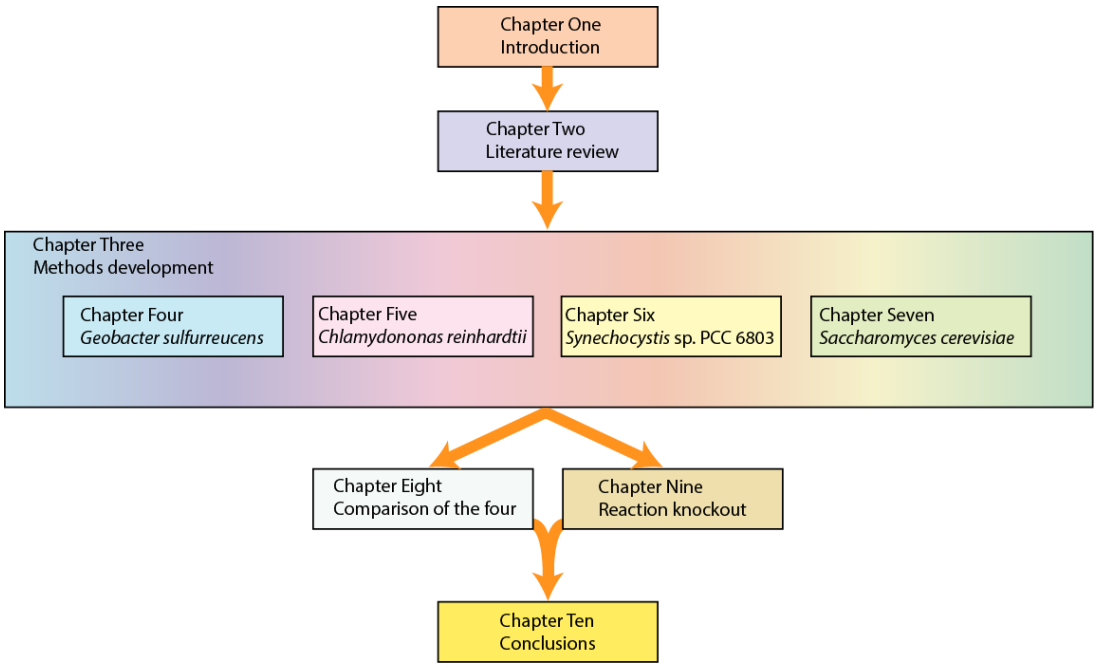

Figure 1-3: The logical flow of the thesis

CHAPTER 2 Literature Review

Part of the work in this chapter has been published previously in [47].

2.1 Microbial fuel cells (MFCs)

Microbial fuel cells (MFCs) are unique devices that can use microorganisms as catalysts for transforming chemical energy directly into electricity [48]. The biggest advantage of an MFC is that it can generate combustion-less, pollution-free bioelectricity directly from the organic matter in biomass [2]. In an MFC, the energy stored in chemical bonds in organic compounds is converted to electrical energy through enzymatic reactions by microorganisms. Thus, the electricity production by MFC is associated with the normal living processes of bacteria capturing and processing energy.

In a typical MFC configuration (Figure 2-1), microorganisms are situated in the anodic compartment and use the biomass for growth, while forming electrons and protons [22]. The electrons are transported out of cells to an electrode using redox mediators or directly expelled by some microorganisms for reducing the substrate. The protons or H^+ ions are diffused through the electrolyte to the cathode where it is oxidized to water. The cathode can be in a separate chamber (i.e, double chambered MFCs) or in the same chamber (i.e., single chambered MFCs). A single chambered MFC eliminates the need for the cathodic chamber by exposing the cathode directly to the air. The only byproduct released by MFCs is carbon dioxide, which can be fixed by plants for photosynthesis.

MFCs can operate under a wide range of environmental conditions due to the adaptability of microbial species. Factors affecting the MFC's efficiency include electrode material, pH Buffer and electrolyte, proton exchange system, and operating conditions in both the anodic and the cathodic chambers. MFCs are usually operated at ambient temperature, atmospheric pressure, and at pH conditions that are neutral or only slightly acidic [20].

MFCs harness the electrons from these systems in three main operation modes: mediated electron transfer (MET), direct electron transfer (DET) and product mode. Photosynthetic MFCs use photosynthesis as the electron source and can also be operated in the same modes.

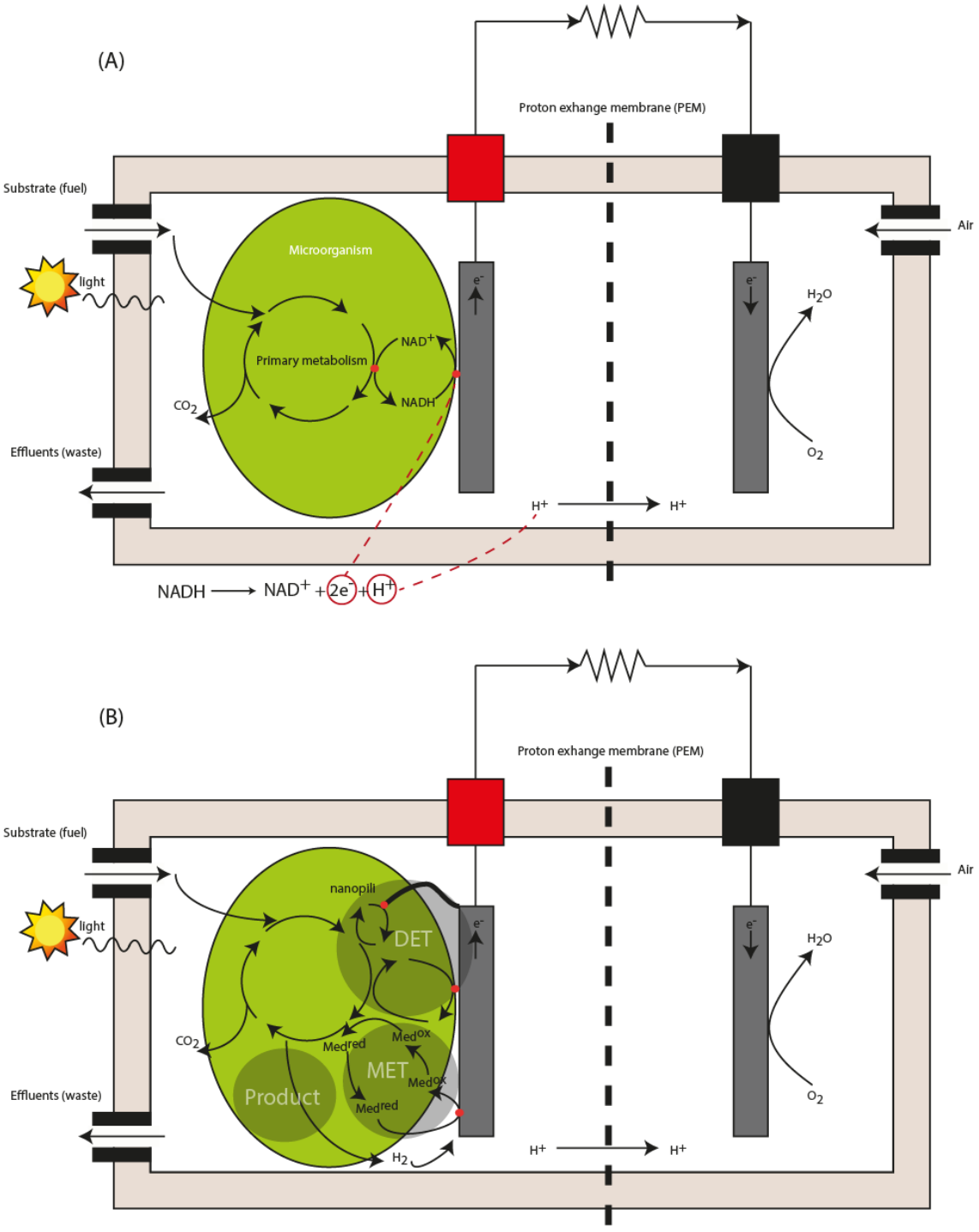

Figure 2-1: The working principle of a microbial fuel cell.

(A) A bacterium in the anode compartment transfers electrons obtained from an electron donor (glucose or light in the case of photosynthetic organisms) to the anode electrode. Protons are also produced in excess during electron production. These

protons flow through the proton exchange membrane (PEM) into the cathode chamber. The electrons flow from the anode through an external resistance (or load) to the cathode where they react with the final electron acceptor (oxygen) and protons.

(B) Three electron transfer modes: (i) directly via membrane-associated components (DET), (ii) mediated by soluble electron shuttles (MET) or (iii) primary product (Product) e.g., H_2 can act as a fuel to be oxidized to provide electrons for the electricity circuit. Med, redox mediator; Red oval, terminal electron shuttle in or on the bacterium.

2.1.1 Microbial fuel cell – a type of bioelectrocatalysis

Bioelectrochemical systems are based on use of biological entities to conduct interconversion between chemical and electrical energy at lower overpotentials. The biological moieties (biocatalysts) can be classified according to their nature in three classes: (i) redox enzymes, (ii) enzyme arrays or organelles (e.g., mitochondria) and (iii) microbial cells [49].

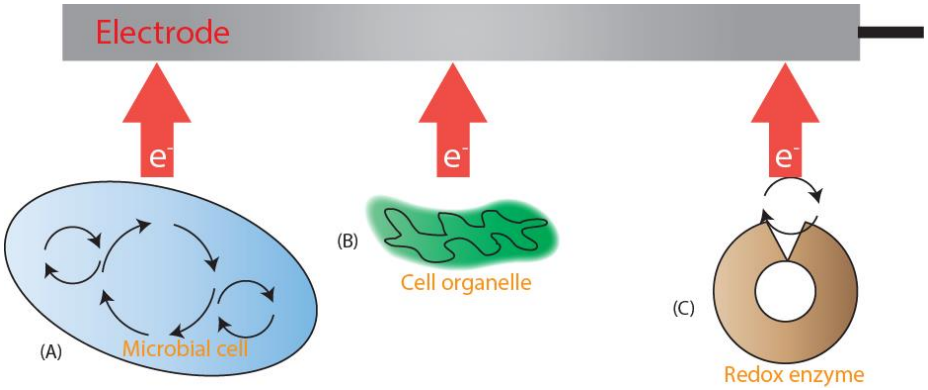

Figure 2-2: Simplified sketch of bioelectrocalytic systems.

A) microbial cells, B) cell organelles and C) redox enzymes (relative size not true to scale; and possible mediators not displayed). inspired by [49]

In a recent review paper [28], individual enzymes and enzyme arrays/organelles were considered as a combined group since they shared similar characteristics when compared with microbial cells. The research fields in enzymatic and microbial catalysis have developed in parallel (or even in competition). These two fields can interact and collaborate exchanging chemical and biological knowledge from each side.

The microbial cells can be divided into two classes: i) anode catalysts that convey electrons from an electron donor to an electrode, ii) cathode catalysts that transport electrons from an electrode to an electron acceptor.

2.1.2 Comparison of enzymatic and whole-cell based electrochemistry

Until quite recently, bioelectrochemical reactions were mostly studied with purified enzymes [28]. The desired enzymes are obtained from the cultures of bacteria producing such enzymes through a series of harvesting steps: cell lysis, enzyme extraction and purification [50]. Then, the collected enzymes can be used in enzymatic bioelectrocatalysis via direct electron transfer (DET) or mediated electron transfer (MET) (that involves use of a suitable soluble (or surface-bound) redox mediator for conveying electrons between enzyme and electrode).

Compared with enzymatic electrochemistry, the use of whole microbial cells for bioelectrochemcial processes have advantages in three aspects [28]: 1) The enzyme production and purification process is not required because the microorganisms can naturally regulate their metabolisms to produce the necessary enzymes for survival in different environmental conditions. 2) Enzyme activity is stable inside living cells since microbial cells create suitable conditions for enzymes activity and regulate synthesis of enzymes according to metabolic needs and degradation rates. 3) Unlike enzymatic electrochemistry which relies on a single reaction, living cells contain all kinds of enzymes required for forming complete biochemical pathways and thus provide opportunities to exploit the use of multiple enzymes or paths for electrochemistry.

Despite these advantages over enzymatic systems, whole cell bioelectrochemistry has disadvantages: 1) Microbes demand continual supply of nutrients for growth. 2) Microbial growth relies on multiple metabolic pathways and thus can consume a range of substrates, which lead to some unwanted by-products. This nature makes microbial bioelectrochemical systems not suitable for compound-specific biosensing applications [28].

2.1.3 Mediated electron transfer (MET)

MET is defined as where a mediator molecule acts as an electron relay that repeatedly cycles between the reaction sites and the electrode [12]. MET is the most common electron transfer mode used in MFCs and can be classified into two sub-types [12]:

- Indirect transfer systems that involve freely diffusing mediator molecules (i.e., diffusive MET).

- Indirect transfer systems in which the mediator is integrated into the electrode or the cell membrane (i.e., non-diffusive MET).

In diffusive MET, the mediators enter the cell membrane and exchange electrons between cellular metabolism inside the cell and the electrode outside it. In the non-diffusive MET, the mediator can collect the electrons from the cell membrane without penetrating the cell.

Based on the type of mediators, diffusive MET can also be classified into three sub-categories:

- MET via exogenous (artificial) redox mediators.

- MET via secondary metabolites

- MET via primary metabolites.

The detailed mechanisms in those three classes are discussed in [51]. Because the terminal electron transfer to or from the electrode determines the overall cell potential, potential (Voltage) losses can be minimized by using a mediator that has a reaction potential near that of the biological component.

2.1.3.1 The properties of an ideal mediator

The oxidized mediator captures and transfers electrons to the anode. At the anode the mediator is oxidized releasing electrons to the anode and changing back its reduced state. The ideal mediator should possess the following characteristics [5, 52-55]:

(i) It should display a reversible redox reaction to function as an electron shuttle;

(ii) It should have appreciable solubility in an aqueous solution and stability, and should not adsorb on the bacterial cells or electrode surface;

(iii) It should facilitate the electron transfer; the redox potential of the mediator should match the potential of the reductive metabolite. None of the oxidation states of the mediator should interfere with other metabolic processes. The electrochemical kinetics of the oxidation process for the mediator-reduced state at the electrode should be fast.

(iv) It should have low formal potential*. The lower the formal potential, the larger the cell voltage since it is the difference between the cathode and anode potentials

(v) It should also have a redox potential close to the redox potential of NAD+/NADH couple.

(vi) It should have low cost

(vii) It should be non-biodegradable and non-toxic to microbes

(viii) It should easily penetrate through the bacterial membrane to reach the reductive species inside the bacteria.

* The formal potential is the reduction potential that applies under a specified set of conditions (including pH, ionic strength, and concentration of complexing agents), Biochemists call the formal potential at pH 7, E_0' (read "E zero prime").

2.1.4 Direct electron transfer (DET)

DET is defined as the case where electrons cycle directly between a microorganism and an electrode. DET can be achieved through two naturally occurring mechanisms:

- Membrane bound c-type cytochromes, which exist in the cell membrane in some organisms [56, 57] to provide electron transfer capacity. For example, multi-heme proteins have especially evolved in sediment inhabiting metal reducing microorganisms such as *Geobacter* [58], *Rhodoferax* [59] and *Shewanella* [60]. In

their natural environment, iron(III) oxides act as the solid terminal electron acceptors, but in the case of an MFC the anode is used as the solid electron acceptor.

- Electronically conducting nanowires. The DET via outer membrane cytochromes requires the cytochrome (the bacterial cell) to be physically adhered to the fuel cell anode. When a biofilm is formed, only bacteria in the first monolayer at the anode surface are electrochemically active [58]. Thus, the maximum cell density in this bacterial monolayer usually influences the MFC's performance. However, it has been shown that some *Geobacter* and the *Shewanella* strains can evolve electronically conducting molecular pili [61] (nanowires of 20-30 μm long, made of fibrous protein structures) that make the microorganism able to reach and use more distant solid electron acceptors [26, 62]. The pili are connected to the membrane-bound cytochromes and allow transference of the electrons to the distant electron acceptors without cellular contact (Figure 2-1b). Thus, thicker electroactive biofilms can be formed to increase anode performance. It was found that the *Geobacter* nanowires exhibit metallic like conductivity independently of other cytochromes [63], which is different from *Shewanella* that relies on *c*-type cytochrome of OmcA and MtrC for nanowire-faciliated electron transfer. In practice, the fuel cell performance can be increased up to ten-fold upon nano-wire formation of *Geobacter sulfurreducens* [26].

2.1.5 Product type

In product type MFCs, microbes metabolize the substrate, releasing a secondary fuel product such as hydrogen that then diffuses to the electrode and is oxidised or reduced (as appropriate) to form a final waste product, which is discharged [12]. The product operation is similar to conventional fermentation processes, in that products of the microbial metabolism are used as the fuel at the electrode.

The product system is made up of two independent stages: one is storage of the microbial reaction product, the other one is the product being fed to a conventional fuel cell process driven by non-biological catalysis, such as in the case of a proton exchange membrane fuel

cell , where H_2 is converted into electricity [64]. These stages may also be physically separated in different containment vessels. However, a product system only truly belongs to biofuel cell system when the microbes and the electrode are together in the same anode compartment [12]. Nowadays, the fermentation (mostly to hydrogen gas) usually takes place in the fuel cell itself [65, 66].

Product systems have two main drawbacks, one is that the efficiency of the conversion of the biological substrate to hydrogen is quite low, and the other is that hydrogen oxidation require high fuel cell temperatures. Also, the produced biofuel gas is always contaminated with other byproducts such as CO, H_2S and (poly) siloxanes making it not sufficiently pure for direct use in a fuel cell [67].

2.1.6 Photosynthetic MFCs

Photosynthetic MFCs are MFCs that generate electricity from a light source rather than a fuel substrate and require the mediator involved to be light stable [68]. Conventionally two operating modes exist for photosynthetic MFCs:

- Energy is produced and stored by the microorganism during illumination and then released and processed in the same way as in a non-photosynthetic biofuel cell.

- The energy produced during illumination may be directly extracted in the form of electrons for creating an external electrical circuit.

A single photosynthetic MFC may possess both of these two modes of action. However, it is recently thought better to classify photosynthetic MFCs into categories based on seven approaches that integrate photosynthesis with MFCs – photosynthetic MFCs [68]:

(1) Photosynthetic bacteria at the anode with artificial mediators.

(2) Hydrogen-generating photosynthetic bacteria with an electrocatalytic anode.

(3) A mixed culture, with photosynthetic bacteria supplying organic matter to heterotrophic electroactive bacteria at the anode.

(4) Photosynthesis in plants, supplying organic matter via rhizodeposits to heterotrophic electroactive bacteria at the anode.

(5) An external photosynthetic bioreactor, where only biomass or metabolic products are transferred to the anode compartment to feed heterotrophic electroactive bacteria.

(6) Direct electron transfer between photosynthetic bacteria and electrodes.

(7) Photosynthesis at the cathode to provide oxygen.

These subtypes have been discussed in detail by Rosenbaum *et al*. [68].

2.1.7 Microorganisms suitable for MFCs

Most microorganisms are unable to donate sufficient electrons outside of cells to produce usable currents, because the outer layers of most microbial species are made up of non-conductive lipid membrane, peptididoglycans and lipopolysaccharides which restrain electron transfer to the anode [69]. Since the 1980s, it has been found that artificial water-soluble electron shuttles (i.e., methylene blue, thionine, neutral red and 2-hydroxy-1,4-naphthoquinone) can be used as mediators that transport the electrons from electron carrier molecules inside the cell (e.g., NADH, NADPH or reduced cytochromes) to the anode surface [69]. For example, an MFC based on *Proteus vulgaris* used thionine as a mediator to generate electricity from sucrose [70].

Since the 1990s, some bacterial species such as *Pseudomonas aeruginosa* [71] and *Clostridium butyricumcan* [72] have been found to be able to self-mediate extracellular electron transfer using their own metabolic products. Meanwhile, direct transfer of electrons (DET) that involves use of electrochemically active redox enzymes (i.e., cytochromes) have been discovered in a number of bacterial species such as *Shewanella putrefaciens* [56, 57, 73],

Shewanella oneidensis [74], ***Geobacter sulfurreducens**** [58, 75], *Rhodoferax ferrireducens* [59], and the oxygenic phototrophic cyanobacterium ***Synechocystis* sp. PCC6803*** [62]. These microorganisms are termed as exoelectrogens and among them *S. oneidensis* and *G. sulfurreducens* have evolved electronically conducting molecular pili (nanowires) to further facilitate the DET [26, 62]. Besides the DET mode, *S. oneidensis* can conduct MET using self-produced mediator [76]. The exoelectrogens in MFCs are thought to actively use electrodes to conserve electrochemical energy required for their growth and thus ensure high rates of fuel oxidation and electron transfer for the production of electrical energy [5].

In most of the previous MFC studies, bacteria have been used for electricity generation. On the other hand, since 2000, eukaryotes such as microalgae (e.g., ***Chlamydomonas reinhardtii****) and yeast (e.g, ***Saccharomyces cerevisiae****)** have also emerged as good choices for MFC use. These eukaryotes have been studied as model microorganisms in the lab and have been widely used in the industry for a long time, and their benefits for MFC uses are reviewed in Section 2.4.

(* Microorganisms in boldface are investigated in the present study)

2.2 Current directions of MFC research

2.2.1 Engineering design and biological aspects

Most previous studies tended to improve power densities of MFCs by optimizing the reactor configuration and operation parameters [77, 78], such as modifications of the electrode materials to incorporate metals that contain current collectors [79, 80], use of metals highly optimized for bacterial adhesion and metals possessing high electrical conductivity to minimize ohmic losses[11], and application of a biocathode that can increase an MFC's performance by improved oxidation of hydrogen at the cathode [81]. Applications of chemical treatments and precious metals to electrodes in order to increase power production in the laboratory have also been investigated [82, 83]. However, these modifications, like the use of larger laboratory reactors, may increase the cost and lead to compromises on performance

based on material costs. Many bottlenecks also exist for improving those physical and chemical properties.

Since the fundamental source of electrons is the cellular metabolism, it is particularly important to focus on biological processes that take place in the microbial cells. In this regard, further clarification is needed of the factors relevant to the anodic catalysis process, such as the diversity of the electrochemically active microorganisms [84] and especially the electricity generation mechanisms in relation to normal metabolic states.

2.2.2 Mediator-less, mediator self-producing and artificial mediator-based MFCs.

Mediator-less MFCs are a more recent development relying on the evolved ability of exoelectrogens for disposal of electrons originating from substrate oxidation. This type of MFC has been increasingly preferred, because use of mediators complicates the cell design and these mediators are usually toxic, costly and unsustainable, limiting MFC development [51, 85-88]. In addition, mediator involved MFCs usually produce low current densities (0.1-1 A m^{-2}) [51]. Unfortunately, mediator-less MFCs may not yet find a wide range of applications since the discovered exoelectrogens are still few in number and it is non-exoelectrogens that are largely used in the agricultural and industrial area [89]. Thus, an important direction of MFC research is development of MFCs using non-exoelectrogens without exogenous mediators [89].

However, problems arise from the fact that redox molecules used in electron-transfer reactions are not situated on the outer membrane, but in the cytoplasmic membrane. One way is to develop direct electron transfer using carbon nanoparticles that can contact the redox centres that are incorporated in the interior cell membrane[89]. Another way is to identify and develop self-produced mediators (e.g., in the case of *Shewanella* species mentioned above) through engineering methods [84].

2.2.3 Conventional photosynthetic MFCs

It is appealing to study whether phototrophic microbes can be used in an MFC generating electricity from sunlight, because sunlight is an unlimited energy resource and more solar energy reaches the earth in 1h (4.1×10^{20} J) than the energy consumed on the planet in a year [84, 90, 91]. In addition, the development of a self-sustainable photosynthetic MFC is important to meeting energy requirements at remote locations, where routine addition of fuel would be technically difficult and expensive [84].

Photosynthetic MFCs can generate electricity indirectly or directly. For example, in the indirect way, *Rhodobacter sphaeroides* in the MFC can produce H_2 that is oxidized at a platinum coated anode to generate electricity [92, 93], whereas in the direct way *Rhodopseudomonas palustris*, a photosynthetic purple non-sulfur bacterium, can generate electricity in a biofilm anode MFC by direct electron transfer [94].

There are also more traditional photosynthetic MFC configurations, where photosynthetic organisms live with other microbes and supply products to heterotrophs [95]. Photosynthetic microorganisms (e.g., cyanobacteria or microalgae) and heterotrophic bacteria exhibit synergistic interactions [96] that can be used in self-sustained phototrophic MFCs [90]. An indirect synergistic relationship between photosynthetic organisms and electricigens has been exemplified in a recent study, in which algal photobioreactors were used to supply organic matter produced via photosynthesis to an MFC for electricity generation [97]. The operation of this type of photosynthetic MFC is CO_2-neutral and does not need buffers or exogenous electron transfer mediators [95]. However, the photosynthetic MFC power densities obtained are quite low when compared with those that are currently reported for conventional MFCs, e.g. 0.95 mW m^{-2} for polyaniline-coated and 1.3 mW m^{-2} for polypyrrole-coated anodes [98] versus values in the W m^{-2} range for conventional cells. The photosynthetic MFCs usually have a lower energy efficiency as due to shadowing effects light cannot practically reach all the microbes within the MFC system.

2.2.4 MFCs based on the photosynthetic electron-transfer chain

Recently, the photosynthetic electron transfer chain has been considered as a source of the electrons harvested on the anode surface, which is different from the previously designed anaerobic MFCs, sediment MFCs, or anaerobic photosynthetic MFCs [98]. A single chamber photosynthetic MFC based on two photosynthetic cultures, planktonic cyanobacteria *Synechocystis* sp. PCC 6803 and a natural fresh-water biofilm, has shown a positive light response (i.e., immediate increase in current upon illumination) [98]. This phenomenon proves that it is possible to extract electrons directly from the photosynthetic electron-transfer chain, and not only from the respiratory transfer chain or through oxidation of hydrogen [99].

2.2.5 Improving MFC systems and processes by fuel cell modelling

The application of an MFC system is limited by a number of factors. The most important factor is that the power density of an MFC is several orders of magnitude lower than that of chemical fuel cells [100]. The power generation of an MFC is influenced by a range of different parameters [22], including the amount of bacterial cells, mixing and mass transfer phenomena in the reactors, bacterial kinetics, cathodic reactions, and the efficiency of the proton-exchange membrane. Therefore, construction and analysis of MFCs involve multidisciplinary knowledge of microbiology, electrochemistry, materials science, and engineering. Many intra-system phenomena and the effects of operating factors are poorly understood [14].

The MFC system can be improved through three ways: 1) Use of modern materials such as membranes, ceramics, semi-conductors, conductors, nano-materials can improve the efficiency of microbial community with the material [101]. 2) Engineering innovation can create systems that are reliable and cost-effective [102]. 3) Modelling and other forms of quantification (e.g., follow the electrons) can relate the microbial energy metabolism to mass transport, kinetics, and other engineering principles. The modelling relying on computational tools investigate system parameters avoiding costly and time-consuming laboratory experiments and are easily modified to simulate various configurations and operating

conditions. This can be complementary to the chemical engineering approach that is required for construction and development of an MFC [12].

Mathematical modelling has been used as a tool to study the complex systems of MFCs in a few previous studies [13, 15, 103-105]. The previous models have dedicated great efforts into description of electrochemical transfer mechanisms between the microbes and anode, electric circuit, biofilm formation, mass transport and reactions in biofilm and bulk liquid(s), which are quite variable for different MFC systems. However, none of the previous modelling studies have gone further regarding the change of complex mechanisms inside cells. The reason for that is thought to be due to the fact that 1) The previous limited modelling work stem from methods for traditional chemical fuel cells and centre on integration of knowledge of the microbial community with other engineering factors; 2) The biological system is far more complex than all other processes taking place in MFCs and there was no proper method to model such a complex system. Therefore, all these models overlook characterization of fundamental molecular mechanisms for electric current generation. In addition, the use of Monod equation in these modelling studies would have numerical meaning for microbial growth, but lacks the biological basis other than a regression-based mathematical formula [106].

The processes occurring in the MFC anode can be divided into a number of submodels (Figure 2-3): electrochemical reactions, biochemical reactions of methanogenic and electricigenic communities, biofilm formation, mass transport, reactions in biofilm, and reactions in bulk liquid.

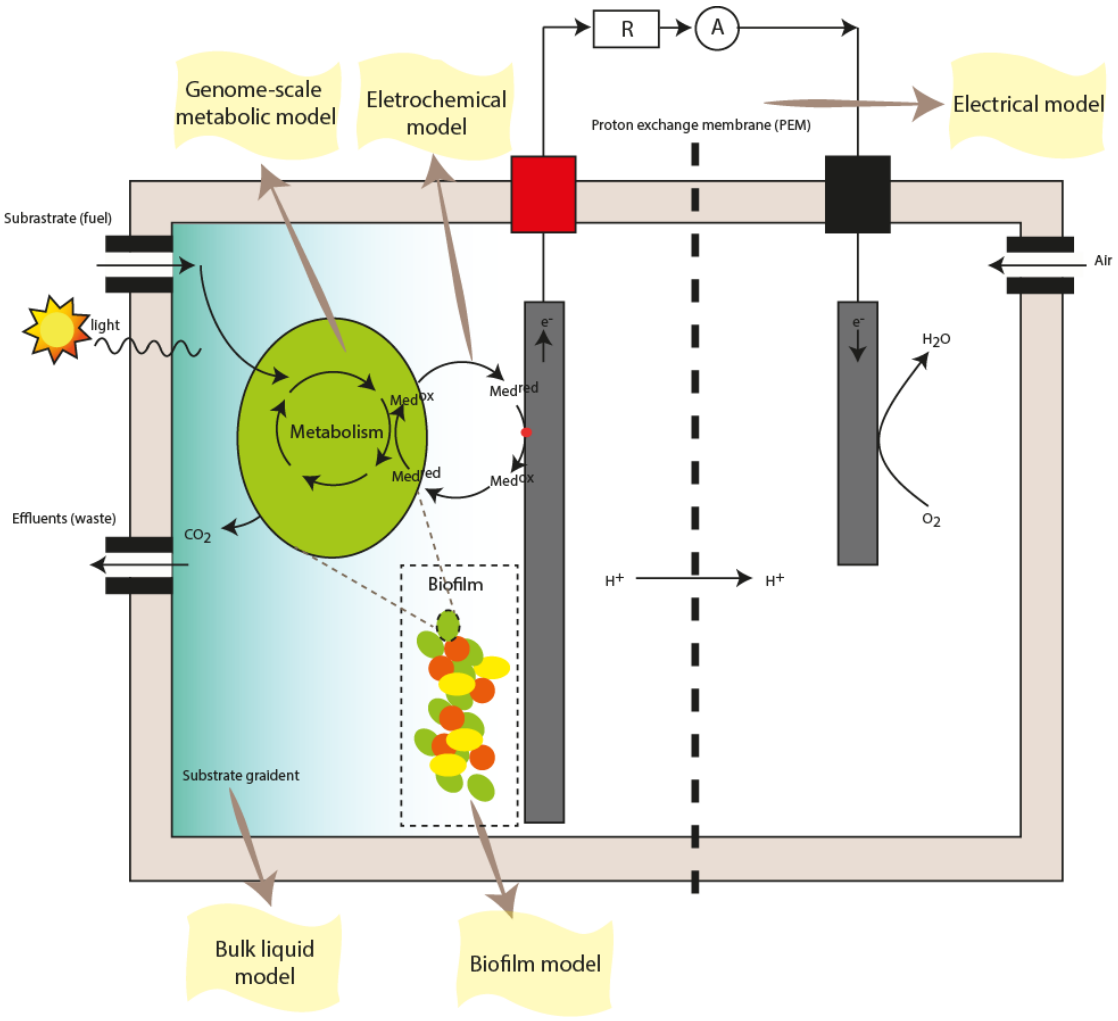

Figure 2-3: Construction of MFC models.

The anode compartment of the MFC comprises several processes, which can be represented by corresponding models: microbial reaction; electrochemical reactions with redox mediator on the anode; biofilm formation; mass transport and reactions in biofilm and bulk liquid. R, internal impedance component; A, current. Inspired by [16].

2.2.6 *In silico* systems study of microbial behaviours in MFCs

Traditionally, the development of highly productive microbial strains has relied on time-consuming methods such as random mutagenesis and screening. On the other hand, the systems biology methods such as mathematical modelling can test the capability of the microbial system for desired metabolic compound production, reveal previously unknown but essential life functions of special bacteria and predict the outcomes of different genetic manipulations and engineer new strains by performing gene deletions or additions leading to a

higher productivity of the desired chemicals. The results of *in silico* modelling can direct the metabolic engineering to manipulate microbial systems in favour of the extraction of electrons from microorganism to the electrode of MFCs for electricity generation.

2.3 Traditional reductionist approaches and systems biology

Systems biology is the newly emerging discipline in modern biology established in the past decade and relies on the idea that a biological organism can be described as a system, a closed organization of interacting distinguishable components including internal components, organelles: membrane surrounded compartments with different functions. These components are mutually dependent and interconnected to form and define the whole [107]. This system also communicates and interacts with the environment.

Because of the complexity of biological systems such as elaborate networks and mutual dependency of cellular processes and compartments, traditional reductionist approaches relying on insufficient data on isolated pathways and regulatory processes do not allow an understanding of the interaction of a biological system, which is indispensable for its function and biotechnological improvement [108]. Instead, systems biology provides *in silico* models that incorporate biological data, metabolic flux data and different physico-chemical constraints like the conservation of mass and energy, thermodynamics, redox-balance, *etc.* [108], and thus provides an opportunity to identify the crucial bottlenecks hidden in a complex network of interactions and cellular compartmentation [109].

2.3.1 Categories of systems biology tools

Microorganisms can be addressed in a global quantitative way by systems biology, which is dependent on the rise of the genomic and proteomic (collectively referred to as 'omic') high-throughput technologies and current computer power [110]. Systems biology tools include 1) gene detection (genomics), 2) gene expression (transcriptomics), 3) protein expression and modifications (proteomics), 4) primary and secondary metabolites production (metabolomics), 5) measurement and estimation of reaction rates (fluxes) for a network of

reactions that occur in an organism (fluxomics) [111] (Figure 2-4) and 6) large-scale literature mining (bibliomics) [110-112].

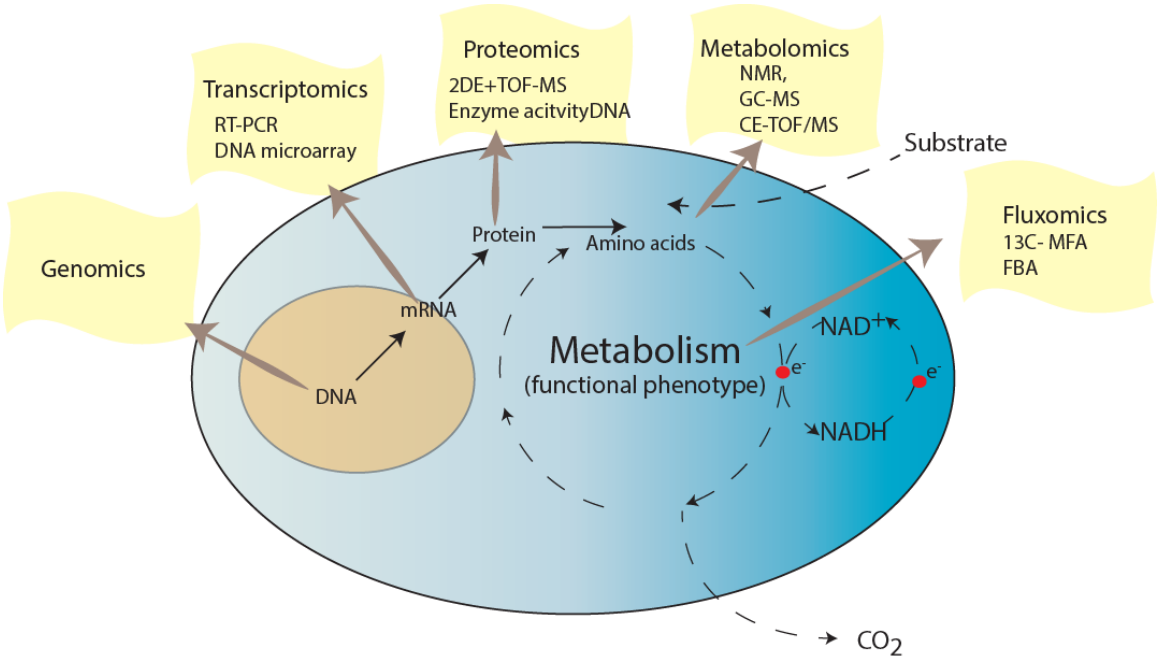

Figure 2-4: Conceptual figure of systems biology.

Systems approaches tend to make genome-wide, transcriptome-wide, or proteome-wide measurements on a system. Techniques for quantitative analyses of metabolic system components (metabolites and proteins) and output (fluxes) are available

These ‘omics’ technologies have different focuses in characterizing the function or dysfunction of engineered microorganisms for strain engineering or improvement. The usefulness of ‘omics’ technologies are addressed as follows:

Genomics integrates genetics, high-throughput analytical tools and bioinformatics to study all genes of a cell, identification of entire DNA sequences and analysis of function/interaction of genes within the entire genome's network [113]. Compared to genomics, transcriptomics is quite dynamic, and it characterises a gene expression pattern by quantification of all the RNA molecules. For such an analysis, the methods/techniques include RT-PCR, alternative splicing arrays like cross-linking immunoprecipitation (CLIP), RNA-tag sequencing like SAGE [114], and DNA microarrays, whole RNA sequencing and gene expression arrays, for example, Affymetrix or Agilent [115]. The next step after genomics and transcriptomics is

proteomics, which studies the structures and functions of proteins through large-scale experimental analysis involving protein purification and mass spectrometry. While an organism's genome is more or less constant, the proteome differs from cell to cell and from time to time and subsequently proteomic experiments are difficult to reproduce [116].

Metabolomics involves the global analysis of all measurable intracellular and extracellular metabolite concentrations (small-molecule content of cells, or other biological samples, such as carbohydrates, fatty acids, and amino acids) and their changes over time under given genetic/environmental perturbations. Therefore, metabolomics can be referred to as concentration-based 'omics' [117, 118].

The tools for analysis of the microbial metabolome usually consist of two technologies: 1) chromatographic techniques that allow an initial separation of extracts and 2) spectrometry-based techniques, e.g., Liquid chromatography–mass spectrometry (LC-MS), Gas chromatography–mass spectrometry (GC-MS), Capillary electrophoresis–mass spectrometry (CE-MS), Nuclear magnetic resonance (NMR), Matrix-assisted laser desorption/ionization - mass spectrometry (MALDI-MS) and capillary electrophoresis time-of-flight mass spectrometry (CE-TOFMS)-based metabolomics techniques [119]. These 'omics' and their control systems can be framed in the context of flux analysis (fluxomics)**.** Fluxomics quantifies the reactions rates that describe the time-dependent passage of metabolites through a reaction. The difference between metabolite concentrations and fluxes can be exemplified through the relationships between the number of cars on a street versus their traffic pattern [117, 118].

The flux distribution through all the reactions in a whole network is the phenotype of the network. Thus, this technique can be used to identify the metabolic interactions and predict physiological phenotypes in metabolic networks and consequently allows for rational design of biological hosts for desired cellular functions and analysis of global physiological changes caused by genetic changes [117, 120].

Flux analysis can be combined with cell biology and subcellular biochemistry to reveal the functionality and efficiency of the enzymes associated with cell biological components or structures [121]. Metabolic regulation can be deeply understood only when multiple system

components are examined simultaneously. This kind of analysis has been conducted in microbial and medical research in recent years.

Flux determinations can produce results that are hardly predictable from observed changes in transcript or protein levels because most of metabolic control takes place at post-translational levels and enzyme activities are often not correlated with changes in transcript or protein levels [121]. The incorporation of data from enzyme platforms should make the functionality of genomics strategies more clear. System-wide metabolic flux characterization is an important part of metabolic engineering [121].

Metabolic flux measurement can be performed by 13C-based metabolic flux analysis (13C-MFA), in which a 13C isotopic labelled carbon source is used to culture microbes and then intracellular fluxes can be quantitatively determined by tracing the transition path of the labelled atoms between metabolites in the biochemical network [122]. However, 13C-MFA faces two major limitations:

1) 13C-MFA can only obtain labelling information of amino acids rather than other free metabolites, which causes the resultant flux information to be restricted to central metabolism and this method is not suitable for large-scale network analysis. To date 13C-MFA has only been applied to two large-scale networks comprising more than 300 reactions, but most of the fluxes in the two studies are not accurately determined due to insufficient constraints [123, 124]. Thus, the genome-scale 13C-MFA still needs further improvements in experimental and computational techniques [125].

2) 13C-MFA is difficult to perform since the metabolite labelling measurement involves a combination of different analytical tools (GC-MS, LC-MS and NMR) to obtain extensive labelling information [126]. In 13C-MFA, cells are cultured in 13C-labelled medium and the isotope-labelled cells are then extracted and quenched by using a solution spiked with unlabelled metabolite standards of known concentration. Intracellular concentration for individual metabolites can be calculated by the isotope ratio-based approach [127]. Thus, to get a confident result requires quick sampling, rapid metabolite extraction, and a high-resolution LC-MS instrument [128, 129].

Due to these two limitations, 13C-MFA aims at understanding the conceptual operation of a simple metabolic network using labelled precursors and is used as a complementary method to *in silico* mathematical approaches that compute flux distribution based on reconstructed genome-scale metabolic networks (GEMs) of organisms [113], which serve as frameworks that integrate all of the massive '-omics' data derived from systems biology research [112].

2.3.2 Genome-scale metabolic network (GEM)

A high-quality GEM is built from a variety of biological knowledge sources such as genome annotations, metabolic databases (e.g., KEGG and BRENDA) and published biochemical information in a quality-controlled and bottom-up fashion [130-132]. These large-scale networks are developed to include as large a part of the cell metabolism as possible and as much biological information as possible [133]. In other words, these networks provide a detailed representation of biological reaction networks and their functional states [134], and can be used as an analysis platform for constraint-based modelling [112]. Nonetheless, characterization of GEMs are still far from comprehensive in databases [135] and even in the best-understood organisms the majority of kinetic parameters remain undetermined.

The GEM reconstruction consists of four main stages 1) Creating a draft reconstruction, 2) Manual reconstruction refinement, 3) Conversion from reconstruction to mathematical model, 4) Network evaluation (i.e, debugging mode). The procedures in each stage are described previously in detail by [132]. Due to the advance in high-throughput 'omics' technologies and computer power, there has been an exponential increase in GEMs reconstructed for a wide variety of organisms since the first GEM was built in 1999 [136].

2.3.3 Stoichiometric matrix

The GEMs can be converted into a mathematical format as a stoichiometric matrix that is fundamentally required by all *in silico* modelling approaches [137]. Stoichiometry is the calculation of quantitative relationships of the reactants and products in chemical reactions. Metabolic networks are represented by a stoichiometric matrix S with each column of the stoichiometric matrix corresponding to a chemical or transport reaction and each row

corresponding to the metabolites [138, 139]. The elements in S are the stoichiometric coefficients of the associated reactions. The negative and positive coefficients indicate the directionality of the reaction, i.e., the substrate metabolites have negative coefficients, whereas the product metabolites have positive ones. Usually in a real situation, the number of reactions (n) is always larger than that of compounds (m), which indicates that there are more unknown variables than equations and thus the system of equations has more than one solution [140]. The stoichiometric matrix can be annotated by including other important information linked to either the reactions or the metabolites, such as the genome and gene expression data for use in certain applications [137]. The stoichiometric matrix, based on a reconstructed metabolic network, serves as a backbone for mathematical modelling approaches to perform predictive, hypothesis-driven *in silico* experiments [141]. These modelling approaches can be divided into three categories: 1) characterizing the general network structure through nullspace analysis such as singular value decomposition (SVD), 2) analysing all possible flux distributions in a network trough extreme pathway analysis (EM) and elementary mode analysis (ExPA), and 3) constraint-based flux analysis, specifically flux balance analysis (FBA) that identifies the flux distribution of a particular network states [137]. However, constraint-based modelling is the only approach that enables a genome-scale description of metabolic process.

2.3.4 Flux characterization of cellular phenotypes by constraint-based flux modelling

A constraint-based modelling approach is used to predict possible cellular phenotypes by interrogating capabilities of the GEM through the imposition of physicochemical constraints. The constraints are formulated based on the consideration of stoichiometry, thermodynamics, flux capacity, and regulatory restraints under which reactions operate in a metabolic network [142, 143]. These constraints are applied to reduce range of attainable flux distributions or metabolic phenotypes achievable for an organism. As a result, a steady-state flux space is defined that contains all possible functional states of the network [144].

Since much fewer model parameters are needed for the analysis of a metabolic network, constraint-based stationary analysis can be performed on a GEM. Nonetheless, this method

generally offers no information about metabolite concentrations or about the temporal dynamics of the system [145-147]. Although the other quantitative approach, i.e, kinetic modelling, can characterize the detailed mechanisms of the metabolic reaction systems, obtaining a large number of kinetic parameters is not an easy task. In addition, many of the kinetic values cannot be trusted because they are acquired from the *in vitro* rather than *in vivo* measurement [148]. Therefore, compared with kinetic modelling, constraint-based modelling is the more appropriate tool for *in silico* engineering complex biological systems. The cornerstone of the constraint-based modelling approach is flux balance analysis (FBA) [149].

2.3.5 Flux balance analysis (FBA)

FBA relies on data-driven constraints and linear optimization theories [150]. The constraints used in FBA can be classified into three groups: physicochemical, topological and environmental constraints. Physicochemical constraints are physical laws such as the stoichiometry of the reactions and thermodynamics on reaction directions; topological constraints represent spatial restrictions on metabolites within cellular compartments; and environmental constraints include nutrient availability, pH and temperature [150]. FBA can analyse metabolic networks to relate genotypes to phenotypes because all expressed phenotypes of a given biological system must satisfy basic physicochemical, topological and environmental constraints that are imposed on the functions of all cells [151, 152]. Once constraints are set, to evaluate the performance of the biological system at various perturbations, FBA requires a physiologically relevant objective function. Objective functions can be in many forms such as physiologically meaningful objectives or design objectives for the interrogation or exploitation of a given system. Examples of common objective functions include maximizing biomass, cell growth maximizing ATP production or maximizing the rate of synthesis of a particular product [153]. Because the physicochemical constraints are readily defined from the annotated genome sequence and measured enzymatic capacities, FBA needs a minimal amount of experimental data.

FBA was specifically designed to compute quantitative growth phenotypes [138, 154], by maximizing the biomass reaction flux (representing the growth rate) given a set of bounded intake rates for external substrates [155]. In FBA, the biomass equation is usually set as a linear formulation of a range of macromolecular components, including proteins, DNA, RNA,

lipids, lipoteichoic acids, peptidoglycan and polysaccharides, which account for all known biomass constituents and their fractional contributions to the overall cellular biomass [132, 156]. This equation is used to reflect the observation that the cell growth requires synthesis of a range of metabolites from a modelling perceptive. The individual composition of every precursor metabolite in the biomass equation is maintained at a fixed stoichiometry, which is determined by examining the relevant literature or adapting known biomass compositions of related organisms [155]. The stoichiometric combination makes the equation consumeeach biomass precursor metabolite in proportion to its ratio in the biomass composition [138] and is thus independent of the specific growth rate [156]. The detailed method to formulate biomass reactions for genome-scale network reconstruction can be found in [132].

FBA is based on the assumption that microbes evolve to optimize their metabolisms for maximizing biomass production (growth rate) [154, 157-159]. This assumption has been confirmed by experiments in many cases [158, 160, 161]. It was also found that the metabolic network did not initially operate according to the optimal growth principle, but under selection pressure on glycerol, *E. coli* evolved to eventually maximize their growth rate [160]. Flux balance models have also been successfully applied for different metabolic engineering purposes, such as production of lycopene and vanillin [162-165].

A previous study used a central metabolic model of *E.coli* to evaluate the prediction accuracy of FBA with different objectives and the results showed that maximization of ATP or biomass yield per unit flux could achieve higher accuracy under specific condition, such as unlimited growth on glucose under aerobic conditions, than maximization of biomass production ("growth rate") [166]. However, this indication is questioned by a later study based on a genome-scale model of *E. coli* [167]. The study found that there was very little difference between maximizing biomass production rate and biomass yield per unit flux for predicting gene expression changes seen after adaptive evolution and both of these two objectives achieved high prediction accuracy. On the other hand, maximizing ATP yield led to poor prediction involving few genes. It was thought that maximization of ATP selects against the usage of biosynthetic pathways since the end products are not included in this objective [167]. Overall, maximization of ATP per unit flux can predict the intracellular flux distribution in accordance with some experimental data, but a maximal growth rate phenotype can still occur after adaptive evolution, or through prolonged experimentation in the laboratory [168].

The biomass objective function is now built into almost every metabolic network of microorganisms for simulating microbial growth through the objective-driven optimization (i.e., FBA), which can circumvent the need to define regulatory and signalling networks of organisms. On the other hand, if metabolic, regulatory and signalling networks are all reconstructed, extrinsic objectives will not be required for a growth-phenotype simulation [149].

2.3.5.1 Mathematical basis of FBA

The mathematical procedure to implement FBA involves computing a basis of the underlying polyhedral cone and identifies one or more optimal flux distribution points within the cone using linear optimization. The principle of the linear optimization underlying FBA modelling comprise four major stages (Figure 2-5): 1) Metabolite balancing and stoichiometry under steady-state assumption (connectivity) to be mathematically expressed as subspace of universal flux space. 2) Reversibility of biochemical fluxes (convex) to be mathematically expressed as convex space. 3) Minimum and maximum fluxes (capacity) to be mathematically expressed as confined convex space. 4) Maximization or minimization of objective function fluxes to be mathematically expressed as a solid plane that touches the polyhedral convex cone in the optimal point that represents a state of the flux distribution to achieve the objective function.

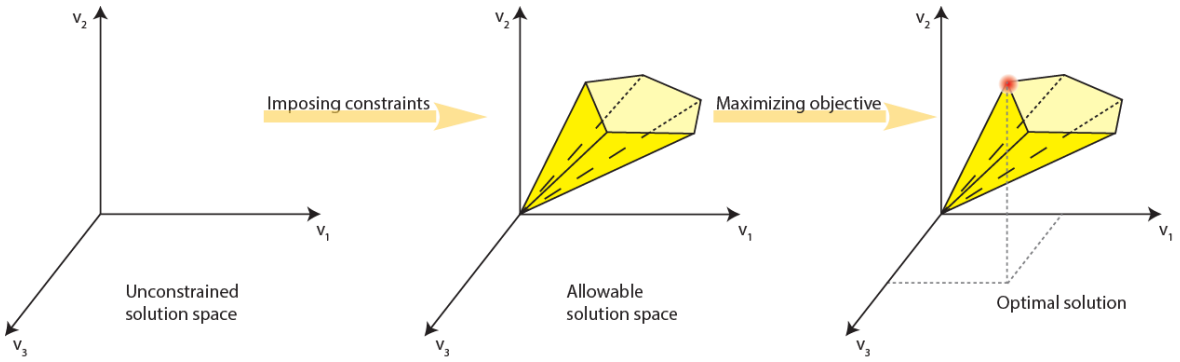

Figure 2-5: The conceptual basis of FBA.

A three-dimensional flux space based on a hypothetical metabolic network is depicted here. Without any constraints, the fluxes can take on any real value. After addition of constraints such as stoichiometric, thermodynamic and enzyme capability rules, the total flux solution space is shrunk into a polyhedral cone, termed the allowable solution space, and the biological infeasible steady-solution space is eliminated. Any point outside of the polyhedral cone violates one or more of the applied constraints and are biologically infeasible. Liner optimization that can maximize or minimize a defined objective such as biomass production can further reduce the steady-state solution space to a single solution, which circumvents the need for complete knowledge of the biochemical reaction networks. Inspired by [140, 169].

2.3.5.2 Comparison of FBA and 13C-based metabolic flux analysis (13C-MFA)

Both FBA and 13C-MFA require the use of a metabolic network and the assumption of steady state for internal metabolites, disregarding dynamic intracellular behaviour. However, FBA characterizes the "optimal" metabolism for the desired functional metabolic output (phenotype) and can be implemented on a genome-scale metabolic network, whereas 13C-MFA profiles *in vivo* metabolic flux distribution in a metabolic network and current technique only allows it to work on a small-sized central metabolic network [113]. Nevertheless, as the 13C-MFA approach determines enzymatic rates at a specific growth conditions experimentally, its resultant flux values are more precise than the prediction results of FBA. The metabolic fluxes experimentally measured by 13C-MFA can be complementary to the metabolism predicted by FBA for identifying competitive pathways or toxic by-products, and thus help in reducing gene targets underlying the enzymatic hurdle for improving desired product yield [170].

2.3.5.3 Variants of FBA

FBA has been considered as a general guideline and a viable first step for metabolic engineering of microorganisms for improving biosynthetic yield [171]. However, *in silico* prediction results of FBA could be different from in vivo observation. In an attempt to resolve this inconsistency, a number of optimization algorithms and computational strategies have been proposed to constrain the solution space of FBA, e.g., energy balance analysis complementary to FBA can take into account thermodynamic principles to improve theoretical prediction [171, 172]. However, energy balance analysis can only be conducted on small-sized network and requires biochemical thermodynamics parameters of all reactions. On the other hand, to better describe metabolic behaviours divergent from optimal prediction, FBA can be performed under a bi-level optimization framework to estimate the potential trade-off between the maximisations of biomass production rate and the other desired product yield [173]. FBA can also use other objective functions such as MOMA (minimization of metabolic adjustment) and ROOM (regulatory on /off minimization). MOMA has been successfully used to engineer strains with increased production of many products such lycopene [174, 175], valine [176], threonine [177], and polylactic acid [178]. On the other hand, transcriptional regulation is incorporated into several variants of FBAs, such as

regulatory FBA (rFBA) [179], steady-state rFBA (SR-FBA) [180] and probabilistic regulation of metabolism (PROM). These variant approaches centre on predicting the immediate behaviour of knockout strains, which is different from ordinary FBA that is used to predict cellular behaviours after strains have undergone adaptive evolution [159]. The computational tools to implement FBA and its derivative techniques is summarised in a recent review article [181].

FBA can also be combined with metabolic pathway analysis, such as elementary mode (EM) and extreme pathway analysis (ExPA), which can characterise all metabolic routes in a metabolic network without prior knowledge of reaction rates. The computation of EMs and ExPAs are restricted to metabolic networks of moderate size and connectivity because the number of modes and the computation time rise exponentially with increasing network complexity [182]. For example, 71 million EMs were found in a medium size metabolic network of *S. cerevisiae* (230 reactions and 218 metabolites) [183]. Computation of EMs for a central metabolism network of *Escherichia coli* (106 reactions and 89 metabolites) results in about 26 millions [182]. Also, according to our empirical observation, computation of EMs for the metabolic network of *G. sulfurreducens* (709 reactions; performed with CellNetAnalyzer 9.9 on an i7 four cores CPU, 8 GB memory and solid state disk home computer) could not terminate after several days. The large number of EMs are biologically meaningless and could only be interpreted due to the fact that the network contains a large quantity of parallel (redundant) pathways.

Furthermore, an FBA algorithm typically only produces one optimal solution for metabolic flux values through a network and neglects the existence of multiple, equally valid, optima that span an optimal solution space. The whole optimal solution space can be explored by flux variability analysis (FVA), which can calculate the feasible range of flux values for each reaction [184]. FVA is an extension of FBA that can calculate a full range of possible numerical values for each reaction flux in a network for achieving a particular objective function. This can help clarify the entire range of achievable cellular functions and examine the redundancy in metabolic network.

2.4 Microorganisms for *in silico* study of MFC functioning

2.4.1 Categories and representatives

Because the electricity generation in MFCs is based on the metabolic activity of living microorganisms, experimental screening of different microorganism for better anodic activity has long been recognised as a fundamental way to improve MFC performance. It is also possible to improve the performance by culturing microorganisms under selective pressure for enhanced power production [58, 185].

Compared to experimental studies, *in silico* modelling is less constrained to a particular MFC design and operating mode. Clearly no single organism is likely to be optimal for all of the varied designs discussed before. To date, every microorganism used in previous MFC studies has advantages and disadvantages. Its selection depends on a variety of factors such as types of application, capability of power generation, the availability of types of energy source for bacterial survival and the ability of extracellular electron transfer, in that electrodes are not natural electron acceptors.

From the modelling perspective, a broader view is possible. Categories of microbes can be identified to cover the range of operating modes, and within these individual organisms selected that will allow different modes to be individually studied and also compared quantitatively.

MFC microbial communities can be divided into three groups: heterotrophic cells, photoheterotrophic cells, and sedimentary cells [10]. The distinction between phototrophic and heterotrophic metabolism is fundamentally important in determining the operating mode. Another key distinction is between prokaryotes and eukaryotes. Compared to prokaryotic species and mixed cultures that have been mostly studied for different MFC applications, fewer studies involve eukaryotes as biocatalysts in MFC operations [186]. This is because the metabolic processes of eukaryotic cells take place in the membrane-surrounded cell organelles (e.g., chloroplasts) and is thus thought to be difficult for some commonly used redox mediators such as HNQ to get access to [23, 85]. While prokaryotes have the advantage that

their simpler cell membranes and internal structures are more amenable for physical electron extraction, the more complex metabolism of eukaryotes may be more efficient and be able to support a larger diversion of redox carrier flux without undue harmful effects on the organism.

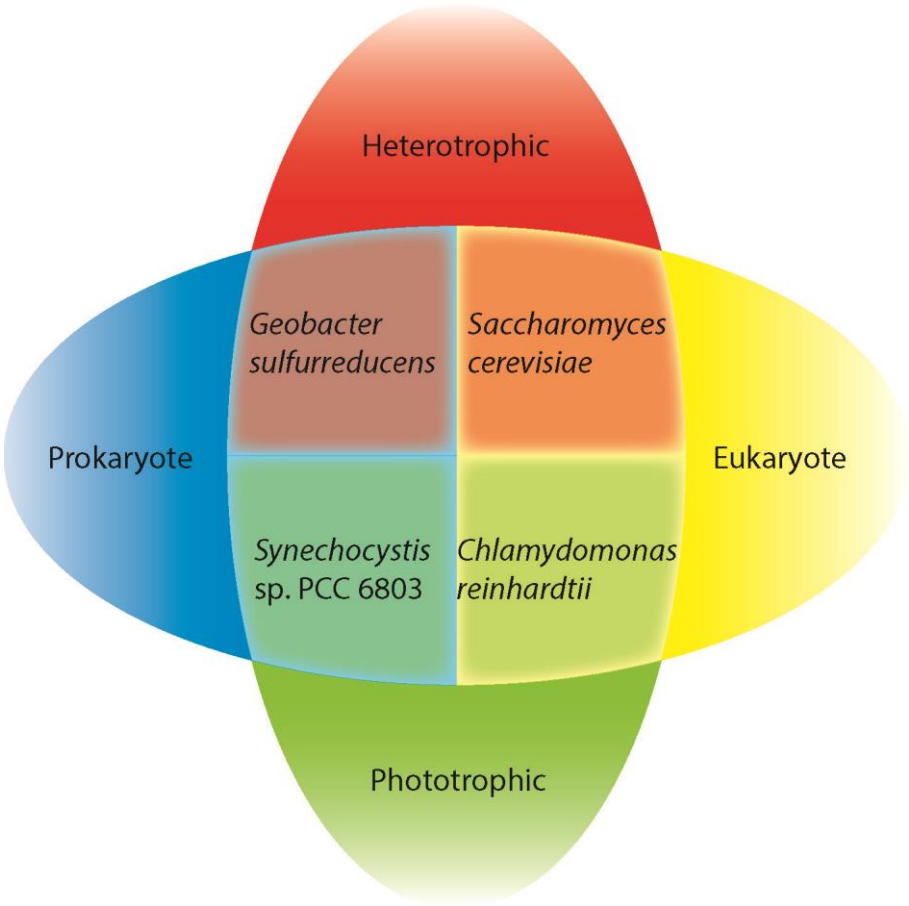

Figure 2-6: Classification of proposed microbes

The four anodic microorganisms: *Chlamydomonas reinhardtii*, *Synechocystis sp.* PCC 6803, *Saccharomyces cerevisiae* and *Geobacter sulfurreducens* each combine a different pair of key features, and are proposed as good candidates for MFC *in silico* characterization.

As illustrated in Figure 2-6, *C. reinhardtii* and *S. cerevisiae* are eukaryotes, whereas *Synechocystis sp.* PCC 6803 and *G. sulfurreducens* are prokaryotes. The four organisms also cover the three groups of the MFC microbial communities mentioned above, i.e., *C.*

reinhardtii and Synechocystis sp. PCC 6803 are photoheterotrophic cells; *S. cerevisiae* are heterotrophic cells, and *G. sulfurreducens* is a typical sedimentary cell.

C. reinhardtii and *Synechocystis sp.* PCC 6803 are photosynthetic organisms that are also capable of producing hydrogen. The comparison of organisms with/without photosynthesis can be used to study exploitation of photosynthetic and respiratory electron transport chains to supply MFC current.

A further consideration in a modelling study is whether the data is available and computationally manageable. All four microorganisms have been studied extensively as model organisms and used in various industries for a long time and thus related molecular tools and biological mechanisms are abundant. In particular, genome-scale metabolic networks have been reconstructed and are regularly updated for these four organisms. Based on a literature review, the most updated models are shown in Table 2-1. These models include the natural redox mediators (i.e., NADH) that are well balanced for the cellular energy metabolisms (e.g., oxidative phosphorylation, glycolysis, Calvin cycles and TCA cycles) and are thus practicable for MFC modelling.

Table 2-1: The scope of the genome-scale models of the four selected organisms

	Chlamydomonas reinhardtii	*Synechocystis sp. PCC 6083*	*Geobacter sulferreducens*	*Saccharomyces cerevisiae*
Gene	1080	1811	617	918
Metabolite	1068	465	644	1655
Reaction	2190	493	709	2110
Compartment	10	3	2	17
Date	2011	2011	2009	2012
Reference	[187]	[188]	[189]	[190]

It is noted that only the network models of *C. reinhardtii* and *S. cerevisiae* fulfil current standards of model annotation as requested by MIRIAM (Minimum information requested in the annotation of biochemical models [191]), whereas the models of *Synechocystis* and *G. sulferreducens* do not. The lack of such unifying nomenclature makes systematic comparisons unnecessarily difficult.

The biological features of the four microorganisms are summarized in Table 2-2 and the relevance of each of these microbes is reviewed in more detail in the following sections:

Table 2-2: Comparison of four selected microorganisms

Name	***Geobacter sulfurreducens***	***Chlamydomonas reinhardtii***	***Synechococcus sp. 6803***	***Saccharomyces cerevisiae***
Domain	Prokaryote (Gram-negative)	Eukaryote	Prokaryote (Gram-negative)	Eukaryote
Mitochondria	N/A	Multiple	N/A	Multiple
Chloroplast	N/A	Single chloroplast occupies two thirds of the cell.	Chloroplast analogy	N/A
Hydrogen synthesis enzyme	N/A	Fe hydrogenase	NiFe hydrogenase	N/A
MFC mode	DET	Product mode	Photosynthetic DET	MET DET (output extremely low)
MFC performance	1.88 W m^{-2} 43 W m^{-3}	0.4 W m^{-2} 3.3 W m^{-3}	0.02 W m^{-2} 0.007 W m^{-3}	1.5 W m^{-2} 90 W m^{-3}(MET) 0.003 W m^{-2} (DET)
Optimum growth temperature	30 - 35 ℃ [192]	20-25 ℃ [193]	30-33 ℃ [194]	25–35 ℃ [195]
Growth mode	Heterotrophic & Sedimentary (soil inhabitant)	Autotrophic Heterotrophic Mixotrophic	Autotrophic Heterotrophic Mixotrophic	Heterotrophic

N/A, not applicable.

2.4.2 Chlamydomonas reinhardtii

C. reinhardtii is a unicellular green alga that belongs to the *Chlorophytes* division, which diverged from the *Streptophytes* division (including land plants) more than one billion years ago [196]. *C. reinhardtii* is a ~10-μm, unicellular, soil-dwelling green alga with an eyespot, a nucleus, multiple mitochondria, two anterior flagella for motility and mating, and a single cup-shaped chloroplast that accommodates the photosynthetic apparatus [197, 198].

Like plants, *C. reinhardtii* has a cell wall and can grow in a medium lacking carbon and energy sources when illuminated [198]. Unlike angiosperms (flowering plants), this microorganism has functional photosynthetic apparatus even when in dark conditions and with an organic carbon source [198]. In the dark, acetate is the sole carbon source used by wild-type *C. reinhardtii in vivo* [199].

Because of the relative adaptability and quick generation time, *C. reinhardtii* has been used as a model to study eukaryotic photosynthesis, eukaryotic flagella and basal body functions and the pathological effects of their dysfunction [200, 201], and investigated for water bioremediation and biofuel generation [198, 202-204]. The cDNA, genomic sequence and mutant strains of *C. reinhardtii* are publicly available through the *Chlamydomonas* Center [205].

Advantages of algae: *C. reinharditii* inherits all potential advantages of algae for industrial use and scientific study, including [206-208]: (1) Algae biomass can potentially be produced at extremely high volumes and this biomass can yield a much higher oil (1 000-4 000 gallon/acre/yr) than soybeans and other oil crops [208]. (2) Algae do not compete with traditional agriculture because they are a non-food based resource which can be cultivated in large open ponds or in closed photobioreactors located on low productive or non-arable land. (3) Algae have a good adaption to different climate and water conditions and can be grown in a wide range of water sources, such as brackish, saline, fresh or waste water; (4) Algae can make use of resources that would otherwise be considered waste as substrates for growth [208]. (5) Algae can use and sequester CO_2 from many sources such as flue gases of fossil fuel power plants and other waste streams. (6) Algae can be processed into a wide range of products such as biodiesel, bioethanol, methane, bio-oil and biochar, and high protein animal feed. (7) The 'simple' photosynthetic alga *C. reinhardtii* is an excellent model organism for a systems biology approach compared to a complex vascular plant [108].

Biofuel and electricity production by algae: Due to the advantages listed above, algae have been examined in many studies for the generation of energy products, such as bio-oil, methane, methanol and hydrogen [209]. Nevertheless, these technologies have one disadvantage in that the fuel produced must be stored, transported and further processed to produce electricity. To circumvent these problems, an MFC is used as an alternative way to directly generate electricity in only one process unit by means of hydrolysis and fermentation of algae and makes use of energy originating from sunlight.

However, algae are not exoelectrogens and the conventional mediators do not perform well in the extraction of the redox potential for algae based MFCs because the redox species are produced through the metabolic mechanisms that take place in membrane-surrounded cell

organelles in algae such as mitochondria and chloroplasts [23]. Since MET current production has recently been achieved on eukaryotic microorganisms such as *S. cerevisiae*, *C. reinhardtii* would be a promising candidate biocatalyst for the MET mode based on the advantageous biological features discussed above.

Previous studies tend to use algae in MFCs of the product mode that depend on the production of hydrogen molecules, which is then oxidised at the anode for electron transfer to the MFC circuit. Another mechanism is where algae produce organic matter that is used as a substrate for electrochemically active bacteria, which then supply electrons for MFCs from oxidization of the organic matter [97].

In one landmark study of MFCs using algae, C. *reinhardtii* was used in a product mode MFC to produce hydrogen for oxidation at the anode. A maximum hydrogen production rate of 7.6 ml/l culture h^{-1} [210] was achieved, at a current yield of 9 mA at a constant electrode potential of 0.2 V. Using the culture's volume and electrode dimensions this corresponds to power densities of 0.4 W m^{-2} and 3.3 W m^{-3}. In another study [209], *Chlorella vulgaris* microalgae were used as a biomass source to feed a mixed microbial culture, producing a maximum power density of 0.98 W m^{-2} (277 W m^{-3}).

Furthermore, algae have been inoculated into a bioelectrode to generate oxygen as the electron acceptor [211]. Under illumination, algae produced oxygen as the electron acceptor for the MFC cathodic reactions, changing the bioelectrode into biocathode mode; while in darkness, the algal oxygen production stops and the bioelectrode mainly functioned as the bioanode. The reversible bioelectrode can relieve the pH membrane gradient generated by the acidification at the anode and the alkalisation at the cathode during normal MFC operation [211, 212].

Hydrogen production by C. reinhardtii: Only a specific group of green microalgae and cyanobacteria, e.g., microalga *C. reinhardtii*, have evolved the additional ability to harness the huge solar energy resource to drive molecular H_2 production [213-219]. The release of hydrogen by *C. reinhardtii* under light exposure was first reported in 1942 [216]. In 2000, sustained hydrogen production was achieved using induced sulfur depletion in a culture

medium containing acetate, a carbon source that is used to cause the shift from aerobic to anaerobic state [218].

C. reinhardtii is one of the best eukaryotes for H_2 production [220]. The available experimental information, including genomics, indicates that *C. reinhardtii* possesses a complex metabolic network containing aerobic respiration and molecular flexibility associated with fermentative metabolism. The molecular flexibility is accomplished with adjustments in the rates of accumulation of organic acids, ethanol, CO_2 and H_2 [197, 221-226] and underlies the cell's adaptive ability for hypoxic and anoxic conditions.

Compared to other H_2-producing organisms such as chemotrophic and phototrophic bacteria, *C. reinhardtii* is more practical for H_2 production as it can be easily and efficiently grown in bioreactors using solar light, grows rapidly (doubling-times of the order 6 h or less) and has a flexible metabolism [227]. The genome of this model microorganism was fully sequenced in 2007 [197], which makes it possible to increase production yields of H_2 from water by optimization of cell metabolism.

Limitation of hydrogen production by C. reinhardtii: Hydrogen production by *C. reinhardtii* still cannot meet the commercial requirement because of several biochemical and engineering shortcomings, for example, hydrogen production demands anoxia because oxygen can suppress transcription and function of hydrogenase(s). However, the anoxia is constrained by the function of the photosystem II (PSII), which provides electrons and protons from water and conducts oxygen evolution in the photosynthetic electron transport chain. Economic assessments have suggested that microalgae should achieve an efficiency of 10% in the conversion of solar energy to bioenergy to be competitive with other H_2 production methods, such as biomass gasification or photovoltaic electrolysis [228]. This is a more than a fivefold increase in efficiency from current levels. Exploiting hydrogen production directly in a product-type MFC may help to bridge this gap.

2.4.3 *Synechocystis* sp. PCC 6803

Synechocystis sp. PCC 6803 is a unicellular cyanobacterium, one of the earliest groups of

microbes to evolve on Earth. The first primitive bacteria on Earth are dated at 3.8–3.6 billion years ago [229]. It is thought that cyanobacteria flourished during the period from 3.5 to 1.8 billion years ago, consuming CO_2 and providing Earth with oxygen, making possible the development of the different forms of aerobic life. At present, cyanobacteria deliver amounts of oxygen to the atmosphere similar to those that are produced by higher plants [229]. Moreover, cyanobacteria harness 0.2% to 0.3% of the total solar energy (178,000TW) that reaches the Earth [217] and convert the solar energy into biomass-stored chemical energy at the rate of ~450 TW, contributing to 20-30% of Earth's primary photosynthetic productivity [230].

Until 1982 the cyanobacteria were called blue-green algae because they can photosynthesize and look like chloroplasts. Since then, cyanobacteria were re-classified as prokaryotes [231]. It is suggested that cyanobacteria entered into a symbiosis with cells, which were not capable of absorbing CO_2 and release oxygen, and later became photosynthetic organelles of plants [232]. Nowadays many species of cyanobacteria, e.g., *Synechocystis sp.* PCC 6803, are widely distributed in nature.

Synechocystis sp. PCC 6803 and plants have similar oxygen-evolving apparatus and are thus used for studying photosynthesis in plant cells. The difference is that *Synechocystis sp.* PCC 6803 grow much faster than plants, and they are relatively easy organisms for genetic manipulations [229]. Also, plants are fixed at places where they grow and they have less adaptation abilities for their growth and propagation than cyanobacteria.

Synechocystis sp. PCC 6803 grow photoautotrophically on carbon dioxide and light, as well as heterotrophically on glucose. Like *C. reinhardtii* , *Synechocystis sp.* PCC 6803 is one of several hydrogen yielding species of cyanobacteria [233]. After its genome was fully sequenced in the 1990s [234, 235], this cyanobacteria species has become a popular model photosynthetic organism studied by many researchers.

Advantages of cyanobacteria: Cyanobacteria, besides other photosynthetic microorganisms such as microalgae, can establish synergistic relationships with heterotrophic bacteria, for instance in a microbial mat [96]. Thus, they could be potentially manipulated to establish an indirect synergistic relationship with electricigens in phototrophic MFCs [97]. However,

phototrophic MFCs usually have a low conversion efficiency [90] and the study of phototrophic MFCs is in its nascent stages [90].

Since *Synechocystis sp.* PCC 6803 is a photoautotroph that divides rapidly, it has been enlisted as a platform for production of biofuels by using sunlight as an inexpensive energy source [236, 237]. This feature makes this species suitable as a candidate for MFCs of product mode.

Electrogenic activity of cyanobacteria, Unlike other exoelectrogens, such as *G. sulfurreductens*, in which the electrons are derived from biochemical oxidation of organic compounds via the respiratory electron transfer chain [238], cyanobacterial electrogenic activity does not need exogenous organic fuel and is entirely dependent on the energy of light, which drives the biophotolysis of water through the photosynthetic electron transfer chain in the cyanobacteria, releasing electrons [239, 240]. The electrogenic activity of cyanobacteria may represent a form of overflow metabolism to protect cells under high-intensity light [98, 240]. This light-driven electrogenic activity is conserved in diverse genera of cyanobacteria and is an important microbiological channel of solar energy into the biosphere [240].

The electrogenic activity of *Synechocystis* sp. PCC6803 has been captured in an MFC for electricity generation. The MFC can achieve a steady power density of 6.7 mW m^{-3} (peaking at 7.5 mW m^{-3}) [241, 242]. These power densities are still much lower than the values achieved by the other microbes under discussion. Despite that, it is included in the selection list because it offers the unique combination of photosynthetic activity that is plausibly accessible to direct mode electron transfer. The quoted measurements are quite recent, and it is worth exploring if this organism has the potential to deliver competitive power densities in the future.

Hydrogen production by cyanobacteria: Cyanobacteria have a similar process for hydrogen production as algae, except that they use NiFe-hydrogenases rather than Fe-hydrogenases in microalgae and the hydrogenase of cyanobacteria is 100 times less active than those of the green algae *C. reinhardtii* [217]. These hydrogenases contain [Ni-Fe] catalytic centres that are extremely sensitive to inactivation by O_2, one of the major barriers to hydrogen production. Natural mechanisms such as consumption by respiration, chemical reduction via PSI, and

reversible inactivation of PSII O_2 evolution can reduce intracellular O_2 content and thereby increase H_2 production.

2.4.4 Saccharomyces cerevisiae

The *Saccharomyces* genus currently contains eight species [243]. *Saccharomyces cerevisiae*, *Saccharomyces bayanus* and *Saccharomyces pastorianus* are associated with anthropic environments, whereas *Saccharomyces paradoxus*, *Saccharomyces kudriavzevii*, *Saccharomyces cariocanus*, *Saccharomyces mikatae* and the recently described *Saccharomyces arboricolus* are mostly isolated from natural environments [244, 245]. These *Saccharomyces* species can play a major role in food or beverage fermentation. However, the ale yeasts involved in alcoholic fermentation mostly belong to the species *S. cerevisiae* [243]. Besides its important role in baking and brewing, this yeast species has been used as a eukaryotic model organism in molecular and cell biology; for example, the characteristic of many proteins can be discovered by studying their homologs in *S. cerevisiae*.

S. cerevisiae cells are round to ovoid, 5–10 micrometres in diameter, reproduce by a budding process and can grow aerobically on glucose, maltose, and trehalose but not on lactose or cellobiose. In the presence of oxygen, it is even able to operate in a mixed fermentation/respiration mode. The ratio of fermentation to respiration varies slightly among strains but is approximately 80:20 [246].

Furthermore, *S. cerevisiae* can be processed to produce potential advanced biofuels such as long chain alcohols and isoprenoid- and fatty acid-based biofuels, which have physical properties that more closely resemble petroleum-derived fuels [247].

Advantages of yeast for MFC: Yeast is sometimes thought to be impractical as a biocatalyst, due to difficulties with transferring electrons out of cellular organelles [54]. However, since yeasts are robust, easily handled, mostly non-pathogenic, have high catabolic rates and grow on substrate spectrum, they are well worth considering as promising biocatalysts for MFCs [248]. In addition, several other merits may exist for using *S. cerevisiae* in MFCs. First, *S. cerevisiae* can survive and function in anaerobic conditions that are required for the anode

compartment of a traditional MFC. Second, the optimal growth temperature for *S. cerevisiae* is around 30 ℃, which is a convenient ambient temperature. Third, the metabolism of this species is well understood, which helps locate mechanisms responsible for electricity generation in MFCs. Lastly, yeast based fuel cells could be retrofitted into ethanol plants for *in situ* power generation [249].

Yeast for in situ power generation: In anaerobic conditions, yeasts usually switch to fermentation reactions where one glucose molecule is consumed for the production of two molecules of pyruvates. Pyruvate is further transformed into alcohol or organic acid by recycling NADH to NAD^+, which is a key step to sustain the glycolysis process [250]. This glycolysis reaction takes place in the cytosol of the cell rather than in the mitochondria, so NADH could be easily accessed by the mediator molecule present in the cell membrane of the yeast [186]. The glycolysis and the oxidation of NADH to NAD^+ are not influenced by the energy extraction process in the MFCs. Based on these characteristics, MFCs using yeast can be directly applied in fermenters for *in situ* power generation [249].

Limitation of S. cerevisiaes for MFC use: Limitations exist for *S. cereviseae* to be used in MFCs. First, *S. cereviseae* has a weak ability to oxidise the substrate to supply the maximum number of electrons available for yeast based MFC. In the mitochondrial process of *S. cereviseae*, there is a total of only 14 ATP per glucose molecule produced, which is much less than a net 28–30 ATP typically achieved by most aerobes [248]. Also, mediators are commonly required to facilitate the transfer of electrons to the anode, which makes exogenous mediators necessary to MFCs based on *S. cerevisiaes* because this yeast is thought incapable of producing such mediators indigenously [249].

The output of S. cerevisiae based MFCs: In general, yeast based MFCs perform better than cyanobacteria but still have a lower power output than bacterial fuel cells [248]. It was shown that methylene blue mediated *S. cerevisiae* MFC can give a power density of 1.5 W m^{-2} [251], which is less than the maximum of 6.86 W m^{-2} reported by Fan, *et al* (2008) [246] for a mixed culture MFC. The corresponding volumetric density, based on the specified anodic chamber volume of 10 ml, is 90 W m^{-3}.

A recent MFC that employs *S. cerevisiae* as the electron donor in the anodic half-cell and *Chlorella vulgaris* as the electron acceptor in the cathodic half-cell can reach a maximum power at 90 mV and a load of 5000 Ω, giving a power density of 0.95 mW m^{-2} of electrode surface area [252]. This power density is still very low.

Another study investigated the possibility of *S. cerevisiae* to transfer electrons to an extracellular electron acceptor through DET mode and found that the cells adhered to the anode were able to sustain power generation in a mediator-less MFC. However, the power performance of this MFC was extremely low (0.003 W m^{-2}) [253].

2.4.5 Geobacter sulfurreducens

G. sulfurreducens are rod shaped gram-negative, anaerobic bacteria capable of coupling oxidization of organic compounds to reduction of metals. This organism is one of the predominant metal-reducing bacteria in soil and hence plays an important ecological role in biotechnologically exploitable bioremediation. The activity of *Geobacter* species in the subsurface can be stimulated to remove organic and metal contaminants such as aromatic hydrocarbons and uranium from groundwater [254-256].

The genome sequence of *G. sulfurreducens* is available, and a system for genetic manipulation has been developed for this organism [257]. Since it was discovered in 1994 [258], this bacteria has been extensively studied for MFC applications. It has been reported that (i) *G. sulfurreducens* can completely oxidize electron donors by using only an electrode as the electron acceptor, (ii) it can quantitatively transfer electrons to electrodes in the absence of electron mediators, and (iii) this electron transfer was found different from those observed for electron transport to Fe(III) citrate [259].

Advantages of Geobacter sulfurreducens: *G. sulfurreducens* is the most abundant species on anode surfaces in MFCs grown with more than one bacterial species [25, 30, 260]. It can form biofilms on the anodes, which make all the cells participate in electron transport to the anode and thus increase the current production [261]. *G. sulfurreducens* is an anaerobe, but can withstand low levels of oxygen and may use oxygen as an electron acceptor to support growth under aerobic conditions [262].

This *Geobacter* species can produce large amounts of electrical energy since it possesses multiple mechanisms that involve either pili or c-type cytochromes to facilitate the electron transfer to electrode in MFCs (discussed before in Section 2) [25]. Also, with the electron transfer to electrodes, the *Geobacter* species can effectively oxidize acetate [75, 263]. A current density of 4.56 A m^{-2}, corresponding to power densities of 1.88 W m^{-2} and 43 W m^{-3} , measured for *G. sulfurreducens* is among the highest reported for a pure culture [264]. By reducing the anode compartment volume to a fraction of a millilitre, the volumetric density was in fact increased to 2.15 kW m^{-3}. While the lower value is more realistic for comparison to other studies, this does show that very high densities are achievable in principle with this organism. In addition, *G. sulfurreducens* converts acetate to current with coulombic efficiencies of over 90% [260, 264].

Previous studies have shown that when a high selective pressure for high rates of current production at high coulombic efficiencies is imposed on complex microbial communities, it is the organisms closely related to *G. sulfurreducens* that are routinely enriched on anodes of the MFCs [83, 263, 265-267]. Thus, *G. sulfureducens* can also be used to study adaptation for enhanced power production.

Metabolism of Geobacter species: The metabolism of *G. sulfurreducens* was investigated by constraint-based modelling [268]. In contrast to *Escherichia coli*, which primarily produces energy and biosynthetic precursors through sugar fermentation, *Geobacter* completely oxidizes acetate and other electron donors via the tricarboxylic acid (TCA) cycle [269, 270], which makes it necessary to transfer electrons to terminal electron acceptors for regeneration of cytoplasmic and intramembrane electron acceptors and ATP synthesis. In *G. sulfurreducens* this is accomplished by electron transfer to extracellular electron acceptors, i.e., Fe(III) oxides [271].

Since the rate of cytoplasmic proton consumption is lower than that of proton production during the reduction of extracellular electron acceptors such as Fe(III), the energy consumption with extracellular electron acceptors is lower compared to that associated with intracellular acceptors [268]. The use of extracellular electron shuttles make the *Geobacter* species circumvent the metabolic cost of producing the electron shuttles and consequently

more energetically competitive than shuttle-producing Fe(III) reducers in subsurface environments [268].

In silico analysis suggested that the metabolic network of *G. sulfurreducens* contains pyruvate-ferredoxin oxidoreductase, which catalyzes synthesis of pyruvate from acetate and carbon dioxide in a single step, indicating the synthesis of amino acids in *G. sulfurreducens* more efficient than in *E. coli* [268].

Limits and applications: MFCs powered by *G. sulfurreducens* are far away from being commercialized as a practical biofuel source [261], because up until now the current levels of these MFCs are around 14 mA which could be used to power very simple components [25] but still not big enough to drive complex mechanisms. However, the actual current densities that could be generated from MFCs based on *G. sulfurreducens* are still unclear and require further investigation [260].

Comparison of Geobacter sp. and Shewenella sp.: *Geobacteraceae* and *Shewanellaceae* are classic models in MFC research as their metabolism and versatility have been studied extensively [185, 272]. As mentioned before in Section 2, they are both capable of being used for DET mode in MFCs, because both *Shewanella sp.* and *Geobacter sp.* possess nanowires, electrically conductive bacterial appendages, to transport electron from cells to solid electron acceptors such as graphite anodes in MFCs [26, 62, 271]. Despite those similarities, differences also exist when compared, regarding the engineering design and performance of the MFCs.

Geobacter-based MFCs generate high coulombic efficiencies [273], but require strict anaerobic conditions which limits their applicability. In contrast, *Shewanella*-based MFCs can be operated with air-exposed cultures [51]. Unlike *Geobacter* sp. that requires direct contact to the electrode surface [185], *Shewanella* sp. can use additional mediators to facilitate electron transfer outside the cell membrane [51]. Importantly, besides utilizing nanowires to mediate the electron transport [274], they can synthesize their own redox mediators (i.e, flavins) for extracellular electron transfer under diverse environmental conditions [272, 275]. These two electron mediated mechanisms determine the efficiency of the current generation in *Shewanella* based MFCs [276].

A maximum power density of 24 mW m^{-2} (in the presence of an additional mediator) was reported for *Shewanella* [277]. This value appears low in comparison to bacterial cells, but that is because it was referred to the true microscopic area of a porous electrode. When expressed, as customary, in terms of macroscopic MFC dimensions, the equivalent power densities are 3 W m^{-2} and 500 W m^{-3}. These values compare favourably with *Geobacter*. When dissolved oxygen was deliberately fed into the anode chamber, a *Shewanella* based MFC was still able to produce a power output of 6.5 mW m^{-2} and 13 mA m^{-2}. The MFC used lactate as the fuel source and relied on self-excreted mediators of *Shewanella* [46].

In fact, the previously described *Shewanella*-based system would not be directly applicable to powering electronics and is required to use aerobic water [278]. For instance, a complex pumping system is necessary to continuously recirculate the anolyte between the anode and the large anolyte reservoir, but this pumping system at the anode could consume more power than the *Shewanella*-based MFC produces. Since *Shewnella sp.* cannot use oxygen as the electron acceptor, ferricyanide needs to be added as catholyte. However, ferricyanide is a non-renewable and toxic electron acceptor and can thus not be deployed in the field in the long term. Moreover, the coulombic efficiencies were found to be low (<6%), when calculated based on the incomplete oxidation of lactate to acetate [278].

Conversely, *G. sulfurreducens* can effectively oxidize acetate with electron transfer to electrodes [75, 263] and convert acetate to current with coulombic efficiencies of more than 90% [260, 264]. *G. sulfurreducens* is an anaerobe that can withstand low levels of oxygen and may use oxygen as an electron acceptor [262]. It has recently been shown that with a new configuration, MFCs based on *G. sulfurreducens* can become 100% aerobic, allowing for floating and/or untethered applications. At the same time the performance of the MFCs is similar to their anaerobic/aerobic counterparts [278]. It is expected that with this aerobic configuration, power could be produced in a *G. sulfurreducens* MFC suspended in aerobic seawater [278].

CHAPTER 3 Methods

This chapter discusses a number of global methodologies chosen and developed for modelling the current production states of the four microorganisms. The objective formulations and parameters set-up for the respective microorganisms are presented in Chapters 4-7 and are not covered here. An extract of the work in this chapter has been published in [279] and [280]. In addition, the MFC optimization toolbox (MFCoT) for study of the metabolism of MFC biocatalysts has been developed based on the method framework presented here and published in [281]. Description of the functionality of MFCoT can be seen in Appendix 4 (p. 251).

3.1 Framework for modelling metabolisms under redox perturbation

This framework starts with the selection of the reconstructed metabolic networks that integrate biochemistry, genomics and physiology knowledge about the selected microorganism. Then, the four microorganisms are respectively modelled for identification of their electricity generation potential and the metabolic pathways (key reactions) underlying the high current production. After accomplishment of modelling all the cases of the four microbes, a general framework for modelling MFC biocatalysts is established. The implementation of the framework follows the five steps:

Step one

Verification of the models by FBA simulation of the published network models.

This step can give greater understanding of the network with regard to parameter set-up and to what degree the network has been experimentally verified. For example, most networks are verified for their capabilities for predicting growth rate and gene expressions upon a particular simulation. Also, if extrinsic reactions are added into the network, the impact of the added

reaction on the prediction capability of the network needs to be considered, for example, the potentially affected pathways.

Step two

Preparation of parameters (we use the optimal growth condition).

An SBML file is produced containing the metabolic model with proper parameters defined. The environmental conditions are modelled by acting on the exchange rates of external metabolites (e.g., substrate, CO_2, H_2O and etc.) with the extracellular space (i.e., environment). In real cases, most of the parameters on the uptake or excretion of these external metabolites are discussed and referenced in the publications of the models. Imposing proper bounds on the exchange reactions can ensure that the cell is modelled in a way that reflects the experimental observations.

Some published networks are stored in Excel format and cannot directly be used by modelling software. Therefore, models in Excel format need to be converted into BioOpt format (http://129.16.106.142/tools.php?c=bioopt), which are then parsed into SBML using the converter integrated in the NetSplitter [282].

Step three

Incorporation of the hypothesis into the model (we use multiple-objective optimization to model the stressed metabolic state under electricity generation, the formulation of multiple-objective function is described in a later section)

Step four

Conduct computation using the developed methods with COBRA or OptFlux

1. FBA is used to elucidate the theoretical maximum current output and impact of electron extraction on the metabolism

2. FATMIN is employed to identify the metabolic strategies underlying the identified high current output (FATMIN is an extension to ordinary FVA and can further reduce the solution space by eliminating futile solutions, and is described in detail below).

3. Robust analysis is conducted to examine the effect of varying substrate uptake on the desired electron transfer rate for current generation. In other words, at the identified metabolic states optimized for electricity generation, the current output is mathematically formulated as a function of carbon and/or energy consumption rates.

Step five

Comparison of the metabolic characteristics among four representative microorganisms.

Calculations of power output and coulombic efficiency.

Using biochemical knowledge to interpret flux values and identify dominating pathways.

3.2 The steady-state

In a microbial culture, individual cells can have various metabolic states underlying different physiological status such as healthy or diseased. Among all metabolic states, only steady state in optimal growth condition can be used to assess the maximum capability of the metabolism of a particular species. The steady state assumes metabolic concentrations and reaction rates to be constant on longer time scales. In other words, when the network is at steady state, for every intermediate metabolite the net production and synthesis rates are balanced.

A steady-state condition requires 1) Definition of the boundary of the metabolic network (Figure 3-1); 2) Stoichiometric balancing rule is applied to the metabolites inside the boundary of the network, typically called internal metabolites [283]; 3) Balancing does not apply to metabolites outside the boundaries of the system (external metabolites), which are typically input/output metabolites and (sometimes) cofactors. These rules make sure that only the production and consumption of the internal metabolite are captured with the reactions in

the network for modelling study [284]. The steady-state condition and its underlying boundary definition can provide fundamental insights into biological metabolism.

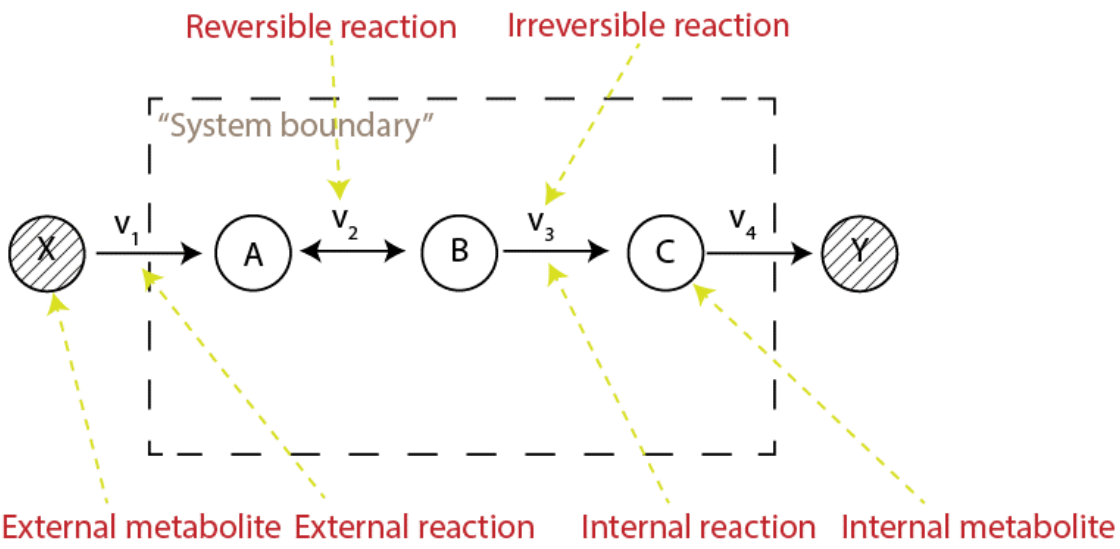

Figure 3-1: The steady state of a toy metabolic network.

In a metabolic network (equivalently called "metabolic graph") where compounds and reactions are nodes linked by edges representing substrate/product relationships. The simple metabolic network consisting of four reactions, two external metabolites (X and Y) that act as source or sink, and three internal metabolites (A, B and C).

3.3 Linear formulation of FBA

The metabolic flux distribution of the GEM models are calculated using FBA. FBA aims to predict a feasible flux distribution through a metabolic network under a given environmental and genetic condition, by maximizing or minimizing a given objective (e.g., biomass production) while satisfying a stoichiometric mass-balance constraint, and enzymatic directionality and capacity constraints embedded in the network.

In FBA, all reactions in which a metabolite participates are considered, which can be represented by a mass balance equation:

$$\frac{dx_i}{dt} = \sum_j s_{ij} v_j \quad (1)$$

Where S_{ij} is the stoichiometric coefficient of metabolite x_i for flux v_j. The equation neglects the metabolite dilution because this effect on concentration is negligible compared to the fluxes for each reaction in which the metabolite participates [285].

For FBA, the metabolic reactions of the metabolic model are converted into a stoichiometric matrix as aforementioned. The system is assumed in steady state, i.e. the concentrations c of internal metabolites are constant [286]. The maximum and minimum ranges of the flux for each reaction are defined. These constraints provided a feasible space of the flux distribution in the metabolic model. FBA defines these constraints as a system of linear equations, which are solved by application of a linear programming (LP) technique to obtain a unique flux distribution in the feasible space with maximization or minimization of an appropriate objective function. This LP problem is represented by the following equation:

$$\begin{aligned} &\text{maximize: } Z = c^T \cdot v \\ &\text{subject to: } S \cdot v = 0 \quad (2) \\ &v_{\min} \le v \le v_{\max} \end{aligned}$$

Where *Z* denotes the biological objective to be optimized (i.e., maximized or minimized as appropriate); *c* is a vector that represents the linear objective function to be maximized or minimized. In general, published network models always include an experimentally formulated biomass reaction as the objective function (*Z*). The flux through this reaction is the growth rate (h^{-1}) predicted by modelling. *S* is the $m \times n$ stoichiometric matrix of all the reactions in the metabolic network, m is the number of metabolites, *n* is the number of fluxes (reaction rates) and *v* denotes a vector of flux of each metabolic reaction. *v* min and v max represent the minimum and maximum flux of each reaction to define the constraint for maximal enzymatic reaction rate, constant uptake from the environment and irreversibility of reaction. Also, thermodynamic constraints on reactions may exist to restrict the directional flow of the reaction along with capacity constraints that provide potential upper limits to the flux levels of the reactions. These constraints are obtained from the literature where the models are retrieved.

For a cellular metabolism, the number of metabolites defines the number of balance equations in (2) while the number of reactions represents the number of unknowns in (2). If the number

of reactions n is larger than the number of metabolites *m*, the system has a mutual degree of freedom $F = n - m$. Hence, if a system has a number of measured fluxes less than F the system becomes underdetermined by nature. In general, every metabolic network of an organism is an underdetermined system.

The network stoichiometry and media composition are represented by upper bounds on exchange reactions. The flux (or reaction rates) are expressed in mmol per gram dry weight and hour [mmol/(gDW/h)]. Under physiological conditions, each reaction will have a limited maximal flux due to thermodynamic constraints. v_{min} is limited to zero for irreversible reactions. The exact *in vivo* limits are usually not known, but it is biologically meaningful to restrict the reaction rates to a high value (e.g., 10000 mmol/gDW/h) that act as additional constraints in the modelling. These high values are also known as explicitly-encoded infinity constraints i.e. bounds on reactions represented by a large number.

$$0 \le v \le 10000$$
$$-10000 \le v \le 10000$$

To further constrain the underdetermined system based on that in which no unique flux can be calculated, it may be possible to calculate the unknown rates after a range of reaction rates (normally the exchange reactions representing substrate uptake and/or by-product output) are set to fixed values or a proper range measured by experiments.

The static nature of FBA makes the model structure identification for this modelling framework significantly different from others based on dynamical modelling systems of ordinary differential equations (ODE). Additional introductory expositions of formulation of FBA can be found in recent three papers [140, 168, 287].

3.4 Robustness analysis: varying one (or two) parameter(s)

The sensitivity of the optimal properties of a network can be assessed by changing parameters over a given range of values and repeatedly computing the optimal state [286]. Here, we examine the uptake rate parameters of the substrate, organic matter or sunlight. These

parameters were varied in a stepwise fashion and the LP problem solved for every incremental value.

$$\text{maximize } Z = c^T \cdot v$$
$$\text{subject to } v_j = c_k$$
$$Sv = 0$$
$$\text{and } v_{i,\min} \le v_i \le v_{i,\max} \quad i = 1,...,n, \quad i \ne j$$

Where Z, c and v denote the same concepts as defined in the linear formulation of FBA (see p. 60). c_k is varied in *l* increments between two values, a and b, and $c_{k+1} = c_k + \frac{b-a}{l-1}$. Solving the LP problem for *l* times generates a series of *l* values for Z ($Z_k, k \in [1,l]$).

In similar fashion, two parameters can be varied simultaneously.

3.5 Linear formulation of flux variability analysis (FVA)

FVA test for the range (min, max) of certain fluxes that fit the optimal solution. FVA can be formulated as:

$$\text{minimize or maximize } v_i \text{ for all } i \in \{1,...,n\}:$$
$$\text{subject to } Sv = 0$$
$$Z = c^T \cdot v = Z_{\text{optimal}}$$
$$v_{i,\min} \le v_i \le v_{i,\max}$$

Where *Z* is a known optimal value for a biological objective; *S* is a $m \times n$ stoichiometric matrix which consists of *m* rows (i.e., metabolites) and *n* columns (i.e., reactions with the respective stoichiometric coefficients for the participating metabolites); *v* is the flux of each reaction in the model that is mathematically formulated as a system of linear (metabolite balancing) equations. FVA shares the same central assumption with FBA, i.e., the system is in steady state which means the concentrations of internal metabolites are constant. FVA results

address the variability of *v* and thus can capture the effect of perturbations to the metabolic reactions in terms of the changes in flux output range.

Specifically, FVA calculates each unknown reaction v for the minimal possible flux and for the maximal possible flux that a reaction can carry in any flux distribution that is consistent with the constraints. In other words, the information obtained from FVA is the physiologically feasible flux range for the unknown reactions. Moreover, if the computed minimal and maximal rate of a reaction coincide, $r_{i,min} = r_{i,max}$, the reaction rate that follows will be uniquely determined.

In contrast to FBA, FVA, as described above, does not make any assumption about biological objectives [140]. The objective function $Z_{optimal}$ is only used as a tool to define a desired metabolic state (such as a redox perturbed state) for FVA to compute the feasible flux ranges. The relationship between FBA and FVA is illustrated in Figure 3-2 below.

The figure visualizes a 3-dimensional flux space, and shows that the FBA solution space is a projection on the plane represented by a fixed (maximal) objective value. In the illustrated case it is a polygon, and the vertices are extreme points that satisfy the FBA constraints represented by the finite convex cone. Any point inside the polygon, is a flux combination that is both feasible and gives the same objective value, and can be mathematically constructed by a suitable combination of the edge vectors of the polygon. Hence knowledge of all vertices would be enough to fully specify the FBA optimal solution space. Note that an FBA calculation only gives a single vertex; and since all vertices have the same objective value, it is essentially random which one. Minor changes to constraints, a different linear optimizer or even the ordering of variables, can produce a different vertex. Hence it is virtually impossible to get full specification of the optimality space from FBA especially for large networks.

In an FVA calculation, one flux at a time is allowed to vary while all others are kept fixed. For example, Figure 3-2B shows the case where the feasible range of flux v_1 is explored while v_2 and v_3 are kept fixed. This corresponds to the determination of two flat parallel planes, perpendicular to the v_1 axis, that touch the polygon at opposite vertices. Repeating this for all fluxes, the result is a cubical bounding box containing the optimality polygon. So FVA yields

only an approximation to the optimality space, as the intersection of the optimality plane and the bounding box; the actual polygon is contained within this, but it could also contain points that are outside the polygon and hence infeasible. Nevertheless, this approximate description is a major improvement on simple FBA and may suffice for practical use.

The situation illustrated by Figure 3-2, where the optimality space is a finite polygon, is simpler than most real network models where the convex cone and hence the optimality subspace is unbounded in some directions. This is more fully discussed in section 3.7 below but a similar comparison between FBA and FVA solutions can be developed in that case.

(A)

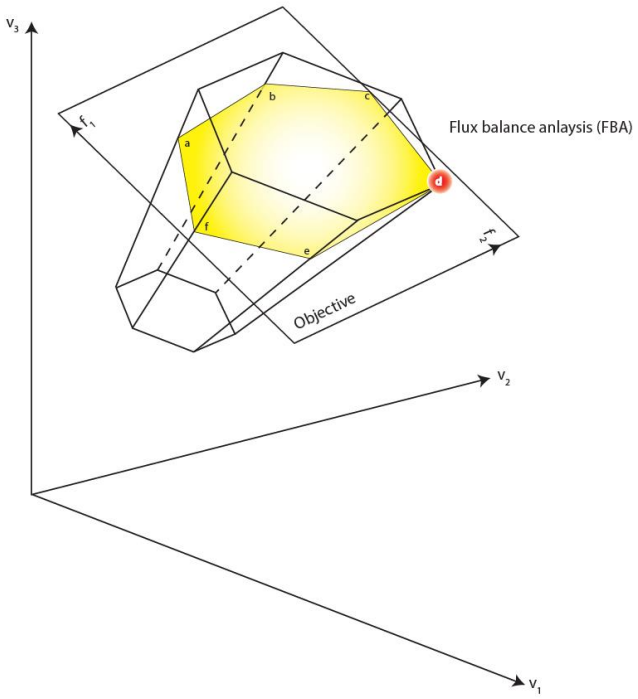

(B)

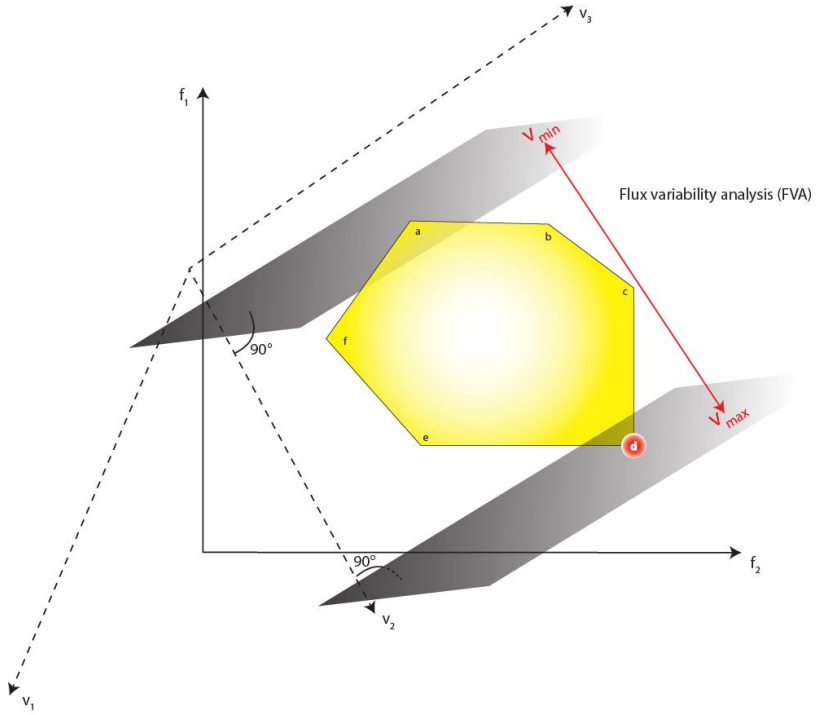

Figure 3-2: The optimization principles underlying FBA (A) and FVA (B).

A schematic 3D depiction of the feasible space resulting from FBA and the yellow polygon represents the optimal solution space that contains points computed by maximizing the objective function (the objective plane). The coordinates are three arbitrary representative fluxes, which is a simplified version of the multidimensional flux space.

(A) A polyhedral solution space. The solution space results from mass-balance and capacity constraints ($v_{i,min} \leq v_i \leq v_{i,max}$) and contains all feasible flux states. Objective is two-dimensional (a plane). (B) FVA to identify the possible range of each flux such that the objective value does not degenerate.

3.6 Exploration of alternate optimal solutions (AOS) and futile loops

FBA relies on linear programming to find the optimal solution for reaction fluxes, which maximizes or minimizes a given objective function. However, the identified solution may not be unique and an infinite number of different flux vectors may exist producing an identical optimal objective value. In the context of metabolic models, these flux vectors are called alternate optimal solutions (AOS) or equivalent phenotypic states [184, 288-290]. Previous methods for the determination of AOS include: 1) vertex enumeration such as extreme pathway or elementary mode analysis [289, 291, 292], and 2) flux variability analysis (FVA) [293]. However, the computation of extreme pathways and elementary modes are too time-consuming and sometimes impossible, even for a medium-sized network model (up to one hundred reactions), and FVA results may contain large futile values due to the presence of loops in the network.

3.6.1 Futile loops

In constraint-based modelling, the constraints mainly used are mass balance and metabolite uptake rates. The thermodynamic limitations associated with the reactions are difficult to implement and thus commonly overlooked. Without thermodynamic constraints, non-physical fluxes can be computed for some metabolic reactions if they form an internal cycle (Figure 3-3). Such a cycle of reactions violate a "loop law" that is analogous to Kirchhoff's second law for electrical circuits, as discussed previously by Beard *et al.* [294]. These futile cycles are not formed for any biologically meaningful purposes.

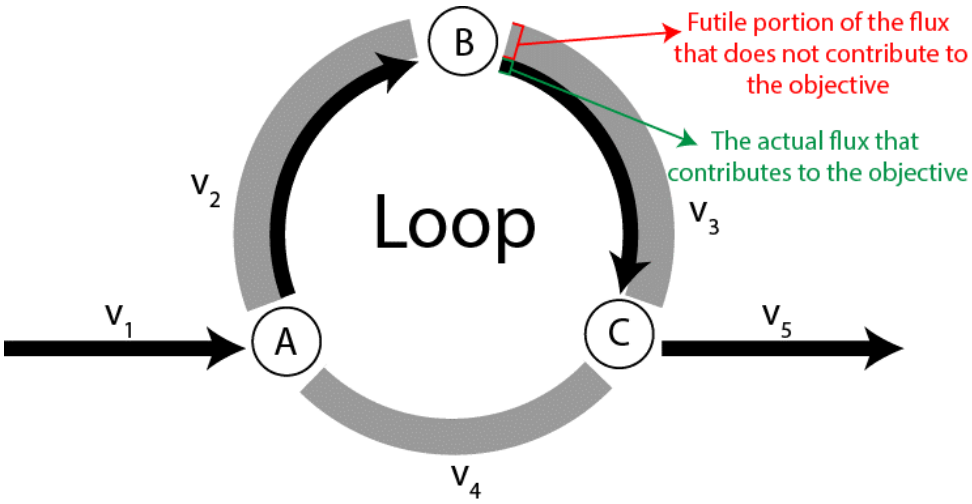

Figure 3-3: An example set of reactions that form a loop cycling three metabolites internally.

The capital letters represent hypothetical metabolites. FBA and FVA can particularly not resolve reversible, circular and parallel reactions.

Importantly, it should be noted that futile cycles that consume biochemical energy are not necessarily "futile" [295]. Since this particular type of futile cycles consumes energy, their associated flux values are limited by the available energy and consequently do not display the behaviours of reaching an "explicitly encoded infinite". This futile reactions of this type should not be eliminated from the GEMs; the removal of them would pose a risk to over-constrain the problem beyond the elimination of the loops themselves.

Although the exact metabolic function of futile cycles has not been fully elucidated, their activities have been suggested as mechanisms of biochemical regulation [295-297]. The amount of energy expended by (or the change of the flux through) a futile cycle determines the magnitude of changes in the effective equilibrium constants for biochemical reactions and the sensitivity and robustness of intermediate concentrations [295]. Also, the cellular ATP/ADP ratio could be dependent on the specific growth rate and environmental conditions [298]. Furthermore, futile cycle activity in *Geobacter metallireducens* might be associated with the regulation of the substrate utilization for gluconeogenesis and the oxidative TCA cycle [299].

In practical FBA calculations, the presence of a futile loop is often signalled by implausibly high flux values for some reactions. It is common practice to set an artificial upper limit e.g.

10000 on all fluxes, simply to avoid numerical problems in the optimization algorithm. Fluxes of loop reactions are often observed to reach values of this magnitude, but simple strategies, such blocking these reactions by constraining their fluxes to zero, only work in the simplest cases (as exemplified in the case of the simple method in Section 3.6.2 below).

One reason for this is that individual loop reactions may simultaneously participate in non-futile fluxes carried by productive pathways. In this case flux values along the loop may all be high, but with different values, because the observed fluxes result from superimposing productive and futile fluxes. This has to be disentangled without affecting productive fluxes. This problem is particularly common when loops involve a currency metabolite such as NADH.

Another reason is that as loop fluxes do not contribute to the objective value, it is conceivable that some such fluxes may have another value, even zero, in the particular flux distribution that is selected from the solution space by the optimization algorithm.

Elaborate strategies that have been proposed to remove these thermodynamically infeasible futile cycles, include known flux directionality [300], energy-balance equations [294], known [301-306] or predicted [307] thermodynamic parameters, and nonlinear constraints to eliminate flux distributions that utilize reactions which cannot be thermodynamically feasible under physiological conditions [308]. But these thermodynamic constraints are difficult to obtain and nonlinear constraints can make application to large-scale systems computationally challenging [302]. Therefore, the listed methods above cannot be applied on genome scale systems [302].

In addition, another algorithm, called loopless-COBRA, was recently proposed to eliminate loops [309]. This method imposes the second law of thermodynamics by using a mixed-integer linear programming (MILP) approach to constrain flux solutions so that they obey the loop law and does not require additional data such as metabolite concentrations or thermodynamic parameters. This method was mathematically proved not to over-constrain the problem beyond the elimination of the loops themselves [310]. However, such method was unable to be conducted with the commonly used solver GLPK and necessitates a commercial solver (TOMLAB/CPLEX package (Tomlab Research, Pullman, WA)).Besides, the algorithm

is computationally intensive and its running time is significantly increased with the network size.

Another previous study indirectly constrains the futile loops by coupling reaction flux to enzyme synthesis costs, but this approach necessitates comprehensive knowledge of the transcriptional and translational machinery [290].

Alternatively, loops can be removed by minimizing network total flux [167, 301, 311, 312]. The application of flux minimization can produce a most likely stationary flux distribution. The notion behind this method is that the flux through any reaction of a metabolic network requires some 'effort' and a metabolic network is inclined to fulfil the same biological objective, such as growth, with minimum metabolic effort [301]. A drawback of this approach is that the use of the minimum sum of all fluxes in the network as an auxiliary criterion in FBA by previous methods, can forestall variability within optimal flux distribution.

Below, we present a simple method that resolves some accidently activated futile values in the FBA results. The simple method can remove the futile cycle without impacting simulations of the cellular phenotype such as biomass growth. On the other hand, for concurrently determining AOS and efficiently eliminating the flux loop, we also devised another method termed **F**lux variability **A**nalysis with **T**arget flux **Mi**nimization (FATMIN) that combines the functions of FVA and FBA to determine AOS and efficiently eliminate flux loops in large metabolic networks. Importantly, FATMIN requires the least amount of information to quantify the fluxes and analyse the metabolic system.

3.6.2 A simple method to remove futile reactions encountered in FBA modelling

An example of a network fragment that contains a superposition of productive fluxes and a futile loop, is shown in Figure 3-4.

A simple method to remove those loops without affecting productive fluxes, is to constrain the flux with the smallest absolute value to zero in order to break the loop. This still allows other fluxes in the loop to attain the values they contribute to productive (non-loop) pathways.

In the toy network of Figure 3-4, fluxes towards I, J and K are considered to be constrained while the yield of product H is to be maximized. In the optimal solution, all flux contributions necessary to supply the constraints and yield are taken as productive. However, the solution illustrated in Figure 3-4(B) additionally contains a circulating flux. Because it is the sum of circulating and productive fluxes for a reaction that is limited by the explicitly encoded infinite capacity constraints as shown in Figure 3-4(A), it seems plausible to expect the smallest absolute flux value to be in the link along the loop that carries only the circular flux component. Constraining this flux (v_{11}) to zero, indeed produces a feasible steady state flux distribution (v_1,v_2,…v_{11}) = (40,40,40,10,30,10,20,10,10,10,0) without loops as shown in Figure 3-4(C).

However, this is not the only compatible distribution; for example the flux vectors (40,30,30,10,20,10,10,10,0,10,-10) and (40,0,0,10,-10,10,-20,10,-30,10,-40) satisfy the same conditions as would suitably normalized combinations of these vectors. These alternative distributions only occur because by assumption, all loop reactions in the toy network are reversible. In real networks, that is often not the case and so the simple method is adequate to eliminate futile loops. Even if this does not apply, depending on the purpose of the modelling it may only be required to produce one distribution free of futile loops, regardless of whether others also exist.

The simple method also has the drawback that it may overlook some hidden futile cycles, as sometimes those futile cycle reactions could have flux rates in a particular FBA solution within a reasonable range (e.g., the absolute flux value is less than 100 mmol/gDW/h) and appears to be ‘normal’. For these reasons, we have developed a more elaborate method to deal with futile loops as described in the next section 3.6.3.

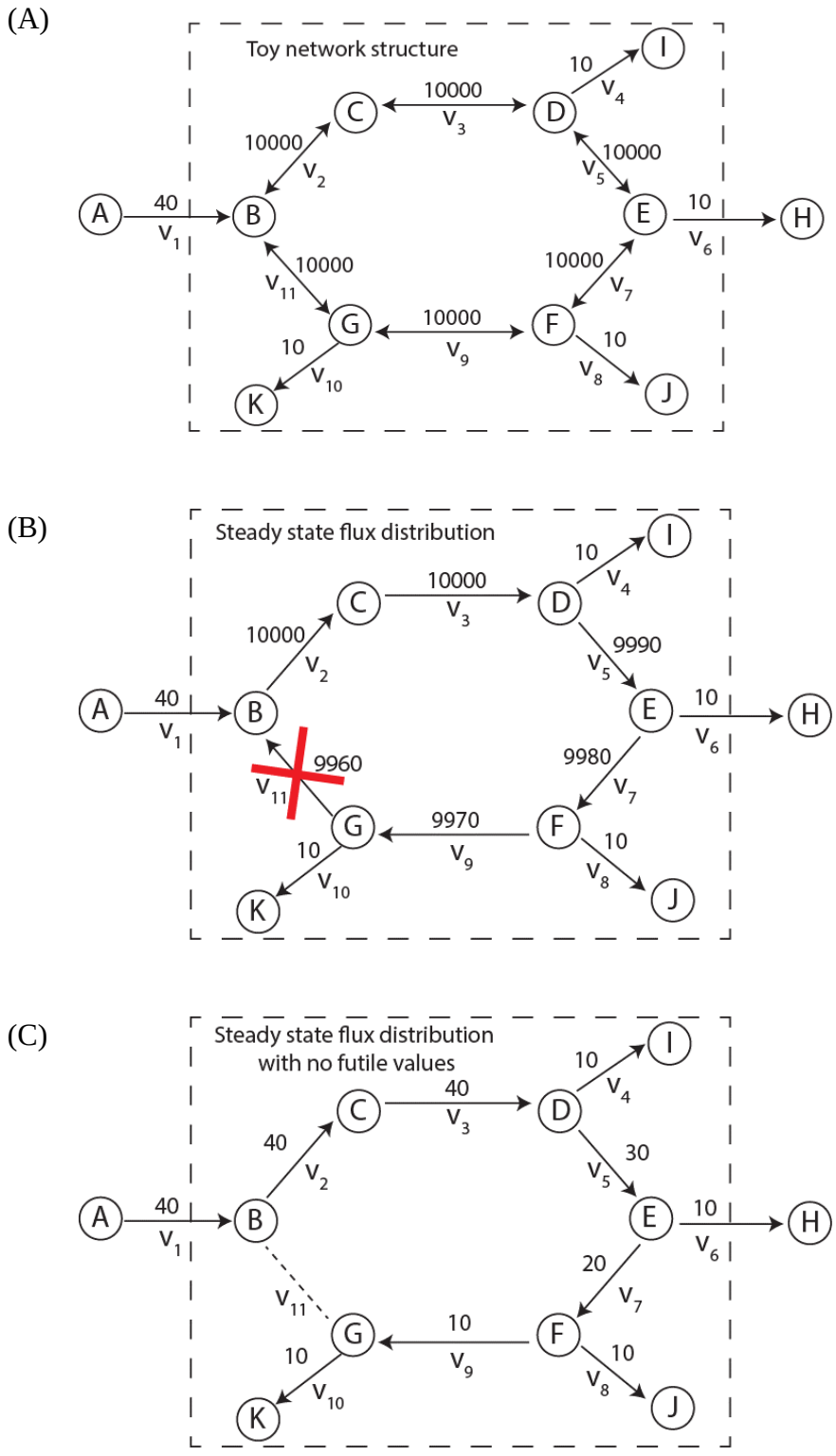

Figure 3-4: A toy network with loop for illustrating the method to remove futile flux values.

(A) The structure of the network and the reaction bounds are represented graphically. Reactions v_2, v_3, v_5, v_7, v_9 and v_{11} form a loop. Reactions v_4, v_8, v_{10} are constraints. v_1 is the exchange reaction providing source for the network. v_6 is the reaction that should be maximized. (B) FBA returns a solution that contains a loop and an objective value of 10. To eliminate the less meaningful flux values in this case, v_{11} is constrained to zero as it has the lowest absolute flux value. (C) By eliminating reaction v_{11}, biologically meaningful flux values for v_2, v_3, v_5, v_7 and v_9 are obtained without degenerating the objective of 10.

3.6.3 The FATMIN algorithm

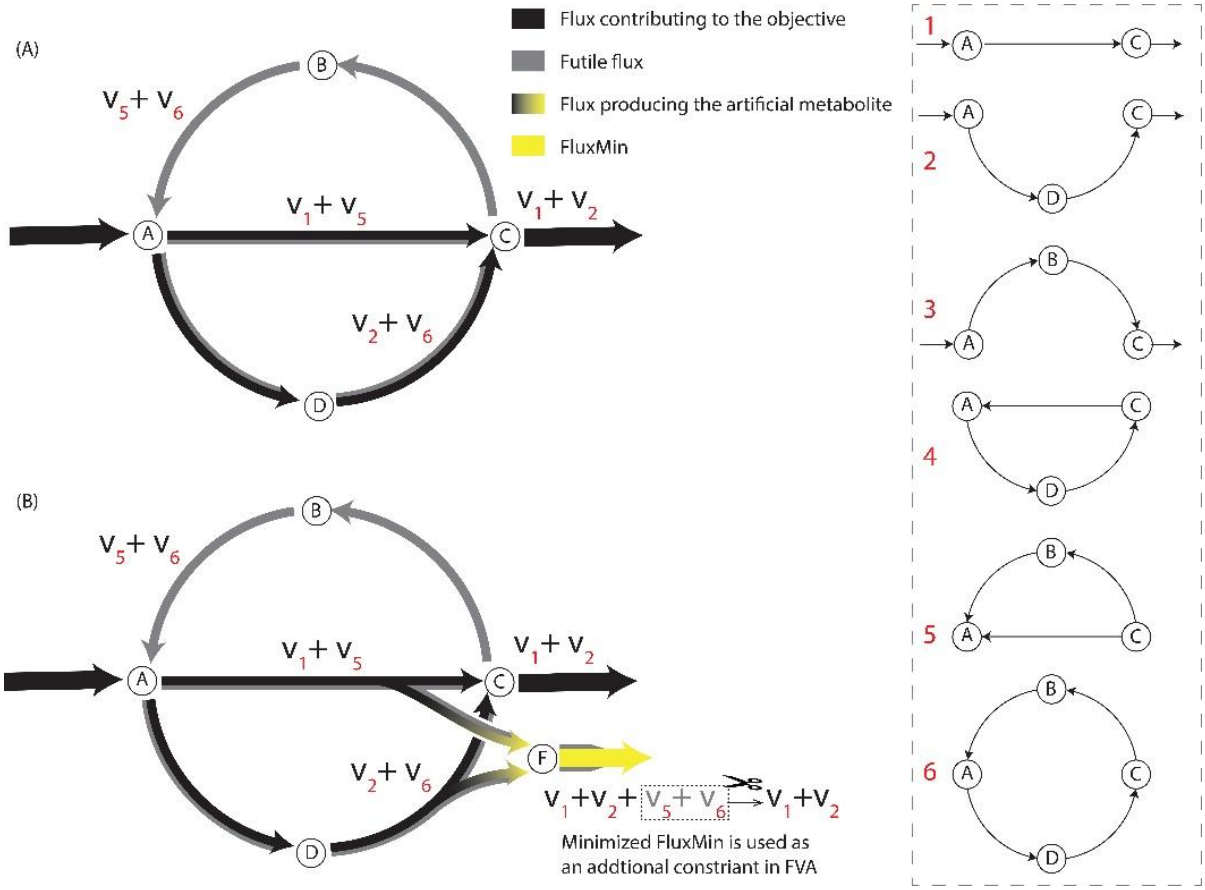

Figure 3-5: The schematic diagram of elimination of the futile cycle in an imaginary network by the FATMIN.

(A) Flux distribution at steady state without employment of the FATMIN; (B) The minimization in the FATMIN to identify another constraint that can remove the futile values associated with cycles 5 and 6. The inset shows alternate path through the network, with numbers used as flux indices in the main figure. Path 3 and 4 carry no flux with reaction directions as shown, but are examples of paths that become active if reactions are made reversible.

The basis of FATMIN is FVA, which is used to probe the feasible flux ranges of desired reactions, such as NADH involved reactions in the present study. Importantly, the method can constrain the pointlessly high flux values of the loop reactions to a biologically meaningful value. It is intended to deal with such loops involving one or more *target metabolites* that are of specific interest; here this is NADH.

All reactions that produce the target metabolite and carry a flux higher than a threshold value (that is chosen to be higher than any realistic flux value) are identified as *target reactions*. To identify which portion of the high value is compulsory to achieve the value of the FBA

objective function, we add an artificial metabolite to each target reaction, and add another reaction (e.g, reaction ID: FluxMin) that only comprises the artificial metabolite. FluxMin acts as a drain reaction for the artificial metabolite, and its flux is the sum of all production fluxes. Minimizing this flux while maintaining the objective value, in effect eliminates futile fluxes.

The idea is demonstrated in Figure 3-5 (A). Metabolite C is taken as the target metabolite that this simple network produces. The network contains two alternative routes (1 and 2) for producing C and two cycles (5 and 6). All reactions are irreversible, so with paths through the network chosen as indicated, all flux values are non-negative. A new metabolite labelled "F" is added to both reactions that produce C, as well as the associated drain reaction, to give the augmented network in Figure 3-5 (B). Balancing fluxes at all nodes of the augmented network shows that although the net production of C (made up of the contributions v_1 and v_2) is independent of the futile fluxes, the flux of the added reaction FluxMin is $v_1 + v_2 + v_5 + v_6$. Since the value of $v_1 + v_2$ remains fixed for a chosen objective value, and negative values for v_5 and v_6 are not allowed, minimization of FluxMin reduces both of the cyclic fluxes to zero. The resulting minimal value is subsequently used as a constraint on FluxMin in a repeated FVA calculation for the augmented network.

Although the explanation above referred to fluxes along individual pathways – in effect, elementary modes – the strength of the FATMIN method is that these do not in fact have to be identified to apply the method. Simply adding FluxMin to the network and minimizing its flux, ensures that the cyclic components implicitly contained in it are eliminated.

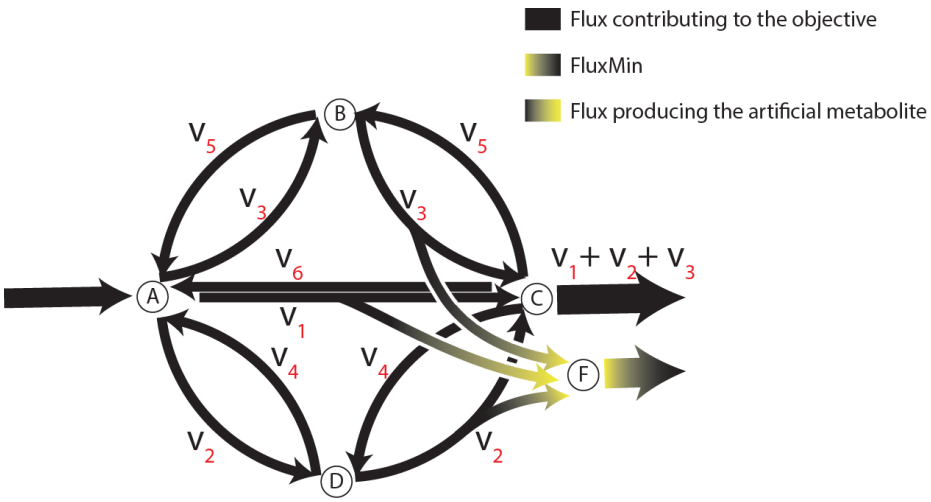

Figure 3-6: Illustration of all possible flux paths in an imaginary network

This result relies on the fact that negative flux values are excluded. Realistic networks containing reversible reactions are usually handled in FBA by allowing positive and negative flux values. To maintain the exclusion of negative fluxes, in the FATMIN minimization step reversible reactions involving the target metabolite are conceptually split into two counter directional reactions, and the artificial metabolite only entered into the branch that produces the target metabolite. This is illustrated in Figure 3-6.

In practice, because the other branch does not contribute to FluxMin, it can be omitted. So the procedure followed is that where the FVA range of a target reaction exceeds the threshold on both negative and positive fluxes, the negative lower limit constraint is replaced by zero for finding the minimal FluxMin flux value. We stress that for the subsequent FluxMin-constrained FVA calculations the lower limit is restored to its original value.

Another point illustrated by the example is that the FATMIN strategy does not restrict the optimal solution space; e.g. all v_1 and v_2 value pairs allowed by the original objective value remain viable in the augmented network. Finally, we remark that the strategy described here is easily extended for multiple target metabolites by simply introducing a unique artificial metabolite and drain reaction for each.

Overall, FATMIN can be summarised as a modelling sequence FBA+ FVA +FBA +FVA, which is implemented as a computational pipeline consisting of the following steps, where we take NADH as the target metabolite:

1. Perform FBA to calculate the optimal objective $Z_{optimum}$. Then set the obtained optimal $Z_{optimum}$ as the constraint and perform flux variability analysis (FVA) to calculate a feasible flux range for each reaction.

2. Extract NADH reactions and calculate the feasible range of NADH flux values associated with each reaction by multiplying reaction rate with the NADH stoichiometry coefficient.

3. Any reaction with an absolute value of the NADH flux boundaries higher than a threshold T (here, we chose T = 100 mmol/gDW/h) is identified as a target reaction. If the target reaction is reversible and the absolute value of the lower limit is higher than T, we decompose the reversible reaction into two reactions in forward and backward direction respectively.

4. Extend the network by adding an artificial metabolite F as a product to each target reaction, and an F drain reaction FluxMin to the network model.

5. Use the FBA optimum ($Z_{optimum}$) as the constraint and minimize the flux of reaction FluxMin.

6. Perform FVA on the augmented network while using the obtained minimal flux value obtained at step 5 as a constraint for the flux of FluxMin.

7. Re-calculate the numerical range of NADH flux values using the method in step 2

This method shares some ideas with [313], in which the solution space is described in terms of three key characteristics: linealities which are the reversible (bi-directional) infinite reactions, rays which are the irreversible infinite reactions, and vertices which are the corner points of the shape formed by interception of the polyhedral cone representing the convex

constraint space with the objective plane. However, there could be millions of vertices, from which one cannot identify biological significance. Therefore, FATMIN intends to remove only the rays and linealities, which matched irreversible and reversible cycles. The rays and linealities are independent of the growth medium [313]. Since FATMIN is based on FVA, the method inherits the function of the FVA in elucidating the phenomena of equivalent optima in the network. Nonetheless, unlike the results of FVA that could contain infeasible, futile values, the result of FATMIN are the feasible flux ranges for the reactions.

The drawback of FVA is that this tool only produces the outline of a rectangular cuboid or 'box' encompassing the polygon of the solutions, but cannot illustrate the real shape of the polygon, which indicates that FVA results cannot reflect the relationships between different reaction fluxes, e.g, how the increase in the fluxes of some reactions influence the fluxes of the other reactions. The solution 'box' is discussed in the case of the MET (The MET mode section of the Results and Discussion of Chapter 4).

3.7 Mathematical explanation for the optimal solution space of FBA

There are two ways to describe the set of optimal solutions of a FBA problem:

In the first description, optimal solutions arising from FBA are defined by a finite number of, i.e., (a) linear inequalities, i.e., the constraints in the LP (1) and (b) equalities, i.e., the constraint that the objective value of the LP is equal to the optimal value. Therefore, the optimal solution space is a polyhedron (or polytope, when bounded, i.e., when none of the fluxes can reach minus or plus infinity). This representation of a polyhedron is called the "outer description" and can be mathematically formulated as follows:

$$P = \left\{ x \in R^n \middle| Ax = 0 \right\}$$

$$A \in R^{m \times n}$$

The other description of a polyhedron is termed an "inner description" or "parametric representation", which involves use of Minkowsky sum to decompose polyhedron into three sets: a linear combination of so called lines (columns of matrix L), and a positive combination of extremal rays, which form a cone (columns of matrix R), and a convex combination of vertices (columns of matrix V). Thus, Minkovski characterization of any optimal flux vector can be formulated as follows:

$$P = \left\{ x \middle| x = L\lambda + R\mu + V\upsilon, \mu, \upsilon \geq 0, \sum \upsilon = 1 \right\} \qquad (2)$$

where λ, μ and υ denote lineality, ray and vertex.

Linealities and rays correspond to reversible and irreversible cycles in the network respectively [313]. In linear algebraic terms, for any flux v in this lineality space and any optimal flux *v*', the flux $v' + \mu v$ is also optimal for every value of μ. And for any flux v in the cone of rays and any optimal flux *v*', the flux *v*' + υ *v* is also optimal for every value of $\upsilon >$ 0. The rays and the linealities do not belong to the optimal solution space themselves and thus they do not contribute to optimization of the metabolic objective. In fact, the rays and linealites only carry the information about the directions in which the solution space is unbounded. Conversely, vertices are feasible and optimal flux vectors and they correspond to corner points of (a suitably chosen projection) of the polyhedron describing the solution space. Therefore, any optimal flux vector can then be written as a linear combination of the linealities plus a positive linear combination of the rays of the cone plus a convex combination of the vertices of the polytope, as shown in formula (2) [313]. This Minkovski description indicates that it is the μv of linealities ($v' + \mu v$) and the υ v of rays (*v*' + υ *v*) which are removed by the minimisation of the flux through the FluxMin reaction in the FATMIN algorithm.

Compared with the elimination of the linealities and rays, identification of all the vertices in a network is much more difficult, because such a task is highly computational challenging. The vertices are reaction paths through the network that give rise to the maximization of an objective and the total number can in general be much larger than the number of reactions in the system. For example, when the FBA of growth of the *E. coli* (model version iJR904) on glucose in a mineral medium indicated that only 59 reactions out of 1066 reactions in the

model are variable, but that these give rise to 17280 vertex solutions [313]. Thus, this suggests the enumeration of vertices in a genome-scale metabolic network would not help elucidation of the metabolic behaviours of the microorganisms from a biological perspective. For characterization of the phenotypes of microorganisms, the algorithm that aims at removing the linealities and rays present in the solution space, such as FATMIN, would be sufficent.

3.8 Assumptions for present modelling

MFCs built in the literature are not only different in their performance, such as power output and robustness (operation time), but also configuration. This indicates that there is no such an MFC configuration as a standard reference for modelling. Since an MFC's performance is fundamentally determined by a microorganism's capability to supply reducing equivalents towards mediators or anode, releasing electrons to the electric circuit, this study centred on elucidating such a capability of the cell by way of modelling thirteen representative electron transfer cases of four microorganisms.

This study assumed an optimal mediator for microbial catalysed anodic electron transfer. Artificial redox mediators possess the great advantage of fairly well known redox and chemical properties. For example, eNR ($E^{\circ\prime}$= −325 mV) can enter the cytoplasm and extract electrons from intracellular NADH [314]. The use of mediators is a useful tool to tune the microbial growth and metabolism in the anode.

The anodic compartment is operated under anaerobic conditions because oxygen is usually a more efficient oxidant than the anode, competing with the desired electrochemical process. However, an aerobic MFC that allows the existence of oxygen in anodic chamber has also been recently developed [46, 278]. Hence, in present modelling, we studied both anaerobic and aerobic metabolisms as appropriate for particular organisms.

To model metabolism under electricity generation, a few assumptions were made: 1) the putative MET mode relies on a putative ideal mediator that can enter the cytoplasm and transfer electrons from NADH/NAD+ cycle (or ferredoxin/quinone in the case of

Synechocystis) to anode. The study did not focus on NADPH/NADP+ cycle, since the interconversion of the two molecules are unconstrained in the metabolic models, due to lack of proper enzymatic and/or themodynamic constraints. Exposition of the difference between the metabolic functions of NADH and NADPH are elaborated before in Section 1.3 of Chapter 1. 2) The *c*-type cytochrome in the electron transfer chain is the electron source for the DET mode; in some microorganisms, such as *Geobacter sulfurreducens*, the DET mode can be facilitated by nanowires and, in that case, we presume that the intracellular electron source is still *c*-type cytochrome. 3) Only pure culture is used for electricity generation. 4) The MFC reactor is a chemostat that can provide optimum conditions to meet all the needs of microbial growth.

Subsequently, in order to ensure that the cells are not limited by substrate uptake rates, the model is allowed to adjust substrate uptake rate within a proper range as necessary for optimal growth. The range constraints on the reaction used in the modelling are specified in each case-study chapter. Moreover, since the carbon and energy sources were limited to a proper range, there was no necessity to use a two-step optimization strategy, i.e., the first to maximize biomass with no constraint and the second to minimize energy usage while fixing the biomass, as described in [268, 315, 316]).

3.9 Objective equation

The extraction of electric current in an MFC creates a new metabolic environment, in which the cell needs to produce excess current carriers in addition to its needs for normal growth. To judge the maximum capabilities to convert low energetic co-substrates (NAD) to their highly energetic counterparts (NADH), the FBA optimization needs to represent a range of priorities for these competing metabolic demands and allows us to evaluate the impact of the enhanced current extraction on cellular metabolism.

Optimization of two competing objectives is a well-studied problem and gives rise to the concept of a Pareto front [317], which is a range of solutions that interpolate between two

extremes. At each extreme, one objective is optimized on its own; in between, the objectives are combined in varying proportions. This is represented in our study by defining the objective as follows in terms of the biomass growth flux F_B and the NADH_mfc flux F_N:

$$o = (1-\lambda)\ F_B + \lambda\ g\ F_N$$

A unit conversion factor g is explicitly provided because in the model, F_N and F_B are measured respectively in mmol/gDW/h and g/gDW/h or (h^{-1}). This ensures that λ is a dimensionless fraction that can be directly interpreted as the relative contribution of the NADH flux to the combined objective.

Use of a dual objective with adjustable relative contributions is a standard computational device, and has also been discussed for metabolic modelling elsewhere [161]. In the present context, λ = 0 represents the metabolic state where no external current is drawn from the MFC, while λ = 1 is the other (in practice non-viable) extreme where all metabolic resources are devoted to support the external current. In this sense, the value of λ can also be interpreted as a measure of the degree of NADH perturbation caused by the mediators of MFCs.

Practical calculations are done by maximizing o for a series of fixed λ values. As commonly found [317], equally spaced λ values do not yield equally spaced points on the Pareto front. Suitable values were therefore chosen by trial and error to resolve the range where biomass and NADH flux values change significantly. These give rise to the points plotted on the curves in Figure 4-3, Figure 5-2, Figure 6-2 & Figure 7-2. As the λ values tend to be closely clustered near the value 1, it is sometimes convenient to characterise the points by an equivalent parameter, the ratio of objective contributions which is also sometimes referred to as a coefficient of importance or coi:

$$coi = \frac{g\,\lambda}{1-\lambda}$$

A biological perspective on the dual objective, is that it is also a way to represent regulatory mechanisms of the cell to increase the electron transfer rate in the MFC environment, while trying to maximize the cellular growth rate. The mediator in MFCs deprives the cell of

electrons, and the cell metabolism reacts to the deprivation by regulating the metabolism to increase NADH production because the cell requires NADH for growth. So we used the growth objective to model the normal cell metabolism and then introduced the λ to model the regulation process of the cell. The varying of λ can also be considered a way to force the cell to reallocate the metabolic resource between the two objectives, one is desired by the cell (growth), the other by the MFC operator (current output).

Objective One (Maximization of growth rate)	←	Regulation (modelled by way of λ)	→	Objective Two (Maximization of election transfer in MET, which mimics the metabolic perturbation caused by MET for electricity generation)

3.10 Fractional benefit analysis

The concept of a dual objective is based on the premise that each term contributing to it, represents a benefit to the system. While the objective function is a useful computational tool, it is not a good measure of the combined benefit that is obtained from an optimized state. This is demonstrated by considering either extreme; even though only one of the objective terms is maximized, the other term also has a value and will contribute (positively or negatively) to the overall benefit.

To construct a better measure of this, we express each of F_B and F_N as a fraction of the maximal values F_B^* and F_N^* they can ever achieve, i.e. the values when each is independently maximized. As the maximum of each of these fractions is 1, a plausible measure of the combined benefit achieved in any particular metabolic state is the value of the quantity we denote as the fractional benefit *B*:

$$B = \frac{1}{2}\left(\frac{F_B}{F_B^*} + \frac{F_N}{F_N^*} \right)$$

This measure was used in Figure 4-4, Figure 5-3, Figure 6-3 & Figure 7-3 to highlight the way that different growth conditions produce different responses in terms of combining cell growth and external current yield.

3.11 Performance unit

It is difficult to compare MFC performances from literature, because different MFC studies use different configurations involving different operating conditions, surface area and type of electrodes and different microorganisms. Besides, different units are used to denote the performance of an MFC. The most common one is current density, which can be represented as the current generated per unit area of the anode surface area (mA/cm^2) or current generated per unit volume of the cell (mA/m^3). Nevertheless, the electrode dimension and the maximum cell densities are difficult to obtain. Therefore, for the sake of comparison in the present study, the current density is calculated into mA/gDW. This allows the values to be applied to any MFC configuration by taking into account the cells that are actually contributing to current generation in that situation, for example based on the thickness of a biofilm.

3.12 Conversion of units of flux and current

Current (in amperes) was integrated over time and converted to electrons recovered by using the following conversions: 1 C = 1 A $\times$ 1 s, 1 C = 6.24×10^{18} electrons, and 1 mol = 6.02×10^{23} electrons (Faraday's constant 96485 C/mol). Therefore, one flux unit (mmol/g/h) can be converted into A/g as follows:

$$1\ \text{mmol/g/h} = \frac{1\ \text{mol}}{1000\text{g} \times 3600\text{s}} \times \frac{96485\ \text{C}}{\text{mol}} = 0.0268\ \text{A/g}$$

3.13 Calculation of theoretical power outputs of the tested modes.

The calculations in the present study are only based on a flux balance viewpoint and thus do not take into account ohmic resistances, concentration polarization and kinetic constraints during an MFC operation. For the sake of simplification the calculations of cell voltage (i.e., cell potential) are based on formal potentials (at pH 7) of the involved biological and electrochemical redox processes. Therefore, this calculated Electromotive force (EMF) provides an upper limit for the cell voltage and the actual potential derived from the MFC will be lower due to various potential losses [48]:

$$\Delta E^{\circ'}_{\text{cell}} = E^{\circ'}_{\text{cathode}} - E^{\circ'}_{\text{anode}}$$

Where $\Delta E^{\circ'}_{\text{cell}}$ is the standard cell potential (aka., electromotive force); $E^{\circ'}_{\text{cathode}}$ is the standard potential of cathode oxidation; $E^{\circ'}_{\text{anode}}$ is the standard potential of anode reduction.

The formal potentials of the anode and cathode used for calculation of power density in the three operation modes are summarized in Table 3-1.

The calculation of standard cell potential of an MFC (Table 3-2) shows that as long as the same electron donors are used as fuel, there is little that can be done in terms of discovering bacteria capable of creating stronger potentials.

Table 3-1: The standard potential of the anodic and catholic reactions funneling electrons to the electrode, measured at pH 7, versus standard hydrogen electrode [SHE].

		Redox couple	$E^{\circ\prime}$ (V)
Anode	MET	Ferredoxin(Fe^{3+})+e^-→Ferredoxin(Fe^{2+})	−0.420 [22]
		NAD^++H^++2e^-→NADH	−0.320 [318]
		Ubiquinone+2H^++2e^-→Ubiquinone H_2	+0.100 [318]
	DET	Cytochrome *c* (Fe^{3+})+e^-→Cytochrome *c* (Fe^{2+})	+0.254 [318]
Cathode		O_2+4H^++4e^-→2H_2O	+0.51 [51, 319, 320]

Table 3-2: The theoretical limit of standard anode potentials of MFC.

Electron transfer mode	$E^{\circ'}_{anode}$	$E^{\circ'}_{cathode}$	$\Delta E^{\circ'}_{cell}$
MET	-0.32	0.51	0.83
DET (*c*-type cytochrome)	0.254	0.51	0.256
DET (quinol)	0.10	0.51	0.41
DET (reduced ferredoxin)	−0.42	0.51	0.93

3.14 Calculation of the viable growth rate

A slow growth rate could cause biomass decay, a phenomenon in which only a small fraction of microbial cells are metabolically active. This problem is often overlooked in batch and chemostat experiments but is important to real-world applications [102]. To maintain reliability and stability of the treatment system, the actual growth rate can be much lower (between 5- and 100-times smaller) than the maximum possible [102]. However, the lower limit of the viable growth rate for a microorganism is usually unclear. Several modelling works assumed 1% of the maximum theoretical biomass yield as the viability threshold for computational identification of the lowest growth rate [321, 322]. Nevertheless, we chose 5% of the maximum theoretical biomass yield in this study since this value is more conservative and more likely to be practically viable.

3.15 Analysis technique

The growth rates and electron production were computationally determined using Flux Balance Analysis (FBA) [140, 142]. Computational simulations were performed using OptFlux (version 2.4.3) [323] and COBRA Toolbox [324] on MATLAB (The Math-Works Inc., Natick, MA, USA). LibSBML [325] was used to handle files in the SBML format and the GNU Linear Programming Kit (GLPK) (http://www.gnu.org/software/glpk) was used as linear programming solver to execute all linear programming computations. The FATMIN is a pipeline comprising FBA and FVA and thus can be performed with either COBRA or OptFlux according to users' preference. The maximum reducing equivalent production rates for arbitrary growth rates between the data points were calculated using the interpolation function in Mathematica 8.0 (Wolfram Research, Inc. Champaign, IL, USA). All the data and

operations other than solving optimization models are processed in Excel 2013 (Microsoft, Inc., Redmond, Washington, USA).

For reproduction of the simulations in the present study, we have developed a computational toolbox, MFCoT. The introduction to MFCoT can be found in Appendix 4 and its implementation requires COBRA toolbox and GLPK linear solver. The Matlab variables that store the network models are provided (See Appendix 4 for the download link). On the other hand, for users who prefer OptFlux, which possesses a graphic interface, we provide the SBML files that include all the constraints and modifications, such as the added MET reactions, FluxMin reaction for FATMIN and a series of compound objectives with different λ (See Appendix 2 for the download link).

CHAPTER 4 Elucidation of the inherent capability of *Geobacter sulfurreducens* for mediated and direct electron production

Most of the work discussed here has been published in [280]

4.1 Introduction

Geobacter sulfurreducens has been extensively studied for MFC applications since discovered in 1994 [258]. The electrons in the metabolism of *G. sulfurreducens* can be converted to a comparatively large amount of electrical energy through the DET established between reducing processes and the MFC electrode. DET relies on membrane bound c-type cytochromes and electrically conducting nanowires [25], and allows MFCs based on this microbe to obviate the need to replenish exogenous mediators. DET has been suggested to resemble mechanisms observed for electron transport to Fe(III) citrate [326].

Although *G. sulfurreducens* do not excrete redox shuttles [327, 328], exogenous redox shuttles can be added to pull electrons from the reduced intracellular carriers (e.g., NADH) to sustain power generation in MFCs in a mediated way [328]. The electron shuttle compounds allow bacteria to utilise a remote electron acceptor (anode) that is not directly accessible to the cells, enhancing the electron transfer efficiency between the cellular metabolism and the electrode [51]. Therefore, the MET mode could also be advantageous for some MFCs in which the microbes are not grown on the anode.

For the mediated electron generation process, the intracellular electron-shuttling compound NADH has received considerable attention, since it is used to accept the electrons released from an organic substrate and donates them to various oxidoreductase enzymes and electron acceptors (such as quinone and ferredoxin) in the respiratory electron transfer chain of all living cells [19-24]. Exogenous mediators, such as bromocresol green (BG) and neutral red (NR), may target any steps of NADH regeneration in the intracellular electron-transfer pathways in cells and convey the electrons to an extracellular electrode (anode) [36, 37, 40].

Besides, it has been proposed that the theoretical limit of MFC voltage output is the potential difference between NADH and the reaction in the cathode if microorganisms are used as a biological catalyst [22, 41]. Therefore, targeting NADH as the electron source in MFCs of MET mode can liberate the maximum power achievable for a microorganism.

Furthermore, a putative mixed operation mode (Mixed mode) involving both the DET and MET may exist when the cells are grown on the anode and the redox shuttles are added to the anodic reactor of the MFC. The putative Mixed mode may not be practical since different anode potentials could be required to accept the electrons from c-type cytochrome and the reduced mediators, but study of the Mixed mode can help elucidate the metabolic connection between the MET and DET modes.

Scanning the previous literature regarding MFCs based on *G. sulfurreducens* indicates that there are two questions needed to be answered: 1) What is the maximum potential of *G. sulfurreducens* for current output in MFCs under the three aforementioned operation modes? 2) Since a variety of reactions inside a cell are associated with NADH regeneration, what is the best metabolic strategy to choose NADH supply reactions, to maximize the current output in the MET and Mixed modes?

To address these two issues, in this study, we employed FBA to examine the maximum amperage output of metabolic-driven electricity generation based on *G. sulfurreducens* in three electricity generation modes, namely, the c-type cytochrome dependent DET mode, the NADH-dependent MET mode and a Mixed mode combining the DET and MET modes (Table 4-1). We then demonstrated theoretical trade-offs between amperage yield and the biomass production (growth) rate. For elucidation of the metabolic strategies for sustaining free NADH flux for electricity generation in the MET and Mixed modes, we conducted FATMIN to identify the enzymatic mechanisms that could be used by the cell to regenerate NADH at a high rate, subject to the network stoichiometry and substrate uptake. Finally, we analysed the effect of varying substrate uptake rate on the growth rate and the amperage output in the three modes.

Table 4-1: The metabolism and electron transfer types investigated in the present metabolic modelling.

Organism	Transfer type	Electron source (Terminal bacterial electron shuttle)	Metabolic type
G.sulfurreducens	DET (Membrane-driven)	c-type cytochrome	Anaerobic & Heterotrophic
	MET (Mediator-driven)	NADH	
	The Mixed mode (Membrane-driven and Mediator-driven at the same time)	c-type cytochrome & NADH	

4.2 Methods

4.2.1 Modelling electrode interactions

The interactions with an electrode were captured by introducing three reactions into the model reconstruction (Table 4-2). These reactions represent the net reaction that takes place between the reducing equivalents and the mediators (or electrode) in MFCs. Introduction of these reactions create additional channels for electrons to escape from the metabolism and the fluxes of these reactions are subject to the mass balance rule in the FBA modelling. Because NADH and NAD are native metabolites of the microorganisms, these added equations did not lead to non-native by-product production. The reducing equivalent represents NADH in the MET mode, whereas it denotes an assumed product of the reaction catalysed by cytochrome *c* reductase for the DET mode. In both cases, one cycle of the electron transfer yields two electrons. The process is schematically shown in Figure 4-1.

Scanning previous MFC studies indicates that the electron-transfer property of mediators can be specific to each cell design and vary between cells and operational conditions even for the same reaction. This indicates that there is no such a certain mediator ‘supreme’ for all MFCs. Therefore, to avoid limiting the scope of the present study to a particular mediator and leave room for researchers to refine the electron-mediating properties of mediators, we choose to model the function of mediators, skipping their properties such as electric potential and the ability to penetrate the cellular membrane.

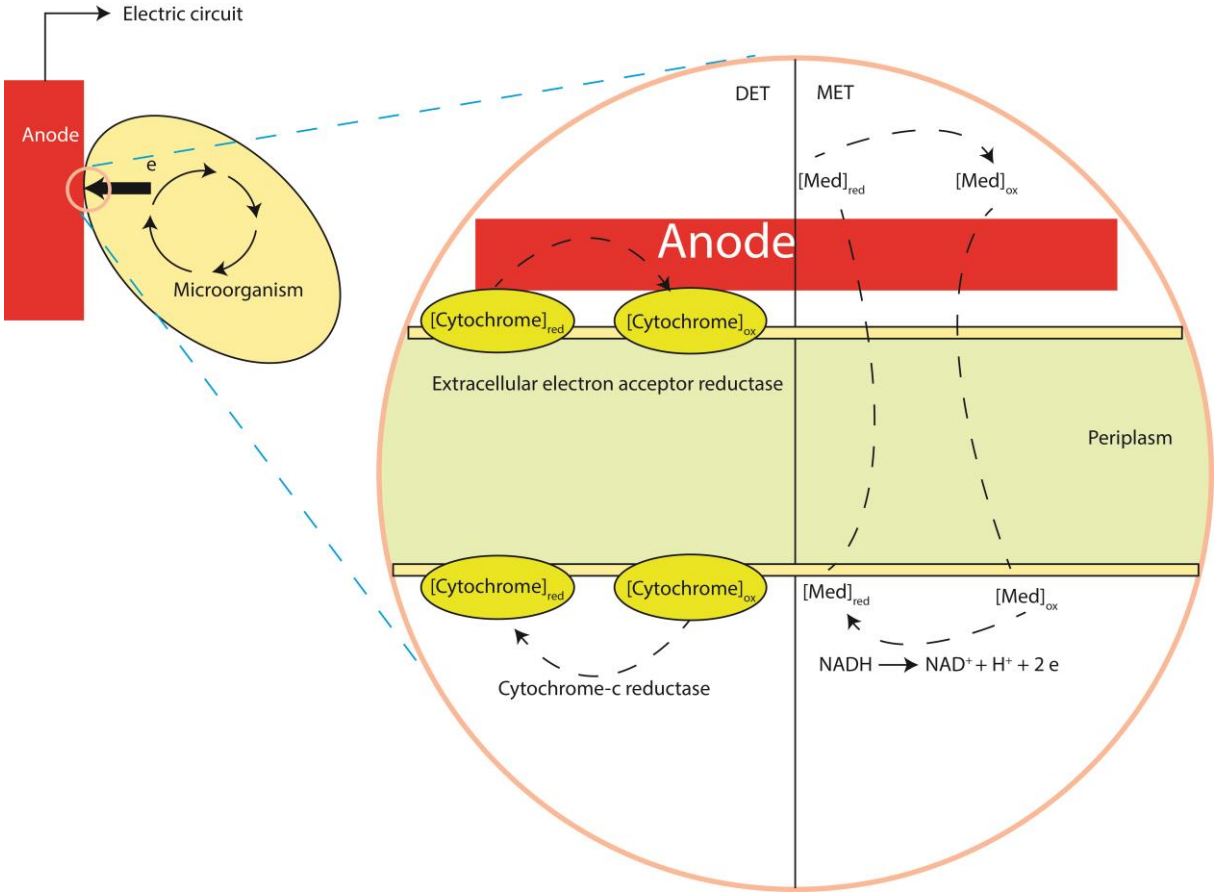

Figure 4-1: A schematic of the anodic mechanisms in MFCs based on *G. sulfurreducens*.

(i) DET, the electron transfer involving c-type cytochrome. (ii) MET, the electron transfer driven by a mediator used process; red, reduced form; ox, oxidized form. Microbes take up substrate generating carbon dioxide and protons. This process yields electrons for metabolic benefit, i.e., growth, and reduces Med_{ox} in the cytosol into Medred. Med_{red} diffuses into contact with the electrode, where Med_{red} reduces the electrode generating electrical current. The oxidized form, Med_{ox}, diffuses back through anolyte for reuse by the microbes. Periplasm only exist in gram-negative bacteria such as *G. sulfurreducens*.

Table 4-2: The added reactions for modeling the interaction of the microorganisms and the electrode in MFCs.

Operation mode of the MFC	Reaction ID	Reaction
MET	1NADHmfc	nadh --> nadh_mfc
	2NADHmfc	nadh_mfc --> nad + h_emm
DET	3Cytcmfc	h_edm --> h_edm_out

nadh_mfc: the NADH available for MET mode of MFCs;

h_emm: the H ions as the by-product released from the reaction 2NADHmfc;

h_edm: the H ions as the by-product released from cytochrome-c reductase (CROR1m) catalysed reaction;

h_edm_out: the extracellular form of h_edm.

4.2.2 Locating the target site in the DET mode

The c-type cytochromes is the electron source for the DET mode (Figure 4-2) [329]. In the network model, the reaction that captures the c-type cytochrome production and the direct electron transfer to the exogenous electron acceptor are retrieved and listed in Table 4-3.

The reaction CYOR1m makes the model suitable for studying direct electron transfer in the case of an MFC. The availability of the c-type cytochrome for extracellular electron transfer is determined by the flux of this reaction. It is assumed that one round of this reaction cycle produces two quotients of the reduced c-type cytochrome for the extracellular electron transfer reaction (FERCYT), equivalent of two quotients of electrons for the electric circuit.

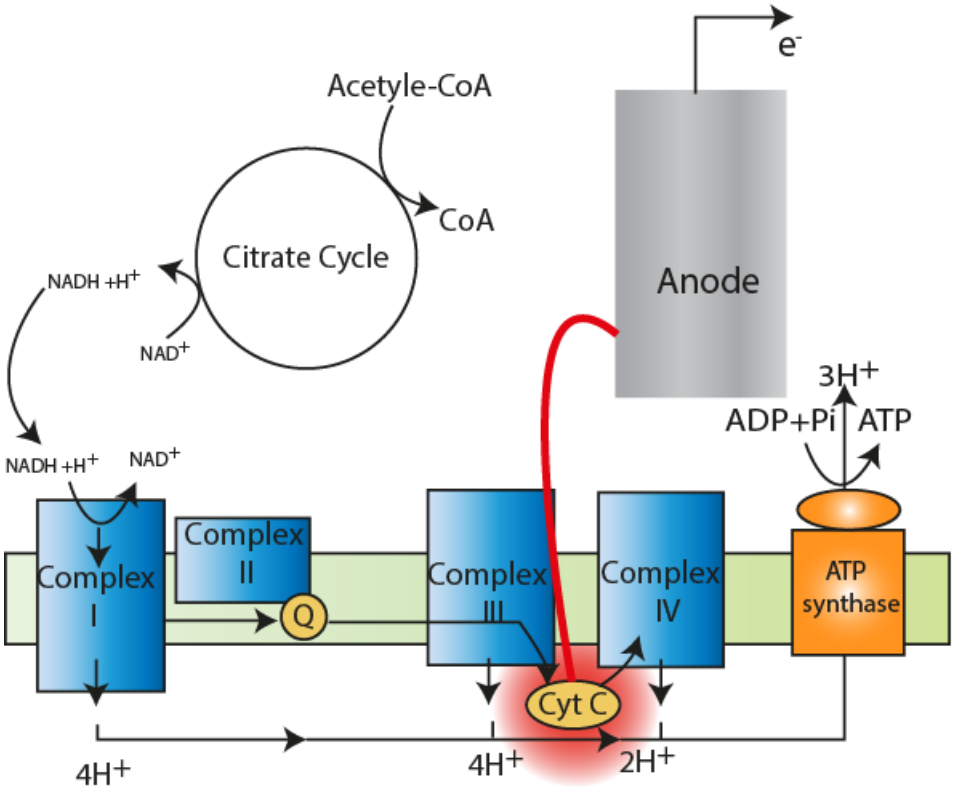

Figure 4-2: A schematic illustration of the electron source in DET mode of *G. sulfurreducens*.

Cyt C, Cytochrome *c*, which is not part of an enzyme complex and moves between complex III and IV as a freely soluble protein.

Table 4-3: The reactions of the extracellular electron transfer in *G. sulfurreudcens*

Reaction ID	Enzyme	Reaction
CYOR1m	cytochrome-c reductase	(2) ficytcc[c] + mql7[c] --> (2) focytcc[c] + h_edm [e] + h[c] + mqn7[c]
FERCYT	Fe (III) Reductase	fe3[e] + focytcc[c] --> fe2[e] + ficytcc[c]

(The reaction and metabolite abbreviations were described in Sun, *et al* (2009) [189] and also in the Appendix 3)

4.2.3 Objective equations

For modelling the maximum metabolic potential for current production and the pertinent metabolic behaviours in the MET mode, the cells were tested for their capabilities to convert low energetic co-substrates (NAD) to their highly energetic counterparts (NADH). For the DET mode, the oxidation rate of c-type cytochrome by the exogenous electron acceptor (i.e., the anode) was maximized. For the Mixed mode, the maximization of the rates of the MET

and DET were equally combined. Hence, the Mixed mode was just a special case of the MET mode with the reduced c-type cytochrome as an additional electron supplier.

The present study used an optimization based framework based on a hypothesized objective function produced by a weighted combination of fluxes (Table 4-4). Characterizing changes to NADH yield and biomass growth rate can aid in understanding the impact of the enhanced current extraction on cellular metabolism. We used a compound objective function comprising maximizations of NADH and biomass concurrently.

Table 4-4: Formulation of objective functions for modelling perturbed metabolisms under electricity generation

MET	Biomass production + (COI_{DET}) NADH_mfc
DET	Biomass production + (COI_{MET}) h_edm_out
Mixed mode	Biomass production + (COI_{MET}) NADH_mfc + (COI_{DET}) h_edm_out

*NADH_mfc denotes the NADH flow that contributes to the electricity generation; h_edm_out represents the flux of the DET reaction that involves the cytochrome *c* reductase

4.2.4 Coulombic efficiency (CE)

One of the parameters commonly used to quantify the performance of MFCs is the Coulombic efficiency (CE); the CE is defined as the ratio of electrons transferred to the anode to that in the starting substrate. For the characterization of the energy efficiency of the metabolism, the full oxidation of acetate with oxygen as the oxidant (as follows) will be used as the reference reaction.

Acetate oxidation reaction: $CH_3COOH + 2\ H_2O \rightarrow 2\ CO_2 + 8\ H^+ + 8\ e^-$.

Based on such stoichiometric information, 1 mol of acetate was converted into 8 mol of electrons (1 mol of acetate = 8 mol e^-) [330].

$$CE\% = \frac{C_{output}}{C_{substrate}} \times 100\% = \frac{\text{reducing equivelent produced (mmol/gDW/h)}}{\text{acetate uptake rate (mmol/gDW/h)} \times 8}\%$$

4.3 Results and discussion

4.3.1 Impact of the redox perturbation on the biomass production

Figure 4-3 shows how reduction equivalent is allocated to internal use (i.e. maintenance of the cell metabolism) and supply to the external circuit, for various cell growth rates.

The increase in production of reducing equivalent drove the fluxes through electron transfer reactions in the three MFC operating modes towards their maximum allowable values and corresponding biomass formation rates to their minimum values. This reflects that at a low growth rate, only a small part of the energy is available to microorganisms in MFCs for their growth, as a large part is converted to electricity.

The present modelling allowed free selection of the acetate uptake rate in a proper range (0-18 mmol/gDW/h) to maximize the objectives, i.e., biomass production rate, and NADH or c-type cytochrome involved electron transfer rates. Since acetate is the main source for producing biomass, NADH and c-type cytochrome, the acetate uptake rate stayed at the maximum (18 mmol/gDW/h) in all the simulatinon results. This suggests that the increased fluxes through the NADH and reduced c-type cytochrome regenerating reactions did not result from the increased availability of acetate, but were associated with the redirection of electron flux for biomass formation towards mediators in the MET mode or the electrode in the DET mode.

In the Mixed mode, the total electron flux available for current production was the sum of the fluxes through the c-type cytochrome dependent and NADH-targeted pathways, which are individually exploited by the DET and MET modes respectively. The current production influenced the combined production of the NADH and the reduced form of the c-type cytochrome in the same way as observed for the cases of MET and DET modes. Since relative importance (λ) were equally assigned for DET and MET, the two electron transfer rates were nearly the same. Equal weighting may not necessarily represent actual physiological

priorities, but is appropriate to evaluate how DET and MET mutually influence each other. Figure 4-3 also shows that the Mixed mode did not produce significantly higher electron flux than either MET or DET alone. This result suggests that the DET competed with the MET for the metabolic resources.

(A) DET

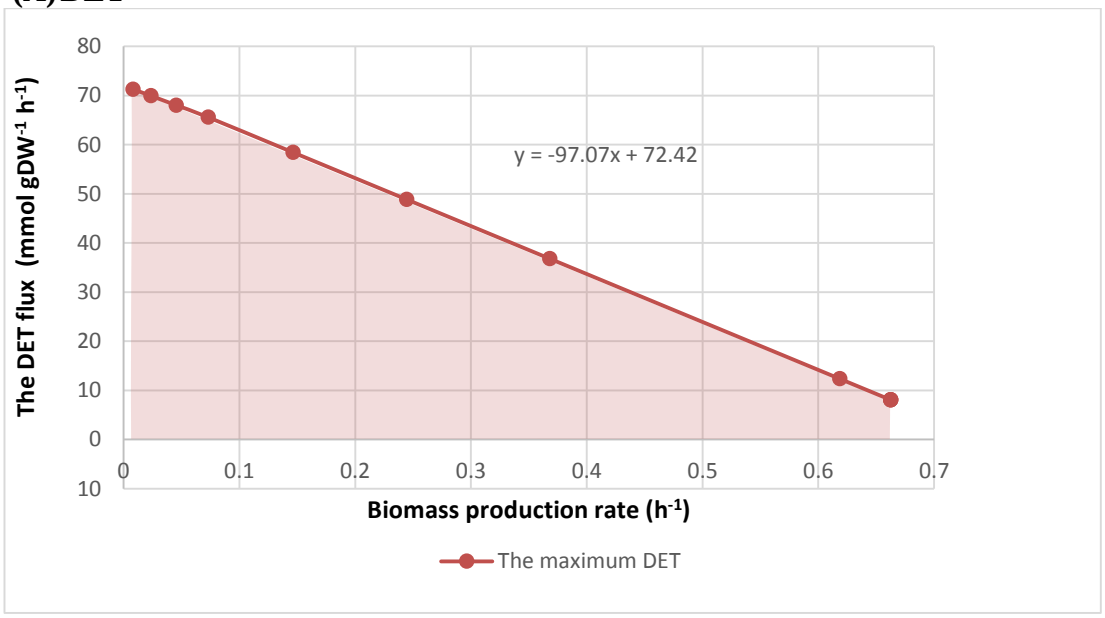

(B) MET

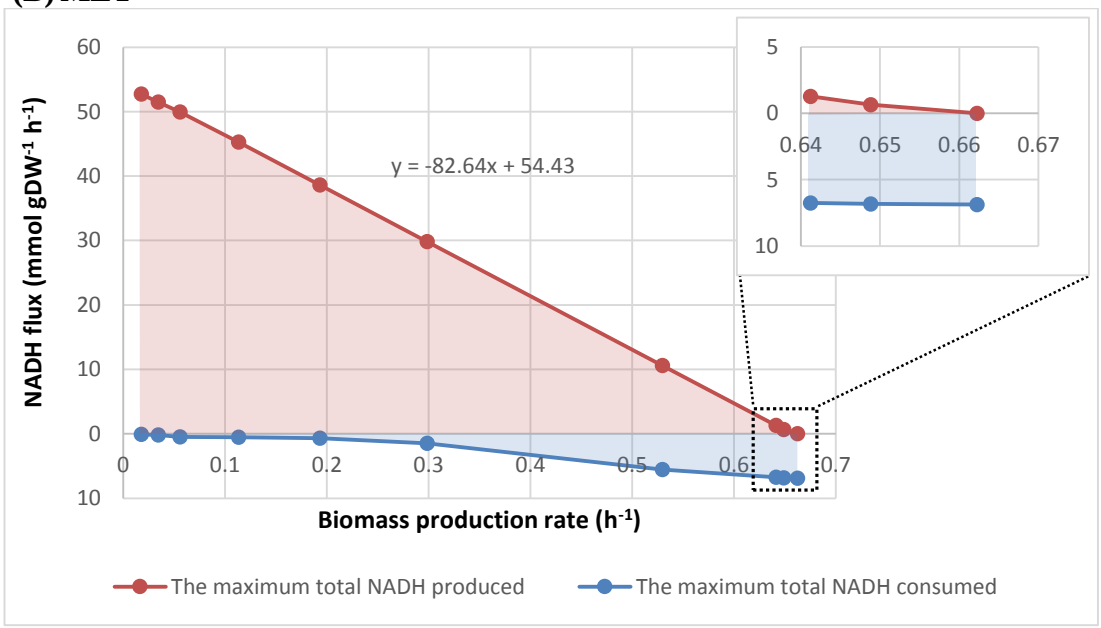

(C) Mixed mode

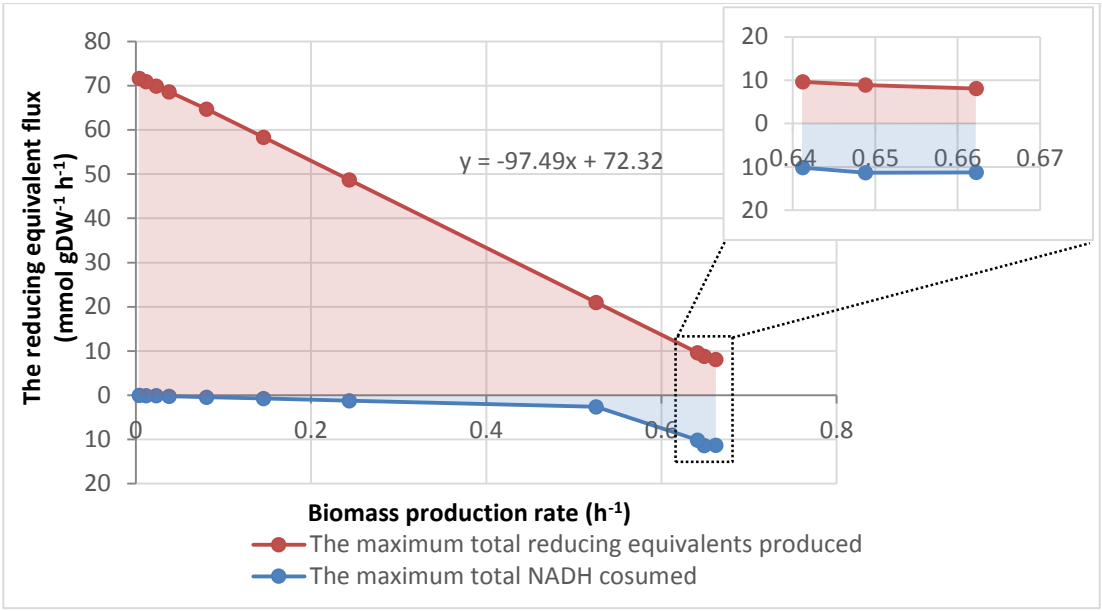

Figure 4-3: The relationship of the biomass production and electron transfer rates.

The reducing equivalent supplying rates in the (A) DET, (B) MET and (C) Mixed modes, and the NADH consumption rate for cellular use in the (B) MET and (C) Mixed modes, as functions of biomass yield. The line represents the maximal electron transfer rates and biomass production rate, while any point within the pink area represents all allowable electron transfer rates and biomass production rates. The blue area represents the total NADH-consuming flux for normal cellular function. The distance between the two lines across the pink and blue areas represents the total available NADH flux in the cell at a metabolic state related to a specific biomass production rate; inset, enlargement of boxed area. The reducing equivalent represents NADH in the MET mode, whereas it denotes an assumed product of the reaction catalysed by cytochrome *c* reductase for the DET mode.

Generally, MFC current production competes with biomass production for metabolic resources. The increase in the electron transfer rates is linearly correlated with a decrease in biomass yield in the three operation modes. For DET mode (Figure 4-3 (A)), the optimal metabolic state that resulted in the maximum growth rate of 0.6622 h^{-1} necessitates a flux of 8.092 mmol/gDW/h through reaction CYOR1m. This indicates that disposal of some electrons to exogenous Fe(III) can benefit the growth of *G.sulfurreducens*. When the λ associated with CYOR1m increased to 0.9998, which resulted in a highly perturbed metabolic state corresponding to around the upper limit of current output, the capability of the metabolic network for the electron transfer in DET mode increased by 8.65 fold (765%) to 69.69 mmol/gdW/h (not specified on the plot) compared with the optimal state.

Unlike the DET mode, which relies on one single enzymatic contribution (c-type cytochrome involved reaction), there were 51 internal reactions with potential to generate or consume NADH for the MET mode in the network model. Sum of the fluxes of all NADH producing reactions gives the total NADH production rate at a particular metabolic state, whereas sum of

the fluxes of all NADH consuming reactions is the total NADH consumption rate for maintenance. The net yield of NADH reactions is the total NADH production rate available for MFCs (i.e., NADH_mfc).

For MET mode (Figure 4-3 (B)), the total NADH production rate (sum of the fluxes of the NADH_mfc and NADH_consumed) increased from 6.865 mmol/gDW/h at the optimal growth rate of 0.6622 h^{-1} to 52.80 mmol/gDW/h at the growth rate of 0.01757 h^{-1} (λ = of 0.9998). In the metabolic state simulated by λ of 0.9998, the metabolism was capable of increasing the NADH_mfc yield by up to 7.5 fold (653%) compared with the base state optimised for growth. The increase in the flux of NADH_mfc was predicted to result from a combination of two mechanisms, i.e., increasing the NADH production and decreasing the NADH needed for biomass production and maintenance.

In addition, the rise in NADH regeneration rate by increasing λ accidently activated some NADH-consuming futile cycles, leading to very high flux values (larger than 100 mmol/gdW/h) through some NADH-consuming reactions. Increasing flux through these futile cycle reactions did not change the growth rate and the net NADH production rate. Since the total NADH flux for normal cellular function was taken as the sum of all NADH-consuming fluxes, the contained futile values could make the calculated total NADH flux much higher than the actual ones. Because the task to eliminate all futile cycles in the whole network diverges from the purpose of the present study, we did not carry out the analysis of all futile pathways using methods such as elementary mode or extreme pathway, which can only be performed on a small-scale network [331].

Instead, in an attempt to eliminate flux contributions of those futile cycle reactions to the total NADH consumption rate associated with growth and non-growth maintenance, several sub-sets of constraints were used for the simulations with different λ according to a simple method (Section 3.6.2). This was used instead of the relatively complex pipeline in the FATMIN algorithm, because the present section simply uses a single FBA rather than elucidation of the detailed flux range of individual reactions for which FATMIN was developed.

Unlike DET and MET modes, the Mixed mode relied on the metabolic capability for concurrent regeneration of NADH and reduced c-type cytochrome. The analysis showed that

the metabolism could increase the regeneration capability of the two metabolites by 3.7 fold (267.1%), compared with its base state, to 71 mmol/gDW/h (λ of 0.9998). The increase was attributed to a combination of three mechanisms, i.e., increasing the NADH and reduced c-type cytochrome regeneration rate and decreasing the NADH needed for biomass production and maintenance.

The discussion above makes it clear that while reducing equivalent production competes with biomass growth for metabolic resources, not all gains in reducing equivalent production come at a cost to the growth rate, because some gains are also derived from reconfiguration of the metabolism. To quantify this observation we introduce a measure called the fractional benefit B, as discussed in Chapter 3. Briefly, B is the sum of the fractions of maximal growth and reducing equivalent production respectively, achieved in a particular metabolic state. It indicates the combined benefit from both considerations. So a metabolic state would attain the maximum B value of 100% if it reaches the utopian ideal of simultaneously producing the maximal growth rate and the maximal reducing equivalent production. On the other hand, the wild type phenotype of maximal growth rate and no reducing equivalent, has a B-value of 50%, as has the other extreme of the Pareto frontier where reducing equivalent is, by definition, maximal while the growth rate is zero. Values above 50% signify that the gain in one objective contribution outweighs the losses in the other, and vice versa for values below 50%.

Figure 4-4 shows the result of this measure applied to the reported simulations. There is a steady drop in the B values from near 56% at wild type growth rates (right hand side of the figures) to about 50% at the heavily suppressed growth rates (left hand side). The high B value (around 56%) in the wild type indicates that the two objectives, i.e., the DET and growth, are well balanced at the control metabolic state, which corresponds to Figure 1 (A) that shows DET is needed and favoured for optimal growth. The subsequently declined B values indicate that the forced increase in the DET is hostile to biomass production. On the contrary, the fractional benefit curve of the MET mode fluctuates around 50%. As the growth rate decreased as a result of elevated current production, the B values dropped below 50%, bottomed out at the growth rate of 0.6488 h^{-1} and then increased steadily, peaking at about 51%, before experiencing another drop. The fluctuation indicates that a small redox disturbance causes an adverse effect on the growth, but further increase in the degree of the redox perturbation can improve the metabolic output of the combined two goals. However,

since the maximum B value could not exceed 51%, it is indicated that MET could not liberate the maximum metabolic capability of cell for growth-coupled current production. Similar to the B value curve of the DET mode, the Mixed mode exhibits a decrease over the whole growth rate range. Notably, a clear drop in the fractional benefit was observed at high growth rates (0.6488 – 0.6622 h^{-1}), which correlate with the appearance of the B-value curve of MET mode.

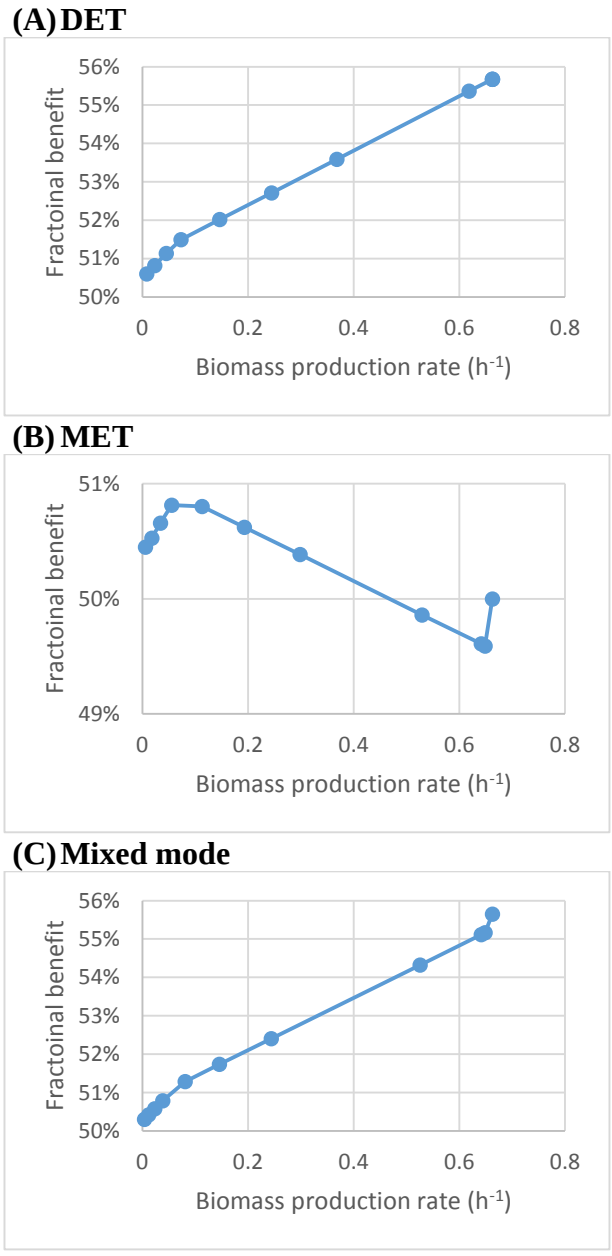

Figure 4-4: The effect of varying biomass production on the fractional benefit.

The fractional benefit B plotted on the vertical axis, is a measure of success in achieving the combined goals of maximal growth rate and MET flux. Maximizing one of these at a time, as at the endpoints, gives only B = 50%. The graphs show that relative to this, gains in MET flux can more than offset losses of growth rate in the *G. sulfurreducens* metabolism.

The mechanisms by which the NADH is additionally produced for current output are elucidated in the next section.

4.3.2 Metabolic strategies for sustaining a high flux of NADH under the MET and Mixed modes.

In this study, the maximization of the reducing equivalent for electricity production and the biomass growth were two objectives desired to be optimised during the modelling. The relative importance between two objectives was regulated by a coefficient λ, which is discussed in detail under 'Objective equation' in Methods chapter (CHAPTER 3). For elucidation of the enzymatic mechanisms underlying the high current production in the three modes, we chose metabolic states modelled with λ of 0.9998 as the references, because a further increase in λ can barely increase the electron transfer rates when the λ was above 0.999. In fact, for identifying the metabolic behaviours under high electron transfer rates, it does not matter whether the metabolism is extremely perturbed (such as the metabolic state modelled by λ of 0.9998 or higher) or just a little bit less extremely perturbed (λ of 0.999), as they all represent the metabolic states at which nearly all metabolic resources have been relocated from for biomass production to the current production. The λ = 0.9998 value corresponds to COI = 3000.

4.3.2.1 The MET mode

Table 4-5: The identified reactions that contribute significantly to the predicted maximum NADH production rate in the MET mode.

Reaction ID	NADH flux (mmol/gDW/h)		Enzyme	EC. No.	Reaction	Subsystems
	Min	Max				
AKGD	0	17.73	2-oxoglutarate dehydrogenase	2.3.1.61	[c] : akg + coa + nad --> co2 + nadh + succoa	Central Metabolism
ALAD_L	0	52.77	L-alanine dehydrogenase	1.4.1.1	[c] : ala-L + h2o + nad --> h + nadh + nh4 + pyr	Amino Acid Metabolism
GLUDx	0	52.72	glutamate dehydrogenase (NAD)	1.4.1.3	[c] : glu-L + h2o + nad <==> akg + h + nadh + nh4	Amino Acid Metabolism
GSADH	0	52.77	L-glutamate 5-semialdehyde dehydrogenase	1.2.1.38	[c] : glu5sa + h2o + nad --> glu-L + (2) h + nadh	Amino Acid Metabolism
HDMAT7	-0.00007	52.77	Hexadecanoyl-[acyl-carrier protein]:malonyl-CoA C-acyltransferase	1.3.1.9	[c] : nad + palmACP <==> h + hdeACP + nadh	Fatty Acid Synthesis
ME1x	0	52.77	malic enzyme (NAD)	1.1.1.37	[c] : mal-L + nad --> co2 + nadh + pyr	Central Metabolism
P5CD	0	52.77	1-pyrroline-5-carboxylate dehydrogenase	1.5.1.12	[c] : 1pyr5c + (2) h2o + nad --> glu-L + h + nadh	Amino Acid Metabolism
PDH	0	52.77	pyruvate dehydrogenase	1.2.4.1	[c] : coa + nad + pyr --> accoa + co2 + nadh	Central Metabolism
PGCD	0.0196	52.79	phosphoglycerate dehydrogenase	1.1.1.95	[c] : 3pg + nad --> 3php + h + nadh	Amino Acid Metabolism
TDMAT6	-0.00404	52.77	Tetradecanoyl-[acyl-carrier protein]:malonyl-CoA C-acyltransferase	1.3.1.9	[c] : myrsACP + nad <==> h + nadh + tdeACP	Fatty Acid Synthesis

(The reaction and metabolite abbreviations are listed in Appendix 2).

When the mediator deprives NADH of electrons forming NAD+, the NAD+/NADH ratio in the metabolism is changed and consequently the cell has to adjust its metabolism to regenerate NADH from NAD+ in order to maintain a proper redox balance for survival. To elucidate the metabolic adjustments induced by heavy NADH loss (COI=3000), the range of variability of intracellular fluxes were calculated. The results show that although many reactions in the network can produce NADH, under heavy NADH demand, only a few reactions can sustain large NADH drain, while other NADH producing reactions become deactivated to leave the metabolic resource for the highly efficient NADH producers.

In total, ten out of fifty-one NADH involved reactions were identified as capable of regenerating NADH at a high rate under the redox perturbation (Table 4-5). Among the ten reactions, one reaction (AKGD) (EC 2.3.1.61) had a potential to produce NADH at up to a flux rate of 17.73 mmol/gDW/h. Each of the other nine reactions possessed the capability to solely supply almost all of the 52.80 mmol/gDW/h, which was the maximum total NADH flux that could be achieved for the metabolism of *G. sulfurreducens* at COI of 3000. Therefore, the probed maximum NADH production rate could result from any combination of lesser fluxes of the nine reactions that made up that value. This indicates that the number of optimal solutions will be unlimited. The non-uniqueness of the obtained solution corresponds to the alternative optima in the linear optimization and the existence of alternative pathways that result in equivalent mutant phenotypes regarding the required metabolic adjustment.

Among the nine reactions, three reactions (i.e., AKGD, ME1x and PDH) were part of the central metabolism pathway (TCA cycle). Four reactions (i.e., ALAD_L, GLUDx, GSADH and PGCD) were related to the amino acid metabolism. Another two reactions (i.e., TDMAT6 and HDMAT7) were located in the fatty acid metabolism. Therefore, this result extends the previous notion that the TCA cycle is the main source of NADH for *G. sulfurreducens* when acetate is fed as the electron donor [270].

Except the nine reactions, all other NADH involved reactions were found to have very low or no variability ($v_{i\ min}/v_{i\ max}>0.99$) under high current output. The rigid variability may be attributed to the fact that NADH is a highly connected metabolite ensuring a degree of network connectivity sufficient to limit the availability of alternative flux distributions because of cascading effects on other metabolites.

The analysis presented does not fully specify the solution space. The Max/Min limits in Table 4-5 describe a rectangular cuboid in 10 dimensions, that encloses the feasible flux points but would, in general, still contain flux value combinations that are not feasible even if the values do add up to the 52.80 mmol/gDW/h value that was determined as the combined maximum. A full specification requires determination of all vertices of the solution space. Elucidation of these vertices is the task targeted by techniques such as elementary mode and extreme pathway analysis, but applications of these tools are restricted to small- and medium-scale

networks of limited connectivity [182] and not suitable for the network size of *G. sulfurreducens* used here.

4.3.2.2 The Mixed mode

Table 4-6: The identified reactions that contribute significantly to the predicted maximum NADH production rate in the Mixed mode.

Reaction ID	NADH flux (mmol/gDW/h)		Enzyme	EC. No.	Reaction	Subsystems
	min	max				
NADH producing reactions						
AKGD	0	35.48	2-oxoglutarate dehydrogenase	2.3.1.61	[c] : akg + coa + nad --> co2 + nadh + succoa	Central Metabolism
ALDD2x	8.855	35.32	aldehyde dehydrogenase (acetaldehyde, NAD)	1.2.1.3	[c] : acald + h2o + nad --> ac + (2) h + nadh	Amino Acid Metabolism
GCCc	4.427	17.66	part of glycine-cleavage complex	1.8.1.4	[c] : dhlpro + nad --> h + lpro + nadh	Amino Acid Metabolism
NADH consuming reactions						
GAPD	-52.96	-0.04026	glyceraldehyde-3-phosphate dehydrogenase (NAD)	1.2.1.12	[c] : g3p + nad + pi <==> 13dpg + h + nadh	Central Metabolism
GLUSx	-52.92	0	glutamate synthase (NADH2)	1.4.1.14	[c] : akg + gln-L + h + nadh --> (2) glu-L + nad	Amino Acid Metabolism
NADH5	-10.58	0	NADH dehydrogenase (Menaquinone 7 & 2 protons)	1.6.5.3	(3) h[c] + mqn7[c] + nadh[c] --> (2) h[e] + mql7[c] + nad[c]	Energy Metabolism
DET						
CYOR1m	35.48	35.48	cytochrome-c reductase (menaquinol 7: 1 protons)	1.7.2.2	(2) ficytcc[c] + mql7[c] --> (2) focytcc[c] + h[e] + h[c] + mqn7[c]	Energy Metabolism

(The reaction and metabolite abbreviations are listed in the Appendix 2)

Similar to the case of the MET, a continuous range of solutions for achieving the high electron transfer rate in the Mixed mode involving an combination of six reactions for NADH regeneration plus one c-type cytochrome dependent DET reaction (Table 4-6) was obtained. It is shown that the electrons leaking from the site of the c-type cytochrome influenced the possible cellular strategies to supply high NADH flux. The metabolic strategies probed for the Mixed and MET modes shared one common reaction, AKGD (EC: 2.3.1.61), to sustain high NADH flux. Nonetheless, the other eight reactions that could regenerate NADH at high rates

in the MET mode were not active in the Mixed mode, which chose two new reactions, ALDD2x (EC: 1.2.1.3) and GCCc (EC: 1.8.1.4) located in the amino acid metabolism as the NADH suppliers. Besides, in the Mixed mode, another three reactions were identified capable of consuming NADH at high rates. These NADH consuming reactions were deregulated to balance the excess NADH produced by the identified three producing reactions, making up a net sum flux of NADH of 70.96 mmol/gDW/h (obtained when COI=3000). Since a range of reactions (nine for MET and three for Mixed mode) in different biological sub-systems could be targeted as the efficient NADH suppliers, NADH-dependent electricity generation should be more robust against momentary shifts in environmental conditions than the pure DET mode.

In the case of MET, NADH production was increased by directing the electrons towards the reactions in the Krebs cycle and fatty acid biosynthesis, so fewer electrons are available for the downstream pathway of oxidative phosphorylation, which is associated with DET, to produce energy for the cell maintenance and growth. This accounts for the phenomenon shown here that MET and DET competed with each other for electron resources in the Mixed mode and a combination of both did not double the current output of MET or DET alone.

To demonstrate how nutrient uptake is channelled to biomass growth and current yield respectively, Figure 4-5 compares the corresponding fluxes at different uptake rates.

4.3.3 Effect of varying acetate uptake rate on the predicted biomass and reducing equivalent production rates

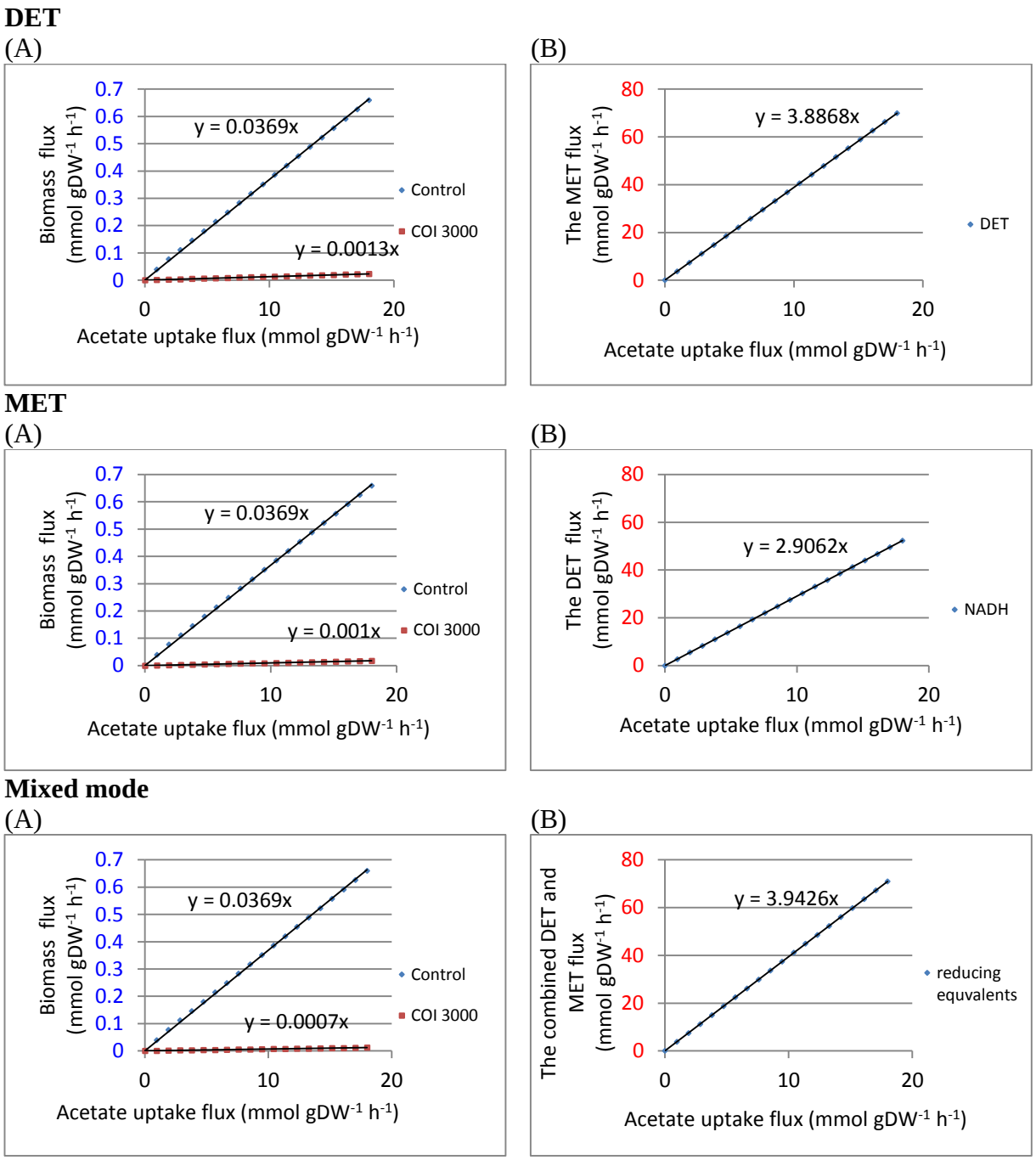

Figure 4-5: The effect of varying acetate uptake rate on the biomass and reducing equivalent production rates.

(A) The effect of varying acetate uptake rate on the biomass growth rates when biomass production is set as biological priority for the organisms (use of only biomass maximization as objective function) and when the electron transfer in the three modes is set as the priority (use of a λ of 0.9998 (COI of 3000) for the reducing equivalent production in the objective function); (B) The effect of varying acetate uptake rate on reducing equivalent production rate flux when a λ of 0.9998 is used for the reducing equivalent production.

The biomass production rates or the electron transfer rates were all linearly proportional to the acetate uptake rate in the three operation modes. This suggests that acetate uptake rate is the major limiting factor for both biomass and current yields. In addition, as seen from the different Y axis scales (i.e., the slopes of the trend lines), the priority set for electricity generation in the three modes lead to the suppression of biomass production and current production was much less acetate-costly than the biomasss production.

The Mixed mode (slope=3.9426) can achieve higher efficiency of converting substrate into electricity in MFCs than the DET (slope=3.8868) and MET (slope=2.9062) modes. The high conversion efficiency reached by the Mixed mode is attributed to the fact that two by-products, reduced c-type cytochrome and NADH, were both acceptable for electricity generation, leaving more freedom for the metabolism to adjust to maximize the objective than only one byproduct, such as in the either case of DET or MET.

Finally, the three operation modes are compared for their theoretically maximum current output in Figure 4-6 and Table 4-7.

4.3.4 Comparison of amperage output of the three operations modes

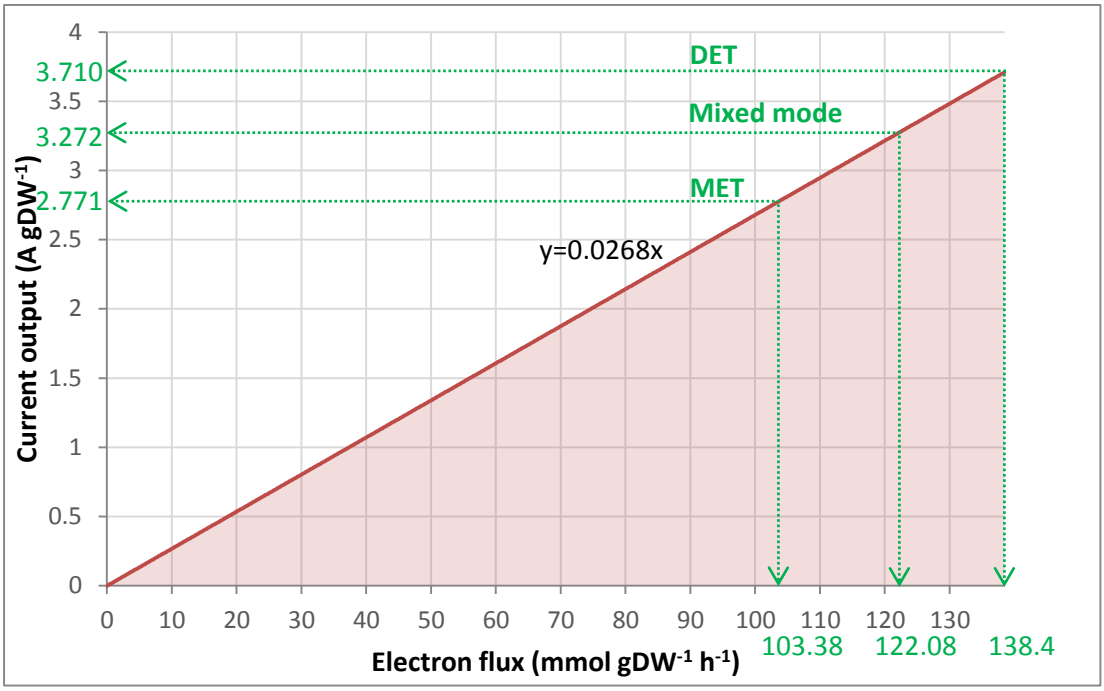

Figure 4-6: The current output (A/g) as a function of electron flux.

The dark red line denotes the maximal current outputs and NADH_mfc production rate, while the area represents all allowable current outputs and electron production rates. The round dotted arrow line indicates the maximal current output and corresponding electron production rate when the growth rate is set to 5% of the predicted maximum growth rate (0.033 h^{-1}).

Table 4-7: Comparison of predicted amperage and power output of three modes under acetate limiting condition and under theoretical maximum current output condition

	Conditions	Biomass growth rate (h^{-1})	Electron (mmol gDW^{-1} h^{-1})	Amperage (A gDW^{-1})	Coulombic efficiency (CE%)	Theoretical limit of the power output (W gDW^{-1})
DET	The growth rate achieved in the acetate limiting condition)	0.06	133.2	3.570	92.50%	0.9139
MET			98.94	2.652	68.71%	2.201
Mixed mode			116.8	3.131	81.13%	2.599
DET	5% of Maximum growth rate	0.033	138.4	3.710	96.12%	0.950
MET			103.4	2.771	71.79%	2.300
Mixed mode			122.1	3.272	84.78%	2.716

* c-type cytochrome *c* and NADH have different standard potentials. The power density for the Mixed mode was calculated by sum of the power contributions from the DET and the MET, i.e., the current output of DET and MET were multiplied with their appropriate voltages respectively.

A growth rate of 0.06 h^{-1}, which is achievable in the experiment [332], was also chosen as a reference value in addition to the 5% optimal growth rate. Among the three tested electron transfer modes, DET delivered the highest maximum limits of the current output, whereas MET achieved the lowest maximum limit. This could be attributed to the fact that *G. sulfurreducens* can conserve energy for cellular growth during the process of disposing electrons to exogenous electron acceptors [86] and consequently less additional energy resources (i.e., acetate) are required for the DET mode to achieve the same level of current output as the MET. Therefore, these organisms can gain an energetic advantage by growth on, or near, the electrode. Nonetheless, despite its higher current output, the maximum power output of the DET mode was lower than those achievable by the other two modes, due to the low standard potential of the c-type chromosome used by the DET mode.

For the MET, mediators are needed to extract the redox potential out of cells and thus the cells that are located far away from electrode surface can still contribute to the current production. On the other hand, the DET depends on the 20-30 μm long pili of *G. sulfurreducens* to deliver the electrons from the outer membrane to the anode [26, 271]. Consequently, compared with the MET, the DET requires a much closer distance between the cell and the anode surface, and thus the actual current output will be restricted by the number of electrochemically active cells that are near the surface area of the electrode.

The result shows that the maximum output of the Mixed mode was a little bit higher than MET. However, based on this, it cannot be concluded that the Mixed mode is more competitive than MET. In effect, the Mixed mode may require independent circuits to collect the power output from the DET and MET concurrently. Furthermore, the Mixed mode requires involvement of mediators, large surface contact between the cells and special electrode design that can accept electrons from the two reducing agents with different potentials. This creates more demands for the engineering design and has impacts on power density and the long-term stability of the MFCs. The extra complication probably does not justify the design effort needed for mixed mode operation.

The DET and Mixed mode both involved higher coulombic efficiencies than the MET mode, which implies that more electron flows were directed to current production rather than cellular synthesis. In a previous MFC review article, the MET system was suggested to have lower

coulombic efficiency than the DET [51]. This is because part of the electrons from the substrate are used by the cell to form some electrochemically inactive side products [51].

The present study computed the theoretical maximum CE% achievable for the DET as 79.34% based on the stoichiometry in the network, indicating the acetate-fed MFCs using *Geobacter* species can effectively oxidize acetate with electron transfer to electrodes. However, the computed value is still much lower than the values reported by several previous studies, which claimed that *G. sulfurreducens* in MFCs could convert acetate to current with CEs of 89% [333] and above 90% [260, 264]. Some studies assumed a CE of 100% for the DET via c-type cytochromes [58, 185].

The reasons for such a discrepancy between the computed CE in this study and previous reported ones are speculated to be as follows: 1) The acetate consumed by the cell was calculated by measuring the change of concentration of acetate in the culture media. The measured point is always far away from the cells. A gradient of acetate concentration exists in the distance between the measured point and the cell surface, i.e., the acetate concentration is lower at the cell surface and much higher at the point where the measurement takes place, because starting with a homogenous acetate concentration, after MFC operation the concentration will drop more at the cell surface than at the measurement point. Thus the measured acetate uptake rate is lower than the actual uptake rate. According to the formula: $\text{CE\%}=\frac{\text{Acetate used for current production}}{\text{Total acetate consumed by the cell}}$, an underestimated total acetate uptake rate could increase the resulting CE%. 2) Microbes can consume other nutrients in the media or reserved in the cells, such as other dead cells, for electron production, but this factor was not taken into account for calculating the total substrate consumed by the cell.

Microorganisms have a strong propensity to aggregate and proliferate into biofilm on the solid surfaces [334]. A previous MFC study reported a current output of 1.4 A/m^2 and a power density of 0.5 W/m^2 by a biofilm of wild-type *G. sulfurreducens* [260]. The cell protein density of the biofilm was measured as 0.571 g protein $/m^2$ [260]. With an assumed protein content of 46% of cell dry weight [268], the cell density of the biofilm is estimated to be 1.241 g/m^2 and the previously reported current flow (1.4 A/m^2) and power density (0.5 W/m^2) can be converted into 1.128 A/gDW and 0.4028 W/gDW respectively. Clearly, these

values are much lower than the computed ones (3.710 A/gDW and 0.95 W/gDW) for the DET mode in the present study. The difference between the *in silico* predicted maximum electric outputs and observed ones may be attributed to the fact that some electrons and potential would be lost during the electron transfer between the biofilm and the electrode, and consequently the actual current and power density will be lower than these computed values. Understanding and optimizing the micro-electrode interaction is another challenge to overcome in MFC research.

It is commonly observed that mixed cultures usually produce much higher current densities at high coulombic efficiency compared with pure cultures, due to many advantageous features arising from the mutualism among microbial diversity [24, 335, 336]. However, by improving the engineering design, the MFC based on *G.sulfurreducens* can produce a power density similar to those reported with various mixed cultures while maintaining high coulombic efficiency [264].

4.4 Conclusions

Analysis of the metabolic flux models predicted that *G. sulfferreducens* in the DET mode achieved the highest current output (3.710 A/gDW), followed by the Mixed mode (3.272 A/gDW), and MET the lowest (2.771 A/gDW). In the DET mode, the enzymatic activity of one reaction determined the current generation in MFCs. On the contrary, in the MET mode, the reducing molecule, NADH, could be efficiently regenerated and supplied from ten identified reactions, while in the Mixed mode the number of possible reactions supplying NADH was reduced to three. The decreased reaction number indicates that the DET and MET compete with each other for the metabolic resources, as is also evident from the fact that the total current output in the mixed mode is not additive but instead interpolates between the DET and MET values . The increases in the electron transfer rates in the three modes were linearly correlated with the drop in growth rate, which was, however, achieved by the increasingly rising metabolic ‘cost’ (modelled by λ).

The multiplicity of reactions capable of individually supplying the maximal current output, indicates a range of feasible solutions rather than just a single idealised metabolic state. This

leaves room for good performance to be obtained from different cellular phenotypes and suggests robustness to changes in environmental or metabolic conditions.

CHAPTER 5 Comparison of the mediated current generation capacity of *Chlamydomonas reinhardtii* in photosynthetic and respiratory growth modes.

The materials in this chapter have been submitted for publication [337].

5.1 Introduction

C. reinharditii inherits all potential advantages of algae for industrial use and scientific study, which have been reviewed in previous studies [47, 206-208]. Due to these advantages, algae have been examined in many studies for the generation of energy products, such as bio-oil, methane, methanol and hydrogen [209]. These technologies require that the fuel produced must be stored, transported and further processed to produce electricity. Although it would be an advantage if an MFC is used for remote power generation, this is a disadvantage where the electricity produced by MFC is to be consumed locally, To circumvent these problems, a microbial fuel cell (MFC) could be used as an alternative way to directly generate electricity in only one process unit by means of conversion of the metabolic energy of the cell to electricity. Previous studies tend to use this microbe as a hydrogen supplier in MFCs of product type that depend on the production and oxidation of hydrogen molecules at the anode to supply electrons to the MFC circuit. However, the hydrogen production is subject to several biochemical and engineering shortcomings, such as a necessitation of a light-dark cycle and anoxia condition, safety issues arising from hydrogen combustion at high pressure, and the MFCs of product type have quite a low power performance [210].

Another possibility is to extract the redox power of the metabolic activity inside the cell for current production in MFCs by direct or mediated electron transfer (DET or MET) modes. However, previous studies of these two operational modes of MFCs commonly relied on diverse prokaryotic species and mixed culture as the biocatalysts and fewer studies involve eukaryotes as biocatalysts in the MFC operations. This could be attributed to the fact that the metabolic processes of eukaryotic cells are difficult for some conventional redox mediators to get access to [23, 85]. However, recent works have shown that eukaryotes such as *S.*

cerevisiae can be used in MFCs of MET mode reliant on the cytoplasmic redox potential of the cell [61, 186, 249]. The more complex metabolism of eukaryotes may be more efficient and be able to support a larger diversion of redox carrier flux without undue harmful effects on the organism. Since the characteristics of *C. reinhardtii* show very promising merits for being exploited in MFCs of MET mode and using algae as biocatalysts in MFCs is an ongoing research area, it would be desirable to know the maximum potential of *C.reinhardtii* for electricity generation and the available metabolic mechanisms for this microorganism to sustain a high current output.

For the mediated electron generation process, NADH has been suggested as the optimal intracellular electron-shuttling compound to be targeted for mediated electricity generation [36], because NADH is the universal electron carrier connecting many different cellular processes in all living cells. Some NADH flux may originate from NADPH in other organelles. Also, it has been proposed that the theoretical limit of MFC voltage output, if microorganisms are used as a biological catalyst, is the difference between the redox potential of the carrier and the cathode potential [22, 41], and NADH has a relatively low (negative) redox potential [22]. Therefore, study of the current production in MFCs linked to the $NADH/NAD^+$ cycle could be considered as a way to probe the maximum metabolic potential for the ideal electricity generation. This would also serve as a reference method and a starting point for elucidation of other potential redox molecules available from eukaryote metabolism for mediated electron transfer in the future.

The present study intends to provide *a priori* information about *C. reinhardtii* for its use in MFCs of MET mode. To achieve this goal, 1) we performed FBA to examine the maximum amperage output of metabolic-driven electricity generation based on *C. reinhardtii* in three cultivation conditions, namely, mixotrophic, photoautotrophic and heterotrophic growths (Table 5-1), since these nutritional modes generally govern the metabolic efficiency for current production in MFCs; 2) We then demonstrated theoretical trade-offs between amperage yield and the biomass production (growth) rate; 3) For elucidation of the metabolic strategies for sustaining free NADH flux for electricity generation in the MET mode, we implemented FATMIN to identify the fundamental metabolic mechanisms chosen by the cell to regenerate a surplus of NADH for current output, subject to stoichiometric balance and substrate uptake; 4) In the end, we analysed the effect of varying substrate (i.e., the acetate and photon) uptake rate on the growth rate and the amperage output in the three conditions.

Table 5-1: The metabolism and electron transfer types investigated in the present metabolic modelling.

Organism	Transfer type	Electron source (Terminal bacterial electron shuttle)		Metabolic type
C. reinharditii	Mediator-driven	NADH	Aerobic	Mixotrophic
				Photoautotrophic
				Heterotrophic

5.2 Methods

5.2.1 Modelling electrode interactions

The interactions with an electrode were captured by introducing two reactions into the model reconstruction (Table 5-2). These reactions represent the net reaction between the reducing equivalents and the electrodes in MFCs, with mediators not shown because they act as intermediates only. Introduction of these reactions creates an additional escape channel for electrons, and their fluxes are subject to the mass balance rule in the FBA modelling. Because NADH and NAD are native metabolites of the microorganisms, the added equations do not cause production of non-native by-products. The process is schematically shown in Figure 5-1.

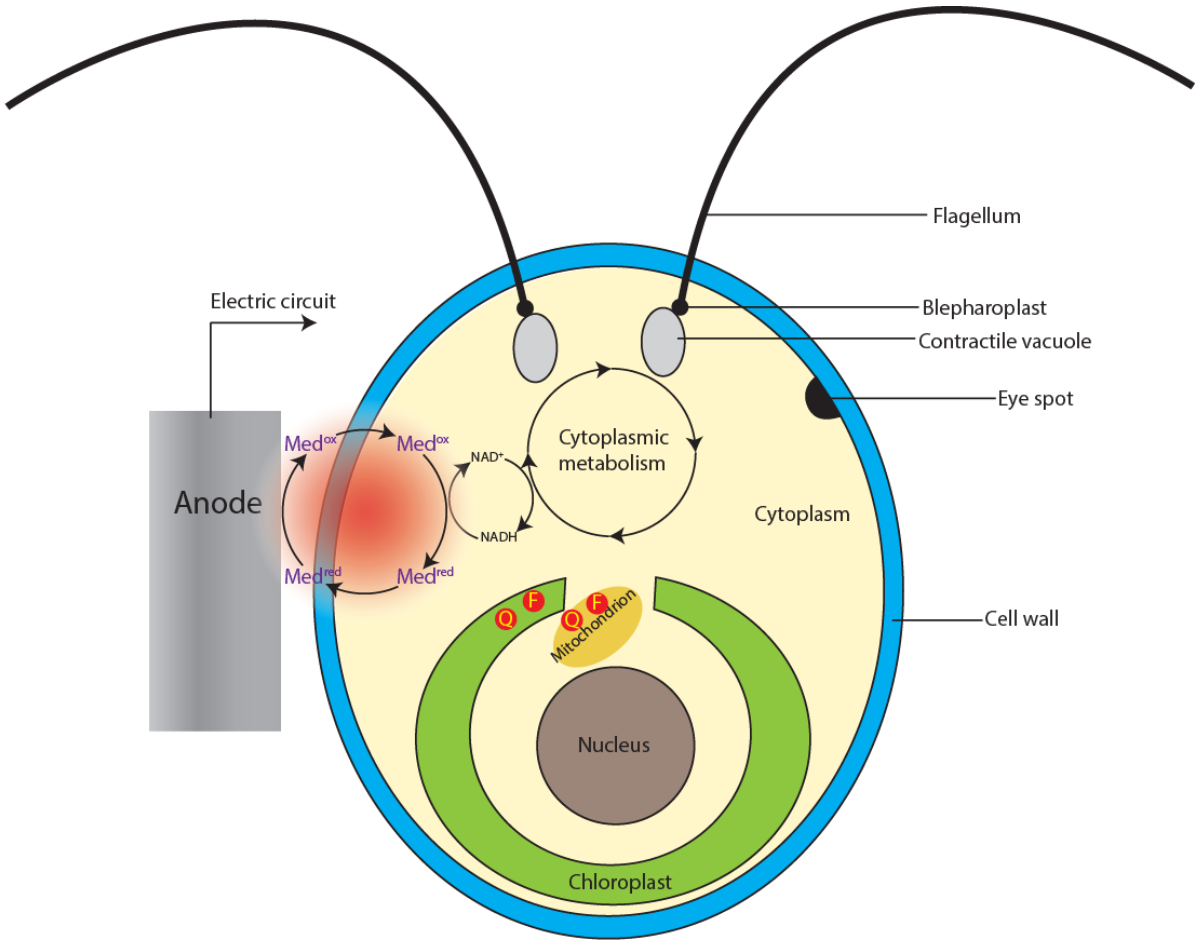

Figure 5-1: A schematic of the modeled anodic mechanisms where the cytoplasmic NADH/NAD$^+$ cycle as the electron supplier.

Microbes consume substrates (i.e., acetate and/or light) generating carbon dioxide and proton. This process yield electrons for metabolic benefit, i.e., growth, and reduces Med_{ox} in the cytosol into Med_{red}. Med_{red} diffuses into contact with the electrode, where Med_{red} reduces the electrode generating electrical current. The oxidized form, Med_{ox}, diffuses back through anolyte for reuse by the microbes. Radial red circle highlights the redox cycle supplying the electron to the anode, which is investigated in the present modelling. The iron/sulfur proteins such as ferredoxin (F) and quinone pool (Q) formed in the photophosphorylation and oxidative phosphorylation may also be a potential electron source to be targeted for current production.These reducing species are located in the membrane-surrounded organelles and are not studied in the present modelling. Other cellular compartments, such as flagellum and eyespot etc., are inclcuded in the genome-scale network model, but NADH contained in these compartments is not investigated since no evidence indicates that the mediators could reach the reducing power inside these organelles.

There is no empirical use of *C. reinhardtii* in MET-mode electricity generation. Scanning previous MFC studies indicates that the electron-transfer property of mediators can be specific to each cell design and vary between cells and operational conditions even for the same reaction. In addition, there is a continuous need for identifying or engineering the ideal mediator that possesses the favoured characteristics, as reviewed in [5, 52-55]. Since this study aimed at elucidation of the electricity generation potential of this microorganism, we only model the function of mediators. Once a useful theoretical ability for current generation

has been demonstrated, further investigation to identify a mediator and devise a device that can practically extract the electrons out of the *C. reinhardtii* will become justified.

Table 5-2: The added reactions for modeling the interaction of the microorganisms and the electrode in MFCs.

Operation mode of the MFC	Reaction ID	Reaction
MET	1NADHmfc	nadh --> nadh_mfc
	2NADHmfc	nadh_mfc --> nad + h_emm
nadh_mfc: the NADH available for MET mode of MFCs;		
h_emm: the H ions as the by-product released from the Reaction 2NADHmfc;		

5.2.2 Calculation of coulombic efficiency (CE)

The energy efficiency of converting acetate into MFC current is calculated the same way as described for *G. sulfurreducens* (CHAPTER 4).

To define a similar measure of how efficiently light uptake is converted to external MFC current, it is first noted that in each of the four photosynthetic reactions in the *C. reinhardtii* model (Table 5-3), one photon of an appropriate wavelength liberates one electron.

Therefore, the maximal electron count for a given illumination is given by its number of incident photons of these wavelengths. Starting from the spectral distribution of solar light, a "stoichiometric" representation in terms of eight discrete wavelengths was presented in reference [187]. Furthermore, the same work established that the 80% maximum O_2 photoevolution is consistent with an overall absorbed flux of 145 mmol/gDW/h (mE/gDW/h). The stoichiometric coefficients of the 4 active wavelengths add up to 0.4537, giving the value of 0.4537*145 = 65.79 mmol/gDW/h of electrons at full conversion. This yields the coulombic efficiency:

$$CE\% = \frac{C_{output}}{C_{substrate}} \times 100\% = \frac{\text{The MET flux (mmol/gDW/h)} \times 100}{\text{solar light uptake rate (mmol/gDW/h)} \times 0.4537}\% = \frac{\text{The MET flux (mmol/gDW/h)} \times 100}{65.79\ \text{(mmol/gDW/h)}}\%$$

Simple addition of the four coefficients as done above is questionable, in view of the fact that there appears to be some overlap between the spectral bands associated with the eight discrete wavelengths [16]. However, as all eight values add up to a value close to (although not equal to) 1, this is taken as sufficiently accurate for the present purpose.

Table 5-3: List of four light-dependent reactions in the network model [187].

photosystem I (blue light-activated)	[u] : fdxox + (2) pccu1p + (2) **photon437** + (2) h --> fdxrd + (2) pccu2p
photosystem II (blue light-activated)	[u] : (2) h2o + (4) **photon438** + (2) pq --> o2D + (2) pqh2
photosystem I (red light-activated)	[u] : fdxox + (2) pccu1p + (2) **photon680** + (2) h --> fdxrd + (2) pccu2p
photosystem II (red light-activated)	[u] : (2) h2o + (4) **photon673** + (2) pq --> o2D + (2) pqh2

The stoichiometries of the four active wavelength in these redox reactions indicate that each absorbed photon of the indicated wavelength carries one electron, since pqh2 and fdxrd each carries 2 electrons in *C. reinharditii* [187, 338]. The abbreviations of the metabolites are listed in [187].

5.2.3 Simulating the growth of *C. reinhardtii*

Mixotrophic, autotrophic and heterotrophic growths were modelled according to [187] by appropriately setting reaction flux constraints including environmental exchanges, non-growth associated ATP maintenance, O_2 photoevolution, starch degradation, and light- or dark-regulated enzymatic reactions. Particularly, for photoautotrophic and mixotrophic growth, the effective photon uptake rate was set to 145 mmol g DW^{-1} h^{-1} (37.795 μE m^{-2} s^{-1}), which corresponds to 80% maximum O_2 photoevolution [187]. For heterotrophic and mixotrophic growth, the maximum acetate uptake rate was constrained to 10 mmol g DW^{-1} h^{-1} [187].

5.2.4 Analysis technique

In this study we chose a metabolic network of *C. reinhardtii*, named iRC1080, as the computational analysis foundation. It is noted that two genome-scale network models, AlgaGEM [339] and iRC1080 [187] were published in the same period for *C. reinharditii*. Compared to AlgaGEM that focuses on capturing the metabolic mechanisms of hydrogen production [339], iRC1080 is a light-source-specific model containing the prism reactions that can accurately reduce the space of possible flux distribution relevant to any of the 11 different light sources. [187]. This allows the present study to model a growth dependent on solar lithosphere light. In addition, iRC1080 has considered the regulatory effects resulting from

lighting conditions as the light and dark conditions have been shown to affect metabolic enzyme activity in *C. reinhardtii*. Furthermore, iRC1080 has been thoroughly validated through simulations of 30 gene knockouts that exhibit characteristics in accordance with experimentally produced phenotypes.

5.3 Results and discussion

5.3.1 Impact of the redox perturbation on the biomass production

Figure 5-2 shows how production of mediated electron transfer (MET) aimed at cytosolic NADH competes with biomass production for metabolic resources. MET influenced the production of the NADH and biomass in the same way among the three studied nutritional modes. Specifically, the increase in MET drove the fluxes through the electron transfer reactions in three cultivation conditions towards their maximum allowable values and corresponding biomass formation rates to their minimum values. When only a small part of the energy is available to microorganisms in MFCs for their growth, a large part is converted to electricity.

(A) Heterotrophic growth

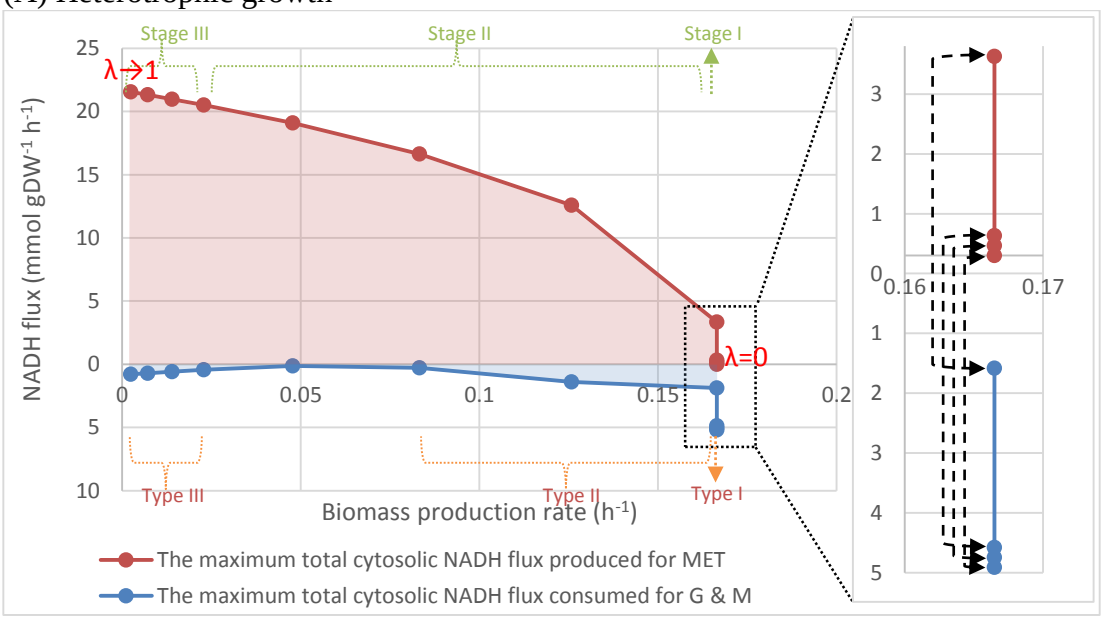

(B) Photoautotrophic growth

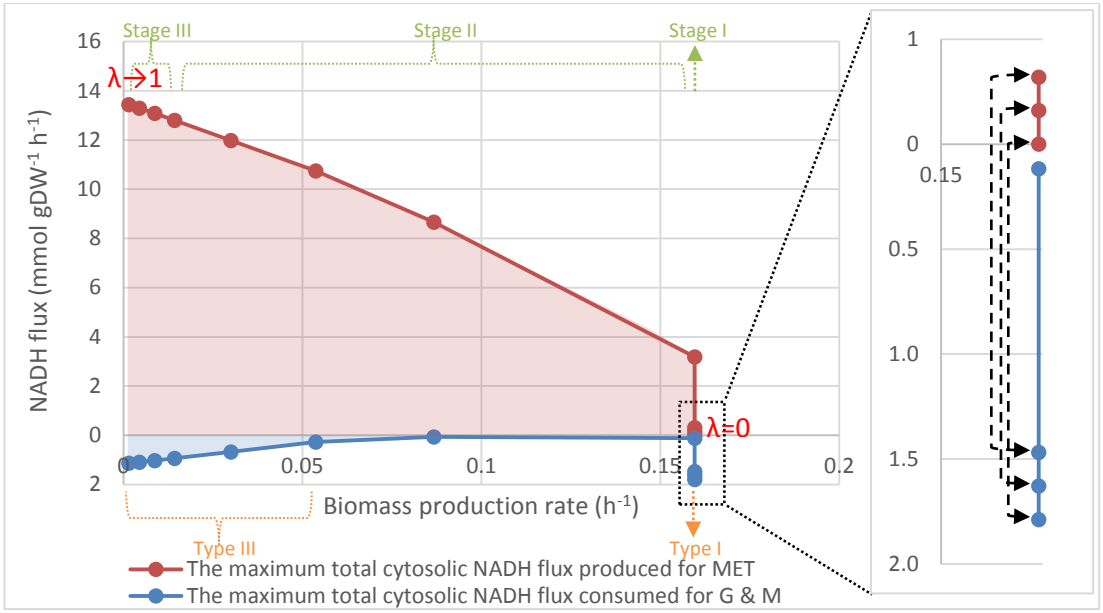

(C) Mixotrophic growth

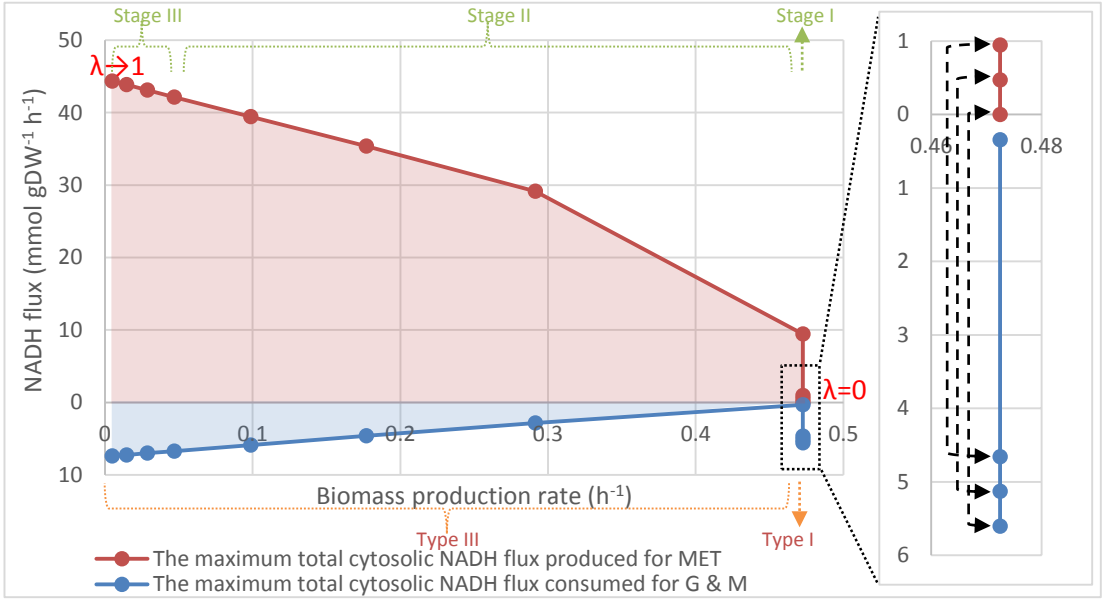

Figure 5-2: The relationship of the biomass production and electron transfer rates.

The NADH supplying rate in the MET mode and the NADH consumption rate for cellular use, as functions of biomass production rate. The red line represents the maximal NADH supplying rate for a feasible biomass production rate, while any point within the pink area represents all allowable NADH supplying rates and biomass production rates. The blue area represents the maximum total NADH-consuming flux for normal cellular function. The distance between the two lines across the pink and blue areas represents the total available NADH flux in the cell at a metabolic state related to a specific biomass production rate; inset, enlargement of boxed area; dashed line with arrowheads indicates which two data points are paired up. Types I-III (indicated by the orange brace and the arrow) are discussed in the context of the article.

Overall, compared with the base state optimised for growth, the heterotrophic, photoautotrophic and mixotrophic metabolisms had a potential to increase their NADH regeneration rates by about 4.292 (329%), 8.147 (715%) and 9.233 (823%), folds respectively under the highly NADH-perturbed metabolic states. The highest NADH_mfc flux modelled

here was about 21.56 mmol gDW^{-1} h^{-1} for the heterotrophic growth, 13.44 mmol gDW^{-1} h^{-1} for the photoautotrophic growth and 44.33 mmol gDW^{-1} h^{-1} for the mixotrophic growth, which were achievable when biomass production rate was suppressed by the external NADH demand to 0.0024, 0.00149 and 0.00493h^{-1} in the heterotrophic, photoautotrophic and mixotrophic modes respectively.

The present modelling limited the acetate uptake rate to a realistic range (0-10 mmol/gDW/h) to maximize the objectives, i.e., biomass production rate and cytosolic NADH-dependent electron transfer rates, in the three cultivation modes, and used a solar lithosphere light uptake rate of 145 mmol/gDW/h for the simulations of the mixotrophic and photoautotrophic nutritional modes. In the mixotrophic simulation, the acetate uptake rate stayed at the maximum (10 mmol/gDW/h) indicating that acetate is used maximally as an auxiliary energy source. This suggests that the increased fluxes through the NADH regenerating reactions did not result from the increased availability of acetate but were associated with the redirection of electron flux for biomass formation towards mediators in the MET mode.

In the mixotrophic mode, the respiratory and photosynthetic metabolisms were both activated and the maximum cytosolic NADH fluxes available for current production (44.33 mmol/gDW/h) was higher than the sum of the NADH fluxes (35 mmol/gDW/h) in the photoautotrophic (13.44 mmol/gDW/h) and heterotrophic modes (21.56 mmol/gDW/h). This synergetic relationship suggests that the substrate-to-NADH efficiency is improved by the combined functions of photosynthesis and respiration in the mixotrophic mode. The cellular energy of the algae can be supplied from two main sources: photophosphorylation and oxidative phosphorylation, but in the heterotrophic mode, in the absence of the light, photophosphorylation is inhibited. Then only oxidative phosphorylation functions are available to convert the energy released from the oxidation of acetate into the universal reducing shuttles, NADH, which is then used by cellular reactions to synthesize the required precursor metabolites (e.g., ATP, sterol and fatty acids) for growth. Since a number of light-dependent metabolic pathways are suppressed, the acetate efficiency is reduced in the heterotrophic metabolism.

The MET production rates shown in the top parts of Figure 5-2 for the three growth condition cases, only show a linear dependence on biomass growth for small growth rates. Starting from

the unperturbed state of zero MET production at the right hand side of the plots, the relationships between varying biomass production rate and the MET (NADH_mfc) rate can be divided into three stages (see Figure 5-2): 1) Stage I, the increase in the MET rate did not change the biomass production rate2) Stage II, further increase in the MET rate not only reduced the biomass production rate, but also decreased the conversion efficiency of metabolic resource into the MET flux. This is reflected by the downward curve associated with decreasing slopes of the lines between the data points, as the curve is followed from right to left. 3) Stage III, at the left hand side tail of the net NADH production curve, the rise in the MET rate was linearly proportional to the drop in biomass production rate.

The slope of the NADH production versus biomass growth curve as in Figure 1 gives a direct measure of the efficiency of the underlying pathways. A large slope means that NADH production increases by a large amount for a given cost in terms of biomass production and is therefore highly efficient, and vice versa. In the discussions below, we base interpretations of reallocations of metabolic resources to pathways with different efficiencies on this evidence directly derived from the modelling results.

On the other hand, as a result of increasing MET, the relationships between the varying biomass production rate and the NADH consumption for maintenance (Figure 5-2) can also be classified into three types: Type I is a decrease in the NADH consumption rate without changing the biomass production rate; Type II represents a decrease in the NADH consumed for maintenance, associated with a drop in biomass production rate; Type III describes a rise in NADH consumption resulting from a decline in the biomass production. Type I and III were found in the photoautotrophic and mixotrophic modes, whereas all the three types appeared in the heterotrophic metabolism.

Looking at the net NADH production (MET) curve, the Stage I relationship indicates that solutions exist for improving the flux of the NADH_mfc without compromising the growth rate. This is not inconsistent with the competition between biomass growth and NADH production that is observed in the other stages. For example, NADH that is here diverted to electricity production, may alternatively be used by the cell to produce secondary metabolites or other metabolic objectives, or simply be potentially available if e.g. the carbon uptake rate is increased.

The Stage II shows that further attempts to improve NADH_mfc production caused degradation in the other goal (i.e., to maximize growth rate), but the NADH production versus biomass (parametric sensitivity graph) plotted for *C. reinharditii* was non-linear, which is different from the linear relationship computed for *G. sulfurreducens* [280]. This indicates that different organisms have different metabolic mechanisms involved to cope with the heavy NADH drain. The shape of the curve could reflect the efficiency of NADH production in the different organisms. When the current output is low, many metabolic pathways are available to cope with the demand for the small increase in NADH diversion and thus the metabolism tends to choose those metabolic pathways with higher efficiency in converting the metabolic resource originally for the biomass production to the current output. As the current output augments, which means that the conversion efficiency becomes less important than the flux capability, the metabolism has to abandon the pathways with high conversion efficiency but lower maximum capability and reallocate the metabolic resources to those with higher flux capability. The non-linear curve shape corresponds to the complexity of the eukaryotic metabolism.

The Stage III behaviour sets in at very low growth rate values (less than about 10% of the maximum growth rates) in each of the three modes. In this range, as the demand for NADH_mfc increased, some NADH producing reactions were inactivated and the NADH regenerating mechanism switched to other reactions for higher production efficiency. It is thought that, due to the limited metabolic resources, the metabolism has to repress reactions with lower efficiency in NADH production, leaving the resource to those with higher catalytic rates to sustain the extremely high current output. As a result, the decrease in the biomass production rate was linearly proportional to the increase in the MET flux. This indicates that the solution space has been greatly reduced by the high MET rate and the remainder solutions are rigid in selection of reactions.

There is a partial correspondence between the three types of NADH consumption behaviours and the stages displayed by the MET production curves. Firstly, Stage I and Type I behaviours coincide, since in this range the increase in the MET is accompanied by a drop in the NADH consumption for cellular maintenance. This suggests that the increase in the flux of NADH_mfc results from a combination of two mechanisms, i.e., increasing the NADH production and decreasing the NADH needed for biomass production and maintenance.

Stage II (non-linear MET production) does not appear to be associated with any particular consumption type; it coincides with Type II consumption for heterotrophic growth and with Type III for mixotrophic growth.

Different from the heterotrophic growth mode, neither photautotrophic nor mixotrophic growth displays type II consumption as was found for the simpler metabolism of *G. sulfurreducens* [280], This difference suggests that in the mixotrophic condition where the acetate and light are both available, the metabolic characteristics of the *C. reinhardtii* are more similar to that of the photoautotrophic than to that of the heterotrophic, which lacks the metabolic activity of the Calvin-Benson cycle in the stoma of the chloroplast. The same feature has been found with another photosynthetic microorganism, *Synechocystis* sp. PCC6803, of which the mixotrophic and photoautotrophic metabolic characteristic are alike [340].

Stage III is well correlated with Type III in all three nutritional modes at low biomass production rates. This is interpreted to reflect that the solution space is extremely shrunk and the choice of reactions by the cell for NADH regeneration and for maintenance is limited. Type III behaviour is counterintuitive: a reduction in biomass growth would be expected to reduce the NADH consumption rate. The reason for this behaviour can be understood from differences in the reactions that mainly contribute to NADH consumption in the three nutritional modes, as further discussed below and summarised in Tables 1-3. Type III behaviour is most pronounced for mixotrophic growth, and this case Table 3 shows a notable NADH consumption by the nitrite oxidation reaction (ID: NITR), and its flux value of -7.193 accounts for very nearly all of the net consumption of NADH shown on the left of Figure 1(C). Similarly, the photoautotrophic flux of -1.06 in Table 2 is virtually identical with the net consumption shown for the maximum NADH_MFC production in Figure 1(B). Comparison of the flux values of NITR in the supplementary data confirms that this holds for all type III behaviour points, including the short type III range for heterotrophic growth in figure 1(A). So it is this single reaction that causes the somewhat anomalous behaviour. The NITR reaction can be seen as a key reaction to maintain the redox balance. It is also active in the absence of the external NADH drain, when its flux initially reduces as the biomass growth reduces. However, at some point the increasing external NADH demand upsets the NADH-NAD+ balance, and the flux of this reaction accordingly starts to increase giving rise to type III behaviour.

Overall, it is shown that mixo-/photoautotrophic and heterotrophic growth involve different combinations of stages of NADH production and types of NADH consumption curves. The way they are combined, may be not only specific to metabolism types, but also to different organism types (as exemplified by the distinction between *C. reinhardtii* in the present study and *G.sulfurreducens* in another study [280]). Since NADH is a currency molecule universal in all organisms, it would need to be considered how NADH production and consumption behaviours combine in different nutritional modes and organisms, in order to promote beneficial cooperation in a mixed microbial community such as biofilm.

The discussion above makes it clear that while NADH_mfc production competes with biomass growth for metabolic resources, not all gains in NADH_mfc production come at a cost to the growth rate, because some gains are also derived from reconfiguration of the metabolism. To quantify this observation we introduce a measure called the fractional benefit B (detailed in Methods section 3.10). In short, B is the sum of the fractions of maximal growth and NADH production respectively, achieved in a particular metabolic state. It indicates the combined benefit from both considerations. Figure 5-3 shows the result of this measure applied to the reported simulations. Starting from wild type growth rates (right hand side of the figures) the increased B values that result from type I behaviour is displayed, but moreover it is shown that in both heterotrophic and mixotrophic growth modes even further gains are achievable over a limited range of biomass rates. Only in the phototrophic mode is there a steady decline in the fractional benefit from the high achieved by type I. Even so, the combined benefit stays above the single objective baseline for all growth conditions and metabolic states. This observation supports the suitability of *C. reinhardtii* for cytosolic NADH targeted applications.

(A) Heterotrophic growth

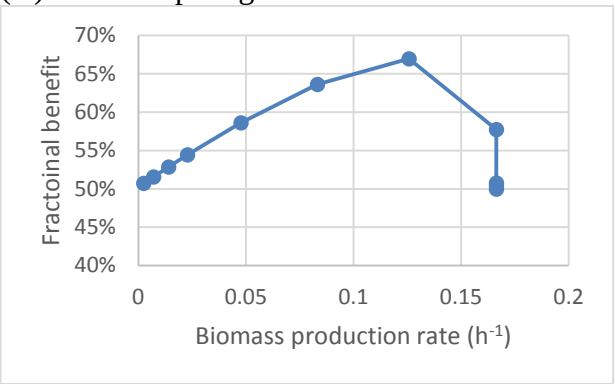

(B) Photoautotrophic growth

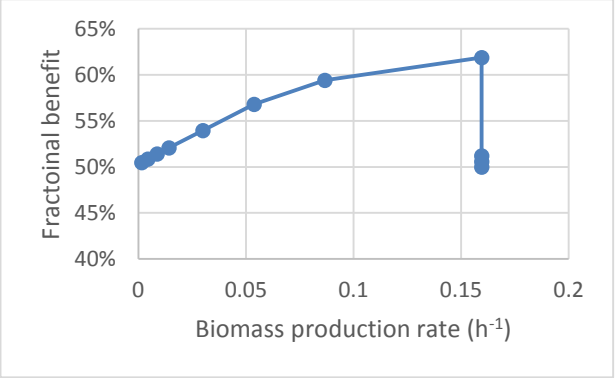

(C) Mixotrophic growth

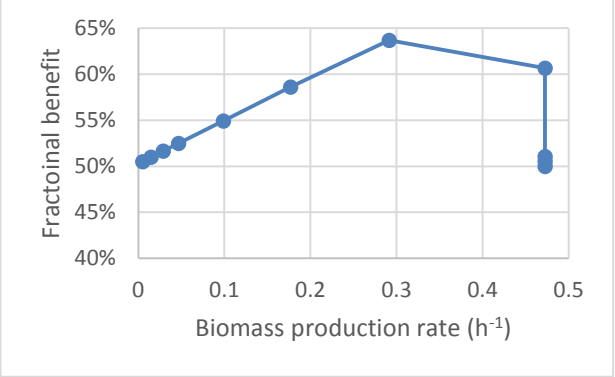

Figure 5-3: The effect of varying biomass production on the fractional benefit.

The fractional benefit B plotted on the vertical axis, is a measure of success in achieving the combined goals of maximal growth rate and MET flux. Maximizing one of these at a time, as at the endpoints, gives only B = 50%. The graphs show that relative to this, gains in MET flux can more than offset losses of growth rate in the *C. reinhardtii* metabolism.

The metabolic mechanisms underlying the high NADH regeneration rate in the three modes are elucidated in the next section. Table 5-4, Table 5-5 and Table 5-6 summarize a list of reactions (enzymes) that were responsible for the enhanced diversion of the cytosolic NADH flux towards current production.

5.3.2 Metabolic strategies for sustaining a high flux of cytosolic NADH under the three nutritional modes

5.3.2.1 Heterotrophic metabolism

Table 5-4: The identified reactions that contribute significantly to the predicted maximum MET rate in the heterotrophic mode.

Reaction ID	NADH flux (mmol/gDW/h)		Enzyme	EC No.	Reaction	Subsystem
	Min	Max				
ALCD19	-0.05348	13.78	alcohol dehydrogenase (glycerol, NAD)	1.1.1.2	[c] : glyald + nadh + h <==> glyc + nad	Glycerolipid metabolism
HBCO	0	13.78	3-Hydroxybutanoyl-CoA:NAD+ oxidoreductase	4.2.1.17 ;5.3.3.8	[c] : 3hbcoa + nad --> aacoa + nadh + h	Butanoate metabolism
NADH(h)tx	8.225	8.257	NADH transport, glyoxysome	N/A	h[c] + nadh[c] <==> h[x] + nadh[x]	Transport, glyoxysome
NADHth	0	3.664	nadh transport, chloroplast	N/A	nadh[c] <==> nadh[h]	Transport, chloroplast

(see the Appendix 2 for the FATMIN results of all 75 reactions involving NADH in the heterotrophic mode; Reaction ID abbreviations correspond to the names in [187].)

As a response to draining electrons away from NADH, a metabolic mechanism that regenerates NADH from NAD^+ at a high rate had to be activated to restore the redox balance for survival (growth). Two reactions, alcohol dehydrogenase (glycerol, NAD) (EC: 1.1.1.2) and 3-Hydroxybutanoyl-CoA:NAD^+ oxidoreductase (EC: 4.2.1.17;5.3.3.8) contributed significantly to the NADH_mfc flux (Table 5-4) in the heterotrophic mode. Each of these two reactions possessed capability to solely supply 13.78 mmol/gDW/h and thus any possible combinations of these two reaction fluxes that made up 62.50% maximum net NADH flux (22.04 mmol/gDW/h) were viable. This indicates that the number of optimal solutions will be unlimited. The non-uniqueness of the obtained solution corresponds to alternative optima in the linear optimization and the existence of alternative pathways that result in equivalent mutant phenotypes regarding the required metabolic adjustment.

Except the two identified cytosolic reactions, all other seventy NADH involved reactions were found to have very low flux values (absolute flux value < 1 mmol/gDW/h) with no variability ($v_{i\,min}/v_{i\,max}>0.99$) under high current output. The low flux values and rigid variability may be attributed to the fact that NADH is a highly connected metabolite ensuring

a degree of network connectivity sufficient to limit the availability of alternative flux distributions because of cascading effects on other metabolites.

In the heterotrophic mode, some portions of the increased cytosolic NADH flux were produced in the chloroplast and glyoxysome. The chloroplast could supply up to 3.663 mmol/gDW/h NADH flux, and glyoxysome obligately contributed 8.257 mmol/gDW/h, which accounts for 37.46% maximum computed MET flux. The flux of the NADH transport reaction between cytosol and glyoxysome was inflexible, implying that the maximum MET flux and biomass production rate are limited by the metabolic activity in the glyoxysome, which is associated with fatty acid mechanism mediated by a range of oxidoreductases.

5.3.2.2 Photoautotrophic metabolism

Table 5-5: The identified reactions that contribute significantly to the predicted maximum MET rate in the photoautotrophic mode.

Reaction ID	NADH flux (mmol/gDW/h)		Enzyme	EC No.	Reaction	Subsystem
	Min	Max				
ALCD19	-0.00029	5.669	alcohol dehydrogenase (glycerol, NAD)	1.1.1.2	[c] : glyald + nadh + h <==> glyc + nad	Glycerolipid metabolism
HBCO	0	5.669	3-Hydroxybutanoyl-CoA:NAD+ oxidoreductase	4.2.1.17; 5.3.3.8	[c] : 3hbcoa + nad --> aacoa + nadh + h	Butanoate metabolism
HDH	4.340	4.340	histidinol dehydrogenase, cytosol	1.1.1.23	[c] : histd + (2) nad + h2o --> his-L + (2) nadh + (4) h	Histidine metabolism
NITR	-1.060	-1.060	nitrate reductase (NADH)	1.7.1.1	[c] : no3 + nadh + h --> no2 + nad + h2o	Nitrogen metabolism
OGMG	4.339	4.340	4-oxoglutaramate generation (non-enzymatic)	N/A	[c] : 4izp + (2) nad + (3) h2o + h --> 4ogm + for + nh4 + (2) nadh	Nitrogen metabolism; Histidine metabolism

(see Appendix 2 for the FATMIN results of all 75 reactions involving NADH in the photoautotrophic mode; Reaction ID abbreviations correspond to the names in [187].)

Four NADH producing reactions and one NADH consuming reactions were mainly responsible for the identified maximum net NADH flux (13.30 mmol/gDW/h) in the photoautotrophic mode (Table 5-5). Among the five reactions, the fluxes of three reactions were invariable. The two NADH producing reactions, catalysed by histidinol dehydrogenase (EC: 1.1.1.23) and 4-oxoglutaramate generation (non-enzymatic), could each contribute 32.63% of the 13.30 mmol/gDW/h, whereas another reaction, nitrate reductase (NADH) (EC: 1.7.1.1), consumed 1.060 mmol/gDW/h NADH flux for maintaining growth function of cell. The three reactions with rigid flux ranges amounted to 7.619 mmol/gDW/h NADH production rate, which accounted for 57.30% of maximum net NADH flux. The remaining 42.7 % maximum net NADH flux was mainly contributed by any combination of the other two reactions, alcohol dehydrogenase (glycerol, NAD) (EC: 1.1.1.2) and 3-Hydroxybutanoyl-CoA:NAD^+ oxidoreductase (EC: 4.2.1.17;5.3.3.8). Each of these two reactions could contribute up to 42.63% maximum net NADH flux.

5.3.2.3 Mixotrophic metabolism

Table 5-6: The identified reactions that contribute significantly to the predicted maximum MET rate in the mixotrophic mode.

Reaction ID	NADH flux (mmol/gDW/h)		Enzyme	EC No.	Reaction	Subsystem
	min	max				
ALCD19	0	23.95	alcohol dehydrogenase (glycerol, NAD)	1.1.1.2	[c] : glyald + nadh + h <==> glyc + nad	Glycerolipid metabolism
HBCO	0	23.95	3-Hydroxybutanoyl-CoA:NAD+ oxidoreductase	4.2.1.17; 5.3.3.8	[c] : 3hbcoa + nad --> aacoa + nadh + h	Butanoate metabolism
HDH	13.53	13.53	histidinol dehydrogenase, cytosol	1.1.1.23	[c] : histd + (2) nad + h2o --> his-L + (2) nadh + (4) h	Histidine metabolism
NITR	-7.193	-7.193	nitrate reductase (NADH)	1.7.1.1	[c] : no3 + nadh + h --> no2 + nad + h2o	Nitrogen metabolism
OGMG	13.5	13.53	4-oxoglutaramate generation (non-enzymatic)	N/A	[c] : 4izp + (2) nad + (3) h2o + h --> 4ogm + for + nh4 + (2) nadh	Nitrogen metabolism;Histidine metabolism

(see Appendix 2 for the FATMIN results of all 75 reactions involving NADH in the mixotrophic mode; Reaction ID abbreviations correspond to the names in [187]).

The mixotrophic metabolism involved the same set of reactions for NADH production as the photoautotrophic metabolism and relied on mainly four NADH producing reactions and one NADH consuming reaction (Table 5-6). Three NADH involved reactions, histidinol dehydrogenase (EC: 1.1.1.23), nitrate reductase (NADH) (EC: 1.7.1.1) and 4-oxoglutaramate generation (non-enzymatic) (N/A), were found to have inflexible flux ranges and their flux values added up to 19.88 mmol/gDW/h, which contributed 45.33% of the maximum net NADH flux (i.e., the maximum MET flux of 43.84 mmol/gDW/h). In addition, the increasing flux of nitrate reductase (NADH) (EC: 1.7.1.1) mainly underlay the observed elevating NADH consumption for internal use at the low growth rates that increased NADH_mfc in mixotrophic and photoautotrophic conditions (Figure 5-2 B &C). The remaining 54.67% NADH flux (28.96 mmol/gDW/h) was supplied by the other two reactions, alcohol dehydrogenase (glycerol, NAD) (EC: 1.1.1.2) and 3-Hydroxybutanoyl-CoA:NAD^+ oxidoreductase (EC: 4.2.1.17;5.3.3.8). Each of these two reactions possessed capability to solely supply 23.95 mmol/gDW/h and thus any possible combinations of these two reaction fluxes that made up 54.67% maximum net NADH flux (28.96 mmol/gDW/h) were viable.

Comparison of the metabolic strategies in the three nutritional modes indicates that two reactions, alcohol dehydrogenase (glycerol, NAD) (EC: 1.1.1.2) and 3-Hydroxybutanoyl-CoA:NAD^+ oxidoreductase (EC: 4.2.1.17;5.3.3.8), played a key role in supplying NADH flux in all three cases. Unlike the mixotrophic and photoautotrophic metabolisms in which the cytoplasmic reactions were involved to regenerate NADH at high rate, part of the increased cytosolic NADH flux in the heterotrophic mechanism was produced in the chloroplast and glyoxysome.

To elucidate how nutrient uptake is conveyed to biomass growth and current yield respectively, Table 5-7 compares the corresponding fluxes at different uptake rates.

5.3.3 Effect of varying acetate or photon uptake rates on predicted biomass and reducing equivalent production rates

Table 5-7: The summary of linear functions of the biomass production and MET rates

	Metabolic type	Substrate	Growth (g/gDW/h)	MET (g/gDW/h)	MET (mmol/gDW/h)
Aerobic	Hetero-	acetate	y_c=0.0168x y_p=0.0007x+0.0003	$y_{(g/gDW/h)}$=1.4754x	$y_{(mmol/gDW/h)}$=2.2239x
	Photo-	solar light	y_c=0.0011x y_p=3E-05x	$y_{(g/gDW/h)}$=0.064817x	$y_{(mmol/gDW/h)}$=0.0977x
	Mixo-	acetate	y_c=0.0308x+0.1647 y_p=0.001x+0.0045	$y_{(g/gDW/h)}$=2.0256x+8.856	$y_{(mmol/gDW/h)}$=3.0533x+13.349
		solar light	y_c=0.0011x+0.3095 y_p=2E-05x+0.0117	$y_{(g/gDW/h)}$=0.040801x+23.266	$y_{(mmol/gDW/h)}$=0.0615x+35.069

Note: The FBA simulations were performed by changing the photon uptake rate and the acetate uptake rate with the maximization of the objectives. y denotes the MET rate (mmol/gDW/h or g/gDW/h) or growth rate (g/gDW/h), whereas x represents the substrate (i.e., acetate or light) uptake rates (mmol/gDW/h). y_c represents the optimal growth, whereas y_p denotes the perturbed growth under cytosolic NADH deprivation.

The biomass production rates or the electron transfer rates were all linearly proportional to the substrate (i.e., acetate or sun light) uptake rate in the three cultivation conditions (Table 5-7). This suggests that substrate (i.e., either acetate or light) uptake rate is the major limiting factor for both biomass and current yields.

The table shows the linear regression equations first in units (gDW/gDW/h) (column 4) for comparison with the biomass rate, and then in the standard flux units (mmol/gDW/h) in

column 5. Column 3 shows that the slopes of the linear equation for the growth rate versus substrate uptake rate were highly reduced when the cell experienced severe NADH deprivation (modelled by λ of 0.9998). Comparison of columns 3 and 4 indicates that the slopes of the linear equation for the NADH production were all much higher than that for the growth rate, hence the current production was much less substrate-costly than the biomass production.

The mixotrophic metabolism achieved the highest substrate-to-NADH efficiency (slope=3.0533 for the acetate and slope=0.0615 for the photon), followed by the heterotrophic metabolism (slope=2.2239 for the acetate) and the photoautotrophic the lowest (slope=0.0977 for the photon). Under mixotrophic cultivation, although the extra acetate consumption slightly reduced the efficiency of converting light into the NADH (slope =0.0615 in the mixotrophic mode versus slope=0.0977 in the photoautotrophic), the additional uptake of the light increased the acetate-to-NADH efficiency by about 1.4 folds (37%). This may be attributed to the fact that some by-products of the photosynthesis could be the substrates for some NADH-regenerating reactions of the acetate-dependent metabolic processes.

Finally, the three operation modes are compared for their theoretically maximum current output in Figure 5-4 and Table 5-8.

5.3.4 Comparison of amperage output of the three nutritional modes

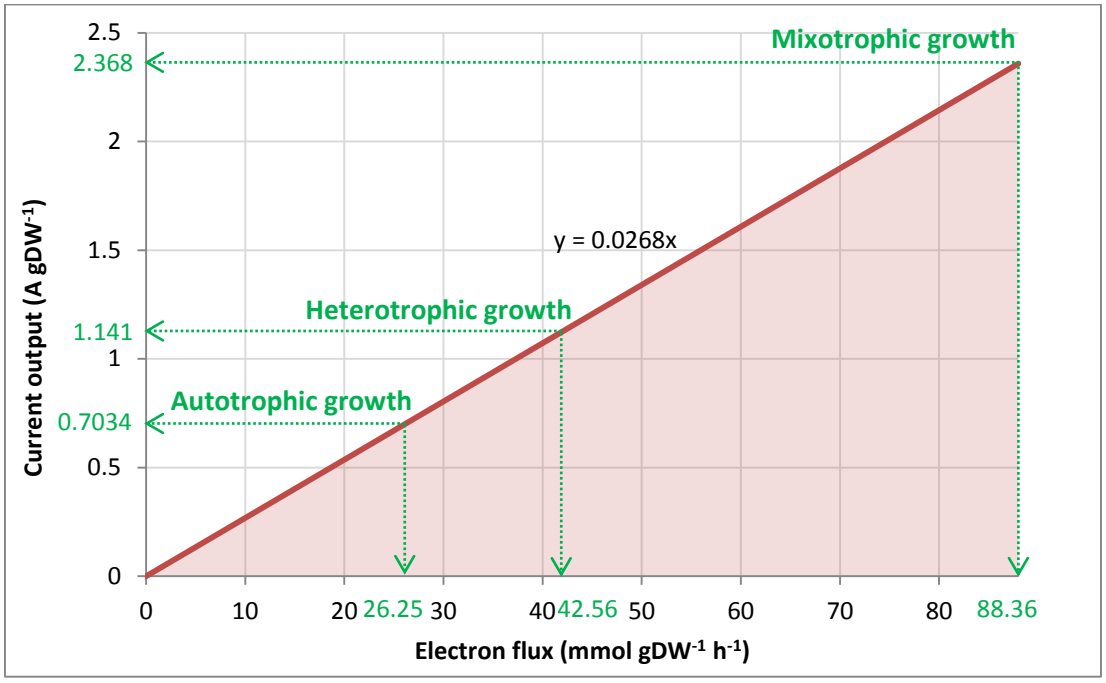

Figure 5-4: The current output (A/g) as a function of electron flux.

The dark red line denotes the maximal current outputs and NADH_mfc production rate, while the area represents all allowable current outputs and electron production rates. The round dotted arrow line indicates the maximal current output and corresponding electron production rate when the growth rate is set to 5% of the predicted maximum growth rate (0.007981h^{-1}).

Table 5-8: Comparison of the predicted amperages and power outputs of the three modes.

Nutritional mode	Conditions	Biomass production rate (h^{-1})	Electron (mmol gDW^{-1} h^{-1})	Amperage (A gDW^{-1})	Coulombic efficiency (CE%)	W gDW^{-1}
Heterotrophic	Boyle's experimental data	0.035	39.71	1.064	49.64%	0.8835
Autotrophic		0.059	26.89	0.7206	40.87%	0.5988
Mixotrophic		0.066	82.31	2.206	56.46%	1.831
Heterotrophic	5% of optimal autotrophic growth rate	0.007981	42.56	1.141	53.20%	0.9467
Autotrophic			26.25	0.7035	39.90%	0.5839
Mixotrophic			88.36	2.368	60.61%	1.966

Two groups of the metabolic states were chosen as the references for the inherent capability of *C. reinahrdtii* for current output and coulombic efficiency. The first group of reference metabolic states was simulated based on the growth rates experimentally obtained [315]. The second group of reference states were based on the assumption that 5% optimal growth would be the minimum viable growth rates in practise. Based on the computed current outputs for the 5% optimal growth, mixotrophic cultivation (2.368 A/gDW and 60.61% CE) is more suitable for the electricity generation than the phototrophic (0.7035 A/gDW and 39.90% CE) and heterotrophic growths (1.141 A/gDW and 53.20% CE). The photoautotrophic metabolism achieved relatively low coulombic efficiency values, because the photosynthesis is much less efficient in conversion of absorbed light into chemical energy than the acetate-dependent respiration. Although photoautotrophic metabolism produced the lowest current (0.7035 A/gDW), this cultivation condition is still competitive for use in MFCs, since the carbon source is no longer required reducing the operation costs.

It is difficult to compare the computed outputs with other MFCs results in the literature, as published values were calculated based on per electrode area and the electrodes have different designs such as mesh, plate or multi layers. Another output unit is based on amperage per litre of the culture, but, as exemplified in a 2005 study of *C. reinhardtii* based MFC [210], the cell density number was usually not provided. Nevertheless, here based on the dry mass of the *C. reinhardtii* of 48 pg/cell [187] and an observed concentration of 1g/L [341], the computed maximum output of *C. reinhardtii* under mixotrophic mode in the present study can be converted into 113.7 pA/cell and about 2.368 A/L respectively. This value is much higher than the previously measured maximum current output of 16.68 μA/(L culture) from an MFC based on *in situ* oxidation of hydrogen photosynthetically produced by *C. reinhardtii* [210].

Two recent studies have evaluated the electrogenic activity of mixed microalgae in anaerobic and oxygenic MFCs under the mixotrophic nutritional mode [264, 342]. The mixed microalgae was dominated by the presence of *Ankistrodesmus, Chlorella, Oscillatoria, Scenedismus, Diatom* and *Cosmarium* [343]. They suggested that it might be the Bc1 complex in the electron transfer chain that is the electron donor for the electricity generation. The results showed that under aerobic conditions, the mixed microalgae produced 8.571 $\mu A/cm^2$ during daytime and 0.1429 $\mu A/cm^2$ during the night [343]. Under the anoxygenic condition, the same mixed microalgae could output a stable current density of 45.71 $\mu A/cm^2$ [342]. Since the cell density was not specified in these studies, these literature data could not be

directly compared with the presently computed amperage output for the pure culture of *C. reinhardtii*.

The present study showed that the current outputs were determined by the uptake of the substrates, i.e., acetate and photons. A maximum observed acetate uptake rate of 10 mmol/gDW/h was used as the upper limit for modelling the three nutritional modes. Nonetheless, a relatively conservative photo uptake rate, 145 mmol/gW/h, was used for modelling the mixotrpohic and photoautotrophic modes. This photon uptake rate is lower than the upper limit used in the original model file, i.e., 646.1 mmol/gDW/h, which indicates that the current outputs calculated for photoautotrophic and mixotrophic growths might be conservatively computed in the present study.

The present study did not regard anaerobic conditions as a prerequisite for modelling the electricity generation and allowed oxygen consumption by the organism. The aerobic metabolism possesses a higher efficiency in degradation of organic compounds in algal species, but the presence of oxygen may intercept the electrons to be diverted to the anode in MFCs in practice [343]. Nonetheless, an aerobic MFC that allows the existence of oxygen in an anodic chamber has also been recently developed [46, 278].

The present flux model was built based on the mass balance and stoichiometric conversion rules with respect to the objective function that maximises the growth rate. Nevertheless, in eukaryotic cells, other objectives such as maximising ATP or entropy could become more dominant in influencing the NADH production than maximization of the growth rate. For example, in a multicellular system, the unlimited growth rate leads to the formation of a tumor and the primary objectives of some pancreas cells could be maximizing production of insulin. Also, regulatory mechanisms could take effect to prevent the NADH flux re-directed outside for MFCs. All these unidentified factors may impose burdens for the cell in achieving the optimal metabolic state for NADH extraction for MFCs.

This study investigated cytosolic NADH as an electron source for electricity generation, since the cytoplasm is where the main cellular metabolism takes place and the putative mediator that passes through the cell membrane should reach the cytoplasm first. It is also possible for the mediator to travel through the cytoplasm to arrive in the next barrier, the membrane of the

mitochondria and chloroplast, and subsequently form a redox cycle with the reducing electron shuttles within these two organelles. Nonetheless, this putative MET mode is expected to be less practical than cycling of a cytosolic NADH/NAD^+ pair to supply electrons to the anode. Future study could extend the present findings to further investigate the organelles such as mitochondria and chloroplast as the electron supplier with the methods provided here. This could be done in a similar way as the electron transfer from c-type cytochrome that was modelled in the study of *G. sulfurreducens* [280].

Although the use of NADH obviates the electrical potential loss during the redox chemical molecules conversion [22, 41] and has been suggested as the optimal intracellular electron source for mediated electron generation process [36], the electricity generation may also target other electron carriers as the election suppliers, including a range of metabolites involved in primary (e.g, NADPH [20], ferredoxin [344] and quinone pool [99]) and secondary (e.g., serotonin [345]) metabolisms. The primary metabolites are the compounds that are essentially connected to the microbial metabolism, whereas secondary metabolites are not directly connected to the main metabolism and consist of a variety of different compounds [51]. Besides, the primary metabolites are similar in all groups of living organisms, while the secondary metabolites can be different for various organisms [51]. It is generally accepted that the availability of NADH determines the production of secondary metabolites and the higher energy organic molecules that are building blocks for the biomass.

The present modelling could not differentiate the regeneration capability of NADH and NADPH. In other words, NADH and NADPH are exchangeable for achieving the same maximum reducing power for current production. This may be attributed to the incomplete set of constraints in the model (e.g. enzyme capacity, regulatory, thermodynamic, or other constraints). For example, the network model used did not consider material fluxes and signalling interactions between compartments. In the future, these fluxes and interaction information can be obtained through isotopic tracers such as 13C, or measurement of compartment concentrations such as using fluorescence resonance energy transfer (FRET) techniques [346].

Generally, NADH is commonly used in reactions related to energy metabolism [21, 31], which is different from the other chemically similar redox cofactor, NADPH, involved in

biosynthesis of cellular components and defence systems against oxidative stresses [32]. In addition, synthesis of NADH is more energetically efficient than NADPH in the heterotrophic nutritional mode [347]. Since the previous experimental MFC studies could not explain the roles of NADH and NADPH in the electricity generation in practice [61] and maintaining a proper NADH/NAD^+ balance is much more important to biomass production [348], here we presume the metabolic perturbation caused by the current output would have a direct impact on the energy metabolism, instead of NADPH-dependent anabolic reactions.

5.4 Conclusions

Analysis of the metabolic flux models predicted that *C. reinhardtii* has a potential to output current at up to 2.368 A/gDW in the mixotrophic nutritional mode, 0.7035 A/gDW in the photoautotrophic mode, and 1.141 A/gDW in the heterotrophic mode. These computed high current values will serve as the theoretical maximum limits of the current output for *C. reinhardtii* and are expected to be achieved through the metabolic engineering strategies such as adaptive evolution and gene knockout strategies. Nevertheless, the practical current production reliant on the metabolic activity elucidated here, necessitates development of proper mediators able to pass through the eukaryotic cell wall and efficiently extract the NADH from the identified enzymes.

This study has also identified a set of essential reactions that can regenerate NADH efficiently to sustain the high current production in each case of the three nutritional modes. It is shown that the three modes shared two common reactions, catalysed by alcohol dehydrogenase (glycerol, NAD) (EC: 1.1.1.2) and 3-Hydroxybutanoyl-CoA: NAD^+ oxidoreductase (EC: 4.2.1.17; 5.3.3.8), for supplying NADH at a high rate. Unlike the mixotrophic and photoautotrophic modes, the elevated current production in the heterotrophic mode involved combined mechanisms of two other organelles, i.e., glyoxysome and chloroplast, which produced NADH and transported them out to the cytoplasm for electron extraction. These results could represent a promising starting point for future studies to tune engineering solutions to harvest optimal current yields with minimal energy costs.

CHAPTER 6 Elucidation of the innate potential of *Synechocystis* sp. PCC 6803 for electricity generation in mediated and direct electron transfer modes

The materials in this chapter have been published in [349].

6.1 Introduction

The previous two chapters have shown that *Geobacter* and *Chlamydomonas* each have specific advantages as MFC biocatalysts. The simple prokaryotic cell structure of *Geobacter* and its ability to grow pili makes it accessible for mediators and allows it to function in both MET and DET modes. *Chlamydomonas*, on the other hand, has a more efficient and resilient metabolism as an eukaryote and can benefit from synergies between its photosynthesis and nutrient-based growth modes. In this chapter, we now explore if it is possible to combine these advantages by using a photosynthetic prokaryote as the biocatalyst.

Synechocystis sp. PCC 6803 has become a popular model photosynthetic organism studied by many researchers after its genome was fully sequenced in the 1990s [234, 235]. Since this cyanobacteria species is a photoautotroph that divides rapidly, it has been enlisted as a platform for production of biofuels by using sunlight as an inexpensive energy source [236, 237]. However, biofuels need to be further processed (e.g., combustion) to be transformed into a usable energy form such as electricity. An alternative way to exploit the energy production potential of *Synechocystis* sp. PCC6803 is to apply this prokaryote as biocatalyst in a microbial fuel cell (MFC), so as to directly convert metabolic activity inside the cell into electricity.

Synechocystis sp. PCC6803 in MFCs can produce current through three mechanisms: MET, DET and product modes [47]. For the product mode, hydrogen produced by *Synechocystis* sp. PCC 6803 can be *in situ* oxidized at the anode, releasing the electrons to the electric circuit. Akin to the green algae *C. reinhardtii, Synechocystis* sp. PCC 6803 relies on hydrogenases for hydrogen generation [233]. However, these enzymes are 100 times less active than the

analogues of *C. reinhardtii* [217] and their activities can be inactivated by O_2. This creates a major barrier for practical hydrogen production. Moreover, the anodic oxidation of hydrogen demands a high pressure that causes safety issues. Due to these biochemical and engineering limitations, it would be impractical to further study the use of *Synechocystis* sp. PCC 6803 in product-mode current production.

In the DET mode, the cytochromes of the electron transfer chain in the cell membrane can directly release electrons to the anode. This operation mode requires attachment of the cell to the anode. Unlike another exoelectrogen, *G. sulfurreducens*, in which the electrons are derived from biochemical oxidation of organic compounds via the respiratory electron transfer chain [238], *Synechocystis* sp. PCC 6803 has an advantage that it obviates the need for exogenous organic fuel and thus its electrogenic activities are entirely dependent on the energy of light [98, 239, 240]. In the DET mode, *Synechocystis* sp. PCC6803 achieved a steady power density of 6.7 mW m^{-3} (peaking at 7.5 mW m^{-3}) [241, 242]. This power density is still much lower than the values achieved by other commonly used biocatalysts. Nevertheless, because the DET mode of this cyanobacterium is directly linked to its photosynthetic activity and the quoted measurement is quite recent, it is worth exploring if this organism has the potential to deliver competitive power densities.

For the MET mode, an exogenous mediator is involved as an electron relay to pull the elections away from metabolism and deliver them to a remote electron acceptor (anode) [51]. *Synechocystis* sp. PCC 6803 are prokaryotes, and their simpler cell membranes and internal structure are more amenable to physical electron extraction than eukaryotes. Two intracellular redox carriers, reduced ferredoxin and plastoquinol, have been proposed to be the electron sources targeted by mediators such as 2-hydroxy-1,4-nepthoplastoquinol (HNQ) [23, 99, 344] in MFCs.

In addition to these two shuttles, the currency molecule NADH has received considerable attention [19-24]. NADH is universally involved in the energy metabolism of all living organisms. Maintaining a proper balance of NADH/NAD+ is a primary biological objective that is important to biomass production [348]. Any steps of NADH regeneration in the intracellular electron-transfer pathways in cells could be targeted by exogenous mediators, such as bromocresol green (BG) and neutral red (NR), which can convey the electrons to an

extracellular electrode (anode) [36, 37, 40]. Importantly, due to the relatively low (negative) potential of NADH, it has been proposed that the theoretical limit of MFC voltage output is the potential difference between NADH and the reaction in the cathode in an MFC [22, 41]. Therefore, targeting NADH as the electron source in MFCs of MET mode can liberate the maximum power achievable for a microorganism.

Since *Synechocystis* sp. PCC6803 has been actively studied as a promising biocatalyst for electricity generation, in this study, we employed computational metabolic engineering tools to elucidate the innate capability of *Synechocystis* sp. PCC6803 for current production. Specifically, 1) we performed FBA to compute the maximum amperage output and pertinent metabolic behaviours of *Synechocystis* PCC6803 in the five electron transfer cases consisting of (Table 6-1): ferredoxin-and quionone-dependent photoautotrophic mode, NADH-dependent photoautotrophic, heterotrophic and mixotrophic modes; 2) We then investigated the trade-offs between amperage output and the biomass production (growth) rate; 3) For elucidation of the fundamental metabolic mechanisms supporting the desired electron transfer in the five cases, we implemented FVA to compute the strategies used by the cell to maximize the current production, subject to stoichiometric balance and substrate uptake; 4) In the end, we analysed the effect of varying substrate (i.e., the glucose and photon) uptake rate on the growth rate and the amperage output in the each of the five modes.

Table 6-1: The metabolism and electron transfer types investigated in the present metabolic modelling.

Organisms	Transfer type	Electron source (Terminal bacterial electron shuttle)		Metabolic type
Synechocystis sp. PCC6803	Membrane-driven	Ferredoxin	Aerobic	Photoautotrophic
		Plastoquinol/ c-type cytochrome (*)		Photoautotrophic
	Mediator-driven	NADH		Photoautotrophic
				Heterotrophic
				Mixotrophic

*. The flux model of *Synechocystis* cannot identify the difference between these two sites for electricity generation.

6.2 Methods

6.2.1 Modelling assumption for DET mode

Although the MFC electricity generation based on the DET mode of the *Synechocystis* has been experimentally observed [239, 240], the molecular mechanisms (what proteins and what reactions) underlying the DET has not been clearly elucidated for this strain (albeit it is proposed that the electron transfer chain in the membrane related to the electrogenic activity). Therefore, to examine the current production potential of the DET mode of the *Synechocystis* in the present modelling, an assumption is made based on the general paradigm of the mechanisms of the DET mode – the c-type chromosome mediated electron transfer. Such a DET mechanism has been well established for the two most commonly used MFC biocatalysts, *Geobacter* sp. and *Shewanella* sp. (reviewed by [47]). These two species possess nanowires, electrically conductive bacterial appendages, to directly transport electrons from cells to solid electron acceptors such as graphite anodes in MFCs [26, 62, 271] and this electron transfer process is fundamentally mediated by the c-type cytochrome in the cell membrane [63, 350]. Since these two microbes and the *Synechocystis* are all gram-negative prokaryotes sharing similar cell membrane structures, the present study presumed that the state-of-the-art DET mechanism in the *Synechocystis* would be mediated by the c-type cytochromes.

6.2.2 Modelling electrode interactions

The interactions with an electrode were captured by introducing six reactions into the model reconstruction (Table 6-2).

Table 6-2: the added reactions for modeling the interaction of the microorganisms and the electrode in MFCs.

Operation mode of the MFC	Reaction ID	Reaction
Ferredoxin-dependent MET	ferred_mfc	ferred --> ferred_mfc
	EX_ferred_mfc	ferred_mfc --> feroxd
Plastoquinol-dependent MET/ Cytochrome *c* dependent DET	qh2_mfc	qh2 --> qh2_mfc
	EX_qh2_mfc	qh2_mfc --> q
NADH-dependent MET	1NADHmfc	nadh --> nadh_mfc
	2NADHmfc	nadh_mfc --> nad + h_emm

ferred_mfc: the reduced form of ferredoxin that supply the electrons to anode

qh2_mfc: the plastoquinol that supply the electrons to anode;

nadh_mfc: the NADH available for MET mode of MFCs;

h_emm: the H ions as the by-product released from the Reaction 2NADHmfc;

Other abbreviations are detailed in [188].

When the electricity generation is linked to the reduced ferredoxin, electrons are deprived of this redox shuttle, accompanied by accumulation of oxidised ferredoxin. Thus, we model this process by introducing the equation. Ferredoxin -> ferredoxin_mfc. Each reduced ferredoxin carries only one electron, which is different from NADH.

The efficiency of the DET mode is dependent on the availability of type-c cytochrome. The production of this cytochrome is catalysed by cytochrome b_6f complex (plastoquinol—cytochrome-c reductase) through the reaction (EC: 1.10.2.2): plastquinol + 2 ferricytochrome c -> plastquinone + 2 ferrocytochrome c. The reaction indicates that the plastoquinol acts as an intrinsic mediator that can reduce the c-type cytochrome [351]. Since the c-type cytochrome production reaction is not included in the original model, it was subsequently added and served as another objective for the FBA modelling. However, from a modelling perspective, it was found that maximization of the flux through this added reaction makes no difference from maximization of plastoquinol available for MFC. This means the plastoquinol dependent MET mode and the cytochrome *c* based DET mode have the same current output potentials.

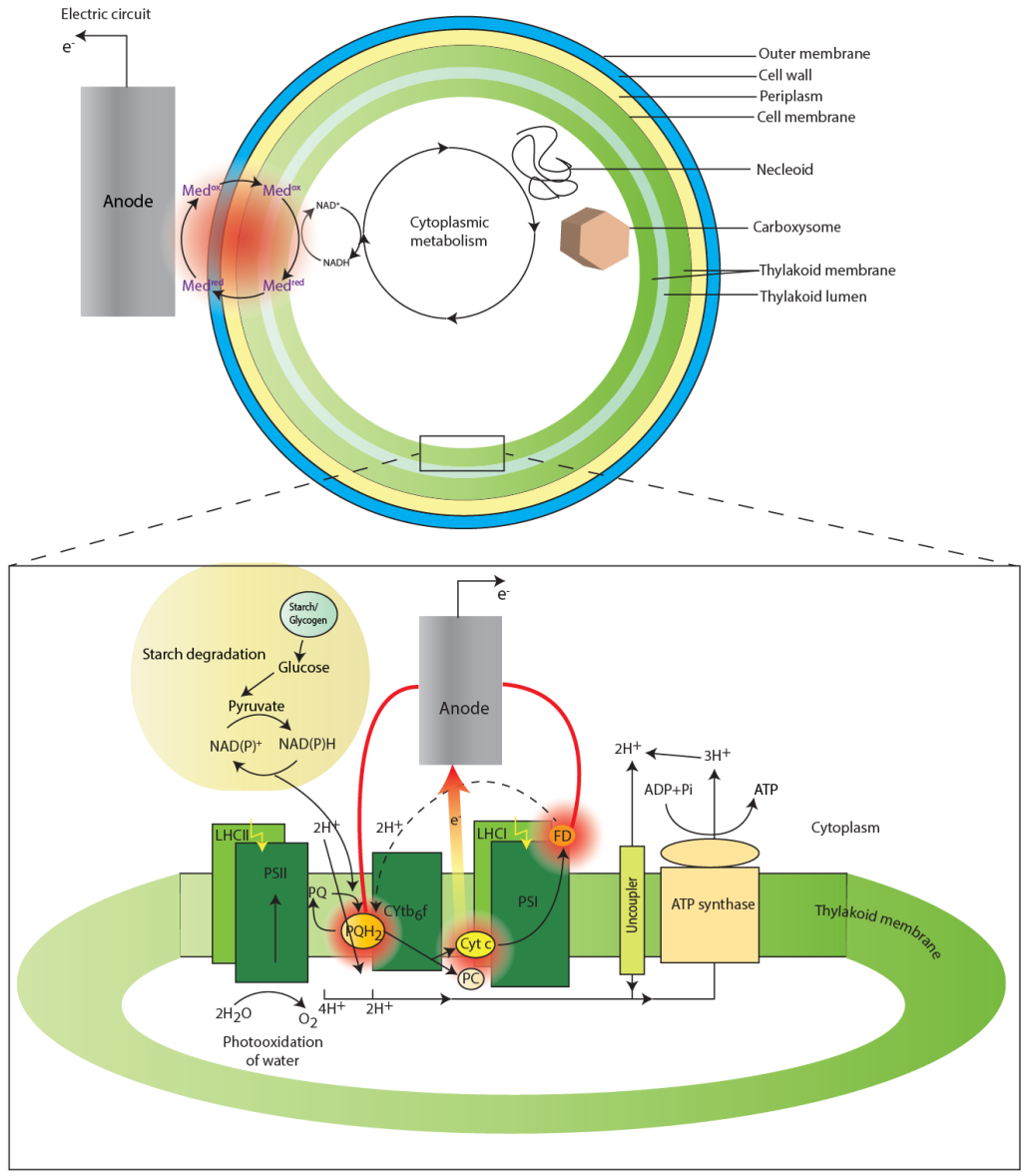

Figure 6-1: The anodic mechanisms of *synethocystis* sp. PCC 6803 modelled in the present study.

The electron transfers are established between an electrode and three potential intracellular electron shuttles: 1) ferredoxin and 2) plastoquinol pool (MET) or type-c cytochromes (DET) in the photosynthetic and respiratory transfer chain, and 3) NADH in the cytoplasmic metabolism in *Synechocystis* sp. PCC6803.

Microbes take up substrates (i.e., glucose and/or light) generating carbon dioxide and proton. This process yields electrons for metabolic benefit, i.e., growth, and reduces Med_{ox} in the cytosol into Med_{red}. Med_{red} diffuses into contact with the electrode, where Med_{red} reduces the electrode generating electrical current. The oxidized form, Med_{ox}, diffuses back through anolyte for reuse by the microbes.

Insert is a schematic representation of the intersecting photosynthetic and respiratory electron transport pathways in thylakoid membranes of *Synechocystis* sp. PCC 6803. Photosysnthesis takes place in a thylakoid membrane and mainly involves two membrane-spanning protein complexes, namely Photosystem 1 (PS1) and Photosystem 2 (PS2). These two complexes are interconnected by a number of enzymes and co-factors, forming a photosynthetic electron transfer chain along which proton-motive gradient are generated across the thylakoid membrane for ATP production. Red thick line, the putative electron tranfer path between the pETC and the electrode, radial red circle highlights the site supplying electrons towareds electrode. Thylakoids are vase-shaped, and occur in pairs. PQ, Plastoquinone; PQH2, plastoquinol; PC, Plastocyanin; Cyt c, C-type cytochrome; PS I, photosystem I; PS II, photosystem II; LHC I, light harvesting complex I; LHC II, light harvesting complex II.

These added reactions (Table 6-2) denote the net reaction between the reducing equivalents and the electrodes in MFCs, with mediators not shown because they act as intermediates only. Introduction of these reactions creates an additional escape channel for electrons, and their fluxes are subject to the mass balance rule in the FBA modelling. Since the reactants (i.e, ferredoxin, plastoquinol and NADH) of these reactions are native metabolites of the microorganisms, the added equations do not cause production of non-native by-products. These processes are schematically detailed in Figure 6-1. NADPH is not expected to be an efficient feedstock for external current production and is not considered further here.

Because this study aimed at elucidation of the electricity generation potential of this microorganism, we only modeled the function of mediators and left room for other ongoing research to identify or engineer an ideal mediator, as reviewed in [5, 52-55], which is suitable for practical extraction of the electrons from the redox metabolites in different configurations of MFCs based on *Synechocystis* sp. PCC 6803.

6.2.3 Simulating the growth of *Synechocystis* sp. PCC6803

Synechocystis sp. PCC 6803 grows photoautotrophically on light, heterotrophically on glucose, or mixotrophically on both light and glucose. For the mixotrophic condition, glucose uptake rate was set to 0.38 mmol g DW^{-1} h^{-1}, which was experimentally obtained [352]. The effective photon uptake rate was set to 15.4 mmol g DW^{-1} h^{-1} (0.889 μE m^{-2} s^{-1}), because this photon uptake rate results in the experimentally obtained flux value of the reaction catalyzed by RuBisCO when the glucose uptake rate was set to the experimentally obtained one (0.38 mmol g DW^{-1} h^{-1}) [188, 352] and illuminated by one circular cool white 32-W fluorescent lamp (the a light intensity of 125 μmol m^{-2} s^{-1}) [352]. For heterotrophic growth, the maximum glucose uptake rate is constrained to an experimentally measured value, 0.85 mmol g DW^{-1} h^{-1} [352], and photon uptake rate was set to zero. Besides, the following external metabolites were allowed to freely transport through the cell membrane: CO_2, H_2O, SO_3, NO_3, and PO_4. Nitrate was assumed as sole nitrogen source, and ammonium uptake rate was set to zero for all simulations [188]. For autotrophic growth, glucose uptake rate was set to zero and the photon uptake rate was set to the given value, the same as for mixotrophic growth.

6.2.4 Photon uptake rate

In contrast to previous studies [188, 316], in which the whole cell surface area was assumed to intercept photon flux during illumination, this study considered the cross section of the exposed orientation of the cell to determine the incident photon flux.

Dimensional photon flux conversion factor

The dry mass of a typical *Synechocystis* cell is taken to be 0.5pg [353] and the diameter of the *Synechocystis* cell is assumed to be 1.75 μm [354] with a spherical geometery. Based on the same assumption as discussed for *C. reinharditii*, the cross sectional area of *S. synechocystis* is calculated to be 2.405 μm^2. With these values, the unit of the photon uptake rate ($\mu E\ m^{-2}\ s^{-1}$) can be converted into the rate of reaction flux (mmol g $DW^{-1}\ h^{-1}$) in the modelling as follows:

$$1\ \mu E\ m^{-2}\ s^{-1} = \frac{1\mu E}{m^2 \cdot s} \times \frac{2.405\ \mu m^2}{0.5\ pg} \times \frac{pg}{10^{-12} g} \times \frac{10^{-12} m^2}{\mu m^2} \times \frac{3600 s}{h} \times \frac{1 mE}{1000 \mu E} = 17.316\ mE\ gDW^{-1}\ h^{-1}$$

$$\text{Conversion}_{\text{Dim}} = \frac{17.316\ \text{mE/gDW/h}}{1\ \mu E/m^2/s}$$

Effective photon flux conversion factor

$$\text{Conversion}_{\text{Eff}} = \frac{15.4\ \text{mE/gDW/h}}{125\ \mu E/m^2/s\ \times \text{Conversion}_{\text{Dim}}} = 0.007115\ \text{effective/incident photon flux}$$

This model indicated an effective photon flux conversion factor of 0.007115 for *Synechosystis* sp. PCC6803, which means 0.7115% of incident photons are absorbed metabolically by the cell. This value is lower than that 3.75% calculated for *C. reinharditii* [187].

6.2.5 Conversion of units of flux and current

Current (in amperes) was integrated over time and converted to electrons recovered by using the following conversions: 1 C = 1 A $\times$ 1 s, 1 C = 6.24 $\times 10^{18}$ electrons, and 1 mol = 6.02 $\times 10^{23}$ electrons (Faraday's constant 96485 C/mol). Therefore, one flux unit (mmol/g/h) can be converted into A/g as follows:

$$1\ \text{mmol/g/h} = \frac{1\ \text{mol}}{1000\text{g} \times 3600\text{s}} \times \frac{96485\ \text{C}}{\text{mol}} = 0.0268\ \text{A/g}$$

6.2.6 Calculation of coulombic efficiency (CE)

We use the full oxidation of glucose with oxygen as the oxidant as the reference reaction to characterize the energy efficiency of the respiratory metabolism:

Glucose oxidation reaction: $C_6H_{12}O_6 + 6\ H_2O \rightarrow 6\ CO_2 + 24\ H^+ + 24\ e^-$

Based on such stoichiometric information, 1 mol of glucose supplies 24 mol of electrons [330].

$$\text{CE\%} = \frac{C_{output}}{C_{substrate}} \times 100\% = \frac{\text{The MET flux(mmol/gDW/h)} \times\ 100}{\text{acetate uptake rate (mmol/gDW/h)}\ \times\ 24}\%$$

The metabolic efficiency of converting photons into external MFC current can be calculated based on the stoichiometries of the photon involved reaction in the network model below (Table 6-3). Each absorbed photon liberates 2 electrons since each qh_2 (plastoquinol) carries two electrons [338].

Table 6-3: Two light-dependent reactions in the network model [188].

Photosynthesis and electron transport chain	2 h2o + 4 photon + 4 q + 8 H -> 4 H[t] + O2 + 4 qh2
	4 qh2 + 2 nadp + 2 H + 4 photon -> 4 q + 2 nadph + 8 H[t]

The abbreviations of the metabolites are listed in [188].

Thus, the coulombic efficiency can be calculated using the formula as follows:

$$CE\% = \frac{C_{output}}{C_{substrate}} \times 100\% = \frac{\text{The MET flux (mmol/gDW/h)} \times 100}{\text{photon uptake rate (mmol/gDW/h)} \times 2}\%$$

6.3 Results and discussion

6.3.1 Impact of the redox perturbation on the biomass production

Figure 6-2 shows that the production of MFC current competes with biomass production for metabolic resources. In the metabolic state of optimal growth, all redox flux was consumed for maximizing the biomass production rate. As the oxidised forms of the reducing metabolites (i.e., reduced ferredoxin, plastoquinol and NADH) were converted into their oxidised counterparts, due to the deprivation of electrons by mediators for current production, the metabolic resources for biomass growth were diverted towards reducing equivalent generation, so as to restore a proper redox balance for maintaining a viable growth state. In all five modelled electron transfer cases, the rise in current production was accompanied by a continuous drop in the growth rates. When the current production rates approached their maximum allowable values, the corresponding biomass formation rates were suppressed to near their minimum values. This indicates that a large portion of energy is converted into electricity and the remaining metabolic resource is only sufficient for a low growth rate.

(A) Ferredoxin-dependent photoautotrophic mode

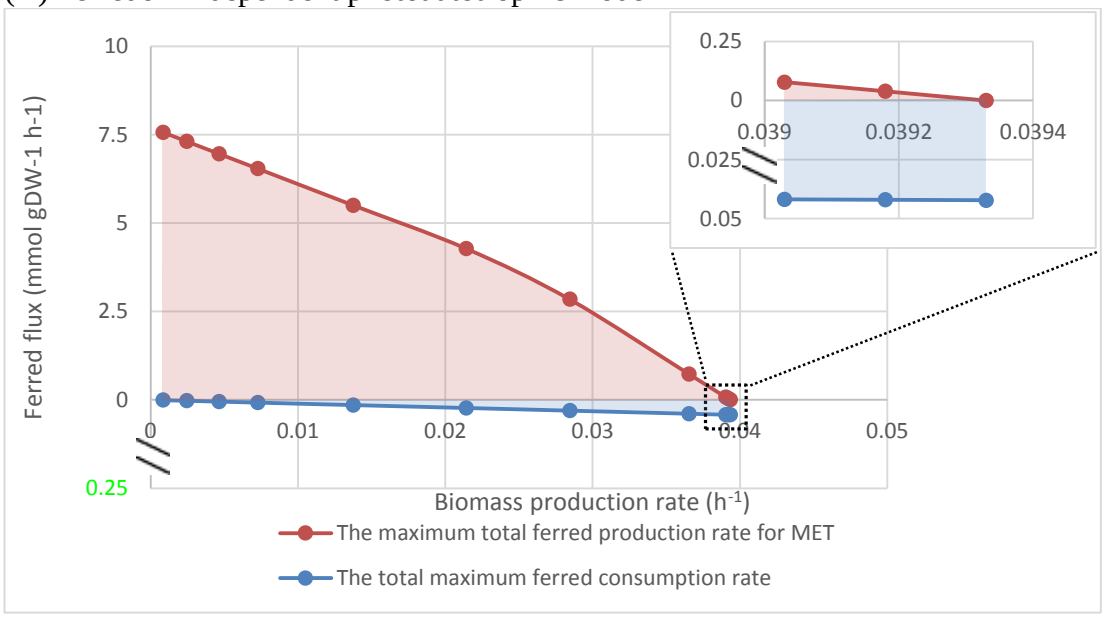

(B) Plastoquinol (QH_2)-dependent photoautotrophic mode

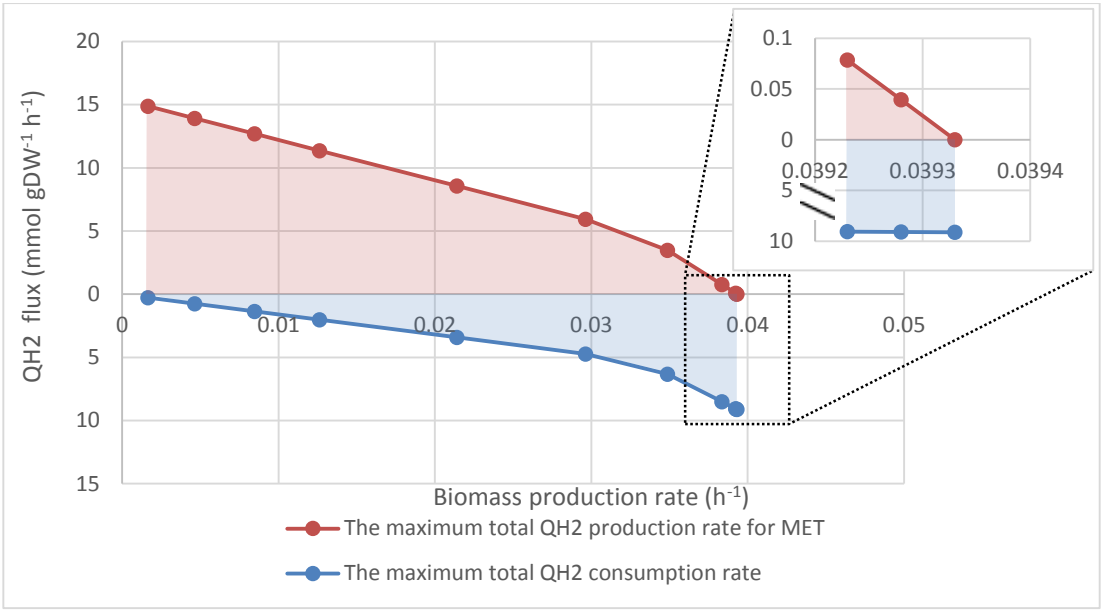

(C) NADH-dependent photoautotrophic mode

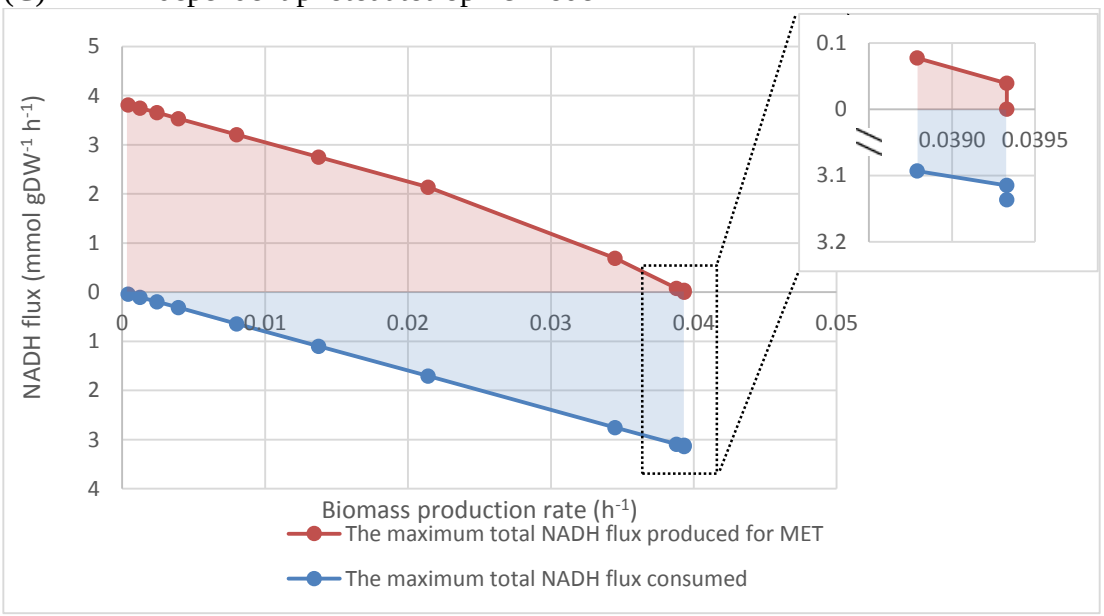

(D) NADH-dependent heterotrophic mode

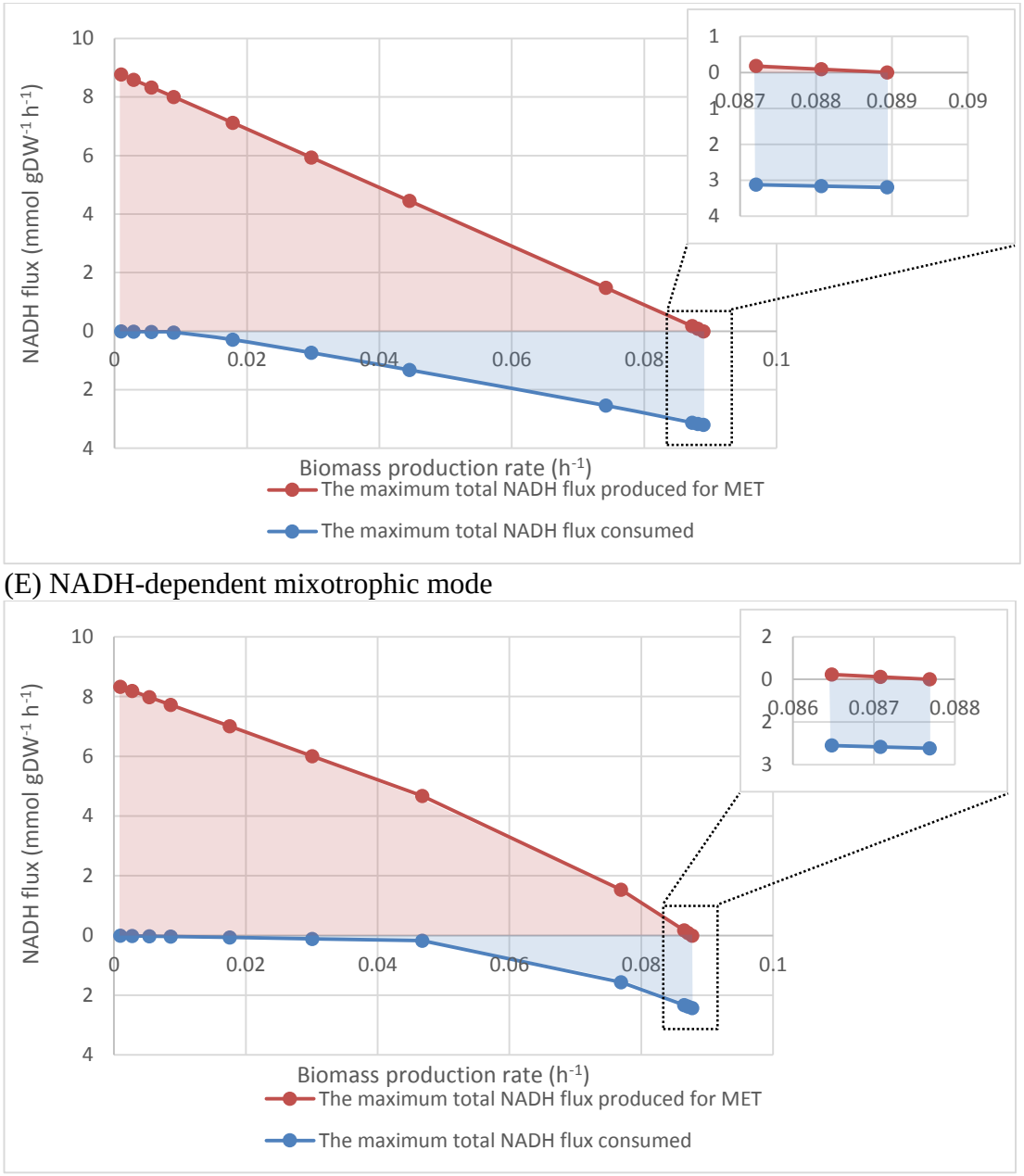

(E) NADH-dependent mixotrophic mode

Figure 6-2: The relationships of the biomass production and electron transfer rates.

The production rate of external MFC current carriers and the reducing equivalent consumption rate for cellular use, as functions of biomass production rate. The red line represents the maximal reducing equivalent supplying rate rate for a feasible biomass production rate, while any point within the pink area represents all allowable reducing equivalent supplying rates and biomass production rates. The blue area represents the total reducing equivalent consuming flux for normal cellular function. The distance between the two lines across the pink and blue areas represents the total available reducing equivalent flux in the cell at a metabolic state related to a specific biomass production rate; inset, enlargement of boxed area. The reducing equivalent denotes reduced ferredoxin, plastoquinol, or NADH in respective cases above. QH2, reduced plastoquinol; ferred, reduced ferredoxin.

Comparison of the regeneration rates of the desired reducing equivalents at optimal growth states and highly perturbed current producing states (Table 6-4), shows that the *Synechocystis* could elevate the plastoquinol regeneration rate more readily than for reduced ferredoxin and NADH. This implies that the metabolism of the cyanobacterium is naturally more tolerant to disturbance of a plastoquinol leak than stress situations resulting from ferredoxin and NADH

perturbation, when light is the sole feedstock. It is found that, compared with the optimal growth state, the cell had a capability to increase the total ferredoxin regeneration rate by about 179.4 folds (17839%), achieving a total reduced ferredoxin flux of 7.567 mmol/gDW/h. This indicates that ferredoxin flux level is not compulsory to survival (growth) of the *Synechocystis*, but it is allowed to up-regulate to eliminate uncontrolled adverse conditions, such as an overoxidized state caused by electron deprivation of the reduced ferredoxin. In addition, *Synechocystis* achieved the highest NADH turnover rate in the heterotrophic mode, followed by the mixotrophic mode, and the lowest in the photoautotrophic mode. This is due to the highest substrate uptake rates set for the heterotrophic mode among the three nutritional modes.

Table 6-4: The increases in the desired redox metabolite production rate at metabolic states optimised for current production compared with their control states optimised for growth.

Operational mode	Control state (mmol/gDW/h)	Maximum current production state (mmol/gDW/h)	Fold change	% increase
Ferredoxin-targeted Photoautotrophic	0.04218	7.567	179.4	17839%
QH2-targeted Photoautotrophic	9.114	15.14	1.661	66%
NADH-targeted Photoautotrophic	3.137	3.850	1.227	23%
NADH-targeted Heterotrophic	3.200	8.779	2.743	174%
NADH-targeted Mixotrophic	2.426	8.339	3.437	244%

The present modelling limited the substrate uptake rate to a realistic range (see Methods section 6.2) to maximize the objectives and allow the metablism to freely adjust. Nevetheless, in all simluations of the heterotrophic and mixotrophic modes, the glucose uptake rates were at the maximum bounds (0.85 mmol/gDW/h for the heterotropic and 0.38 mmol/gDW/h for the mixotrophc condtions). This indiates that the enhanced reducing equvalent regeneration, as presented in Figure 6-2, is mainly associated with the reallocation of metabolic resource from growth towards the desired electron shunt.

The MFC current production rates shown in the top parts of Figure 6-2 for the five cases, show a linear dependence on biomass growth for small growth rates and only deviates slightly from that for larger growth rates. The relationships between varying biomass production rate and the electron transfer rate appears simpler than that found in our previous work on the eukaryote *C. reinhardtii* (CHAPTER 5) and which was characterised by different growth

types and current production modes . For that organism, starting from the unperturbed state of zero MET production at the right hand side of the plots, a Type I, behaviour was described as the increase in the current production rate without any change the biomass production rate; in Figure 6-2 only a single point for the NADH-targeted photoautotrophic mode displays evidence of Type I behaviour. This behaviour demonstrates reallocation of metabolic resources without compromising growth and should repress some possible functional phenotypes, i.e., number of alternative optimal solutions, at the optimal growth rate.

Type II behaviour, where the curvature of the current carrier curve shows that the yield obtained when sacrificing biomass growth progressively decreases, is most pronounced for the QH_2-dependent photoautotrophic mode, less visible for the other cases that involve photosynthesis and totally absent in heterotrophic growth. This behaviour is interpreted as a loss of conversion efficiency, as a higher current demand reduces the feasibility to satisfy this demand by metabolic pathways with high efficiency but comparatively low capacity.

Finally, the linear (Type III) behaviour observed for heterotrophic growth and all other modes at high current demands, shows that when only a small number of pathways remain with the required capacity to supply these demands, efficiency ceases to play a role and there is a straightforward trade-off between biomass growth and current production.

Further support for this interpretation comes from a more detailed comparison of the individual reactions that participate in supplying reducing equivalent, as presented in section 6.3.2 below. For example, in the heterotrophic mode, lack of light input suppresses the photophosphorylation and cascading reactions. The linear correlation between the MFC current production and biomass growth indicates that the remaining reactions associated with electricity production possessed the same efficiency in NADH regeneration. Therefore, there are no slope alteration stages in the electron diversion curve resulting from the switch between the high efficiency and the high capability reactions.

The behaviour of the NADH consumption for maintenance (Figure 6-2) is also much simpler for *Synechocystis* than for *C. reinhardtii.* Again, curved and linear relationships to the growth rates are observed for similar reasons as discussed above for the external current production. However, for *C. reinhardtii* [337] all metabolic conditions showed a range of growth rates

where the NADH consumption increases with a decrease of growth rate, but for *Synechocystis* the NADH consumption monotonically decreases as the growth rate decreases, in all five cases shown in Figure 6-2.

Taken together, the differences from the complex interrelations between MFC current production and the reducing equivalent consumption behaviours in the cases of *Chlamydomonas reinhardtii* [337], indicates that the closer correspondence for *Synechocystis* reflects the simpler prokaryotic metabolism. Since the linear dependence on biomass production was found for the whole heterotrophic curve, but present in only part of the curves for the photoauotrophic and mixotrophic modes, it is indicated that the photoauotrohic and mixotrophic metabolic characteristic of *Synechocystis* sp. PCC6803 were simliar, which is in in accordance with a previous study [340].

The discussion above suggests a general competition between the reducing equivalent shunt and biomass production in all five cases. To further elucidate the change in the metabolic efficiency as the electron shunt augments, we introduce a measure called the fractional benefit B (discussed in Methods section 3.10), to quantify the metabolic optimality regarding the network output in the form of both biomass and reducing equivalent production rates.

Figure 3 shows the result of this measure applied to the reported simulations. Starting from wild type growth rates (right hand side of the figures), the B values generally increased to reach an apex, the best metabolic state for the dual objectives, and then decreased since the further improvement in reducing equivalent generation rate was at a high cost of biomass production rates. This behaviour was easily distinguishable in the photoautotrophic and mixotrophic cases, but not in the heterotrophic mode. The highest combined benefit (near 58%) was achieved with the plastoquinol-targeted photoautotrophic mode. This indicates that plastoquinol-linked MET or the c-type cytochrome targeted DET mode are the most suitable intracellular electron resource for current production. However, this B value (near 58%) is still lower than the lowest maximum values for the NADH-dependent MET mode of *C. reinhardtii* in all three cultivations (i.e., hetero-, photoauto- and mixotrophic). This could imply that the *Synechocystis* is less resilient to redox perturbation than *C. reinhardtii*, a eukaryote. The lowest maximum fractional benefit was found in the case of the heterotrophic mode, where the B values resulted from all the simulations could not even reach 51%. This

suggests that there is a strong competition between the biomass production and the NADH-dependent current production when glucose is the sole metabolic fuel. The peak shown in the insert of Figure 6-3 (C) corresponds to the enlargement in Figure 6-2 (C), and indicates that a small NADH shunt is tolerable to the photoautotrophic growth and thus can improve the metabolic optimality defined here (i.e., fractional benefit B value).

(A) Ferredoxin-dependent photoautotrophic mode

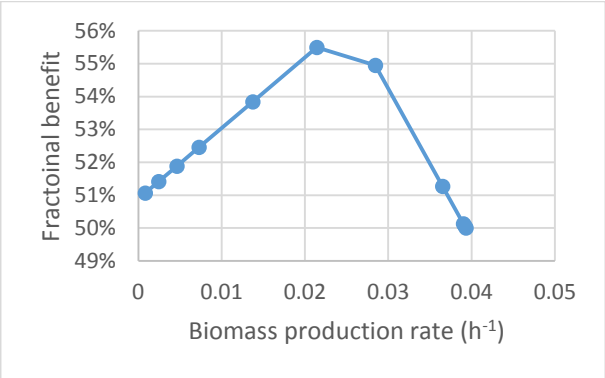

(B) QH_2-dependent photoautotrophic mode

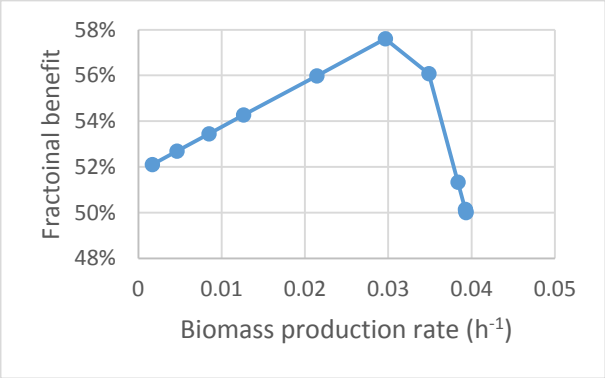

(C) NADH-dependent photoautotrophic mode

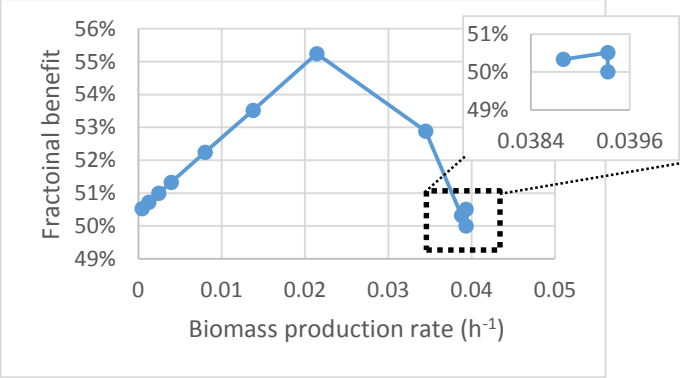

(D) NADH-dependent heterotrophic mode

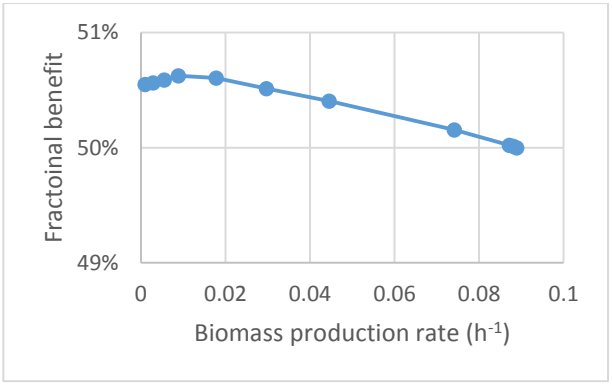

(E) NADH-dependent mixotrophic mode

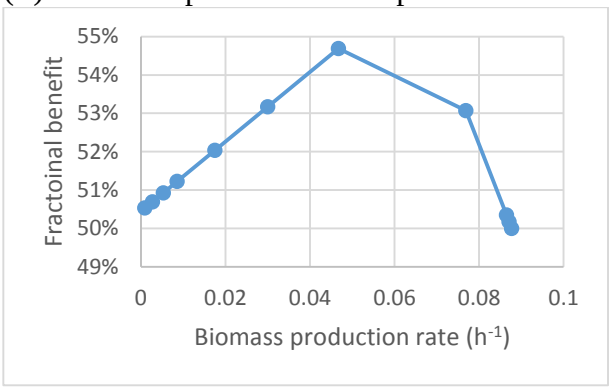

Figure 6-3: The effect of varying biomass production on the fractional benefit.

The fractional benefit B plotted on the vertical axis, is a measure of success in achieving the combined goals of maximal growth rate and MET flux. Maximizing one of these at a time, as at the endpoints, gives only B = 50%. The graphs show that relative to this, gains in MET flux can more than offset losses of growth rate in the *Synechocystis* sp. PCC 6803 metabolism.

The metabolic mechanisms underlying the high reducing equivalent regeneration rates in the aforementioned electron transfer cases are elucidated in the next section. Tables 6.3.2-6 summarize a list of reactions (enzymes) that were chosen by the cell to promote the diversion of the reducing fluxes towards current production.

6.3.2 Metabolic strategies for sustaining a high flux of reducing equivalents in the five electron transfer cases.

6.3.2.1 Ferredoxin (ferred)-dependent photoautotrophic mode

Table 6-5: The identified reactions that contribute significantly to the predicted maximum current output in the ferredoxin-dependent photoautotrophic mode.

Reaction ID	Ferredoxin (mmol/gDW/h)		Enzyme	EC No.	Reaction	Subsystem
	Min	Max				
133	-4.176	0	ferredoxin-dependent glutamate synthase	1.4.7.1	gln-L + akg + 2 ferred -> 2 glu-L + 2 feroxd	Glutamate, glutamine biosynthesis
138	0	0	nitrate reductase	1.7.7.2	nitrate + 2 ferred -> nitrite + h2o + 2 feroxd	Glutamate, glutamine biosynthesis
139	0	0	ferredoxin-nitrite reductase	1.7.7.1	nitrite + 6 ferred + 6 H -> nh3 + 2 h2o + 6 feroxd	Glutamate, glutamine biosynthesis
149	-0.00264	-0.00264	sulfite reductase	1.8.7.1	h2s + 6 feroxd + 3 h2o <=> SO3 + 6 ferred + 6 H	Glycine, serine, cysteine biosynthesis
169	0	0	pyruvate oxidoreductase	1.2.7.1	feroxd + pyr + coa -> ferred + accoa + co2	Glycolysis
279	7.313	11.49	ferredoxin-NADP oxidoreductase	1.18.1.2	2 ferred + nadp + H <=> 2 feroxd + nadph	Photosynthesis and electron transport chain

(Reaction ID and metabolite abbreviations are detailed in [188])

When the mediator deprives reduced ferredoxin of electrons forming oxidised counterparts, the oxidised/reduced ferredoxin ratio in the metabolism is disturbed and consequently the cell has to adjust its metabolic pathways to restore a proper redox balance in order to survive.

Table 6-5 shows that six reactions in the metabolism of *Synechocystis* sp. PCC 6803 involving ferredoxin production, but only one reaction, catalysed by ferredoxin-NADP oxidoreductase (EC: 1.18.1.2), was found to be responsible for the identified maximum output ferredoxin flux (7.310 mmol/gDW/h) for current production. This reaction had a capability to regenerate reduced ferredoxin at rates ranging from 7.313 to 11.49 mmol/gDW/h, which could result in an excess flux of up to 4.177 mmol/gDW/h. The major portion of the excess reduced-ferredoxin flux was balanced by ferredoxin-dependent glutamate synthase (EC:

1.4.7.1) and the remainder was consumed by sulfite reductase (EC: 1.8.7.1), to make up a net sum flux of 7.310 mmol/gDW/h. The present result confirms a previous notion that the ferredoxin-NADP oxidoreductase (EC: 1.18.1.2) is the electron supplying site to reduce the mediator, 2-hydroxy-1, 4-naph-thoquinone (HNQ), in the cyanobacteria-based MFC [99].

In addition, the other three ferredoxin involved reactions had no flux under high current output. This may be attributed to a cellular mechanism that reallocates metabolic resource to those pathways that can regenerate ferredoxin more efficiently, while maximizing the biomass production rate. Compared with ferredoxin-NADP oxidoreductase, the three reactions with zero fluxes probably have lower efficiency or capability to regenerate reduced-ferrredoxin flux to meet the heavy demand at high current output and are thus abandoned by the metabolism.

6.3.2.2 Plastoquinol (QH_2)-dependent photoautotrophic mode

Table 6-6: The identified reactions that contribute significantly to the predicted maximum current output in the plastoquinol dependent photoautotrophic mode.

Reaction ID	QH_2 flux (mmol/gDW/h)		Enzyme	EC No.	Reaction	Subsystem
	Min	Max				
280	0	0	N/A	N/A	2 H + 0.5 O2 + qh2 -> 2 H[t] + h2o + q	Photosynthesis and electron transport chain
281	14.66	14.66	N/A	N/A	2 h2o + 4 photon + 4 q + 8 H -> 4 H[t] + O2 + 4 qh2	Photosynthesis and electron transport chain
284	-0.7414	-0.7414	N/A	N/A	4 qh2 + 2 nadp + 2 H + 4 photon -> 4 q + 2 nadph + 8 H[t]	Photosynthesis and electron transport chain
285	-0.00007	-0.00007	N/A	N/A	fadh2 + q <=> fad + qh2	Photosynthesis and electron transport chain
286	0	0	NADH dehydrogenase	1.6.99.3,1.6.5.3	nadh + 5 H + q -> 4 H[t] + nad + qh2	Photosynthesis and electron transport chain
287	0	0	NADH dehydrogenase	1.6.99.3,1.6.5.3	nadph + 5 H + q -> 4 H[t] + nadp + qh2	Photosynthesis and electron transport chain

(Reaction ID and metabolite abbreviations are detailed in [188])

Akin to the case of ferredoxin-linked MET, only one reaction (reaction ID 281) was identified capable of regenerating plastoquinol at a high enough rate to sustain the theoretical maximum current production (Table 6-6). This reaction could solely supply about 105% of the

maximum net plastoquinol flux (13.92 mmol/gDW/h) towards mediator. Since the identified reaction takes place at a location of the photosystem II of the photosynthetic electron transport chain, the present result is consistent with previous reporting that the site between photosystem II reaction and Q_B (Quinone binding) protein is the main location supplying electrons for the exogenous mediator, HNQ, in a cyanobacteria-based MFC [344].

The 5% surplus plastoquinol flux was consumed by another two reactions (ID 284 & 285) for producing NADPH and $FADH_2$. NADPH is used to provide energy for the Calvin-Benson cycle that produces other carbohydrates such as starch and sucrose, as required for biomass synthesis, whereas $FADH_2$ participates in generating a proton motive force that can drive the synthesis of ATP. This indicates that the plastoquinol-consuming reactions are important to the survival of the cell.

In the conventional paradigm, under normal growth of *Synechocystis* sp. PCC 6803, the plastoquinol pool can be replenished by three sources (Figure 6-1): $FADH_2$, NAD(P)H and photosynthesis light reactions [355] and the actual metabolic source for plastoquinol production during electricity generation is hard to identify. However, the FVA analysis result has elucidated that the plastoquinol available for the electrochemical reaction in MFCs is produced from the photosynthesis light reaction, rather than from the other two sources, i.e., reactions catalysed by NADH dehydrogenase (EC:1.6.99.3,1.6.5.3) or $FADH_2$ in the process of cyclic electron flow.

The discussion above proves that plastoquinol is a good candidate electron source to be targeted by mediators for the MET mode. Recently, it has been found that *Synechocystis* sp. PCC 6803 can perform DET in an MFC without addition of mediators [98] and this cyanobacterium can also produce electrically conductive nanowires (nanopili) to facilitate the DET mode [356, 357]. The DET mode uses an electron transfer mechanism to deposit the electrons from the c-type cyctochome to the anode. As described in the methods section of this chapter, this process was modelled by incorporating another two reactions in the network: one describes the electron transfer from plastquonione to the cyctochome, and the other one captures the mechanism of the electron transfer from the cyctochome to anode, leaving the oxidised form of the protein complex inside the thylakoid membrane. It is found that modelling the availability of plastoquinol for MET is equivalent to modelling the c-type

cytochrome-associated DET. Although this phenomenon is still in keeping with a previous idea that the DET mode of the *Synechocystis* is related to the pastoquionol pool in the electron transfer chain [240], it could also be interpreted that the lack of further detailed mechanisms and constraints regarding the DET mode makes this model unable to tell the difference between DET and MET mode, both of which are influenced by the plastoquinol regeneration capability of the cell.

6.3.2.3 NADH-dependent photoautotrophic mode

Table 6-7: The identified reactions that contribute significantly to the predicted maximum current output in the NADH-dependent photoautotrophic mode.

Reaction ID	NADH_mfc (mmol/gDW/h)		Enzyme	EC No.	Reaction	Subsystem
	Min	Max				
73	0	7.779	NAD(P) transhydrogenase	1.6.1.2	nadph + nad -> nadp + nadh	Energy metabolism
106	-0.0005	7.778	enoyl-ACP reductase	1.3.1.9	dodecaACP + nad <=> tddec2eACP + nadh + H	Fatty acid biosynthesis
140	0.00114	3.890	D-3-phosphoglycerate dehydrogenase	1.1.1.95	3pg + nad <=> 3ppop + nadh + H	Glycine, serine, cysteine biosynthesis
171	-2.722	7.684	glyceraldehyde-3-phosphate dehydrogenase	1.2.1.59	gap + pi + nad <=> bpg + nadh + H	Glycolysis
251	-0.00051	7.778	homoserine dehydrogenase	1.1.1.3	hom-L + nad <=> aspsa + nadh + H	Methionine biosynthesis
288	0	3.889	delta-1-pyrroline-5-carboxylate dehydrogenase	1.5.1.12 1.5.99.8	1pyr5c + nad + 2 h2o -> glu-L + nadh + H	Proline biosynthesis
NADH consuming reactions						
134	-3.941	0	glutamate synthase	1.4.1.14	gln-L + akg + nadh + H -> 2 glu-L + nad	Glutamate, glutamine biosynthesis
381	-3.940	0.00101	2-ketoacid dehydrogenase malate dehydrogenase lactate dehydrogenase	1.1.1.37	mal + nad <=> oaa + nadh + H	TCA cycle

(see the Appendix 3 for the FVA results of all 32 reactions involving NADH, Reaction ID and metabolite abbreviations are detailed in [188])

In the autotrophic mode (Table 6-7), the maximum net NADH flux is computed to be 3.849 mmol/gDW/h, resulting from a combination of six NADH producing routes and two NADH consuming reactions. Each of the four NADH-producing reactions, catalysed by NAD(P)

transhydrogenase (EC: 1.6.1.2), enoyl-ACP reductase (EC: 1.3.1.9), homoserine dehydrogenase (EC: 1.1.1.3) and glyceraldehyde-3-phosphate dehydrogenase (EC: 1.2.1.59) respectively, could solely contribute up to 200% of the maximum net NADH flux. The other two NADH-producing reactions, D-3-phosphoglycerate dehydrogenase (EC: 1.1.1.95) and delta-1-pyrroline-5-carboxylate dehydrogenase (EC: 1.5.1.12 1.5.99.8), could supply up to about 101% of the maximum net value. Any excess percentages of the NADH flux was mainly balanced by a combination of three consuming reactions, catalysed by glyceraldehyde-3-phosphate dehydrogenase (EC: 1.2.1.59), 2-ketoacid dehydrogenase (EC: 1.1.1.37) and glutamate synthase (EC: 1.4.1.14), respectively.

6.3.2.4 NADH-dependent heterotrophic mode

Table 6-8: The identified reactions that contribute significantly to the predicted maximum current output in the NADH-dependent heterotrophic mode.

Reaction ID	NADH flux (mmol/gDW/h)		enzyme	EC	Reaction	Subsystems
	Min	Max				
73	0	3.021	NAD(P) transhydrogenase	1.6.1.2	nadph + nad -> nadp + nadh	Energy metabolism
106	-0.00115	3.020	enoyl-ACP reductase	1.3.1.9	dodecaACP + nad <=> tddec2eACP + nadh + H	Fatty acid biosynthesis
171	1.410	4.431	glyceraldehyde-3-phosphate dehydrogenase	1.2.1.59	gap + pi + nad <=> bpg + nadh + H	Glycolysis
251	-0.00117	3.020	homoserine dehydrogenase	1.1.1.3	hom-L + nad <=> aspsa + nadh + H	Methionine biosynthesis
377	2.772	2.772	dihydrolipoamide dehydrogenase	1.8.1.4	dlipo + nad <=> lipo + nadh + H	TCA cycle
381	1.388	1.388	malate dehydrogenase	1.1.1.37	mal + nad <=> oaa + nadh + H	TCA cycle

(see the Appendix 3 for the FVA results of all 32 reactions involving NADH, Reaction ID and metabolite abbreviations are detailed in [188])

Under heterotrophic growth, the maximum net NADH flux (8.605 mmol/gDW/h) was achieved through six reactions (Table 6-8). However, each reaction alone could only produce a NADH flux ranging from 16.13% to 51.50% of the 8.605 mmol/gDW/h and thus these reactions had to work together to achieve the identified maximum net flux value. Notably, the fluxes associated with dihydrolipoamide dehydrogenase (EC: 1.8.1.4) and malate

dehydrogenase (EC: 1.1.1.37) were inflexible, which indicates that the TCA cycle encompassing these two reactions is necessary to the glucose catabolism for sustaining biomass production. Furthermore, in contrast to the other two cultivation conditions (photoauotrophic and mixotrophic), there were no reactions that consumed NADH at a high rate (>1 mmol/gDW/h).

The reactions identified with potential for a high NADH regeneration rate are distributed in four conventional biological subsystems: energy metabolism, fatty acid biosynthesis, methionine biosynthesis and glycolysis. It is found that the up-regulation of glycolysis was one of four ways to increase the NADH regeneration rate for *Synechocystis*, but not used by *G.sulfurreducens* (CHAPTER 4), which employed strategies of overexpression of enzymes in the TCA cycle, amino acids and/or fatty acids pathways [280]. The involvement of glycolysis in the case of *Synechocystis* could be ascribed to the use of complex carbohydrate (i.e., glucose) as the substrate, which is different from the simple carbon source, acetate, chosen for the growth of *G. sulfurreducens*.

6.3.2.5 NADH-dependent mixotrophic mode

Table 6-9: The identified reactions that contribute significantly to the predicted maximum current output in the NADH-dependent mixotrophic mode.

Reaction ID	NADH flux (mmol/gDW/h)		Enzyme	EC No.	Reaction	Subsystem
	Min	Max				
73	0	10.87	NAD(P)+ transhydrogenase	1.6.1.2	nadph + nad -> nadp + nadh	Energy metabolism
106	-0.0011	10.87	enoyl-ACP reductase	1.3.1.9	dodecaACP + nad <=> tddec2eACP + nadh + H	Fatty acid biosynthesis
140	0.00249	2.723	D-3-phosphoglycerate dehydrogenase	1.1.1.95	3pg + nad <=> 3ppop + nadh + H	Glycine, serine, cysteine biosynthesis
251	-0.00111	10.87	homoserine dehydrogenase	1.1.1.3	hom-L + nad <=> aspsa + nadh + H	Methionine biosynthesis
288	0	2.720	delta-1-pyrroline-5-carboxylate dehydrogenase	1.5.1.12 1.5.99.8	1pyr5c + nad + 2 h2o -> glu-L + nadh + H	Proline biosynthesis
171	-1.784	10.90	glyceraldehyde-3-phosphate dehydrogenase	1.2.1.59	gap + pi + nad <=> bpg + nadh + H	Glycolysis
NADH consuming reactions						
134	-2.720	0	glutamate synthase	1.4.1.14	gln-L + akg + nadh + H -> 2 glu-L + nad	Glutamate, glutamine biosynthesis
381	-2.718	0.0022	2-ketoacid dehydrogenase malate dehydrogenase lactate dehydrogenase	1.1.1.37	mal + nad <=> oaa + nadh + H	TCA cycle

(see the Appendix 3 for the FVA results of all 32 reactions involving NADH, Reaction ID and metabolite abbreviations are detailed in [188])

In the mixotrophic mode, the maximum net NADH flux (8.192 mmol/gDW/h) for MFC current production results mainly from the combined fluxes of eight reactions (Table 6-9). Six of the eight reactions were used for NADH regeneration, whereas the other two reactions balanced any excess NADH fluxes of the production reactions. Among the six NADH-producing reactions, four reactions, $NAD(P)^+$ transhydrogenase (EC:1.6.1.2), enoyl-ACP reductase (EC:1.3.1.9) homoserine dehydrogenase (EC:1.1.1.3) and glyceraldehyde-3-phosphate dehydrogenase (EC:1.2.1.59), are the main routes selected by the cell to sustain the heavy NADH shunt during current production. Each of these four reactions could solely supply up to about 133 % of the maximum net NADH regeneration rate, which was four-folds higher than the other two lower potential reactions, catalysed by D-3-phosphoglycerate

dehydrogenase (EC: 1.1.1.95) and delta-1-pyrroline-5-carboxylate dehydrogenase (EC: 1.5.1.12; 1.5.99.8), each of which had a capability to achieve only up to 33% of the maximum net NADH flux. The 33% NADH excess was mainly consumed by two reactions, glutamate synthase (EC: 1.4.1.14) and 2-ketoacid dehydrogenase/malate dehydrogenase/lactate dehydrogenase (EC: 1.1.1.37). Since these eight reactions were allowed to adjust their fluxes within certain ranges (Table 6-9), any combination of the fluxes of these NADH involved reactions that make up the maximum net NADH production rate is viable. This indicates that there are unlimited metabolic states (each corresponds to a functional phenotype) at which *Synechocystis* sp. PCC 6803 can sustain a high current output if the NADH serves as the electron supplier targeted in the MET mode.

Comparison of the metabolic strategies identified for the NADH-linked photoautotrophic, heterotrophic and mixotrophic modes indicated that the electron supplying metabolic pathways activated in the three modes shared five reactions NAD(P) transhydrogenase (EC: 1.6.1.2), enoyl-ACP reductase (EC: 1.3.1.9), glyceraldehyde-3-phosphate dehydrogenase (EC: 1.2.1.59) , homoserine dehydrogenase (EC: 1.1.1.3) and malate dehydrogenase (EC: 1.1.1.37). Only one reaction, dihydrolipoamide dehydrogenase (EC: 1.8.1.4), was used in the hetereotrophic mode, but not in the other two modes. The mixotrohpic and autotrophic growth employed the same set of reactions to regenerate NADH at a high rate. This is in accordance with the previous notion that the mixotrophic and photoautotrophic metabolic features are similar in *Synechocystis* sp. PCC6803 [340].

To elucidate how nutrient uptake is conveyed to biomass growth and current yield respectively, the following section compares the corresponding fluxes at different uptake rates.

6.3.3 Effect of varying glucose uptake and light uptake rates on predicted biomass and reducing equivalent production rates

Table 6-10: The summary of linear functions of the biomass and the reducing equivalent production rates

	Metabolic type	Substrate	Growth (g/gDW/h)	Reducing equivalent production (g/gDW/h)	Reducing equivalent production (mmol/gDW/h)
Aerobic	Ferred &Photo	light	$y_c = 0.0026x$ $y_p = 0.0002x$	$y_{(g/gDW/h)} = 0.4769x$	$y_{(mmol/gDW/h)} = 0.4747x$
	QH2 &Photo	light	$y_c = 0.0026x$ $y_p = 0.0002x$	$y_{(g/gDW/h)} = 0.782x$	$y_{(mmol/gDW/h)} = 0.9037x$
	NADH &Photo	light	$y_c = 0.0026x$ $y_p = 8E\text{-}05x$	$y_{(g/gDW/h)} = 0.162x$	$y_{(mmol/gDW/h)} = 0.2435x$
	NADH & Hetero	glucose	$y_c = 0.1046x$ $y_p = 0.0034x$	$y_{(g/gDW/h)} = 6.726x$	$y_{(mmol/gDW/h)} = 10.108x$
	NADH & Mixo	light	$y_c = 0.0029x + 0.0446$ $y_p = 9E\text{-}05x + 0.0014$	$y_{(g/gDW/h)} = 0.0.1769 + 2.788$	$y_{(mmol/gDW/h)} = 0.2658x + 4.1895$
		glucose	$y_c = 0.1273x + 0.0393$ $y_p = 0.0039x + 0.0013$	$y_{(mmol/gDW/h)} = 7.778x + 2.495$	$y_{(mmol/gDW/h} = 11.689x + 3.7501$

Note: The FBA simulations were performed by changing the photon uptake rate and the glucose uptake rate with the maximization of the objectives. For the mixoitrophic mode, the two separate sets of equations were obtained by a) varying glucose uptake rate while the photon uptake rate was fixed to a value (as discussed in the method section); b) varying photon uptake rate while the glucose uptake rate was constrained to a given range. y denotes the reducing equvalent produciton rate for current generation (mmol/gDW/h or g/gDW/h) or growth rate (g/gDW/h), whereas x represents the substrate (i.e., glucose or light) uptake rates (mmol/gDW/h). y_c represents the optimal growth, whereas y_p denotes the perturbed growth under cytosolic NADH deprivation.

The effect of varying substrate uptake rates on the biomass production or the electron transfer rates in all five current producing cases can be described using linear equations (Table 6-10). This suggests that substrate (i.e., either glucose or light) uptake rate is the major limiting factor for both biomass and current productivity.

Column 3 of Table 6-10 shows that the slopes of the linear regression equations for the biomass production rates were highly reduced compared to optimal growth, due to the severe reducing equivalent deprivation during electricity generation. Also, the slopes of the linear equations in column 4 are much higher than those of the equations in column 3. This indicates that the cell can produce all the three electron shuttles (i.e., ferredoxin, plastoquinol and NADH) much more efficiently than biomass.

Comparison of the slopes of the equations in column 3 also shows that the glucose rate has greater influence on the biomass and reducing equivalent production than light, since the slopes of plots of cumulative biomass produced versus glucose consumed were higher than

those for the light. This could be attributed to the higher energy content in glucose than in light (8 electrons in each one glucose molecule, versus 2 electrons carried by each photon, as discussed in the methods section of this chapter).

The efficiency of conversion of glucose to biomass in the mixotrophic (slope=11.689) growth was higher than that in the heterotrophic (slope=10.108) growth. And, the efficiency of the conversion of the photon to biomass in the mixotrophic (slope=0.2658) growth was higher than that in the autotrophic (slope=0.2435) growth. Thus, this indicates that the respiratory metabolism complements the photosynthesis in the mixotrophic growth. In other words, the respiratory and photosynthetic metabolisms are interconnected and form a synergetic relationship, due to the fact that the by-products of the photosynthetic reactions could be used as substrates for respiratory reactions and the simultaneous activation of the two energy metabolic pathways can improve the efficiencies of the reactions in each of the two pathways. Taken together, mixotrophic mode performs better in the conversion of the substrates to any of the three reducing equivalents than the photoautotrophic and heterotrophic modes.

By comparison of the line slopes for the three electron transfer cases of the photoauotrophic mode, higher substrate-to-product conversions (i.e., higher slopes of the lines) were seen with the plastoquinol than the other two electron sources, ferredoxin and NADH. This indicates that additional plastoquinol production is more favoured for the *Synechocystis* compared with the other two electron sources, and thus it is a cost effective feedstock for current production.

Finally, the five operation modes are compared for their theoretically maximum current output in Figure 6-4 and Table 6-11.

6.3.4 Comparison of amperage outputs of the five electron transfer cases.

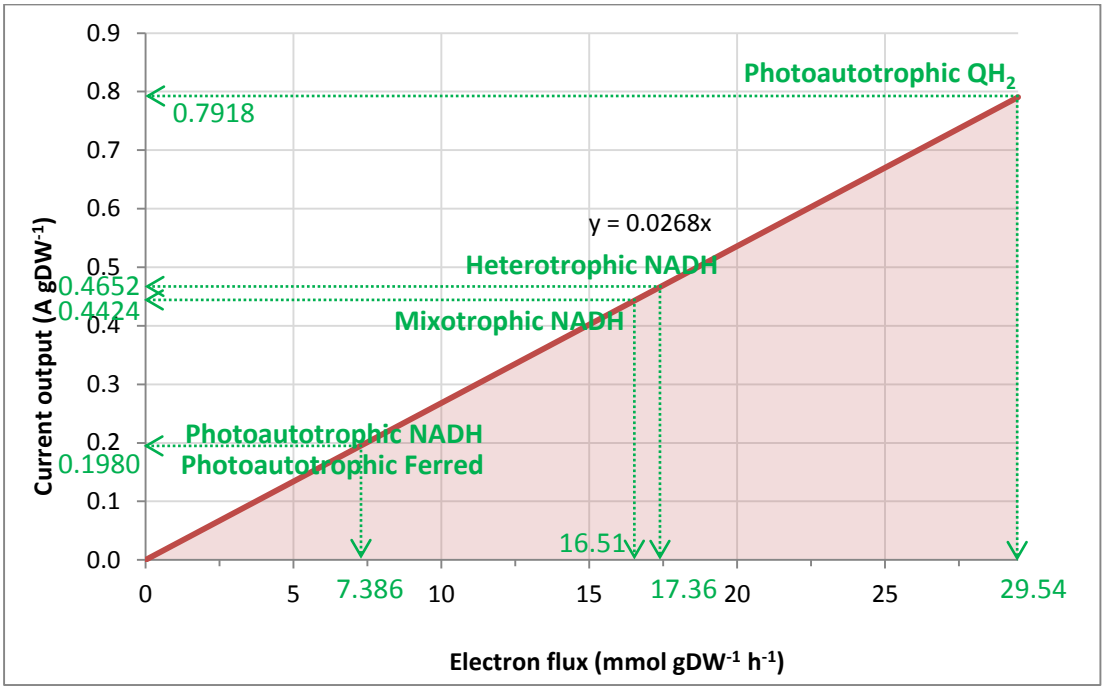

Figure 6-4: The current output (A/g) as a function of electron flux.

The dark red line denotes the maximal current outputs and reducing equvalent production rates, while the area represents all allowable current outputs and electron production rates. The round dotted arrow line indicates the maximal current output and corresponding electron production rate when the growth rate is set to 5% of the predicted maximum growth rate (0.001967 h^{-1}).

Table 6-11: Comparison of predicted amperage outputs of five modes under theoretical maximum current output condition, Ferred, reduced ferredoxin; QH2, plastoquinol; cyt c, C-type cytochrome.

Mode	Condition	Biomass production rate	Electron (mmol gDW^{-1} h^{-1})	Amperage (A gDW^{-1})	Coulombic efficiency (CE%)	W gDW^{-1}
Photoautotrophic Ferred	5% of optimal growth rate	0.001967	7.386	0.198	23.98%	0.184
Photoautotrophic QH2			29.54	0.7918	95.91%	0.325
Photoautotrophic cyt c						0.203
Photoautotrophic NADH			7.386	0.198	23.98%	0.164
Heterotrophic NADH			17.36	0.4652	85.09%	0.386
Mixotrophic NADH			16.51	0.4424	41.35%	0.367

Comparison of the results of five metabolic models for theoretically maximum current output (Figure 6-4 & Table 6-11) shows that the highest current output was 0.7918 A/gDW, which

was achieved by using plastoquinol as the electron source under photoautotrophic growth. The metabolism of *Synechocystis* sp. PCC 6803 could recover the electrons from photon to plastoquinol at a coulombic efficiency of 95.91%. When electricity generation was linked to NADH or reduced ferredoxin, the metabolism produced current at about 0.1980 A/gDW. The coulombic efficiencies for production of these two redox molecules were comparatively low, at 23.98%, suggesting the light-driven metabolism is not efficient in either NADH or ferredoxin regeneration. When NADH was modelled as the electron source for electricity generation, similar levels of current output were obtained for mixotrophic (0.4424 A/gDW) and heterotrophic growth (0.4652 A/gDW). The slightly lower current output of the mixotrophic mode is due to a lower upper limit of glucose uptake rate (0.38 mmol/gDW/h) used in the simulations of mixotrophic growth, compared with a much higher upper bound of 0.85 mmol/gDW/h chosen for modelling heterotrophic growth. These two upper bounds for the two growth modes were experimentally determined in a previous study [352]. In addition, the coulombic efficiency was much lower for mixotrophic growth (41.35%) than for heterotrophic growth (85.09%). This is attributed to the smaller number of electrons liberated from each one photon than from one glucose molecule.

Although the plastquinol and c-type cytochrome-dependent electricity generation produced much higher current than NADH-dependent modes, their power outputs were lower than the NADH-dependent counterparts due to lower formal potential of plastiquinol and c-type cytochrome. Nevertheless, this minor weakness should be outweighed by the other two advantages, i.e., much higher current productivity and the economic operation cost in the photoauotrophic growth, which does not need the organic carbon source. Taken together, these results indicate that plastoquinol-targeted MET or cytochrome complex targeted DET mode is the best electron transfer mode that should be exploited during practical electricity generation than the other three operational cases studied here.

In experiments, the MFC based on *Synechocystis* sp. PCC6803 could reach a maximum power density output of 6.7 of mW m^{-3} in the photoautotrophic growth mode, without addition of exogenous mediator [241]. The cell density in this MFC system was about 6 x 10^{9} cells/mL [241]. For estimation of the theoretical maximum power output in this previous study, an assumed dry weight of 2 x 10^{-13} g per cell [358], together with the measured cell density reported, can be used to convert the presently computed maximum power density for plastquinol and c-type cytochrome targeted electricity generation into 308 W m^{-3} and 192.58

W m^{-3} respectively. These two values serve as the theoretical upper bounds of the DET mode outputs of the *Synechocystis* at the literature cell density (6 x 10^{9} cells/mL) aforementioned. These upper limits of the power densities are at least a thousand times higher than the practically reported ones. Some reasons for such a large discrepancy could be ascribed to the fact that in the calculation, we assume every single cell in a volume of m^3 lives in the optimal metabolic state and can contribute to the power generation to its maximum capability. In practice, only cells attached to the anode can participate in the DET current production and only part of the surface of the cells on the outsides of the culture can intercept light to conduct photosynthesis. Our results nevertheless suggest a large potential for improvement of current yields from currently obtained experimental values.

Comparison of the production capability of the three potential reducing equivalents (i.e., ferredoxin, plastoquinol and NADH) indicates that plastoquinol or pastoquinol-linked c-type cytochrome is the best electron source to be targeted for MFC current production. Previous study has found that the *Synechocystis* sp.PCC 6803 can conduct photosynthesis and respiration simultaneously, because its respiratory and photosynthetic electron transport pathways intersect in the thylakoid membrane and enzymes and electron carriers, such as cytochocome b_6f complex and plastoquinone pool, are shared between the electron transport chains [355, 359]. Therefore, the redox shuttle, plastoquinol or its successively linked cytochrome complex would be ideal for supplying electrons towards the anode not only in the autotrophic mode, but also in heterotrophic or mixotrophic modes, in which the two electron flows through both photosynthesis and catabolism of a carbon source are added up.

However, current output based on the plastoquinol replenished by the electron transfer chains may have a disadvantage in that only one reaction can be targeted as the electron supplier. On the other hand, the results of the present study have shown that a high flux of NADH can be achieved by unlimited combinations of the fluxes of a number of NADH-involved reactions. This indicates that the metabolism is naturally optimised for NADH dependent by-product synthesis and the NADH targeted current production can endure more environmental perturbations since many metabolic states (pathways) can produce the same high level of current. In addition, the relatively low (negative) redox potential of NADH is also another merit for selecting this currency metabolite as the terminal electron shuttle in MFC applications [51].

The metabolic flux model for the *Synechocystis* in the present study was computed based on a genome-scale network. This is different from many other studies that usually conduct modelling on the effective model of the metabolism of *Synechocystis*, considering only nearly 100 reactions [316]. Compared with such simplified networks, the genome-scale metabolic network contains essential and non-essential reactions and is more suitable for modelling microorganisms under extreme conditions such as a higher current generation in MFC conditions in which the non-essential reactions may become activated and consequently responsible for the optimization for the desired metabolite production.

6.4 Conclusions

The present study modelled five cases of the MFC electricity generation based on *Synechocystis* sp. PCC6803. The analysis of the resultant flux models indicates that plastoquinol is the best electron source to be targeted to liberate the maximum capability of the cyanobacteria for current production, since the pertinent electrochemical reaction had a potential to supply a higher electron flux than the reactions based on the other two studied sources (reduced ferredoxin and NADH). The site with the highest potential for plastoquinol regeneration was confirmed to be the electron transfer chain reaction situated between PSII and PSI complexes. Besides, the fractional benefit analysis has further implied the suitability of the plastoquinol /cytochromes targeted MET or DET modes for *Synechocystis* sp. PCC 6803.

Compared with autotrophic and heterotrohic conditions, the photosynthesis and oxidative phosphorylation of the mixotrophic metabolism could form a synergetic relationship, improving the efficiency of converting glucose and photons into NADH. Even though the current output in the simulations was slightly higher for heterotrophic than for mixotrophic growth, this was under the assumption of a much lower glucose uptake rate in the mixotrophic mode. This is a conservative assumption based on the observed uptakes rates in unperturbed growth. It is quite plausible that without this restriction, the glucose uptake rate will be increased when NADH is extracted under mixotrophic growth conditions, to a value that is closer to that shown by heterotrophic growth to be physiologically feasible. In that case, the mixotrophic current output would be considerably higher than those we calculated. The

considerations above suggest that mixotrophic growth is more efficient and can yield a higher current output per unit substrate uptake rate, and consequently is an ideal nutritional condition for the cyanobacterium.

Future studies could employ the metabolic engineering strategies such as adaptive evolution, or rationally devised gene knockout strategies, with the aid of knowledge of the metabolic pathways identified here, to practically achieve a higher current production for MFC using this biocatalyst.

CHAPTER 7 Exploration and comparison of inborn capacity of aerobic and anaerobic metabolisms of *Saccharomyces cerevisiae* for current production.

The materials in this chapter have been published in [360].

7.1 Introduction

Chapter 6 established that the combination of prokaryotic simplicity and photosynthetic ability creates a much larger potential for use of *Synechocystis* as an MFC biocatalyst, than has been experimentally realised so far. To complete the picture of the interplay between the prokaryote/eukaryote and photosynthetic/non-photosynthetic aspects, we finally turn to yeast as a non-photosynthetic eukaryote.

Saccharomyces cerevisiae is associated with anthropic environments and is well known for food or beverage (alcoholic) fermentation[243]. Besides these applications, this yeast species has been employed as an eukaryotic model organism in molecular and cell biology; for example, the characteristic of many proteins can be discovered by studying their homologs in *S. cerevisiae*. Recently, it has been shown that *S. cerevisiae* can be processed to produce potential advanced biofuels such as long chain alcohols and isoprenoid- and fatty acid-based biofuels, which have physical properties that more closely resemble petroleum-derived fuels [247]. Nevertheless, biofuels need to be further combusted to produce usable energy in the form of electricity. To circumvent the disadvantages of biofuel combustion and directly convert the metabolic reducing potential inside the cell into electricity, another device, named an MFC, has also been proposed.

There are two ways of using *S. cerevisiae* in MFCs, namely, DET and MET modes [47]. In the DET mode, the yeast based MFC could produce an extremely low current output, at a scale of μA [361]. In addition, it is unclear what mechanisms on the cell wall are responsible for DET current production[253]. This creates burden for the *in silico* metabolic engineering technique to model the DET mode of the yeast for current output. In the MET mode,

mediators are required to facilitate the transfer of electrons to the anode, because this yeast is thought incapable of producing such mediators indigenously [249]. Because glycolysis occurs in the cytosol of the yeast cell rather than in the mitochondria, the electron shuttle, NADH, is easily accessible to a mediator molecule present in the cell membrane of the yeast and has been proposed as the main electron supplier in a yeast-based MFC [186, 249]. Based on these characteristics, MFCs using yeast can be directly applied in fermenters for *in situ* power generation [249]. Other electron carriers (such as $FADH_2$) may also contribute to current production, but these reduced molecules are regenerated by much fewer reactions than NADH, which is widely used in many reactions of the energy metabolism (e.g., glycolysis and Krebs cycles).

To identify the maximum potential of *S. cerevisiae* to sustain the energy extraction process in yeast-based MFCs, this chapter employed FBA to investigate the metabolic capability of the yeast to supply a excess flux of cytosolic NADH to reduce the oxidsed mediators (or anode), under two broad metabolic types, anaerobic and aerobic growth (Table 7-1). In addtion, FATMIN was implemented to eludcidate pertinent reactions underlying the maximum current output. Finally, robustness analysis was conducted to establish the feedstock costs for the cytosoli NADH-linked electricity generation in *S. cerevisiae*.

Table 7-1: Microbial species and their metabolism and electron transfer types investigated in the present metabolic modelling.

Organisms	Transfer type	Electron source (Terminal bacterial electron shuttle)	Metabolic type	
S.cerevisae	Mediator-driven	NADH	aerobic / anaerobic	Heterotrophic

7.2 Methods

7.2.1 Modelling electrode interactions

The interactions with an electrode were captured by introducing two reactions into the model reconstruction (Table 7-2). These reactions represent the net reaction between the reducing equivalents and the electrodes in MFC, and the pertinent process is schematically shown in Figure 7-1.

Table 7-2: The added reactions for modeling the interaction of the microorganisms and the electrode in MFCs.

Operation mode of the MFC	Reaction ID	Reaction
MET	1NADHmfc	nadh → nadh_mfc
	2NADHmfc	nadh_mfc → nad + h_emm
nadh_mfc: the NADH available for MET mode of MFCs;		
h_emm: the H ions as the by-product released from the Reaction 2NADHmfc;		

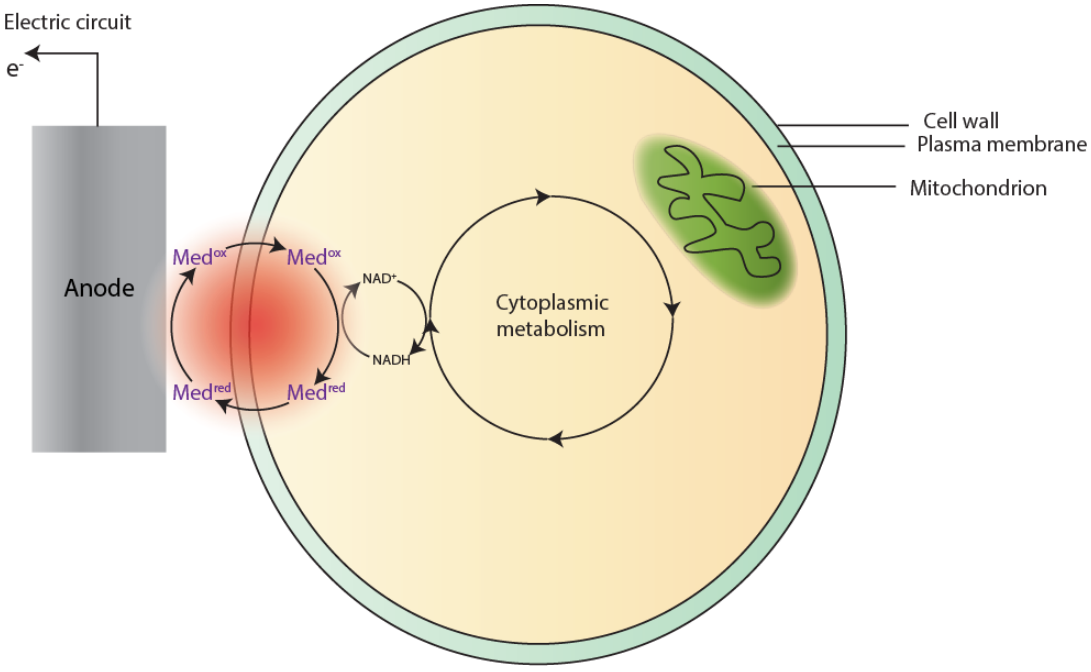

Figure 7-1: A schematic of the modelled anodic mechanisms where the cytoplasmic NADH/NAD$^+$ cycle as the electron supplier.

Microbes take up substrates (glucose) generating carbon dioxide and proton. This process yield electrons for metabolic benefit, i.e., growth, and reduces Med_{ox} in the cytosol into Med_{red}. Med_{red} diffuses into contact with the electrode, where Med_{red} reduces the electrode generating electrical current. The oxidized form, Med_{ox}, diffuses back through anolyte for reuse

by the microbes. Radial red circle highlights the redox cycle supplying the electron to the anode, which is investigated in the present modelling.

7.2.2 Calculation of coulombic efficiency (CE)

The CE is calucated based on efficiency of converting glucose into MFC current as described in the heterotrophic case of *Syncheocystis* sp. PCC 6803.

7.2.3 Simulating *S. serevisiae* growth

A recently published metabolic network of *S. cerevisieae*, Yeast 5 GEM [190] (Version 5.40; November, 2012), was chosen as the analysis backbone for the all the simulations. Compared with previous metabolic networks of this yeast, this network model is a fully compartmentalized and elementally-balanced *S. cerevisiae* metabolic network, which includes more genes and reactions based on genomic, biochemical, and physiological information. The details of existing reactions (substrate and cofactor specificity, reaction reversibility, and compartmentalization) in the network also re-evaluated to update the model based on existing literature. Furthermore, the SBML file compatible for computation with the COBRA toolbox is attached in the publication [324].

All simulations were performed on glucose as the sole carbon source. The exchange of oxygen, ammonium, protons, iron(2+), phosphate, potassium, sodium, sulfate and water were all unconstrained. The maximum rate of the glucose uptake is set to 10 mmol/gDW/h [362]. For aerobic growth, oxygen exchange was unconstrained [190]. For simulation of anaerobic growth, the oxygen exchange reaction was constrained to 0. In addition, ergosterol, lanosterol, zymosterol and phosphatidate were allowed for free exchange and the biomass definition was modified by removing 14-demethyllanosterol and ergosta-5,7,22,24(28)-tetraen-3beta-ol from the “lipid” definition [190].These steps were applied to reflect the observation that yeasts require sterols and fatty acids when cultured under rigidly anaerobic conditions [190].

7.3 Results and discussion

7.3.1 Impact of the redox perturbation on the biomass production

Figure 7-2 shows how production of mediated electron transfer (MET) aimed at cytosolic NADH competes with biomass production for metabolic resources. MET influenced the production of the NADH and biomass in the same way for both anaerobic and aerobic conditions, that is, the increase in MET drove the NADH regeneration rates in the two growth modes towards their maximum attainable values, and the corresponding NADH flux consumed for cell maintenance and biomass formation rates towards zero. This indicates that most of the energy originally for growth is converted to electricity.

(A) Anaerobic growth

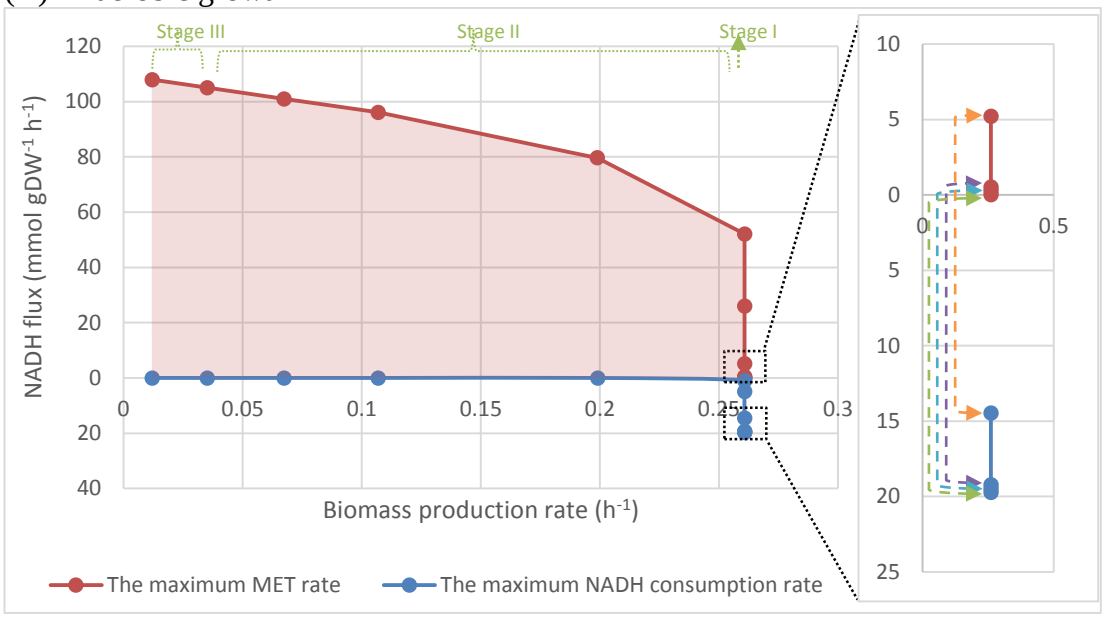

(B) Aerobic growth

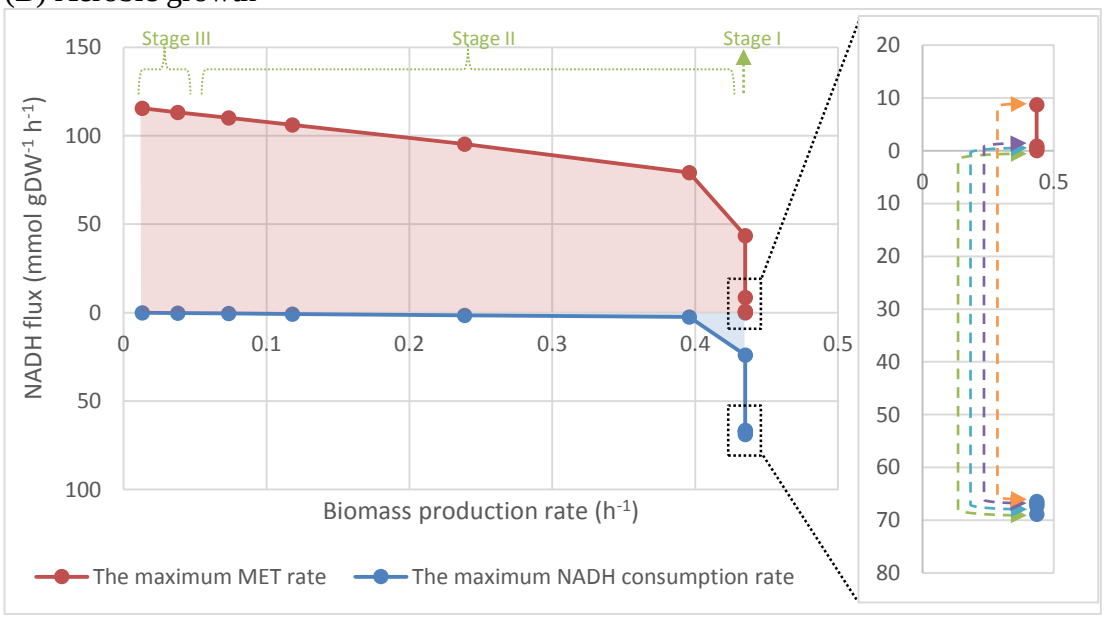

Figure 7-2: The relationships of the biomass production rate and cytosolic NADH flux diverted towards anode (NADH_mfc).

The NADH supplying rate in the MET mode and the reducing equvalent consumption rate for cellular use, as functions of biomass production rate. The red line represents the maximal NADH_mfc flux for a feasible biomass production rate, while any point within the pink area represents all allowable NADH_mfc and biomass production rates. The blue area represents the total cytosolic NADH consuming flux for normal cellular function. The distance between the two lines across the pink and blue areas represents the total available reducing equivalent flux in the cell at a metabolic state related to a specific biomass production rate; inset, enlargement of boxed area. The reducing equivalent denotes reduced ferredoxin, plastoquinol, or NADH in respective cases above; Dashed line with arrowheads indicates which two data points are paired up.

At the base state optimised for growth, the total turnover rate of NADH were 19.74 mmol/gDW/h and 67.34 mmol/gDW/h for the anaerobic and aerobic condition respectively. Compared with the base states, the anaerobic and aerobic metabolisms had a potential to increase their NADH regeneration rates by about 5.469 (447%) and 1.716 (71.6%) folds

respectively under the highly NADH-perturbed metabolic states, achieving the highest NADH_mfc flux values of about 108 mmol gDW^{-1} h^{-1} for the anaerobic growth and 115.6 mmol gDW^{-1} h^{-1} for the aerobic growth, which were achievable when biomass production rate was suppressed to 0.012 and 0.01284 h^{-1} in the anaerobic and aerobic modes respectively. This indicates that aerobic respiration can increase the maximum biomass production rate, but does not influence the metabolic capability for NADH regeneration. At the same substrate consumption rate, the fermentation can regenerate NADH to a level that is sufficient to sustain similar electric current output as aerobic growth.

The MET production rates shown in the top parts of Figure 7-2for the two growth cases, only show a linear dependence on biomass growth for small growth rates. The same for *C. reinhardtii*, starting from the unperturbed state of zero MET production at the right hand side of the plots and based on the slope changes in the lines connecting two neighbouring data points, the relationships between varying biomass production rate and the MET (NADH_mfc) rate can be divided into three stages (see Figure 7-2), which have been detailed for *C. reinhardtii* (CHAPTER 5). Briefly, the relationships between the changes in MET and growth comprise: an increase in MET without changing biomass growth (Stage I), a downward non-linear curve of MET versus growth rates (Stage II) and a linear dependence of the rise in MET on drop in biomass formation (Stage III). Stage III only appears in the left corner of the figures, where the line connecting the points clustered indicates there is a linear relationship between the biomass production and the current output.

Looking at the net NADH production (MET) curve, the Stage I relationship indicates that solutions that are based on reallocation of energy resources inside cells can elevate the slight increase in MET rate, which obviate the degradation of the intrinsic biological objective, to grow. However, rerouting the energy flow through different metabolic pathways could quell some cellular functions, which, for example, are unnecessary in optimal growth conditions, but may be important to survival in adverse conditions. This also implies that maximization of growth rate is not the sole goal for eukaryote.

The Stage II indicates that the metabolic pathways have different efficiencies and capability in NADH regeneration. Some pathways possess higher efficiencies in converting the metabolic resource into NADH but lower maximum capability in turnover rate, and some others *vice*

versa. When the current output was relatively low, the routes with higher efficiencies were selected to minimize the metabolic resource cost in order to maximize growth rate. When the current output rose to a higher level, those pathways with lower efficiencies but higher upper bounds of the NADH flux had to be used instead.

The Stage III behaviour begins at very low growth rate values (less than about 10% of the highest growth rates) in each of the two modes. The Stage III results from the fact that, only a certain set of pathways are able to sustain the very high current output and the flux through these pathways are linearly proportional to current output and biomass production rate.

Figure 7-2 also shows that a rising MET production rate reduces the cytosolic NADH consumption rate until it finally reaches zero, which indicates that no cytosolic NADH fluxes were consumed for cell maintenance. The curve plotted for the NADH consumption rate versus the biomass production can be classified into three types: Type I is a reduction in the NADH consumption rate without changing the biomass production rate; Type II represents a decrease in the NADH consumed for maintenance, associated with a drop in biomass production rate; Type III is the phenomenon that (nearly) no cytosolic NADH flux was consumed for cell maintenance accompanied by a decline in the biomass production.

A correspondence can be found between the types of and consumption behaviours and the stages displayed by the MET production curves. Stage I coincides with Type I, which is reflected by the observation that the increase in the MET is accompanied by a drop in the NADH consumption for cellular maintenance. This indicates that decreasing NADH flux for internal use would be the primary mechanism implemented by the yeast to relieve the redox perturbation. The similar mechanism has also been seen for the NADH-targeted MET mode of *C. reinhardtii*. This suggests that excess cytosolic NADH may be a common occurrence in eukaryotic microorganisms.

The Stage II occurs with both Type II and III. This indicates that in Stage II, there is a continuous adjustment in the metabolic strategies underlying the MET current production. The reduction in NADH consumption for maintenance may contribute to the major portion of the elevated NADH flux diverted to the mediator in MFCs in the beginning (i.e., the metabolic states undergoing a relatively lower degree of the current-producing perturbation).

As the NADH flux shunt further augments, the intracellular pathways that consume cytosolic NADH are disfavoured by the metabolism. The cell opts for metabolic pathways that can excessively produce NADH flux for oxidized mediators, while trying to maximize biomass production rate. When entering Stage III of the MET, the cell redirects nearly all of the metabolic resource to NADH regeneration pathways that can supply a high flux of NADH.

Both Stage I and Type I behaviours occurred in the cases of *C. reinhardtii* and *S. cerevisiae*. The coincidence indicates that the multiplicity of eukaryotic functions make these two microorganisms tolerable to hostile situations, since it is originally reflected that there are more routes of energy flow underlying more physiological conditions. In addition, different from *C. reinahrdtii*, where the shape of cytosolic NADH consumption line changed in a complex manner, the two cases of *S. cerevisiae* is much simpler. This discrepancy may be a result of the photosynthesis which contains a number of energy pathways providing metabolic fuel to the cell growth.

To further elucidate which one of the two growth conditions can better cope with the NADH-related perturbation, we performed fractional benefit analysis. Figure 7-3 shows the result of this measure applied to the reported simulations. Starting from wild type growth rates (right hand side of the figures), an increase in B values can be seen for the Stage I and Type I behaviour. The apex points of the B value curves correspond to the highest achievable combined benefit. The maximum B value for the anaerobic growth is a little bit higher than that for the aerobic growth. This suggests that, even though the aerobic growth has a potential to funnel more excess NADH for current production than the anaerobic condition, but the loss of NADH can cause more adverse effects on the aerobic than the anaerobic growth. Both growth conditions can yield a maximum B value of above 75%, which is much higher than those of all other three microorganisms (*G. sulfurreducens*, *C. reinhardtii* and *Synechocystis* sp. PCC 6803). This indicates that additional NADH perturbations would result in less hostile effects on *S. cerevisiae* than the other three microorganisms and thus *S. cerevisiae* has the greatest suitability for current production among the four.

(A) Anaerobic growth

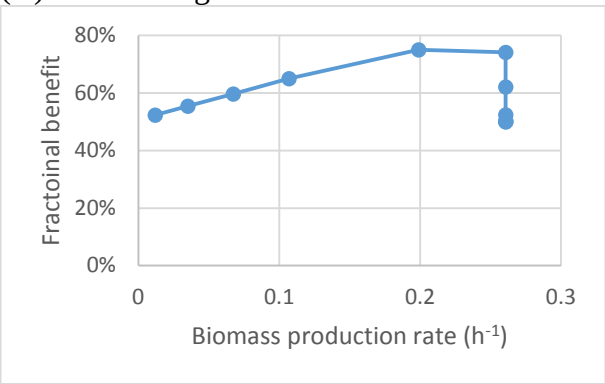

(B) Aerobic growth

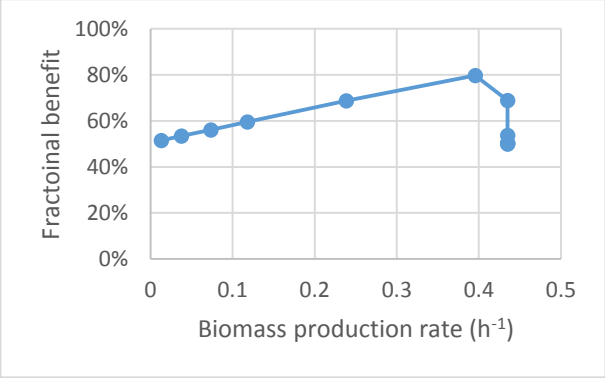

Figure 7-3: The effect of varying biomass production on the fractional benefit.

The fractional benefit B plotted on the vertical axis, is a measure of success in achieving the combined goals of maximal growth rate and MET flux. Maximizing one of these at a time, as at the endpoints, gives only B = 50%. The graphs show that relative to this, gains in MET flux can more than offset losses of growth rate in *S. cerevisiae* metabolism.

The metabolic strategies supporting the high NADH regeneration rate in the anaerobic and aerobic modes are elucidated in the next section. A list of identified reactions (enzymes) that were responsible for the promoted diversion of the cytosolic NADH flux towards current production is summarized in Table 7-3.

7.3.2 Metabolic strategies for increasing flux of reducing equivalents

Table 7-3: Identified reactions that contribute significantly to the predicted maximum NADH production rate.

Reaction ID	NADH flux (mmol/gDW/h)		Enzyme	EC No.	Reaction	Subsystems
	Min	Max				
(B) Anaerobic growth						
r_0163	6.049	6.049	alcohol dehydrogenase (ethanol to acetaldehyde)	1.1.1.1	NAD + ethanol <=> NADH + acetaldehyde	Pyruvate metabolism
r_0445	7.566	7.566	formate dehydrogenase	1.2.1.2	NAD + formate => CO2 + NADH	Methane metabolism
r_0470	-3.948	81.42	glutamate dehydrogenase (NAD)	1.4.1.3	L-glutamate + NAD <=> 2-oxoglutarate + NADH + NH3	Glutamate metabolism (aminosugars metabolism)
r_0486	6.186	6.186	glyceraldehyde-3-phosphate dehydrogenase	1.2.1.12	D-glyceraldehyde 3-phosphate + NAD + phosphate <=> 3-phospho-D-glyceroyl phosphate + NADH	Glycolysis / Gluconeogenesis
r_0731	0	85.37	methylenetetrahydrofolate dehydrogenase (NAD)	1.5.1.5	5,10-methylenetetrahydrofolate + NAD <=> 5,10-methenyltetrahydrofolate + NADH	One carbon pool by folate
r_0891	3.808	3.808	phosphoglycerate dehydrogenase	1.1.1.95	3-phospho-D-glycerate + NAD => 3-phosphonooxypyruvate + NADH	Glycine, serine, and threonine metabolism
(B) Aerobic growth						
r_0163	9.971	9.971	alcohol dehydrogenase (ethanol to acetaldehyde)	1.1.1.1	NAD + ethanol <=> NADH + acetaldehyde	Pyruvate metabolism
r_0470	-0.2163	92.58	glutamate dehydrogenase (NAD)	1.4.1.3	L-glutamate + NAD <=> 2-oxoglutarate + NADH + NH3	Glutamate metabolism (aminosugars metabolism)
r_0486	4.303	4.303	glyceraldehyde-3-phosphate dehydrogenase	1.2.1.12	D-glyceraldehyde 3-phosphate + NAD + phosphate <=> 3-phospho-D-glyceroyl phosphate + NADH	Glycolysis / Gluconeogenesis
r_0714	6.190	6.190	malate dehydrogenase, cytoplasmic	1.1.1.85	2-isopropylmalate + NAD <=> 4-methyl-2-oxopentanoate + CO2 + NADH	Branched chain amino acid metabolism (valine, leucine, and isoleucine)
r_0731	0	92.58	methylenetetrahydrofolate dehydrogenase (NAD)	1.5.1.5	5,10-methylenetetrahydrofolate + NAD <=> 5,10-methenyltetrahydrofolate + NADH	One carbon pool by folate

(see Appendix 3 for the FVA results of all 36 reactions involving NADH and reaction and metabolite abbreviations)

Anaerobic growth

In the anaerobic fermentation, *S. cerevisiae* relied on six reactions to regenerate NADH from NAD^+ at high rate, subject to the stoichiometry and biological constraints applied. Two of six NADH production routes, namely glutamate dehydrogenase (NAD) (EC: 1.4.1.2) and methylenetetrahydrofolate dehydrogenase (NAD) (EC: 1.5.1.15), were the main NADH suppliers. The two enzyme catalysed reactions were capable of producing up to 77.48% (85.37 mmol/gDW/h) and 81.23% (85.37 mmol/gDW/h) respectively of the maximum net NADH supplying rate (105.1 mmol/gDW/h). Nevertheless, only the combined fluxes of these two reactions that made up any percentages within a range of 99.4 to 103.8 % of the maximum net NADH flux were viable. This indicates there are unlimited metabolic states that can achieve the FBA identified maximum net NADH shunt. The overflow (the percentage above 100%) can be offset by the consuming NADH fluxes, for instance, the glutamate dehydrogenase (NAD) catalysed reaction can be reversible and consume up to 3.948 (3.757%) of the maximum net NADH flux.

Another significant portion (22.47%) of the maximum net NADH flux was supplied by four reactions, catalysed by alcohol dehydrogenase (ethanol to acetaldehyde) (EC: 1.1.1.1), formate dehydrogenase (EC: 1.2.1.2), glyceraldehyde-3-phosphate dehydrogenase (EC: 1.2.1.12) and phosphoglycerate dehydrogenase (EC: 1.1.1.95), respectively. These four reactions had rigid flux values, which accounted for 5.76%, 7.20%, 5.89% and 3.62% of the maximum net NADH flux respectively. This indicates that they are essential to growth.

All other NADH producing reactions jointly contributed up to only 0.06% of the maximum net NADH flux. This suggests that, in order to achieve a surplus NADH flux of 105.1 mmol/gDW/h, nearly all of the metabolic resources need to be reallocated towards the four aforementioned reactions. In addition, the rigid variability ($v_{i\ min}/v_{i\ max}>0.99$) of these reaction fluxes under high current output indicates that these reactions were much preferred for the biomass growth, rather than NADH-targeted current production.

Furthermore, it was found that the flux through the reaction catalysed by alcohol dehydrogenase (EC: 1.1.1.1) merely had a flux of 6.049 mmol/gDW/h under the high degree

of NADH perturbation. This is contrary to a previous reporting where alcohol dehydrogenase was suggested as the main NADH sink for mediators [249].

Conventionally, glycolysis, TCA cycle and fatty acid oxidation are considered to be the three main pathways supplying NADH to oxidative phosphorylation for ATP generation [338]. Consequently, it would be appropriate to speculate that these three pathways are the potential NADH suppliers for mediators in the MFC. However, the presently computed metabolic flux model elucidate that the three pathways for NADH regeneration are not the metabolic pathways responsible for the excess NADH regeneration, subject to the stoichiometry and substrate uptake constraints. Instead, two reaction (EC: 1.4.1.2) in nitrogen metabolism and (EC: 1.5.1.15) in folate biosynthesis are the only two routes allowing a high NADH regeneration rate.

Aerobic growth

Under aerobic respiration, five reactions were identified to have a capability to replenish the loss of cytosolic NADH under high current output. Each of the two reactions, catalysed by glutamate dehydrogenase (NAD) (EC 1.4.1.2) and methylene tetrahydrofolate dehydrogenase (NAD) (EC 1.5.1.15), had a potential to solely supply up to 81.71% of the maximum net NADH flux (113.31 mmol/gDW/h); and any combinations of the reaction flux amount to 81.71 – 81.75% of the maximum net NADH flux were attainable.

About 18.06% of the maximum net NADH flux was supplied by alcohol dehydrogenase (EC: 1.1.1.90), glyceraldehyde-3-phosphate dehydrogenase (EC: 1.2.1.12) and malate dehydrogenase (EC: 1.1.1.85). These three reactions had fixed fluxes, implying their enzymatic activities were critical to cell growth.

Comparison of the identified reactions chosen by anaerobic and aerobic growths shows that three reactions, glutamate dehydrogenase (NAD) (EC 1.4.1.2), glyceraldehyde-3-phosphate dehydrogenase (EC: 1.2.1.12) and methylenetetrahydrofolate dehydrogenase (NAD) (EC 1.5.1.15), were used by the two modes to achieve a high NADH regeneration rate. This indicates that 87.70% of the maximum net NADH flux in the anaerobic mode and 85.50% of the maximum flux in the aerobiec mode were generated through the same pathways.

Comparison between aerobic and anaerobic current values

Bearing in mind that oxidation of glucose in aerobic respiration releases 12 electron pairs compared to 2 for anaerobic glycolysis, it is surprising that the final calculated current output is only 20% smaller for the anaerobic operation mode. An explanation may be that the cyclic pentose pathway performs glucose oxidation, and this achieves a high flux value (see flux profile in Appendix 3). This may not be realistic because anaerobic metabolism of the yeast usually devotes substantial metabolic resources towards conversion of glucose to ethanol, but to investigate that further would need knowledge of a realistic constraint for the reactions fluxes of transhydrogenase and pentose phosphsate pathway and as that is not available the matter was not investigated further.

To demonstrate how nutrient uptake is channelled to biomass growth and current yield respectively, Table 7-4 compares the corresponding fluxes at different glucose uptake rates.

7.3.3 Effect of varying glucose uptake rate on predicted biomass and NADH production rates

Table 7-4: The summary of linear functions of the biomass production and MET rates in the heterotrophic, photoautotrophic and mixotrophic modes.

Metabolic type	Substrate	Growth (gDW/gDW/h)	MET	
			(gDW/gDW/h)	(mmol/gDW/h)
Anaerobic	glucose	y_c=0.0261x	$y_{(g/gDW/h)}$=6.971x	$y_{(mmol/gDW/h)}$=10.509x
		y_p=0.0035x		
Aerobic		y_c=0.0435 x	$y_{(g/gDW/h)}$=7.518x	$y_{(mmol/gDW/h)}$=11.332x
		y_p=0.0038x		

Note: The FBA simulations were performed by changing the glucose uptake rate with the maximization of the objectives. y denotes the MET rate (mmol/gDW/h or gDW/gDW/h) or growth rate (gDW/gDW/h), whereas x represents the substrate (i.e., glucose) uptake rates (mmol/gDW/h). y_c represents the optimal growth, whereas y_p denotes The perturbed growth under cytosolic NADH deprivation.

Table 7-4 summarizes the linear functions of biomass and NADH_mfc production rates versus glucose uptake rates. Column 3 shows that the optimal glucose-to-biomass efficiency was heavily suppressed under the high current output condition in both anaerobic and aerobic growth.

The linear regression equations are first in units (gDW/gDW/h) (column 4) for comparison with the biomass rate, and then in the standard flux units (mmol/gDW/h) in column 5. Comparison of columns 3 and 4 indicates that NADH regeneration are much less substrate-costly than the biomass production.

Compared with anaerobic growth, the efficiency of conversion of glucose to biomass was 66.67% higher, but the efficiency for glucose to NADH was just 7.831% higher in the aerobic growth. This implies that the intake of oxygen can promote the biomass production but has fewer effects on NADH regeneration.

Finally, the two operation modes are compared for their theoretically maximum current output in Figure 7-4 and Table 7-5.

7.3.4 Comparison of amperage outputs

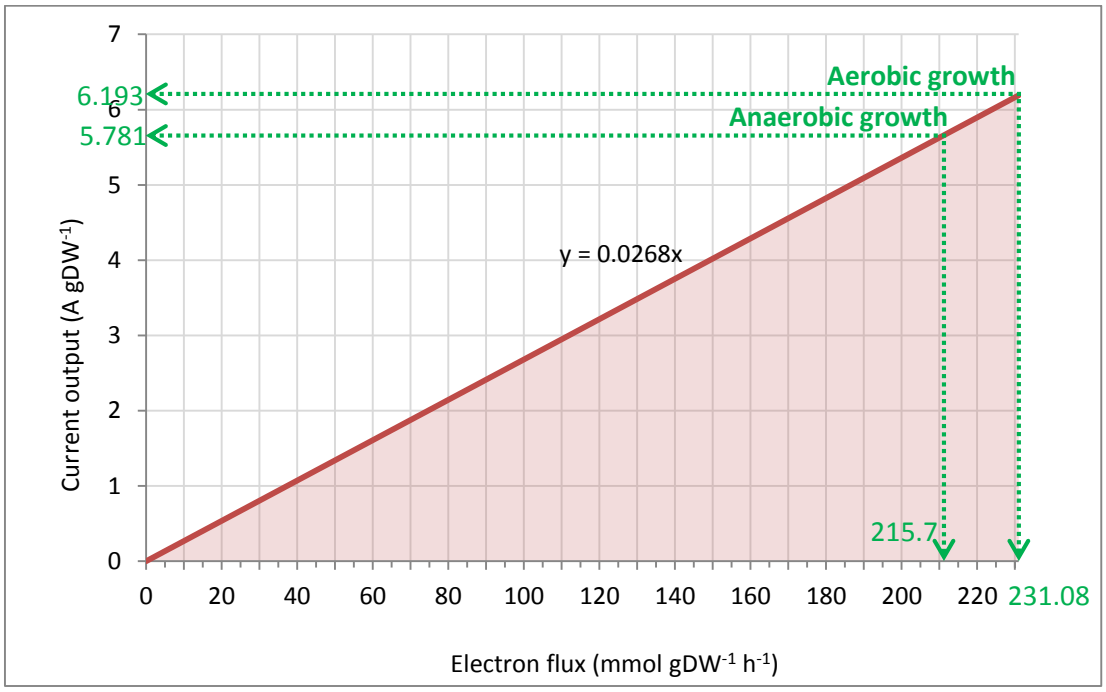

Figure 7-4: The current output (A/g) as a function of electron flux.

The dark red line denotes the maximal current outputs and NADH_mfc production rate, while the area represents all allowable current outputs and electron production rates. The round dotted arrow line indicates the maximal current output and corresponding electron production rate when the growth rate is set to 5% of the predicted maximum growth rate (0.01303 h^{-1}).

Table 7-5: Comparison of predicted amperage output under theoretical maximum current output condition and 5% of optimal growth rate condition

Mode	Conditions	Biomass production rate (h^{-1})	Electron (mmol gDW^{-1} h^{-1})	Amperage (A gDW^{-1})	Coulombic efficiency (CE%)	W gDW^{-1}
Anaerobic	5% of optimal growth rate	0.01303	215.7	5.781	89.87%	4.798
Aerobic			231.1	6.193	96.29%	5.141

Overall, the maximum current output achieved for aerobic growth (6.193 A/gDW) was about 7.14 % higher than for its anaerobic counterpart (5.781 A/gDW). Since aerobic metabolism can more efficiently use substrate than the anaerobic, aerobic MFCs were expected to be capable of generating more current that the anaerobic one. This anticipation is in keeping with the present study's prediction, despite the common observation that fuel cells generate less current when they were supplied with substrate (or anolyte) containing oxygen [19]. The discrepancy between expectations and reality may be ascribed to the deficiency of the engineering design that allows the reduced mediators to be intercepted by the presence of oxygen rather than anode, resulting in low observed coulombic efficiency. Although fermentation produces a lower current than oxidative phosphorylation, anaerobic growth eliminates the need to aerate large volumes of media and thus is more suitable for application in large-scale MFC.

In general, yeast based MFCs perform better than cyanobacteria but still have a lower power output than bacterial fuel cells [248]. An experimentally observed current of 16.09 ± 8 μA was recorded when the cell was operating under its lowest impedance in a previous *S .cerevisiae* based MFC [249]. The anode solution contained 2g of the yeast, and thus the aforementioned amperage output of the MFC system can be converted into 8.45 ± 4 μA/g DW, which is much lower than the maximum current output (5.714 A/g) computed for anaerobic growth in the present study. Another experimental study of a methylene blue mediated *S. cerevisiae* MFC reported a maximum current output of 3 mA [251]. With the cell density of 50 mg/mL and anode volume of 10 mL provided in the same study, 0.006A/g can be calculated [251], which is still much lower than the presently computed value (5.714 A/g). The large discrepancy between the previously reported current per cell gram and the presently

computed one may be attributed to the fact that 1) the cells were not in optimal metabolic states, 2) not every single cell participated in current output, 3) the mediator, i.e., methylene blue (MB), could not penetrate the cell wall and/or cytoplasmic membrane, and thus could not interact with the cytoplasmic metabolic activity efficiently, 4) and the engineering design might not efficiently collect all the electrons funnelled away from the microorganism.

The eukaryotic respiratory chain has a complicated architecture which is advantageous to the cell energy balance [363]. The cell membrane contains higher protein content, which corresponds to the higher rate of redox reactions between cytoplasm and inter-membranous space [363]. This feature has been proposed to facilitate *S. cerevisiae* attached to the anode to convey electrons to the electric circuit without aid of artificial mediators in an MFC [186]. The intracellular redox mediators (i.e., NADH/NAD^+ and FADH/FAD^+) were suggested to sustain a current output of up to 282.83 mA/m^2 [186]. However, without knowledge of the cell density on the anode of the MFC, it is impossible convert the unit (mA/m^2) of the reported current density into a unit of amperage per gram dry weight cell, and therefore we are unable to compare the current output of the yeast cell in this particular MFC to the theoretical maximum value computed here.

Another more recent study investigated the possibility of *S. cerevisiae* to transfer electrons to an extracellular electron acceptor through DET mode and found that cells adhered to the anode were able to sustain power generation in a mediator-less MFC configuration. It is proposed that the surface confined species are responsible for DET [253], however, the power performance of this MFC was extremely low (0.003 W m^{-2} and 0.03 A/m^2) [253]. With a reported cell sample weight of 0.13 g and the anode surface area of 4 cm^2, the current density can be translated into 0.000009231A/g. Since the DET mode is based on surface confined species and it is unclear what those species are, identification of the protein involved in such a DET mode is required, before the *in silico* method presented in this study can be employed to reveal the innate capability of the DET mode based on *S. cerevisiae.*

This chapter investigates the maximum potential of the yeast for current output based on NADH, instead of another chemical similar reduced cofactor, NADPH. We did not model the metabolism into a metabolic state where the two molecules, NADH and NADPH are both up-regulated to cope with the energy extraction during the MFC operation, this is because, in

practise, the exact roles of the NADH and NADPH and their relationships have not been identfied in MFC operation, and it is the cytosolic NADH-dependent pathways that are proposed to be associated with the current output of the MET mode. The primary role of the NADH serves as a reducing cofactor that transfers electrons to oxygen via the electron transport chain, involved in catabolic metabolisms, whereas NADPH donates electrons to anabolic reactions and drives biosynthetic pathways in the cell. Biologically meaningful constraints may be required to clarify interconversion fluxes between NADH and NADPH by NAD(P)H kinases in the present study. To further investigate the metabolic model of synthesis of NADH and NADPH, it may need to establish a thermodynamically constrained metabolic model, to quantitatively differentiate the metabolic costs of the synthesis of the two redox molecules. However, this may diverge from the premise and the objective of the thesis.

7.4 Conclusions

In this chapter, the anaerobic and aerobic growth modes of *S. cerevisiae* were modelled to study its maximum potential for MFC current output and underlying metabolic metabolisms. It was shown that a similar level of maximum current outputs can be achieved for the two growth modes (i.e., 5.781 A/gDW for the anaerobic growth and 6.193 A/gDW for the aerobic growth), whereas under aerobic conditions the yeast achieved nearly twice the anaerobic growth rate. To achieve the highest efficiency of NADH regeneration and maximize the current output, the aerobic and anaerobic metabolisms relied on two reactions, glutamate dehydrogenase (NAD) (EC 1.4.1.2) and methylene tetrahydrofolate dehydrogenase (NAD) (EC 1.5.1.15), for NADH production. Besides, the robustness analysis indicated that the NADH regeneration was much less energy costly than the biomass production rate. Taken together, our findings suggest that *S. cerevisiae* should be re-evaluated and receive more research effort for MFC electricity generation.

CHAPTER 8 Summary and comparison of features of the four microorganisms for electricity generation

This chapter summarizes and compares the metabolic strategies, MFC outputs and substrate-to-current conversion efficiencies among the four organisms, based on the data computed in previous Chapters 3-7.

8.1 Comparison of enzymes involved in the current-supplying pathways selected by the four microorganisms

Comparison of identified reactions supporting energy extraction shows that the four microorganisms commonly relied on reallocation of the metabolic resource from biomass growth to the redox enzymes (oxidoreductases), in order to enhance the thirteen current production cases. These redox enzymes are specialized to catalyse the transfer of reducing equivalents between redox systems [338].

Comparison of all the metabolic strategies discussed in each case for the four microorganisms indicates that most of the metabolic pathways for the maximum current output are different among species. Notably, the three cases of *C. reinhardtii* did not share any enzymatic mechanisms with the *G. sulfurreducens* and the *Synechocystis* for sustaining a high current output. This suggests that despite *C. reinhardtii* and *Synechocystis* sp. PCC 6803 having some similar functional features, such as photosynthesis, hydrogen production and mixotrophic growths, the underlying metabolic mechanisms to maximize NADH-linked MET current production are different. This may be associated with the fundamental discrepancy between eukaryote and prokaryote. The two eukaryotes (*C. reinahrdtii* and *S. cerevisiae*) only shared one enzyme, alcohol dehydrogenase, producing a surplus flux NADH.

Excluding *C. reinhardtii*, the other three microorganisms showed a few similarities in the selection of enzymes (reactions) for maximization of current production.

Table 8-1 shows the results of comparing the enzymes that contribute significantly to high current production among the studied thirteen cases of the four microorganisms. There were only five enzymes shared between the four species in the NADH-dependent MET mode. Three enzymes, malic enzyme (NAD), phosphoglycerate dehydrogenase and dihydrolipoamide dehydrogenase, were chosen by the heterotrophic MET mode and Mixed mode of *G. sulfurreducens*, the hetero-, photoauto- and mixotrophic modes of *Synechocystis* sp. PCC 6083 and hetero- & anaerobic mode of *S. cerevisiae* to achieve the maximum current output. Only one enzyme, glutamate dehydrogenase (NAD), was involved in both the aerobic MET mode of *G. sulfurreducens* and anaerobic mode of *S. cerevisiae*. Another enzyme, glyceraldehyde-3-phosphate dehydrogenase, was used in common among the four organisms. Nevertheless, the enzyme catalyses a NADH-consuming reaction in the Mixed mode of *G. sulfurreducens*, but a NADH-supplying reaction in the *Synechocystis* and *S. cerevisiae.*

Another noticeable trend in the table, is that the prokaryotes each have several reactions that can alternatively supply the full 100% output, whereas in the eukaryotes the metabolism appears more targeted and reactions contribute in more specific ratios to the final current production.

Table 8-1: List of the six enzymes shared by the four studied microorganisms for maximizing current output.

Enzyme name	EC. No.	Subsystem	*G sulfurreducens*		*C. reinhardtii*		*Synechocystis sp. PCC 6083*		*S. cerevisiae*	
			Mode	% of the maximum current output	Mode	% of the maximum current output	Mode	% of the maximum current output	Mode	% of the maximum current output
malic enzyme (NAD)	1.1.1.37	Central Metabolism (TCA cycle)	Hetero & Anaerobic (MET)	100.00%			Auto & Aerobic (MET)	16.13%		
phosphoglycerate dehydrogenase	1.1.1.95	Amino Acid Metabolism (Glycine, serine, cysteine biosynthesis)	Hetero & Anaerobic (MET)	100.03%			Hetero Aerobic (MET)	101.06%	Hetero &Anaerobic (MET)	3.62%
							Mixo Aerobic (MET)	33.24%		
glutamate dehydrogenase (NAD)	1.4.1.3	Amino Acid Metabolism (Alanine, aspartate and glutamate metabolism)	Hetero & Anaerobic (MET)	100.00%					Hetero &Anaerobic (MET)	77.48%
dihydrolipoamide dehydrogenase (part of glycine-cleavage complex)	1.8.1.4	Amino Acid Metabolism (TCA cycle	Hetero & Anaerobic (Mixed)	49.77%			Auto Aerobic (MET)	32.21%		
alcohol dehydrogenase (glycerol, NAD)	1.1.1.2 (C. reinhardtii) 1.1.1.1 (S. cerevisiae)				Mixo	108.06%			Hetero &Anaerobic (MET)	5.76%
					auto	42.63%			Hetero &Aerobic (MET)	8.80%
					hetero	62.50%				
glyceraldehyde-3-phosphate dehydrogenase	1.2.1.12 (G. sulfureducens) 1.2.1.59 (the Synechocystis & C. reinhardtii) 1.2.1.12 (S.	Central Metabolism Glycolysis Gluconeogenesis	Mixed mode	-149.28%			Hetero	51.50%	Hetero &Anaerobic (MET)	5.89%
							Auto	199.59%	Hetero &Aerobic (MET)	3.80%
							Mixo	133.01%		

Note: the grey shaded table cells indicate that the enzyme (row) in the organism (column) is not shared with that in the other three organisms

8.2 Comparison of metabolic and energetic efficiency for biomass and MFC reducing equivalent production

8.2.1 Comparison of the metabolic efficiency

The slopes of the linear relationships obtained for biomass growth and reducing equivalent production versus substrate uptake rates, give quantitative measures of efficiency and are collected together in Table 8-2.

Table 8-2: Summary of the slopes of the linear functions of desired product (biomass or NADH) production rates (y) versus substrate (glucose or acetate) uptake rates (x); Different energy sources are highlighted in different colours, namely, acetate in blue, light in orange and glucose in red.

Metabolic type					Optimal growth (control)	Optimal growth (under perturbation)	Reducing equivalent for MFC (g/gDW/h)	Reducing equivalent for MFC (mmol/gDW/h)	Current yield (A/gDW/$)
G. sulfurreducens	Anaerobic	Hetero	DET	acetate	0.0369	0.0013	2.579	3.887	3469.5
			MET			0.001	3.487	0.2906	259.40
			Mixed			0.0007	2.616	3.943	3519.5
C. reinhardtii	Aerobic	Hetero	MET	acetate	0.168	0.0007	1.475	2.224	1985.0
		Auto	MET	light	0.0011	3E-05	0.04080	0.0977	
		Mixo	MET	acetate	0.0308	0.001	2.026	3.053	2725.3
				light	0.0011	2E-05	0.04080	0.0615	
Synechocystis sp. PCC 6803	Aerobic	Auto ferred	MET	light	0.0026	0.0002	0.4769	0.4747	
		Auto qh_2	MET/ DET	light	0.0026	0.0002	0.782	0.9037	
		Auto	MET	light	0.0026	8E-05	0.162	0.2435	
		Hetero	MET	glucose	0.1046	0.0034	6.726	10.11	9022.3
		Mixo	MET	light	0.0029	9E-05	0.1769	0.2658	
				glucose	0.1273	0.0039	7.778	11.69	10433
S. cerevisiae	Anaerobic	Hetero	MET	glucose	0.0261	0.0035	6.971	10.51	9380.2
	Aerobic			glucose	0.0435	0.0038	7.518	11.33	10115

Note: the grey shaded cells reflect that the current yield (A/gDW/$) is not applicable for the operation mode (row).

For biomass production, *G. sulfurreducens* possessed the highest efficiency of substrate-to-biomass conversion (slope=0.0369). The second highest efficiency was 0.0261, which was achieved by *S. cerevisiae* under anaerobic condition. The other two photosynthetic microbes

had comparatively low substrate-to-biomass efficiency, but *Synechocystis* sp. PCC 6803 possessed higher efficiency than *C. reinharditii* in all three growth conditions (i.e., mixo-, auto- and hetero-trophic).

For *G. sulfurreducens*, the DET mode and mixed mode involved a similar level of conversion efficiency of acetate to NADH (slope=3.8868 and slope=3.9426), which is higher than the MET mode (slope=2.9062). In the case of *C. reinharditii*, the mixotrophic growth acquired much higher efficiency for acetate to reducing equivalent conversion (slope=3.0533) than the other two growth conditions (i.e., autotrophic and heterotrophic). For *Synechocystis* sp. PCC 6803, the highest efficiency obtained for converting glucose to reducing equivalent is found in the cases of mixotrophic (slope=11.689) and heterotrophic (slope=10.108) growth. *S. cerevisiae* converted glucose into reducing equivalents more efficiently under aerobic heterotrophic growth (slope=11.332) than under anaerobic heterotrophic condition (slope=10.51).

Overall, the results imply that the four microorganisms had different efficiencies for biomass production and reducing equivalent regeneration. *G. sulfurreducens* and *S. cerevisiea* are more efficient in biomass production than the other two photosynthetic microbes. In addition, *S. cerevisiae* and *Synechocystic* sp. PCC 6803 can be more efficient at producing reducing equivalent. These differences can be attributed to the different metabolic rates of microbial species. Table 8-2 indicates that the organic energy sources, glucose and acetates, were both more efficient in supporting biomass growth and reducing equivalent production than light. Glucose metabolisms, such as in the cases of *S. cerevisiae* and the *Synechocystis*, had higher efficiency of conversion of substrate to reducing equivalent than acetate metabolisms, such as in the cases of *G. sulfurreducens* and *C. reinhardtii*. The higher conversion efficiency with glucose may be attributed to the higher electrons content (24 electrons) per glucose molecule versus the lower content of 8 electrons of acetate molecule.

Comparison of the reducing equivalents production rates derived from glucose and acetate (Table 8-2) suggests that glucose is the preferred substrate, since each glucose molecule could be converted into a higher number of reducing equivalents than acetate. This is in keeping with a notion that the choice of substrate has a great influence on the electricity generation of MFCs [29]. The substrates range from pure compounds to complex mixtures present in

wastewater. However, wastewater is much more recalcitrant than acetate when used as the substrate for MFCs [364]. It is found that acetate has been chosen as the substrate in most of the MFC studies. Acetate is an ideal carbon source for the growth of electroactive bacteria [263]. On the other hand, glucose is another commonly used substrate in MFCs. In the mixed-cultures used MFCs, glucose can result in a more diverse species of microorganisms than other substrates, because the fermentation by-products generated during glucose degradation can be used to grow a complex, mixed consortium, of diverse electricigens or syntrophic bacteria. The wider community diversity can result in the rapid generation of current without lag time [30].

8.2.2 Comparison based on substrate loading rate and feedstock cost.

Different microbial species had different preferences for nutrients, which makes it difficult to compare the energy efficiency. To obviate the difference in the nutrient usage, it is possible to consider the substrate loading rate and feedstock cost as a basis for comparison of the four microorganisms for current production. The slopes summarized in Table 8-2 are derived from the relationships between substrate (acetate and glucose) uptake rates and biomass or desirable reducing equivalent production rates. Since two organic substrates (acetate and glucose) were used for different microorganisms, a high slope value indicates that a low substrate loading rate (mmol substrate/gDW/h) can result in a high biomass and reducing equivalent production rate.

Whereas light is thought of as a free energy source, acetate and glucose are needed to replenish the MFC bioreactor to sustain oxidative phosphorylation and fermentation. Therefore, there are usually some costs associated with replenishment of these two organic substrates. Each mol of acetate is about three times more expensive than that of glucose (Table 8-3). This indicates that if the two substrates are consumed at the same loading rate, the feedstock cost of acetate for current production is three times higher than that of glucose. Thus, compared with the slopes for glucose cases, the lower slope values for reducing equivalent production rates versus acetate uptake rates indicates higher feedstock costs, corresponding to lower current yield (A/gDW/$) (the rightmost column). This suggests that each NZ dollar ($ NZ) worth of acetate provides a lower amperage output per gram dry cell weight.

Table 8-3: List of the prices of glucose and acetate suitable for cell culture

	Product code (Sigma product)	$NZ/kg	Molar mass (g/mol)	Molecular Formula	Cost (mol/NZ$)
D-(+)-Glucose	G7021-1KG	63.8	180.16	$C_6H_{12}O_6$	5.551
Sodium acetate	S5636-1KG	111	60.05	$C_2H_4O_2$	16.65

Source: http://www.sigmaaldrich.com/

8.3 Comparison of power outputs

Table 8-4: Comparison of the theoretical limit of the MFC performances based on the four selected microorganisms (Growth rate is 5% optimal maximum)

Organism	Electron transfer mode	Substrate uptake rate (mmol gDW^{-1} h^{-1})	Growth rate	Amperage (A gDW^{-1})	$\Delta E_{cell}^{\circ'}$	W gDW^{-1}	Coulombic efficiency (CE %)	The maximum B value
G.sulfurrreducens	MET	18	0.03311	2.771	0.83	2.300	71.79%	50.82%
	DET			3.710	0.256	0.950	96.12%	55.67%
	Combined			3.272	0.83	2.716	84.78%	55.65%
C. reinharditii	Mixotrophic	145	0.00798	2.368	0.83	1.966	39.27%	63.70%
		10						
	Autotrophic	145		0.703	0.83	0.584	18.10%	61.87%
	Heterotrophic	10		1.141	0.83	0.947	53.20%	66.95%
Synechocystis sp. PCC6803	Mixotrophic	15.4	0.00197	0.442	0.83	0.367	41.35%	54.69%
		0.38						
	Autotrophic	15.4		0.198	0.83	0.164	23.98%	55.24%
	Heterotrophic	0.85		0.465	0.83	0.386	85.09%	50.63%
	Autotrophic reduced ferredoxin	15.4		0.198	0.93	0.184	23.98%	55.49%
	Autotrophic QH2			0.792	0.256	0.325	95.91%	57.60%
	Autotrophic cytochrome c			0.792	0.41	0.203	95.91%	57.60%
S.cerevisae	Aerobic	10	0.01303	6.193	0.83	5.141	96.29%	79.72%
	Anaerobic			5.781	0.83	4.798	89.87%	75.03%

Due to distinctive metabolic features among different species, the maximum substrates rates are set differently for the four microbes according to literature. However, the high substrate uptake rate needs to be biochemically processed by the reactions inside cell to produce biomass component and reducing equivalent available for MFC current production. This means the metabolic efficiency of converting substrate to desirable metabolic products is important. To circumvent the effects of any other factors, such as nutritional deficiency, temperature etc. on MFC current production, here we only focus on the maximum (optimal) capability and the most preferable pathways of the cells. Different sets of biological constraints were applied to the four microbes, so as to simulate base (optimal) metabolic states in different electron transfer cases.

Since the upper limit of the potential derived from MFCs is governed by the formal potential of the involved biological and electrochemical redox processes, there is little room for improvement on the metabolism. Only current output accounts for the difference among the metabolic features of the four microorganisms.

Table 8-4 shows that the maximum current and power outputs of the anaerobic and aerobic metabolisms of *S. cerevisiae* were much higher than those of the other three microbes, making the organism a very attractive candidate for MFC use. The maximum power output of *G. sulfurreducens* was about half that of *S. cerevisiae*, but slightly higher than *C. reinhardtii* and a lot higher than that of the other prokaryote, *Synehcocystis*, in which the performance was constrained by the low substrate uptake rates. Although G. *sulfurreducens*, in the DET mode, achieved much higher current output than NADH-dependent MET mode and Mixed mode, the maximum power output of the DET was lower than those achievable by the other two modes, which is attributed to the high (positive) standard potential of the c-type chromosome used by the DET mode. The mixotrophic growth of *C. reinhardtii* resulted in the highest current output among the three nutritional modes, but was still below the MET mode of the *G. sulfurreducens*, which allows higher substrate uptake rate. The maximum electric output of *C. reinhardtii* was higher than *Synechocystis*, but the associated CEs were much lower than all other microorganisms.

In the five cases of *Syncheocystis*, due to its maximum power output, the heterotrophic growth would be more competitive than the other two cultivation conditions for NADH-dependent electricity generation. The plastoquinone or cytochrome-c could generate much more power than ferredoxin and thus were more suitable to serve as the electron supplier to be targeted in MFCs.

The two growth modes of *S. cerevisiae* achieved the highest B values among all the cases. This indicates the greatest suitability of the metabolism of *S. cerevisiae* for cytosolic NADH-dependent current production. In general, both the eukaryotic metabolisms, *S. cerevisiae* and *C. reinharditii* produced higher B values than the other two prokaryotic metabolisms. This may be due to the fact that the compartmentalized and complex eukaryotic metabolisms are more robust against redox balance disruption than the prokaryotic metabolisms and is

therefore more successful in simultaneously satisfying the dual demands of growth and current production.

8.4 Conclusions

There was a distinction in selection of pathways (or reaction) among the four organisms to maximize the current production. For example, even though *C. reinhardtii* and *S. cerevisae* are both eukaryotes, and the environmental roles of *C. reinhardtii* are akin to that of the *Synechocystis*, these features are tangentially coincident with the pathways selected for maximization of redox metabolite turnover rate. In addition, it is found that glucose based metabolisms needed a lower loading rates and are less feedstock costly than acetate-based counterparts.

Based on the computed maximum current outputs, CEs and B values, *S. cerevisiae* was the best candidate for MFC use. Although other microorganisms may have lower MFC performance, other different biological features could justify their use for applications in different situations and engineering configurations. Thus, it is difficult to conclude which one is supreme to the others.

CHAPTER 9 Reaction deletion optimization

While previous chapters have identified the maximum capability of the four microorganisms for current production, this leaves open the question of practical strategies to achieve this potential. One possibility may be a metabolic engineering strategy such as adaptive evolution. In this way, if the right selection pressure is applied, there is a continuous selection for beneficial mutations that can attain the high predicted current output. As an alternative approach, reaction or gene deletion can also be a fast way to generate beneficial mutant strains, facilitated by the reaction knockout identifying algorithms such as OptKnock [161, 169, 365] or its extension, OptGene [163, 366].

In this chapter, we explore the possibility of improving productivity of previously examined reducing equivalents regeneration by employing an OptGene algorithm, which can manipulate interactions among dozens of reactions within the cells to increase the rate of the desired conversion processes. This chapter presents the use of a reaction deletion strategy to make cells voluntarily promote those electron transfer modes in corresponding growth conditions. Based on gene-reaction associations, genes that catalyse the reactions proposed to be deleted can be obtained from online database such as BioCyc (http://www.biocyc.com/)

9.1 Introduction

The development of metabolic engineering and synthetic biology allows new pathways to be constructed in microorganisms to increase productivities of the desired metabolites. Consequently, 1) new strains can be developed to express heterologous enzymes with higher catalytic activities for key intermediates in the new pathways and 2) gene knockouts can be constructed to channel greater carbon flux toward the desired product [367].

Rational gene targets to be over-expressed or deleted can be identified by recently developed computational methods, which can be categorised into three levels: 1) reconstruction of genome-scale metabolic network (GSM), 2) phenotype simulation and 3) strain optimization.

GSMs contain the metabolic information and transcriptional information of a microbe. FBA and its variants such as parsimonious enzyme usage FBA, aim to probe the maximum or minimal value of putative objectives such as cell growth, by solving a linear programming problem subject to stoichiometric and reversibility constraints [167]. Strain optimization formulates a bi-level problem comprising an inner layer, the phenotype simulation method, and an outer-layer, optimization algorithm that searches for the best set of genetic modifications to apply to a microbe. This bi-level optimization framework has been incorporated in several methods such as OptKnock, which suggests gene deletion strategies leading to the overproduction of specific chemical products by simultaneously considering the entire metabolic network [161, 169, 365]. However, application of OptKnock is limited by its time-consuming nature, resulting from the mixed integer linear programming formulation and the restriction of linearity of the objective functions. Extending OptKnock, OptGene uses evolutionary algorithms (EA) to identify near optimal solutions for large problems in a reasonable amount of time [163, 366]. Importantly, OptGene can also identify reaction deletion strategies if gene-reaction rules are not available, which is common in most cases of whole-cell level metabolic models.

In order to increase the rate of channelling electrons from the reducing equivalents to mediators (or electrode in the case of DET), we apply the bi-level OptGene framework to devise reaction knock-out strategies for the microbial strain optimization. A variety of reaction deletions are predicted to promote funnelling electrons towards assumed mediators or electrode. Each of these mutations can increase availability of the reducing equivalents for electricity generation.

9.2 Methods

9.2.1 OptGene algorithm.

Details of the OptGene algorithm are discussed in [163]. The overview of the algorithm can be divided into three steps, 1) Initialization of population: a population of individuals is initiated by specifying a present/absent status for each gene (or reaction) in each of the individuals.2) Scoring fitness of individuals: individuals are scored for their fitness by using

MOMA and the objective function (fitness function). 3) Breeding new populations by evolution: Individuals evolve by application of set-based evolutionary algorithms (SEA), which resemble the natural evolution process through two steps: (i) Individuals are selected for mating based on their fitness score and subsequently crossed to produce new offspring. (ii) Mutations are randomly introduced in individuals at specified mutation rates and thus a new population is obtained. The second and third steps make up a complete cycle of evolution that is repeated until a mutant (or mutants) with the desired phenotypic characteristics is obtained [163].

The OptGene algorithm identifies genes or reactions (if the information on gene-reaction associations are not included in the model) that have to be deleted for the overproduction of the reducing equivalent desired by the current production.

We applied the OptGene with the set-based evolutionary algorithm (SEA) to thirteen case studies of four microorganisms. In these cases, the inner objective function was maximization of the growth rate and the outer objective function was maximization of the electron transfer for electricity generation.

Table 9-1: The parameters used in the strain optimization process

Optimization algorithm	Set based evolutionary algorithm (SEA) (based on the premise of natural evolution)
Simulation method	Minimization of metabolic adjustment (MOMA) (Simulation of the phenotype of the deletion strain))
Fitness function	Biomass-product coupled yield (BPCY) (a non-linear function that aims to simultaneously maximize the biomass and the desired product)
Maximum number of solution evaluations	500 (the number of evaluations needed to find the solution; an increase beyond 125 individuals did not improve the results significantly [163]
Maximum number of knockouts	10
Reaction set size	Variable (the variable size representation allows the automatic finding of the best number of reaction deletions necessary for achieving a given productivity goal)
Environmental conditions	Thirteen conditions profiled before

9.2.2 Set-based evolutionary algorithm (SEA)

Evolutionary algorithms (EAs) are robust, stochastic optimizers roughly based on natural selection evolution [368]. The notion of EAs is to evolve a population, i.e., a set of individuals that encode solutions to target problems in an artificial chromosome.

New individuals (solutions) are produced by the application of reproduction operators to a group of selected parents, which are taken from a pool of the previous population using probabilities. The new individual is evaluated through a fitness function that assigns a score to the solution representing the quality of the encoded solution. The ‘fittest’ solutions are chosen to survive to the next generation. This procedure is iterated until the population converges. The EAs has a limitation due to the fact that the size of solutions (i.e., the number of knockouts) remains fixed throughout the EA's evolution. Consequently, in order to consider a

variant with variable-sized solutions (sets of genes or reactions), a set-based EA (SEA) has been developed that can search for the optimum set size in parallel with the search for the optimum set of gene or reaction deletions. The solution representation and evaluation principle of SEA is explained in detail in [366].

9.2.3 Minimization of metabolic adjustment (MOMA)

Engineered gene or reaction knockouts usually cannot achieve the maximum growth states as they are not exposed to long-term evolutionary pressure. This indicates that the optimization of growth rate, which is commonly used for wild-type organisms, is not appropriate to capture the biological essence of the knockout mutations. Therefore, Minimization Of Metabolic Adjustment (MOMA) is proposed as an algorithm for predicting metabolic flux distributions after gene or reaction knockout and its prediction has been experimentally validated [369]. MOMA relies on the conjecture that the mutant remains initially as close as possible to the wild-type optimum in terms of flux values. In MOMA quadratic programming is employed to identify a point in flux space which is closest to the wild-type point by minimizing the L2 norm (Euclidian distance) between the knockout flux values to wild-type steady-state flux values. The identified flux distribution of the mutant should also satisfy all constraints as in FBA. The MOMA is formulated as follows:

$$\min_{v} \sum_{j} (v_j - w_j)^2$$
$$s.t. \sum_{j} S_{ij} v_j = 0, \ \forall_i$$
$$v_{biom} \geq v_{\text{biom}}^{\text{target}}$$
$$v_j^{\min} \leq v_j \leq v_j^{\max}, \ \forall_i$$

where v_j represents the flux value of reaction j in mutant strains and w_j is the corresponding flux value in wild-type strains that is obtained via FBA ; v_{biom} is defined by summing the metabolite precursors that contribute to the biomass production in FBA . $v_j^{\min}$ and $v_j^{\max}$ are the lower bound and upper bound for v_j, which are determined by the availability of nutrients or the maximal fluxes that can be supported by enzymatic pathways [369].

9.2.4 Fitness function

The fitness function used here is Biomass-Product Coupled Yield (BPCY) [163], given by:

$$BPCY = \frac{P * G}{S}$$

where P stands for the flux representing the excreted product; G for the organism's growth rate (biomass flux) and S for the substrate intake flux.

This objective function allows for selection of mutants that exhibit high growth rates, while optimising for the production of the desired product. The overall process of decoding and evaluating a solution can be found in [366].

9.3 Results and discussion

Table 9-2: Summary of best results of strain optimization for redox product production for each microorganism using the BCPY objective functions for algorithm EA.

		Phenotype simulation			Reaction knockout strain				
		maximum growth rate	**maximum NADH production rate**	**BCPY objective**	**biomass**	**NADH**	**% of the maximum growth rate**	**% of the maximum net NADH production rate**	**A/g**
Geobacter sulferreducens	DET	0.6622	71.3077	0.3016	0.5648	9.6129	85.28%	13.48%	0.2576
	MET	0.6622	63.2158	0.1693	0.5524	5.4595	83.42%	8.64%	0.1463
	Mixed	0.6622	63.5577	0.0142	0.0689	8.1497	10.41%	12.82%	0.2184
Chlamydomonas reinhardtii	mixotrophic	0.4725	44.3340	0.0442	0.1221	3.6157	25.85%	8.16%	0.0969
	Autotrophic	0.1596	13.4427	0.000003	0.0099	0.0422	6.22%	0.31%	0.0011
	Heterotrophic	0.1665	21.5619	0.00004	0.0014	0.3110	0.82%	1.44%	0.0083
Synechocystis sp. PCC 6083	mixotrophic	0.0877	8.2529	0.2188	0.0502	1.6567	57.24%	20.07%	0.0444
	Autotrophic	0.0393	3.8161	0.0002	0.0216	0.1225	54.79%	3.21%	0.0033
	Heterotrophic	0.0889	8.7750	0.0185	0.0179	0.8786	20.14%	10.01%	0.0235
	Autotrophic reduced ferredoxin	0.0393	7.5656	0.0000	0.0010	0.4665	2.64%	6.17%	0.0125
	Autotrophic QH2	0.0393	14.8718	0.0003	0.0236	0.1629	60.08%	1.10%	0.0044
Saccharomyces cerevisiae	Aerobic	0.4350	115.5600	2.3130	0.3147	73.5047	72.34%	63.61%	1.9700
	Anaerobic	0.2607	103.2300	0.9147	0.1354	67.5579	51.94%	65.44%	1.8107

Overall, reaction deletion strategies worked well with *S. cerevisiae* knockout, with more than 60% of the theoretical maximum NADH-dependent electron transfer rate and over 50% of maximum growth being achieved. The mutants were created by a triple reaction deletion (Table 10-4, Appendix 1) in the case of aerobic condition, but by a septuple deletion in the case of anaerobic growth. On the other hand, the deletions could reach up to 20% of maximum electron transfer rates with comparatively high growth rates (more than 50% of the optimal wild-type growth rates) in some cases of *G. sulfurreducen* and the *Synechocystis*, but leads to less than 10% of theoretical maximum electron transfer rates and quite low growth rates (more than 70% reduction in growth rates) for the cases of *C. reinhardtii*.

Of the three case studies of *G. sulfurreducens*, OptGene identified a triple deletion mutant (Table 10-1, Appendix 1) that improved the electron transfer in DET mode up to 13.48% of theoretical limit, which was higher than that in MET (8.64%) and Mixed mode (12.82%). The reaction deletions could keep the growth rate at 85.28% and 83.42% of the optimal parental strain in the cases of DET and MET respectively, but lead to a major drop in the growth rate in the Mixed mode (more than 70% reduction in the optimal parental strain).

In the cases of *Synechocystis* sp. PCC 6083, a double reaction deletion (Table 10-2, Appendix 1) achieved 20.07% of theoretical maximum of the NADH-dependent electron transfer rate and 57.24% of the maximum wild-type growth rate, which is the highest BCPY obtained in all five study cases. In addition, the two suggested reactions were related to CO_2 and L-Glutamine uptake and thus the deletion could be simply achieved by excluding these two nutrients from the growth media. For the cases of heterotrophic and autotrophic-quinone, 10.01% and 3.21% of the theoretical maximum electron transfer rate were reached by the double deletions, with corresponding growth rates at 20.14% and 60.08% of the optimal reference rates. The lowest BCPY was achieved for NADH- and quinone- dependent electron transfer under autotrophic cultivation. In these two cases, the quadruple and double deletions respectively resulted in quite low flux values for NADH- (10.01% of the theoretical maximum) and ferredoxin- (3.21% of the theoretical maximum) dependent electron transfers under autotrophic growth, with low growth rates (10.01% and 2.64% of the optimal wild-type growth rates respectively). In addition, the NADH-dependent autotrophic mode required a deletion of up to nine reactions, and such a high reaction number could cause complexity when implementing the reaction deletions.

For *C. reinharditii*, a single reaction deletion (Table 10-3, Appendix 1) increased the NADH-dependent electron transfer in mixotrophic growth to 8.16% of the theoretical maximum, with a growth rate at 25.85% of optimal wild-type growth rate. On the other hand, to promote the electron transfer to the electrode, six and four reactions were needed to be deleted for the autotrophic and heterotrophic growth respectively. The suggested deletions span the amino acid, vitamin, fatty acid and nitrogen metabolism and some other organelles (transport reactions). Nevertheless, these reaction deletions only resulted in low fluxes through the electron transfer reactions in autotrophic (0.31% of the theoretical maximum) and heterotrophic growth (1.44% of the theoretical maximum). Also, the deletions lead to very

low growth rates for the two cultivation conditions (more than 93% reduction in growth rate), making these identified deletions less attractive.

The comparison of reaction deletion results among the four microorganisms indicates that the metabolism of *S. cerevisiae* is much more flexible than the other three microbes, while the metabolism of *C. reinharditii* is very robust against the reaction pathways modifications.

In addition, the reaction deletion results show that the flux distribution optimized for the biomass production was shifted away from the Pareto surface. The compromise of elevating the lower bound of the NADH-depend current transfer is to reduce the maximum biomass production rate, which means the Pareto surface identified previously is altered (i.e., the surface has been shrunk to somewhat extent; heavily shrunk for *Synechocystis* sp. PCC6803). This phenomena is akin to *Bacillus subtilis* mutants [370].

The repressed growth rates were thought to be attributed to the part objective, MOMA (minimization of metabolic adjustment), which was used to model the metabolic response to the reaction deletions. Therefore, MOMA, which can also be considered as a regulatory mechanism, together with the deletion strategies in effect lead to the electron transfers beneficial to MFCs in all 13 cases. The flux distribution computed by OptGene are the phenotypic characteristics of non-evolved strains, whereas FBA results indicate the phenotypes of strains achieved by evolution. The characteristic of the MOMA produced mutant strains represent short switching times corresponding to small flux adjustments, while FBA predicted strains were a result of long switching times likewise corresponding to large flux adjustments. The mutants account for fast-switching phenotypes that intend to migrate toward Pareto optimality, leading to an in-between flux distribution with suppression of growth rate but augmentation of desired electron transfer rates.

By incorporating the MOMA, OptGene probes part of the operating mechanisms underlying genetic interactions within metabolic networks, in a deletion growth phenotype.

The low current production percentages achieved by most of the knockout strains appear somewhat disappointing at first. However, the MFC case is different from most other bioengineering situations where gene knockouts are used to supply a driving force to

stimulate production of a target metabolite. In an MFC, the main driving force for stimulating production of current carriers comes from the interaction of the cell with its physical environment. The current flowing through an MFC will create a gradient of current carriers in the electrolyte (i.e. the medium that forms the cell environment) that will tend to extract NADH or electrons from the cell. So increased reducing equivalent production is expected as a response to the cell environment, quite independent of the shift in phenotype due to knockouts. Gene knockouts are merely a supporting strategy. Seen from this perspective, the maximum reducing equivalent production rates of the OptGene results can be considered as the new minimum of the achievable rate range by the mutant strains.That is why it is relevant to still investigate the maximal reducing potential in the mutants.

To elucidate the upper limits of current output sustainable by the reaction knockout strains, we use FBA to compute the maximum reducing equivalent production rates at 5% of the optimal growth rates for each operational mode. In this method of modelling, the MOMA mechanism no longer prevents the metabolism allocating more resource towards the desired electron transfers. Figure 9-1 shows the potential of the four knockout strains for MFC current production, in comparison with that of control strains. It is shown that in the case of *G. sulfurreducens*, the identified reaction knockout elevated the lower bound of the DET output and upper bound of the wild strain, but remarkably reduced the maximum achievable reducing equivalent production rate for the MET mode. For *C. reinhardtii*, the proposed knockout strains did not significantly improve heterotrophic and photoautotrophic modes, but raised the lower threshold of the mixotrophic mode. The improvement in the five cases of the *Synechocystis* is not obvious, since the reducing equivalent production rates were relatively lower on the scale when compared to other three microorganisms. The mutants experienced notable decrease on the maximum reducing equivalent production rates in the QH_2 and ferred-dependent photoautotrophic and NADH dependent mixotrophic modes. The other two modes, NADH-targeted photoautotrophic and heterotrophic modes stayed similar with the mutant strains. *S. cerevisiae* remained at almost the maximum capability of NADH_mfc production rate while the lower bound have been significantly increased. Therefore, the reaction deletions identified by OptGene worked efficiently in the two cases of *S. cerevisiae*.

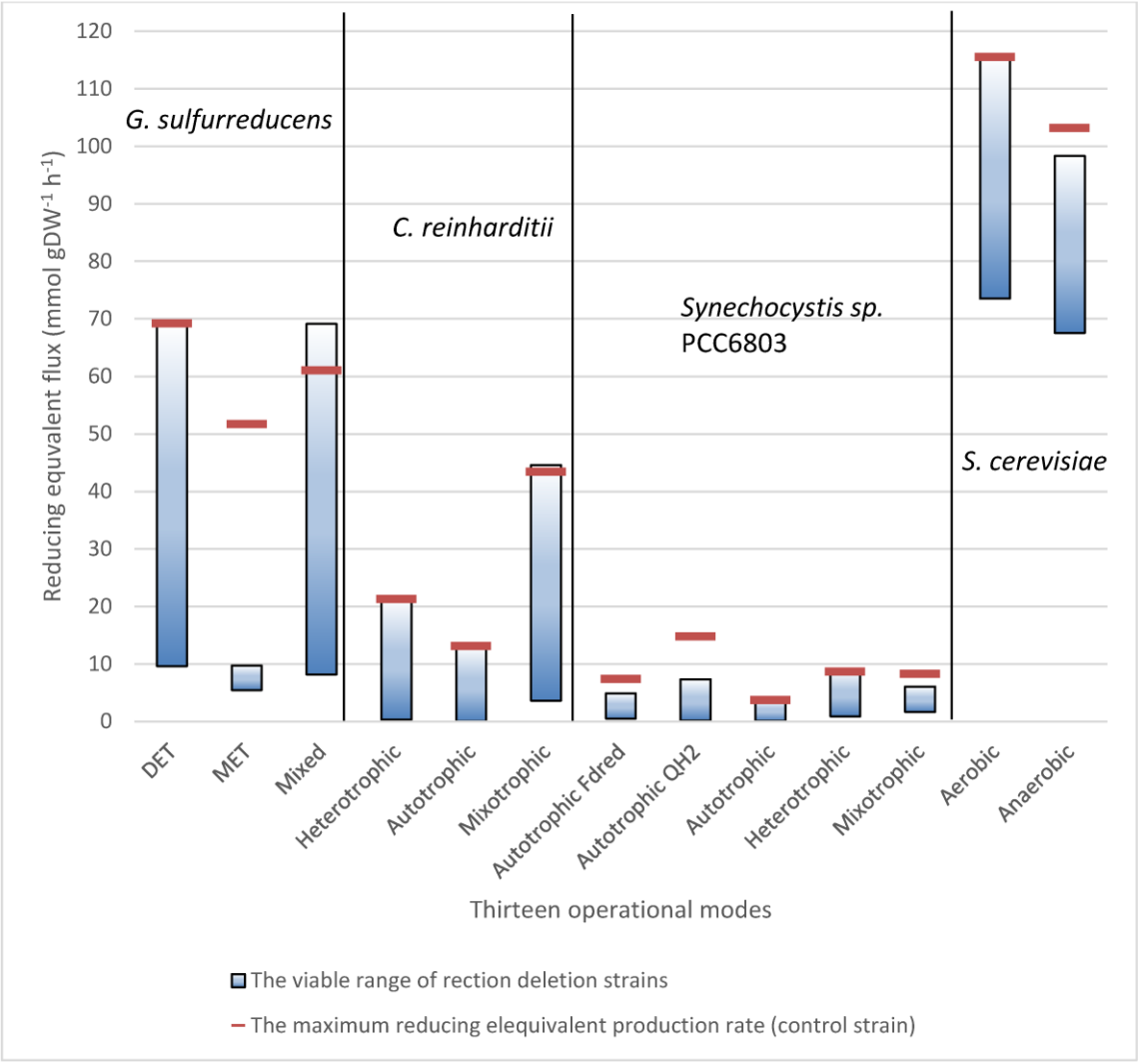

Figure 9-1: Comparison of the current production potential of reaction knockout strains.

The bottom of the gradient blue bar denotes the reducing equivalent production rate of the MOMA produced mutants; the top of the bar represents the FBA predicted the highest achievable reducing equivalent production potential of the mutants after evolution. The Fdred, ferredoxin reduced from. QH2, quinol.

The philosophy of the bi-level optimization framework is similar to that of the compound objective-based optimization. Both techniques use the maximization of biomass production to prune out phenotypes that are non-viable and incorporate a second objective to further search the previously computed viable solutions for a desired solution. Nevertheless, in the way of bi-level-optimization the relationship between the first objective and the second objective functions cannot be elucidated, whereas the compound objective uses λ to weigh the priorities between the two objectives and thus their relationships can be assessed by varying λ.

The MOMA method was used to replace the inner FBA problem in the bi-level optimization procedure. This modification makes the reaction knockout algorithm possess an ability to characterize sources of mispredictions for non-evolved strains. A previous study has shown that MOMA predicts around 10 more lethal genes/reactions than FBA [156].

Similar to many previous studies that involve growth coupling of a bioengineering production objective to perform strain design strategy [163, 173, 371, 372], the proposed reaction knockout solutions are expected to produce the designs through adaptive evolution [373].

9.4 Conclusions

In different electricity generation cases for the four microorganisms, OptGene proposed straightforward but also non-intuitive strategies for reaction deletions. These deletions that resulted in the greatest immediate improvement in electron transfer rate were achieved for *S. cerevisiae,* whereas the deletions resulted in poor immediate improvement in all three cases of *C. reinhardtii*. In addition, despite the reaction knockout elevating the lower bound of current output of *G. sulfurreducens* in the MET mode, the upper bound (the maximum achievable current output value) was greatly repressed. This implies that further development of an engineering method may still be needed to identify and remove metabolic obstacles in these microorganisms to achieve higher productivity, with the aid of the knowledge of maximum potential and pertinent pathways of wild strains computed in previous chapters 4-7. Moreover, future work may conduct detailed analysis to elucidate metabolic pathways to promote electron transfer in these reaction deletion mutant strains.

CHAPTER 10 Conclusions, perspectives and general overview

10.1 General overview

The study centres on the efficiency and capability of genome-scale metabolic mechanisms of the four selected microorganisms to generate desired reducing equivalents, and the flux adjustments to enable the microorganisms to grow in energy extraction situations. This is the only specific context in which the maximum current output can be fundamentally explored. Through the analyses of the genome-scale stoichiometry reaction models, the study has identified metabolic states that can promote the tested electron transfer at high rates in thirteen cases of possible electricity generation for the four representative microorganisms. The results have indicated that *S. cerevisiae* and *G. sulfurreducens* are better candidates for current production due to their higher potential for current output than the other two organisms. Although *C. reinhardtii* and the *Synechocystis* may have lower performance in current output, they may gain advantages from their uniquely biological characteristics such as photoautotrophic growth and good adaptivity for different growth conditions. In general, the innate potential of these microbes for electricity generation are much higher than the reported values from experimental studies. As a way to facilitate liberation of the high current-producing potential of the four organisms, the deletion strategy appears to be an effective way to lift some metabolic burdens and produce strains that are prone to supplying electrons for energy extraction process in MFCs.

The literature review of this thesis indicates that, for optimization of the electron transfer process and fuel cell performance, conventional MFC research focuses on the study of electron transport proteins, development of electrode materials and fuel cell design. The tools used in such research usually include microarrays, proteomics, confocal laser scanning microscopy, electrochemical, protein and metabolite analyses. On the contrary, in addition to these tools, this study has shown that *in silico* constraint-based modelling could be a complementary tool to explore questions concerning the metabolic capability of the biocatalysts. The genome-scale metabolic networks for a number of microorganisms have

been reconstructed. Among them, four microorganisms are selected for the analysis in the present study after taking into account the cell type, operation mode, electron source and the availability of metabolic network specifications.

It could be found that one microorganism has several reconstructed networks available from different research groups, such as in the case of *C. reinharditii* and *Synechocystis* sp. PCC 6803. Each of these two microorganisms has two networks published in the same period. Selection of networks for analysis is not easy, since it would need to investigate into the network model and gather evidence to justify each version of network based on their prediction ability. The selection among the two network versions for modelling *C. reinhardtii* and the *Synechocystis* has been discussed in the methods section of Chapter 5 &7. Nevertheless, the reconstructed networks are usually only validated by their successful prediction on growth rate and the prediction accuracy for other objectives requires additional validations. This creates another burden for model users to decide on network versions published by different research groups. The current opinion on selection of network models accentuates that the complexity is not a proof supporting choosing the complex model unless statistical evidence demonstrates a significant increase in predictive power for a more complex model; the metabolic model should focus on accurate reflection of metabolism in high quality, rather than to make up a maximal number of reactions, most of which are unverified [374]. Since statistical comparison of the prediction abilities of these network models diverges from the purpose of the present study, we did not carry out such a task.

As no published study had conducted genome-scale analysis of the microbial metabolism during MFC operations, we developed a computational framework to produce and study the flux distribution map of the metabolic state perturbed by *in silico* electron diversion. In total, thirteen cases of electron transfer were modelled to obtain a snapshot of behaviour across four organisms in MFCs under the optimal growth conditions. Their potential for MFC use was evaluated based on amperage output per gram, which can reveal *a priori* criteria for ranking the values of microorganisms for MFCs based on their metabolism efficiency. The results also indicate that, due to the different biochemical wiring of the metabolisms, the four microbes implemented different mechanisms for supporting large electron drains in NADH-dependent electricity generation.

The method predicts feasible flux distributions maximizing the production rate of a predefined biomass, while testing for its ability to cope with redox balance disturbance under electron generation. This is achieved by using a dual-objective function formulated through linear combination of the growth objective and the desired objective of electron transfer. The Pareto surface (front) defines the metabolic optimality in the form of (i) biomass and (ii) energy extraction by MFCs. The optimal biomass yield or growth rates have been proved to be meaningful objectives in nutritionally rich and scarce nutritional environment [168]. We did not incorporate another objective, such as minimization of flux adjustment [311], to optimize resource allocation. Such an objective may only be important to accurately predict the flux distribution of microbes in the optimal state for certain bacteria such as *E. coli* and no evidence has supported this objective to be as universal as optimal biomass yield to all microorganisms.

It is thought that under such an extreme current-producing condition, the solution space should be heavily reduced and most of viable flux distributions available in optimal condition would be disabled, and thus there is no need to introduce an extra objective, such as minimization of flux adjustments, to represent the pathway selection process of the cell. Many functional states appearing in the optimal condition should be abandoned to leave resources for growth, in order for microbes to survive. This hypothesis conforms with the up-to-date understanding of the empirical optimality principles (the main purpose) of the microbial metabolism, that is, conversion of nutrients into building blocks and energy for maximal growth rate [131, 149].

The λ was used to weigh the priority of the desired objective relative to the growth. If one wants to avoid use of λ, then a two-stage optimization can be used instead. In this way, first, growth rate is optimized for its maximal value. Then, the obtained growth rate serves as a constraint that is to be decremented in the second stage of the optimization for the desired electron transfer reaction. The constraint of the growth rate is decreased in a stepwise fashion, and for each decremented growth rate the added electron transfer reaction is solved through LP formulation. The obtained maximal NADH production rate is the same as the compound objective method. Nonetheless, the present study did not use the two-step optimization method because λ can be used to model the regulatory mechanisms of the cell and help illustrate at what growth rate the corresponding NADH production rate becomes steady (i.e., hardly increases, observed when λ was at of 0.9998). In addition, the same set of λ can be

applied to model different organisms, and circumvent the need to consider the interspecies difference in growth rate. The λ of 0.9998 was used to simulate a metabolic state for each case of electron transfer modes and as a tool to investigate the metabolic strategies for coping with a highly NADH-perturbed steady state. Other λ above 0.999 were also able to simulate a highly redox-disturbed metabolic state. The metabolic states modelled by the λ of 0.999 or higher were considered the same, since it does not matter whether the state is extremely perturbed or just a little bit less extremely perturbed.

Because the reducing equivalents investigated here are native molecules involved in primary energy metabolisms, the current production linked to these molecules would cause minimal flux adjustments compared with the secondary metabolites. To examine the trade-off between the optimality and adjustment made to metabolisms by energy extraction, we developed fractional benefit analysis, which have quantified additional benefit of the trade-off to the metabolisms between the two objectives (i.e., growth and production of electron shuttles) in the thirteen cases. Importantly, fractional benefit analysis can depict how bi-objective optimization influence metabolic resource allocation.

The method, FATMIN, developed here serves as a foundation for probing the metabolic capability for regeneration of reducing chemicals that are widely involved in many cellular processes. The cornerstone of this method is FBA, which however, alone cannot sufficiently restrict the solution space by removing futile thermodynamically infeasible loops. With FATMIN, it is possible to exclude the futile portion of the flux spectrum without the premise of knowing the metabolite chemical potentials, which in most cases are not easy to obtain. Therefore, FATMIN, which is only based on available stoichiometry, can significantly increase the predictive power of a genome-scale model.

FATMIN relies on an additional selection criteria, i.e., minimization of futile fluxes, to maximize the efficiency of the metabolic resource usage under a highly disturbed metabolic state. This intends to incorporate a common notion that evaluation in a constant environment minimizes the expression of enzymes, in order to reduce the ‘cost’ to produce those enzymes (e.g., growth burden due to production and maintenance of the Lac proteins (cost) [375]) and gain more ‘benefit’ [167, 375].

For NADH-dependent electricity generation, the FATMIN results showed that the metabolic strategies employed by *G. sulfurreducens* involved reactions located in the TCA cycle, amino acid and fatty acid metabolisms. Under mixotrophic and photoautotrophic growth conditions *C. reinhardtii* mainly relied on the reactions participating in the fatty acid and amino acid metabolisms to regenerate NADH at a high rate, whereas under heterotrophic growth, the NADH availability was additionally contributed to by the chloroplast and glyoxysome. In the cases of *Synechocystis*, the high NADH flux could be produced by reactions related to glycolysis, amino acid, fatty acid and energy metabolisms. Finally, *S. cerevisiae* under both anaerobic and aerobic conditions depended on the reactions situated in the nitrogen metabolism and amino acid (folic acid) metabolisms for regeneration of NADH at a high rate. Furthermore, it was found that fluxes through glycolysis could contribute more to the NADH regeneration in the cases of glucose-fed metabolisms (*Synechocystis* and *S. cerevisiae*) than those of acetate-fed metabolisms (*G. sulfurreducens* and *C. reinhardtii*). This indicates that the choice of substrate, rather than the different nature of metabolisms, could have an impact on the metabolic strategies selected by the microorganisms for NADH-dependent electricity generation.

Future studies could employ the same approach here to analyse other organisms in the user-defined conditions by including additional weights for the importance of other objectives and adjusting specific constraints of reactions to more acceptable levels, to reflect a meaningful biological pattern under different growth environments, such as scarce nutritional conditions. There will be an iterative analysis process for associating the *in silico* constraint based modelling to up-to-date experimental results.

10.2 Contributions

The main contributions of this thesis are:

1. Development of a framework for modelling the metabolism of microorganism perturbed by electricity generation. In addition, based on the framework, MFCoT, a computational toolbox, is developed for modelling the metabolism of any interested

microorganism under current production, based on any interested intracellular electron shuttle.

2. Development of the FATMIN algorithm to characterize alternative optimal solutions (AOSs) without disturbance of futile cycles.

3. Elucidation of the inherent capacity of *G sulfurreducens* for electricity generation in the DET, MET and Mixed modes.

4. Comparison of the mediated current generation capacity of *C. reinhardtii* in photosynthetic and respiratory growth modes.

5. Exploration of the maximum current outputs of *Synechocystis* sp. PCC 6803 in MET and DET modes in photoautotrophic, heterotrophic and mixotrophic cultivation conditions.

6. Identification of the metabolic potential of *S. cerevisiae* for MET under aerobic and anaerobic conditions.

7. Comparison and analysis of the underlying metabolic mechanisms chosen by the four microorganisms for maximal amperage output.

8. Exploring the microbial strain design by reaction deletion to improve the electricity generation performance of the four microorganisms.

Overall, we have provided a systematic understanding of how electricity generation can impact cellular metabolism.

The first contribution of this thesis is the development of a framework that has been outlined through a number of steps: selection of microorganisms, retrieval of genome-scale metabolic networks, implementation of a multiple objective approach, setup of SBML file including proper parameters and application of constraint-based modelling methods, i.e., FBA, FVA

and FATMIN. A metabolic network is reconstructed based on knowledge obtained by genomic, transcriptomic, proteomic and metabolomics tools and thus provide the most compact and informative representation of a hypothesis of how a cell works. Constraint-based modelling has successfully been applied to investigate the functional metabolic states of cells. Therefore, taken together, the framework developed based on previous established methods should be able to yield reliable and unbiased prediction results. Besides, the framework method is based on linear programming to find the global optimal in a genome-scale stoichiometry model with a huge space of search parameters. This avoids the calculation complexity that is commonly encountered in non-linear systems at a large-scale.

The method addressed here has two advantages, it is cost effective, i.e., existing previous data and optima can be identified within hours. The predictivity is ensured by the experimental verification of the model in previous publications. The metabolism perturbed by energy extraction can also be studied by high throughput analysis approaches, such as analysis of cellular component levels, transcript levels, metabolite levels, or protein levels (relevant techniques including, genome sequencing, microarrays, or 13-C flux analysis). However, these approaches are not cost-effective and resultant high throughput data can in effect construct a descriptive model, but lack information for the past or future cell states, which can only be predicted and elucidated by the FBA model [171].

The second contribution is the development of the FATMIN algorithm, which is a method pipeline integrated with the functions of FBA and FVA, for computing the metabolic flux flexibility in a context-dependent manner. FATMIN can resolve two problems: 1) flux computed from FBA and FVA may contain futile value. 2) FBA results are hardly likely to be unique, since alternative optimality commonly exists.

FATMIN removes the futile portion of a reaction flux value that has no contribution to the defined objective. As a consequence, the method implicitly eliminates Type III extreme pathways (i.e., a unique set of convex basis vectors of the flux distribution solution space that do not include exchange reactions [291]), which do not contribute to the desired objective. However, the running time for the computation of all extreme pathways increases exponentially with system size [376, 377], which makes it impossible to enumerate all possible cycles in a genome-scale network [378]. As eukaryotic metabolic networks consist of

thousands of reactions, it is worthwhile to consider run-time when devising *in silico* methods, and the presented FATMIN approach, dependent on LP, would be less computational demanding for large-scale network modelling than previous methods based on MILP.

FATMIN uses FVA to identify the existence of alternative optimal solutions due to degeneracy in stoichiometric networks. There can be an infinite number of flux distributions satisfying the given optimality criteria. The size of the optimal flux space can be reduced by adding tighter limits onto each flux in the network. For example, intracellular flux measured by nuclear magnetic resonance (NMR) [379] can be used as a constraint. However, additional constraints can reduce the size of the solution space but not result in a unique solution. The infinite equivalent solutions resulting from *in silico* modelling make it different from the physicochemical sciences where a single and unique solution can be obtained. The mathematical notion of equivalent optimal states *in silico* modelling in biology is considered as an analogy to the biological notion of silent phenotypes [138].

In summary, FATMIN circumvents the need to fully characterize the optimal solution space of genome-scale stoichiometric models (a polyhedron) corresponding to FBA to remove futile cycles and captures the alternate optimal solutions at genome-scale in the form of flux ranges. Because vertices generally appear in large numbers that are quite meaningless to experimental biologists, this approach does not intend to identify all vertices that represent combinations of reaction paths through the network that maximize an objective. Instead, the outcome of the approach is a list of reactions (enzymes) that produce some target metabolite at a high rate. This information would enable experimental biologists to get essential information about candidate pathways for bioengineering, and about biological burdens that restrain high production rates of the target metabolite.

The third contribution is the computation of the fundamental metabolic potential of *G. sulfurreducens* for current output and elucidation of the possible metabolic strategies to sustain the NADH for current production under the MET and Mixed modes. The results showed that *G. sulfurreducens* had a potential to output current at up to 3.710 A/gDW for DET mode, 2.711 A/gDW for MET mode and 3.272 A/gDW for a putative mixed MET and DET mode. Compared with DET, which relies on only one contributing reaction, MET and Mixed modes were more resilient with ten and four reactions respectively for high current

production. Overall, the DET mode can achieve a higher maximum limit of the current output than the MET mode, but the MET has an advantage of a higher power output and more flexible metabolic choices to sustain the electric current. The MET and DET modes compete with each other for the metabolic resource for the electricity generation.

The fourth contribution is the computation and comparison of the NADH-dependent MET mode under three broad nutritional modes: heterotrophic, photoautotrophic and mixotrophic modes. The results showed that *C. reinhardtii* in the mixotrophic growth mode achieved the highest current output (2.368 A/gDW), followed by heterotrophic growth (1.141 A/gDW) and photoautotrophic growth the lowest (0.7035 A/gDW). The significantly higher MET rate in the mixotrophic mode was attributed to the fact that the photophosphorylation improved the efficiency of converting the acetate into biomass and NADH production. The cytosolic NADH-dependent current production was mainly associated with five reactions in both mixotrophic and photoautotrophic nutritional modes, whereas four reactions participated in the heterotrophic mode. The mixotrophic and photoautotrophic metabolisms were alike and shared the same set of reactions for maximizing current production, whereas in the heterotrophic mode, the current production was additionally contributed by the metabolic activities in the two organelles: glyoxysome and chloroplast. Overall, *C. reinhardtii* has a potential to be exploited in MFCs of MET mode to produce a current much higher than the previously studied product mode that was based on *in situ* oxidation of hydrogen produced by the alga. The mixotrophic cultivation is the best nutritional mode for the electricity generation. It is worth further research efforts to liberate the probed current-production potential of *C. reinhardtii*, with the help of the referential metabolic mechanisms elucidated in this chapter.

The fifth contribution is the investigation of the current outputs of the *Synechocystis* under five electron transfer modes, namely, ferredoxin- and plastoquinol-dependent MET and c-type cytochrome-targeted DET under photoautotrophic cultivation, and NADH-dependent MET under photoautotrophic, heterotrophic and mixotrophic conditions. In these five modes, the maximum current outputs were computed as 0.198 A gDW^{-1}, 0.7918 A gDW^{-1}, 0.198 A gDW^{-1}, 0.4652 A gDW^{-1} and 0.4424 A gDW^{-1} respectively. Comparison of the five operational modes suggests that plastoquinol- /c-type cytochrome- targeted electricity generation had an advantage of liberating the highest current output achievable for *Synechocystis sp.* PCC 6803. On the other hand, the analysis indicates that the currency

metabolite, NADH-, dependent electricity generation can rely on a number of reactions from different pathways, and is thus more robust against environmental perturbations.

The sixth contribution is the examination of *S. cerevisiae* for MET based current production under aerobic and anaerobic conditions. The results showed that, in the cytoplasmic NADH-dependent MET mode, *S. cerevisiae* had a potential to produce currents at up to 5.781 A/gDW for the anaerobic and 6.193 A/gDW for the aerobic environments. It is also showed that the aerobic and anaerobic metabolisms are resilient, relying on six and five contributing reactions respectively for high current production. Two reactions, glutamate dehydrogenase (NAD) (EC 1.4.1.2) and methylene tetrahydrofolate dehydrogenase (NAD) (EC 1.5.1.15), were shared in both current-production modes, and contributed to over 80% of the identified maximum current outputs. Notably, it was found that the flux through the reaction catalysed by alcohol dehydrogenase (EC: 1.1.1.1) merely had a flux of 6.049 mmol/gDW/h under the high degree of NADH perturbation. This is contrary to a previous reporting where alcohol dehydrogenase was suggested as the main NADH sink for mediators. It is also shown that the NADH regeneration was much less energy costly than biomass production rate. Taken together, our finding suggests that *S. cerevisiae* should receive more research effort for MFC electricity production.

The next contribution is the comparison of the amperage outputs and metabolic features of the four microorganisms for current generation. The analysis results indicate that *S. cerevisiae*, along with *G. sulffurducens*, are promising biocatalysts with potential to produce higher currents than the other two microorganisms. *C. reinhardtii* and the *Synechocystis* are less competitive in current output, but they possess photo-autotrophic capability which avoids the demand for continuous substrate feed. It is found that the DET mode based on cytochrome *c* could produce higher coulombic efficiency than mediated NADH-dependent electron transfer in the two studied prokaryotes (*G. sulfurreducens* and *Synechocystis* sp. PCC 6803), but at a lower electrode potential that affects the overall power outputs. Compared to the other three microbes, *S. cerevisiae* was found to have an overwhelming advantage in current output and coulombic efficiency. In contrast, the CE% was quite low with *C. reinhardtii* (below 50%), making this organism less favoured for an MFC. Furthermore, the four microorganisms were different in the selection of pathways to maximize the current production. These novel findings are expected to be referential to MFC research communities for further justifying the effort to exploit these species in practical current production.

The last contribution is employment of strain optimization to predict reaction deletion that increases the flux through the target electron transfer reactions in different cases. The identified knockout strategies could elevate the lower limits of the wild type organisms for current production. The reaction deletions did not increase the minimum of the reducing equivalent production rates significantly for *G. sulfurreducens*, *C. reinhardtii* and the *Synechocystis*. The reaction deletion strategy worked effectively on *S. cerevisiae* producing mutants that increased the minimum NADH_mfc production up to two-thirds of the theoretical maximum.

10.3 Limitation of the present study

It should be noted that this study evaluated a comprehensive, but limited, subset of the theoretically infinite number of genetic and environmental parameter values and combinations. This is due to the fact that metabolic flux models created for analysis were based on one particular condition, i.e., optimal growth.

The maximization of biomass production may not reflect what a microorganism tends to do in a given environment, which can make the objective-driven optimization define an inaccurate solution space shape (i.e., this could account for discrepancy between obtained phenotype and experimental observation). Microorganisms can experience any one of three growth conditions, i.e., nutritionally rich, scarce nutritional or elementally limited environments. For the first two conditions, the optimal biomass yield or growth rates are proved to be meaningful objectives based on cumulative data from batch growth (nutritionally rich) and chemostat growth experiments (nutritionally scarce) [168]. Nonetheless, for the case of the elementally limited condition no study has been conducted to verify the prediction ability of the optimality for biomass production [168]. Therefore, the data from the present study can be predictive for microbes grown in nutritionally rich and scarce conditions, but may not apply to those raised in elementally limited environments. In such a growth circumstance, maximization of biomass production may not be suitable to serve as an objective in evaluation of the microbial natural objective coupled electricity production. On the other hand, it could be concluded that the present study investigated the maximum potential of the selected microorganism to convert substrate to electricity, but overlooked the extreme cases of

microbial electricity production, i.e., the metabolic behaviours of microorganisms that experience lacks of element supply and reducing energy drain. Furthermore, the accurate objective of a particular microorganism under the extreme conditions may be elucidated by analysis of its evolutionary history [168].

The premise of the pseudo steady state in FBA avoids the difficulties in developing kinetic models, such as extensive parameterization, and performing intracellular experimental measurements. This feature makes the FBA approach have a wider applicability than kinetic modelling, but consequently loses the ability to explicitly estimate the intracellular metabolite concentrations and to clarify metabolic regulatory mechanisms that can only be described by kinetic modelling. Therefore, the discrepancies between FBA-predicted results and observed results of other '-omic' studies may be ascribed to the unaccounted metabolic regulatory mechanisms. In addition, FBA approach requires *a priori* knowledge of uptake fluxes, which may restrict its use to settings at which they are constrained by experimental data. This is different from the kinetic approach that involves the computation of metabolite levels, allowing for a mechanistic process description linking intracellular conditions to environmental conditions.

Furthermore, in the calculations, the uptake rates used for the modelling were derived from experimentally measured values for optimal growth. Nonetheless, these values may be conservative for the extreme condition - the redox perturbed cases during MFC operation, which might make additional demands on the metabolism to conceivably consume more substrates. This speculated behaviour would increase the current production, and if this type of response is different for different species, it may influence the comparisons made in this study.

Previous MFC studies tend to focus on including the biofuel cell configuration of the MFC, such as electrode area, reactor volume, electrolyte, etc. It is noted that most experimental MFC studies lacks clarification of the cell density during MFC operation. This lead to difficulties of comparing the observed amperage outputs and the theoretical computed ones. Therefore, for better comparison of the *in silico* computed amperage output and the experimentally measured ones, future MFC studies might need to measure or estimate the cell density during fuel cell operation.

The framework and methods presented in this study are only suitable for microorganisms with available GEMs. The prediction accuracy of the framework developed in the present study is mostly determined by the quality of the underlying network models, which serve as analysis skeletons. In particular, the GEMs could be further improved by incorporating additional biological mechanisms, such as transcription and translation regulation. These mechanisms are responsible for the functional consequences upon metabolic perturbations since they can regulate a range of cellular components such as tRNA charging enzymes, the ribosomal proteins, and subunits of the RNA polymerase [380, 381]. Upregulation of these cellular components can increase the growth rate by promoting translation and transcription rates. Unfortunately, the wirings within these regulation behaviours have not been characterized at genome-scale, making it impossible to include the transcriptional regulatory information into the present modelling. However, it would be promising if a GEM model could integrate these three biological mechanisms, so as to provide a complete understanding for the link between genotype and phenotype [112].

It is noted that the network model for *S. cerevisiae* is frequently updated with minor corrections. For the present study, a yeast network version 5 was used (the most updated one in December, 2012), but at present (2013) a newer but unpublished version 6 has been released. Nevertheless, for a large-scale metabolic network, the minor change, such as addition or deletion of one or two reactions, can hardly lead to significant modifications to the network stoichiometry and thus the prediction results should be consistent. Indeed, the way of modelling based on published network has a limitation in that the quantitative results are influenced by the integrity of the genome-scale network.

This thesis primarily consider NADH as the intracellular electron source in order to compare the difference in current output and energy pathways of the four organisms during the MFC operation of the MET mode. However, this may provoke a concern that the present study did not investigate the role of NADPH and its relationship with NADH during the current production of the MET mode. According to our obervations, the metabolic models, such as in the case of *C. reinhardtii*, had the same metabolic efficiency for regeneration of NADH and NADPH. In other words, when either NADH or NADPH alone, or a mixture of both at varying ratios, was modelled as the intracellular electron source for the oxidised mediators, the maximum computed current outputs statyed the same. This implies that these two redox molecules are interchangeable for identifying the maximum potential of microbes for current

production, and the present metabolic models lack the themodynamical constraints to differeniate the metabolic and enegetic costs of the synthesis of the two molecules. In summary, synthesis of NADH is more energetically efficient than NADPH in the heterotrophic nutritional mode, as the NADPH is formed from two major mechanisms [347]: the first is that NADPH is generated from NADH and $NADP^+$ by transhydrogenase; the second is that NADPH is generated from $NADP^+$ by multiple $NADP^+$-dependent enzymes. However, these two mechanisms require $NADP^+$ and/or NADH that is generated *de novo* from NAD^+ kinases at the expense of ATP [347, 382]. On the other hand, in the noncyclic electron transport chain of photosynthesis, the two light-harvesting complexes, photosystem I (PSI) and photosystem II (PSII), generate both ATP and NADPH needed for the Calvin-Benson cycle that produces starch as an additional energy resource to sustain biosynthesis. Since the previous experimental MFC studies could not explain the roles of NADH and NADPH in the electricity generation in practice [61] and study of the interaction of the two reducing molecules deviates from the scope of the thesis, here we presumed the metabolic perturbation caused by the current output would have a direct impact on the energy metabolism, instead of NADPH-dependent anabolic reactions.

OptGene optimization identifies the reaction knockout providing solutions for overcoming the inherent metabolic robustness and host stress at those desired metabolic states with high productivity. However, the knockout solutions might be lethal and thus require further experimental validations. Another limitation of OptGene is that the time taken to obtain a reaction deletion solution could be very long when the algorithm is performed on some large-scale networks using MOMA. For example, in the case of *C. reinhardii*, it took several days to finish the computation.

Furthermore, flux determination in this study assumes that enzymatic reactions are homogenous inside the cell and that there are no transport limitations between metabolite pools. However, the eukaryotes have organelles (compartments) that may have diffusion limitations or metabolite channelling [120, 383, 384].

10.4 Future perspective

Subsequent to this study, the next task is to calibrate the modelling with data from experimental studies and develop electron shuttling compounds that can effectively accept the electrons from these identified reducing equivalent production sites. For eukaryotes, in future it may be worthwhile to explore possibility of the organelles as redox molecules supplier, but this requires identification of redox shuttles that can enter or arrive closely at the organelles. It is noted that, with the rise of nanotechnology, nano-sized mediators could be designed to access the intracellular reducing energy of the cell where traditional mediators cannot reach.

As a direct extension to improve the prediction accuracy of the presented method, it would be possible to measure the fluxes of some certain reactions across a variety of conditions using metabolomics and then employ statistics to the gathered flux data to calculate proper lower and upper bounds that can be used in the steady state calculation. More constrained lower and upper bounds on the reactions in the network can possibly improve the prediction accuracy. Another way is to integrate regulatory constraints in GEM models, which can improve the accuracy of phenotype predictions [385]. Regulation is suggested to account for many phenotypes. However, many regulatory mechanisms are not understood and require further elucidation.

The whole metabolic engineering scheme presented here is malleable and can be adapted for all different kinds of organisms and the different electricity generation mode dependent on various intracellular electron carriers in the future. The experimental subjects used were published GEM models, and thus the predictive power of the whole framework can be improved by incorporating more biological information (e.g., more genes/reactions) into the model. In addition, the augmented GEM would demand more available computing power to conduct strain optimization.

This study is complementary to other MFC studies that focus on the improvement of engineering design and selection of different organisms based on reductionist selective strategies. Further metabolic engineering of MFC biocatalysts may need to consider a range of factors, including (i) the predicted current output of different microorganism for specific growth conditions; (ii) cost and availability of the substrates; (iii) availability of methods for

debottlenecking the pathways to produce the desired product; (iv) negative consequences following adjustment of the metabolic route or expression levels of enzymes.

Another thought would be to test for the best combination of possible variables in the model for higher current output, such as different combinations of substrates. This may lead to development of a 'recipe' for culturing the microbes into a metabolic state in which an optimal organic-to-electricity efficiency is favourably attainable. However, the theoretically infinite number of genetic and environmental parameter values and combinations would make this task impossible to conduct based on available computer power.

It is commonly seen that mixed cultures achieve higher current than pure culture in MFCs. The higher current achieved for the mixed culture may be attributed to the mutualism among microbial diversity. A number of symbiotic mechanisms have been proposed, such as that mediators secreted by one type of microbe improve the electron transfer of the electrogenic species, and the biofilm formed by the mixed culture could increase the number of the electrogenic cells that participate in conveying the electron shunt towards anode by building a solid conductive matrix (networking). Furthermore, a recent study has found that the interaction of microbes can result in living micro-cables in the form of long filamentous bacteria of the *Desulfobulbaceae* and the micro-cable enables the transport of electrons over a distance up to 1 cm [386]. All these mutualistic behaviours should be fundamentally supported and linked at the metabolic level. This indicates that it would be desirable to employ an advanced computational approach to elucidate the metabolic connection underlying the aforementioned symbiotic, syntrophinic and/or synergetic relationships, for exploitation of the electricity generation potential of mixed culture. The four microorganisms have respective advantages for forming a mixture culture for use in MFCs. Since *C. reinhardtii* and *Synechocystis* sp. PCC6803 are photoautotrophic microorganisms that possess high growth rate, *G. sulfurreducens* is an exoelectrogen and *S. cerevieiae* is a cell factory that can produce a wide range of the by-products, it is possible to construct a microorganisms' interaction model to reveal the beneficial outcome of the mutualism of the four microorganisms.

Furthermore, although the reaction deletion strategies proposed by OptGene algorithm have devised strains that can achieve higher initial current output, it is also possible to employ or

develop other optimization algorithms to identify other ways of inducing the expression of more favoured metabolic states of these microorganisms.

10.5 Concluding remarks

The motivation for this thesis was the major research progress in both MFC and *in silico* metabolic modelling methods during the last decade. In summary, our research applied the constraint-based methods to four promising microorganisms to give a portrait of their capacities for electricity generation in MFCs, and revealed the pertinent metabolic characteristics supporting the diversion of electrons to the anode for high current outputs. A modelling framework was also developed and a method that can identify the flux ranges of reactions without interference of futile cycles in a large-scale metabolic network is presented in the thesis (discussed in the methods chapter). The present study appears timely and could serve as a template for elucidation of the electricity-producing potential of microbes and pertinent enzymatic mechanisms by *in silico* modelling. For the long term, the findings and the methods of the present research should be able to contribute jointly to the development of a novel research field, *in silico* biological engineering of MFC biocatalysts.

References

1. Potter MC: **Electrical Effects Accompanying the Decomposition of Organic Compounds.** *Proceedings of the Royal Society of London Series B, Containing Papers of a Biological Character* 1911, **84:**260-276.
2. Rittmann BE: **Opportunities for renewable bioenergy using microorganisms.** *Biotechnology and Bioengineering* 2008, **100:**203-212.
3. Pandyaswargo A, Onoda H, Nagata K: **Energy recovery potential and life cycle impact assessment of municipal solid waste management technologies in Asian countries using ELP model.** *International Journal of Energy and Environmental Engineering* 2012, **3:**28.
4. Eddine B, Salah M: **Solid waste as renewable source of energy: current and future possibility in Algeria.** *International Journal of Energy and Environmental Engineering* 2012, **3:**17.
5. Sharma V, Kundu PP: **Biocatalysts in microbial fuel cells.** *Enzyme and Microbial Technology* 2010, **47:**179-188.
6. Harnisch F, Schröder U: **From MFC to MXC: chemical and biological cathodes and their potential for microbial bioelectrochemical systems.** *Chemical Society Reviews* 2010, **39:**4433-4448.
7. Girguis PR, Nielsen ME, Figueroa I: **Harnessing energy from marine productivity using bioelectrochemical systems.** *Current Opinion in Biotechnology* 2010, **21:**252-258.
8. Li H, Opgenorth PH, Wernick DG, Rogers S, Wu T-Y, Higashide W, Malati P, Huo Y-X, Cho KM, Liao JC: **Integrated Electromicrobial Conversion of CO2 to Higher Alcohols.** *Science* 2012, **335:**1596.
9. Pant D, Van Bogaert G, Diels L, Vanbroekhoven K: **A review of the substrates used in microbial fuel cells (MFCs) for sustainable energy production.** *Bioresource Technology* 2010, **101:**1533-1543.
10. Schwartz K: **Microbial Fuel Cells: Design Elements and Application of a Novel Renewable Energy Source.** *MMG 445 Basic Biotechnology eJournal* 2007, **3**.
11. Logan BE: **Scaling up microbial fuel cells and other bioelectrochemical systems.** *Appl Microbiol Biotechnol* 2010, **85:**1665-1671.
12. Bullen RA, Arnot TC, Lakeman JB, Walsh FC: **Biofuel cells and their development.** *Biosensors and Bioelectronics* 2006, **21:**2015-2045.
13. Kato Marcus A, Torres CI, Rittmann BE: **Conduction-based modeling of the biofilm anode of a microbial fuel cell.** *Biotechnology and Bioengineering* 2007, **98:**1171-1182.
14. Zeng Y, Choo YF, Kim B-H, Wu P: **Modelling and simulation of two-chamber microbial fuel cell.** *Journal of Power Sources* 2010, **195:**79-89.
15. Zhang X-C, Halme A: **Modelling of a microbial fuel cell process.** *Biotechnology Letters* 1995, **17:**809-814.
16. Picioreanu C, van Loosdrecht MC, Katuri KP, Scott K, Head IM: **Mathematical model for microbial fuel cells with anodic biofilms and anaerobic digestion.** *Water science and technology : a journal of the International Association on Water Pollution Research* 2008, **57:**965-971.
17. Picioreanu C, Head IM, Katuri KP, van Loosdrecht MCM, Scott K: **A computational model for biofilm-based microbial fuel cells.** *Water Research* 2007, **41:**2921-2940.

18. Jung S: **Impedance Analysis of Geobacter sulfurreducens PCA, Shewanella oneidensis MR-1, and their Coculture in Bioeletrochemical Systems.** *International Journal of Electrochemical Science* 2012, **7:**11091-11100.
19. Kim BH, Park HS, Kim HJ, Kim GT, Chang IS, Lee J, Phung NT: **Enrichment of microbial community generating electricity using a fuel-cell-type electrochemical cell.** *Appl Microbiol Biotechnol* 2004, **63:**672-681.
20. Du Z, Li H, Gu T: **A state of the art review on microbial fuel cells: A promising technology for wastewater treatment and bioenergy.** *Biotechnology Advances* 2007, **25:**464-482.
21. Wang K, Liu Y, Chen S: **Improved microbial electrocatalysis with neutral red immobilized electrode.** *Journal of Power Sources* 2011, **196:**164-168.
22. Rabaey K, Verstraete W: **Microbial fuel cells: Novel biotechnology for energy generation.** *Trends in Biotechnology* 2005, **23:**291-298.
23. Rosenbaum M, Schröder U: **Photomicrobial Solar and Fuel Cells.** *Electroanalysis* 2010, **22:**844-855.
24. Yang Y, Xu M, Guo J, Sun G: **Bacterial extracellular electron transfer in bioelectrochemical systems.** *Process Biochemistry* 2012, **47:**1707-1714.
25. Nevin KP, Kim BC, Glaven RH, Johnson JP, Woodard TL, Methe BA, Didonato RJ, Covalla SF, Franks AE, Liu A, Lovley DR: **Anode biofilm transcriptomics reveals outer surface components essential for high density current production in Geobacter sulfurreducens fuel cells.** *PLoS ONE* 2009, **4:**e5628.
26. Reguera G, Nevin KP, Nicoll JS, Covalla SF, Woodard TL, Lovley DR: **Biofilm and nanowire production leads to increased current in Geobacter sulfurreducens fuel cells.** *Appl Environ Microbiol* 2006, **72:**7345-7348.
27. Richter H, Nevin KP, Jia H, Lowy DA, Lovley DR, Tender LM: **Cyclic voltammetry of biofilms of wild type and mutant Geobacter sulfurreducens on fuel cell anodes indicates possible roles of OmcB, OmcZ, type IV pili, and protons in extracellular electron transfer.** *Energy & Environmental Science* 2009, **2:**506-516.
28. Freguia S, Virdis B, Harnisch F, Keller J: **Bioelectrochemical systems: Microbial versus enzymatic catalysis.** *Electrochimica Acta* 2012, **82:**165-174.
29. Liu Z, Liu J, Zhang S, Su Z: **Study of operational performance and electrical response on mediator-less microbial fuel cells fed with carbon- and protein-rich substrates.** *Biochemical Engineering Journal* 2009, **45:**185-191.
30. Chae KJ, Choi MJ, Lee JW, Kim KY, Kim IS: **Effect of different substrates on the performance, bacterial diversity, and bacterial viability in microbial fuel cells.** *Bioresource Technology* 2009, **100:**3518-3525.
31. Berrios-Rivera SJ, Bennett GN, San KY: **Metabolic engineering of Escherichia coli: increase of NADH availability by overexpressing an NAD(+)-dependent formate dehydrogenase.** *Metab Eng* 2002, **4:**217-229.
32. Sauer U, Canonaco F, Heri S, Perrenoud A, Fischer E: **The Soluble and Membrane-bound Transhydrogenases UdhA and PntAB Have Divergent Functions in NADPH Metabolism of Escherichia coli.** *Journal of Biological Chemistry* 2004, **279:**6613-6619.
33. Pinchuk GE, Hill EA, Geydebrekht OV, De Ingeniis J, Zhang X, Osterman A, Scott JH, Reed SB, Romine MF, Konopka AE, et al: **Constraint-based model of Shewanella oneidensis MR-1 metabolism: a tool for data analysis and hypothesis generation.** *PLoS Comput Biol* 2010, **6:**e1000822.
34. Pollak N, Dölle C, Ziegler M: **The power to reduce: pyridine nucleotides – small molecules with a multitude of functions.** *The Biochemical journal* 2007, **402:**205-218.

35. Jeong H, Tombor B, Albert R, Oltvai ZN, Barabasi AL: **The large-scale organization of metabolic networks.** *Nature* 2000, **407:**651-654.
36. Park DH, Zeikus JG: **Electricity Generation in Microbial Fuel Cells Using Neutral Red as an Electronophore.** *Appl Environ Microbiol* 2000, **66:**1292-1297.
37. Babanova S, Hubenova Y, Mitov M: **Influence of artificial mediators on yeast-based fuel cell performance.** *J Biosci Bioeng* 2011, **112:**379-387.
38. Park DH, Zeikus JG: **Utilization of Electrically Reduced Neutral Red byActinobacillus succinogenes: Physiological Function of Neutral Red in Membrane-Driven Fumarate Reduction and Energy Conservation.** *Journal of Bacteriology* 1999, **181:**2403-2410.
39. Park DH, Zeikus JG: **Improved fuel cell and electrode designs for producing electricity from microbial degradation.** *Biotechnology and Bioengineering* 2003, **81:**348-355.
40. McKinlay JB, Zeikus JG: **Extracellular iron reduction is mediated in part by neutral red and hydrogenase in Escherichia coli.** *Appl Environ Microbiol* 2004, **70:**3467-3474.
41. Logan BE: **Exoelectrogenic bacteria that power microbial fuel cells.** *Nat Rev Micro* 2009, **7:**375-381.
42. Alberts B, Johnson A, Lewis J, Raff M, Roberts K, Walter P: *Molecular Biology of the Cell.* 4th edn. New York: Garland Science 2002.
43. Quan X-c, Quan Y-p, Tao K: **Effect of anode aeration on the performance and microbial community of an air–cathode microbial fuel cell.** *Chemical Engineering Journal* 2012, **210:**150-156.
44. Rosenbaum M, Cotta MA, Angenent LT: **Aerated Shewanella oneidensis in continuously fed bioelectrochemical systems for power and hydrogen production.** *Biotechnol Bioeng* 2010, **105:**880-888.
45. Biffinger JC, Byrd JN, Dudley BL, Ringeisen BR: **Oxygen exposure promotes fuel diversity for Shewanella oneidensis microbial fuel cells.** *Biosens Bioelectron* 2008, **23:**820-826.
46. Ringeisen BR, Ray R, Little B: **A miniature microbial fuel cell operating with an aerobic anode chamber.** *Journal of Power Sources* 2007, **165:**591-597.
47. Mao L, Verwoerd W: **Selection of organisms for systems biology study of microbial electricity generation: a review.** *International Journal of Energy and Environmental Engineering* 2013, **4:**17.
48. Logan BE, Hamelers B, Rozendal R, Schröder U, Keller J, Freguia S, Aelterman P, Verstraete W, Rabaey K: **Microbial fuel cells: methodology and technology.** *Environmental Science & Technology* 2006, **40:**5181-5192.
49. Bard AJ, Inzelt G, Scholz F: *Electrochemical Dictionary.* 2nd edn. Berlin, Heidelberg: Springer; 2012.
50. Choosri W, Paukner R, Wührer P, Haltrich D, Leitner C: **Enhanced production of recombinant galactose oxidase from Fusarium graminearum in E. coli.** *World J Microbiol Biotechnol* 2011, **27:**1349-1353.
51. Schröder U: **Anodic electron transfer mechanisms in microbial fuel cells and their energy efficiency.** *Physical Chemistry Chemical Physics* 2007, **9:**2619-2629.
52. Kim N, Choi Y, Jung S, Kim S: **Development of Microbial Fuel Cells Using Proteus vulgaris.** *Bull Korean Chem Soc* 2000, **21:**44-48.
53. Shukla AK, Suresh P, Berchmans S, Rajendran A: **Biological fuel cells and their applications.** *Current Science* 2004, **87:**455-468.
54. Wilkinson S: **"Gastrobots" -Benefits and Challenges of Microbial Fuel Cells in FoodPowered Robot Applications.** *Auton Robots* 2000, **9:**99-111.

55. Sund CJ, McMasters S, Crittenden SR, Harrell LE, Sumner JJ: **Effect of electron mediators on current generation and fermentation in a microbial fuel cell.** *Appl Microbiol Biotechnol* 2007, **76:**561-568.
56. Kim HJ, Hyun MS, Chang IS, Kim BH: **A microbial fuel cell type lactate biosensor using a metal-reducing bacterium, Shewanella putrefaciens.** *Journal of Microbiology and Biotechnology* 1999, **9:**365-367.
57. Kim HJ, Park HS, Hyun MS, Chang IS, Kim M, Kim BH: **A mediator-less microbial fuel cell using a metal reducing bacterium, Shewanella putrefaciens.** *Enzyme and Microbial Technology* 2002, **30:**145-152.
58. Lovley DR: **Microbial fuel cells: novel microbial physiologies and engineering approaches.** *Current Opinion in Biotechnology* 2006, **17:**327-332.
59. Chaudhuri SK, Lovley DR: **Electricity generation by direct oxidation of glucose in mediatorless microbial fuel cells.** *Nature Biotechnology* 2003, **21:**1229-1232.
60. Chang IS, Moon H, Bretschger O, Jang JK, Park HI, Nealson KH, Kim BH: **Electrochemically active bacteria (EAB) and mediator-less microbial fuel cells.** *Journal of Microbiology and Biotechnology* 2006, **16:**163-177.
61. Schaetzle O, Barriere F, Baronian K: **Bacteria and yeasts as catalysts in microbial fuel cells: electron transfer from micro-organisms to electrodes for green electricity.** *Energy & Environmental Science* 2008, **1:**607-620.
62. Gorby YA, Yanina S, McLean JS, Rosso KM, Moyles D, Dohnalkova A, Beveridge TJ, Chang IS, Kim BH, Kim KS, et al: **Electrically conductive bacterial nanowires produced by Shewanella oneidensis strain MR-1 and other microorganisms.** *Proceedings of the National Academy of Sciences* 2006, **103:**11358-11363.
63. Boesen T, Nielsen LP: **Molecular Dissection of Bacterial Nanowires.** *MBio* 2013, **4**.
64. Li P, Ki J-P, Liu H: **Analysis and optimization of current collecting systems in PEM fuel cells.** *International Journal of Energy and Environmental Engineering* 2012, **3:**2.
65. Cooney MJ, Roschi E, Marison IW, Comninellis C, von Stockar U: **Physiologic studies with the sulfate-reducing bacterium Desulfovibrio desulfuricans: evaluation for use in a biofuel cell.** *Enzyme and Microbial Technology* 1996, **18:**358-365.
66. Scholz F, Schröder U: **Bacterial batteries.** *Nature Biotechnology* 2003, **21:**3-4.
67. Rabaey K, Lissens G, Verstraete W: **Microbial fuel cells: performances and perspectives.** In *Book Microbial fuel cells: performances and perspectives* (Editor ed.^eds.). City; 2005.
68. Rosenbaum M, He Z, Angenent LT: **Light energy to bioelectricity: photosynthetic microbial fuel cells.** *Current Opinion in Biotechnology* 2010, **21:**259-264.
69. Davis F, Higson SPJ: **Biofuel cells--Recent advances and applications.** *Biosensors and Bioelectronics* 2007, **22:**1224-1235.
70. Bennetto HP, Delaney GM, Mason JR, Roller SD, Stirling JL, Thurston CF: **The sucrose fuel cell: Efficient biomass conversion using a microbial catalyst.** *Biotechnology Letters* 1985, **7:**699-704.
71. Rabaey K, Boon N, Hofte M, Verstraete W: **Microbial phenazine production enhances electron transfer in biofuel cells.** *Environmental Science & Technology* 2005, **39:**3401-3408.
72. Park HS, Kim BH, Kim HS, Kim HJ, Kim GT, Kim M, Chang IS, Park YK, Chang HI: **A Novel Electrochemically Active and Fe(III)-reducing Bacterium Phylogenetically Related to Clostridium butyricum Isolated from a Microbial Fuel Cell.** *Anaerobe* 2001, **7:**297-306.
73. Kim BH, Kim HJ, Hyun MS, Park DH: **Direct electrode reaction of Fe(III)-reducing bacterium, Shewanella putrefaciens.** *Anglais* 1999, **9**.

74. Logan BE, Regan JM: **Electricity-producing bacterial communities in microbial fuel cells.** *Trends Microbiol* 2006, **14:**512-518.
75. Bond DR, Lovley DR: **Electricity Production by Geobacter sulfurreducens Attached to Electrodes.** *Appl Environ Microbiol* 2003, **69:**1548-1555.
76. Lanthier M, Gregory KB, Lovley DR: **Growth with high planktonic biomass in Shewanella oneidensis fuel cells.** *FEMS Microbiology Letters* 2008, **278:**29-35.
77. Logan BE, Regan JM: **Microbial Fuel Cells, Challenges and Applications.** *Environmental Science & Technology* 2006, **40:**5172-5180.
78. Fan Y, Hu H, Liu H: **Enhanced Coulombic efficiency and power density of air-cathode microbial fuel cells with an improved cell configuration.** *Journal of Power Sources* 2007, **171:**348-354.
79. Zhang F, Cheng S, Pant D, Bogaert GV, Logan BE: **Power generation using an activated carbon and metal mesh cathode in a microbial fuel cell.** *Electrochemistry Communications* 2009, **11:**2177-2179.
80. Zuo Y, Cheng S, Logan BE: **Ion Exchange Membrane Cathodes for Scalable Microbial Fuel Cells.** *Environmental Science & Technology* 2008, **42:**6967-6972.
81. Chen G-W, Choi S-J, Lee T-H, Lee G-Y, Cha J-H, Kim C-W: **Application of biocathode in microbial fuel cells: cell performance and microbial community.** *Appl Microbiol Biotechnol* 2008, **79:**379-388.
82. Cheng S, Logan BE: **Ammonia treatment of carbon cloth anodes to enhance power generation of microbial fuel cells.** *Electrochemistry Communications* 2006, **9:**492-496.
83. Liu JL, Lowy DA, Baumann RG, Tender LM: **Influence of anode pretreatment on its microbial colonization.** *Journal of Applied Microbiology* 2007, **102:**177-183.
84. Cao X, Huang X, Boon N, Liang P, Fan M: **Electricity generation by an enriched phototrophic consortium in a microbial fuel cell.** *Electrochemistry Communications* 2008, **10:**1392-1395.
85. Yang Y, Sun G, Xu M: **Microbial fuel cells come of age.** *Journal of Chemical Technology & Biotechnology* 2011, **86:**625-632.
86. Lovley DR: **Extracellular electron transfer: wires, capacitors, iron lungs, and more.** *Geobiology* 2008, **6:**225-231.
87. Shi L, Squier TC, Zachara JM, Fredrickson JK: **Respiration of metal (hydr)oxides by Shewanella and Geobacter: a key role for multihaem c-type cytochromes.** *Mol Microbiol* 2007, **65:**12-20.
88. Oh ST, Kim JR, Premier GC, Lee TH, Kim C, Sloan WT: **Sustainable wastewater treatment: How might microbial fuel cells contribute.** *Biotechnology Advances* 2010, **28:**871-881.
89. Yuan Y, Ahmed J, Zhou L, Zhao B, Kim S: **Carbon nanoparticles-assisted mediator-less microbial fuel cells using Proteus vulgaris.** *Biosensors and Bioelectronics* 2011, **27:**106-112.
90. He Z, Kan J, Mansfeld F, Angenent LT, Nealson KH: **Self-Sustained Phototrophic Microbial Fuel Cells Based on the Synergistic Cooperation between Photosynthetic Microorganisms and Heterotrophic Bacteria.** *Environmental Science & Technology* 2009, **43:**1648-1654.
91. Malik S, Drott E, Grisdela P, Lee J, Lee C, Lowy DA, Gray S, Tender LM: **A self-assembling self-repairing microbial photoelectrochemical solar cell.** *Energy & Environmental Science* 2009, **2:**292-298.
92. Cho YK, Donohue TJ, Tejedor I, Anderson MA, McMahon KD, Noguera DR: **Development of a solar-powered microbial fuel cell.** *Journal of Applied Microbiology* 2008, **104:**640-650.

93. Rosenbaum M, Schröder U, Scholz F: **In Situ Electrooxidation of Photobiological Hydrogen in a Photobioelectrochemical Fuel Cell Based on Rhodobacter sphaeroides.** *Environmental Science & Technology* 2005, **39:**6328-6333.
94. Xing D, Zuo Y, Cheng S, Regan JM, Logan BE: **Electricity Generation by Rhodopseudomonas palustris DX-1.** *Environmental Science & Technology* 2008, **42:**4146-4151.
95. Larsen K, Ibrom A, Beier C, Jonasson S, Michelsen A: **Ecosystem respiration depends strongly on photosynthesis in a temperate heath.** *Biogeochemistry* 2007, **85:**201-213.
96. Stal LJ, van Gemerden H, Krumbein WE: **Structure and development of a benthic marine microbial mat.** *FEMS Microbiology Letters* 1985, **31:**111-125.
97. Strik D, Terlouw H, Hamelers H, Buisman C: **Renewable sustainable biocatalyzed electricity production in a photosynthetic algal microbial fuel cell (PAMFC).** *Appl Microbiol Biotechnol* 2008, **81:**659-668.
98. Zou Y, Pisciotta J, Billmyre RB, Baskakov IV: **Photosynthetic microbial fuel cells with positive light response.** *Biotechnology and Bioengineering* 2009, **104:**939-946.
99. Yagishita T, Horigome T, Tanaka K: **Effects of light, CO2 and inhibitors on the current output of biofuel cells containing the photosynthetic organism Synechococcus sp.** *Journal of Chemical Technology & Biotechnology* 1993, **56:**393-399.
100. Kim B, Chang I, Gadd G: **Challenges in microbial fuel cell development and operation.** *Appl Microbiol Biotechnol* 2007, **76:**485-494.
101. Zhou M, Chi M, Luo J, He H, Jin T: **An overview of electrode materials in microbial fuel cells.** *Journal of Power Sources* 2011, **196:**4427-4435.
102. Rittmann BE: **Microbial ecology to manage processes in environmental biotechnology.** *Trends Biotechnol* 2006, **24:**261-266.
103. Picioreanu C, Kreft JU, Klausen M, Haagensen JA, Tolker-Nielsen T, Molin S: **Microbial motility involvement in biofilm structure formation--a 3D modelling study.** *Water science and technology : a journal of the International Association on Water Pollution Research* 2007, **55:**337-343.
104. Torres CI, Marcus AK, Lee HS, Parameswaran P, Krajmalnik-Brown R, Rittmann BE: **A kinetic perspective on extracellular electron transfer by anode-respiring bacteria.** *FEMS Microbiol Rev* 2010, **34:**3-17.
105. Merkey B, Chopp D: **The Performance of a Microbial Fuel Cell Depends Strongly on Anode Geometry: A Multidimensional Modeling Study.** *Bull Math Biol* 2012, **74:**834-857.
106. Liu Y: **Overview of some theoretical approaches for derivation of the Monod equation.** *Appl Microbiol Biotechnol* 2007, **73:**1241-1250.
107. Trewavas A: **A brief history of systems biology. "Every object that biology studies is a system of systems." Francois Jacob (1974).** *Plant Cell* 2006, **18:**2420-2430.
108. Rupprecht J: **From systems biology to fuel--Chlamydomonas reinhardtii as a model for a systems biology approach to improve biohydrogen production.** *Journal of Biotechnology* 2009, **142:**10-20.
109. Mukhopadhyay A, Redding AM, Rutherford BJ, Keasling JD: **Importance of systems biology in engineering microbes for biofuel production.** *Current Opinion in Biotechnology* 2008, **19:**228-234.
110. Zhu H, Snyder M: **'Omic' approaches for unraveling signaling networks.** *Current Opinion in Cell Biology* 2002, **14:**173-179.
111. De Filippo C, Ramazzotti M, Fontana P, Cavalieri D: **Bioinformatic approaches for functional annotation and pathway inference in metagenomics data.** *Brief Bioinform* 2012, **13:**696-710.

112. Thiele I, Jamshidi N, Fleming RMT, Palsson BØ: **Genome-Scale Reconstruction of *Escherichia coli*'s Transcriptional and Translational Machinery: A Knowledge Base, Its Mathematical Formulation, and Its Functional Characterization.** *PLoS Comput Biol* 2009, **5:**e1000312.
113. Kim IK, Roldao A, Siewers V, Nielsen J: **A systems-level approach for metabolic engineering of yeast cell factories.** *FEMS Yeast Res* 2012, **12:**228-248.
114. Velculescu VE, Zhang L, Vogelstein B, Kinzler KW: **Serial Analysis of Gene Expression.** *Science* 1995, **270:**484-487.
115. Canelas AB, Harrison N, Fazio A, Zhang J, Pitkanen J-P, van den Brink J, Bakker BM, Bogner L, Bouwman J, Castrillo JI, et al: **Integrated multilaboratory systems biology reveals differences in protein metabolism between two reference yeast strains.** *Nat Commun* 2010, **1:**145.
116. Peng J, Elias JE, Thoreen CC, Licklider LJ, Gygi SP: **Evaluation of Multidimensional Chromatography Coupled with Tandem Mass Spectrometry (LC/LC−MS/MS) for Large-Scale Protein Analysis: The Yeast Proteome.** *Journal of Proteome Research* 2002, **2:**43-50.
117. Zamboni N, Sauer U: **Novel biological insights through metabolomics and 13C-flux analysis.** *Current Opinion in Microbiology* 2009, **12:**553-558.
118. Sauer U: **Metabolic networks in motion: 13C-based flux analysis.** *Mol Syst Biol* 2006, **2:**62.
119. Reaves ML, Rabinowitz JD: **Metabolomics in systems microbiology.** *Curr Opin Biotechnol* 2011, **22:**17-25.
120. Feng X, Page L, Rubens J, Chircus L, Colletti P, Pakrasi HB, Tang YJ: **Bridging the Gap between Fluxomics and Industrial Biotechnology.** *Journal of Biomedicine and Biotechnology* 2010, **2010**.
121. Fernie AR, Geigenberger P, Stitt M: **Flux an important, but neglected, component of functional genomics.** *Curr Opin Plant Biol* 2005, **8:**174-182.
122. Toya Y, Shimizu H: **Flux analysis and metabolomics for systematic metabolic engineering of microorganisms.** *Biotechnology Advances*.
123. Suthers PF, Burgard AP, Dasika MS, Nowroozi F, Van Dien S, Keasling JD, Maranas CD: **Metabolic flux elucidation for large-scale models using 13C labeled isotopes.** *Metabolic Engineering* 2007, **9:**387-405.
124. Blank L, Kuepfer L, Sauer U: **Large-scale 13C-flux analysis reveals mechanistic principles of metabolic network robustness to null mutations in yeast.** *Genome Biology* 2005, **6:**R49.
125. Dauner M: **From fluxes and isotope labeling patterns towards in silico cells.** *Curr Opin Biotechnol* 2010, **21:**55-62.
126. Kleijn RJ, Geertman J-MA, Nfor BK, Ras C, Schipper D, Pronk JT, Heijnen JJ, Van Maris AJA, Van Winden WA: **Metabolic flux analysis of a glycerol-overproducing Saccharomyces cerevisiae strain based on GC-MS, LC-MS and NMR-derived 13C-labelling data.** *FEMS Yeast Res* 2007, **7:**216-231.
127. Bennett BD, Yuan J, Kimball EH, Rabinowitz JD: **Absolute quantitation of intracellular metabolite concentrations by an isotope ratio-based approach.** *Nat Protoc* 2008, **3:**1299-1311.
128. Nöh K, Grönke K, Luo B, Takors R, Oldiges M, Wiechert W: **Metabolic flux analysis at ultra short time scale: Isotopically non-stationary 13C labeling experiments.** *Journal of Biotechnology* 2007, **129:**249-267.
129. Shastri AA, Morgan JA: **A transient isotopic labeling methodology for 13C metabolic flux analysis of photoautotrophic microorganisms.** *Phytochemistry* 2007, **68:**2302-2312.

130. Reed JL, Famili I, Thiele I, Palsson BO: **Towards multidimensional genome annotation.** *Nature reviews Genetics* 2006, **7:**130-141.
131. Feist AM, Herrgard MJ, Thiele I, Reed JL, Palsson BO: **Reconstruction of biochemical networks in microorganisms.** *Nature reviews Microbiology* 2009, **7:**129-143.
132. Thiele I, Palsson BO: **A protocol for generating a high-quality genome-scale metabolic reconstruction.** *Nature protocols* 2010, **5:**93-121.
133. Osterlund T, Nookaew I, Nielsen J: **Fifteen years of large scale metabolic modeling of yeast: Developments and impacts.** *Biotechnology Advances* 2011.
134. Price ND, Papin JA, Schilling CH, Palsson BO: **Genome-scale microbial in silico models: the constraints-based approach.** *Trends in Biotechnology* 2003, **21:**162-169.
135. Jaqaman K, Danuser G: **Linking data to models: data regression.** *Nat Rev Mol Cell Biol* 2006, **7:**813-819.
136. Kim TY, Sohn SB, Kim YB, Kim WJ, Lee SY: **Recent advances in reconstruction and applications of genome-scale metabolic models.** *Curr Opin Biotechnol* 2012, **23:**617-623.
137. Terzer M, Maynard ND, Covert MW, Stelling J: **Genome-scale metabolic networks.** *Wiley Interdisciplinary Reviews: Systems Biology and Medicine* 2009, **1:**285-297.
138. Price ND, Reed JL, Palsson BO: **Genome-scale models of microbial cells: evaluating the consequences of constraints.** *Nature reviews Microbiology* 2004, **2:**886-897.
139. Rocha I, Forster J, Nielsen J: **Design and application of genome-scale reconstructed metabolic models.** *Methods Mol Biol* 2008, **416:**409-431.
140. Orth JD, Thiele I, Palsson BO: **What is flux balance analysis?** *Nat Biotech* 2010, **28:**245-248.
141. Chuang HY, Hofree M, Ideker T: **A decade of systems biology.** *Annual review of cell and developmental biology* 2010, **26:**721-744.
142. Varma A, Palsson BO: **Metabolic Flux Balancing: Basic Concepts, Scientific and Practical Use.** *Nat Biotech* 1994, **12:**994-998.
143. Price ND, Papin JA, Schilling CH, Palsson BO: **Genome-scale microbial in silico models: the constraints-based approach.** *Trends in Biotechnology* 2003, **21:**162-169.
144. Price ND, Schellenberger J, Palsson BO: **Uniform sampling of steady-state flux spaces: means to design experiments and to interpret enzymopathies.** *Biophys J* 2004, **87:**2172-2186.
145. Lee JM, Gianchandani EP, Eddy JA, Papin JA: **Dynamic analysis of integrated signaling, metabolic, and regulatory networks.** *PLoS Comput Biol* 2008, **4:**e1000086.
146. Covert MW, Xiao N, Chen TJ, Karr JR: **Integrating metabolic, transcriptional regulatory and signal transduction models in Escherichia coli.** *Bioinformatics* 2008, **24:**2044-2050.
147. Jamshidi N, Palsson Bÿ **Mass Action Stoichiometric Simulation Models: Incorporating Kinetics and Regulation into Stoichiometric Models.** *Biophys J* 2010, **98:**175-185.
148. Teusink B, Passarge J, Reijenga CA, Esgalhado E, van der Weijden CC, Schepper M, Walsh MC, Bakker BM, van Dam K, Westerhoff HV, Snoep JL: **Can yeast glycolysis be understood in terms of in vitro kinetics of the constituent enzymes? Testing biochemistry.** *European Journal of Biochemistry* 2000, **267:**5313-5329.
149. Oberhardt MA, Palsson BO, Papin JA: **Applications of genome-scale metabolic reconstructions.** *Mol Syst Biol* 2009, **5**.

150. Lee JM, Gianchandani EP, Papin JA: **Flux balance analysis in the era of metabolomics.** *Briefings in Bioinformatics* 2006, **7:**140-150.
151. Covert MW, Famili I, Palsson BO: **Identifying constraints that govern cell behavior: a key to converting conceptual to computational models in biology?** *Biotechnology and Bioengineering* 2003, **84:**763-772.
152. Price ND, Reed JL, Palsson BO: **Genome-scale models of microbial cells: evaluating the consequences of constraints.** *Nat Rev Micro* 2004, **2:**886-897.
153. Kauffman KJ, Prakash P, Edwards JS: **Advances in flux balance analysis.** *Current Opinion in Biotechnology* 2003, **14:**491-496.
154. Varma A, Palsson BO: **Stoichiometric flux balance models quantitatively predict growth and metabolic by-product secretion in wild-type Escherichia coli W3110.** *Appl Environ Microbiol* 1994, **60:**3724-3731.
155. Durot M, Bourguignon PY, Schachter V: **Genome-scale models of bacterial metabolism: reconstruction and applications.** *FEMS Microbiology Reviews* 2009, **33:**164-190.
156. Oliveira A, Nielsen J, Forster J: **Modeling Lactococcus lactis using a genome-scale flux model.** *BMC Microbiology* 2005, **5:**39.
157. Famili I, Förster J, Nielsen J, Palsson BO: ***Saccharomyces cerevisiae*** **phenotypes can be predicted by using constraint-based analysis of a genome-scale reconstructed metabolic network.** *Proceedings of the National Academy of Sciences* 2003, **100:**13134-13139.
158. Edwards JS, Ibarra RU, Palsson BO: **In silico predictions of Escherichia coli metabolic capabilities are consistent with experimental data.** *Nature Biotechnology* 2001, **19:**125-130.
159. Fong SS, Palsson BO: **Metabolic gene-deletion strains of Escherichia coli evolve to computationally predicted growth phenotypes.** *Nat Genet* 2004, **36:**1056-1058.
160. Ibarra RU, Edwards JS, Palsson BO: **Escherichia coli K-12 undergoes adaptive evolution to achieve in silico predicted optimal growth.** *Nature* 2002, **420:**186-189.
161. Burgard AP, Maranas CD: **Optimization-based framework for inferring and testing hypothesized metabolic objective functions.** *Biotechnol Bioeng* 2003, **82:**670-677.
162. Lun DS, Rockwell G, Guido NJ, Baym M, Kelner JA, Berger B, Galagan JE, Church GM: **Large-scale identification of genetic design strategies using local search.** *Mol Syst Biol* 2009, **5**.
163. Patil K, Rocha I, Forster J, Nielsen J: **Evolutionary programming as a platform for in silico metabolic engineering.** *BMC Bioinformatics* 2005, **6:**308.
164. Xu P, Ranganathan S, Fowler ZL, Maranas CD, Koffas MAG: **Genome-scale metabolic network modeling results in minimal interventions that cooperatively force carbon flux towards malonyl-CoA.** *Metabolic Engineering* 2011, **13:**578-587.
165. Brochado A, Matos C, Moller B, Hansen J, Mortensen U, Patil K: **Improved vanillin production in baker's yeast through in silico design.** *Microb Cell Fact* 2010, **9:**84.
166. Schuetz R, Kuepfer L, Sauer U: **Systematic evaluation of objective functions for predicting intracellular fluxes in Escherichia coli.** *Molecular systems biology* 2007, **3:**119.
167. Lewis NE, Hixson KK, Conrad TM, Lerman JA, Charusanti P, Polpitiya AD, Adkins JN, Schramm G, Purvine SO, Lopez-Ferrer D, et al: **Omic data from evolved E. coli are consistent with computed optimal growth from genome-scale models.** *Mol Syst Biol* 2010, **6:**390.
168. Feist AM, Palsson BO: **The biomass objective function.** *Curr Opin Microbiol* 2010, **13:**344-349.

169. Reed J, Vo T, Schilling C, Palsson B: **An expanded genome-scale model of Escherichia coli K-12 (iJR904 GSM/GPR).** *Genome Biology* 2003, **4:**R54.
170. Tang YJ, Sapra R, Joyner D, Hazen TC, Myers S, Reichmuth D, Blanch H, Keasling JD: **Analysis of metabolic pathways and fluxes in a newly discovered thermophilic and ethanol-tolerant Geobacillus strain.** *Biotechnol Bioeng* 2009, **102:**1377-1386.
171. Blazeck J, Alper H: **Systems metabolic engineering: genome-scale models and beyond.** *Biotechnology Journal* 2010, **5:**647-659.
172. Boghigian BA, Seth G, Kiss R, Pfeifer BA: **Metabolic flux analysis and pharmaceutical production.** *Metab Eng* 2010, **12:**81-95.
173. Burgard AP, Pharkya P, Maranas CD: **Optknock: a bilevel programming framework for identifying gene knockout strategies for microbial strain optimization.** *Biotechnology and Bioengineering* 2003, **84:**647-657.
174. Alper H, Jin YS, Moxley JF, Stephanopoulos G: **Identifying gene targets for the metabolic engineering of lycopene biosynthesis in Escherichia coli.** *Metabolic Engineering* 2005, **7:**155-164.
175. Alper H, Miyaoku K, Stephanopoulos G: **Construction of lycopene-overproducing E. coli strains by combining systematic and combinatorial gene knockout targets.** *Nat Biotech* 2005, **23:**612-616.
176. Park JH, Lee KH, Kim TY, Lee SY: **Metabolic engineering of Escherichia coli for the production of L-valine based on transcriptome analysis and in silico gene knockout simulation.** *Proc Natl Acad Sci U S A* 2007, **104:**7797-7802.
177. Lee KH, Park JH, Kim TY, Kim HU, Lee SY: **Systems metabolic engineering of Escherichia coli for L-threonine production.** *Mol Syst Biol* 2007, **3:**149.
178. Jung YK, Kim TY, Park SJ, Lee SY: **Metabolic engineering of Escherichia coli for the production of polylactic acid and its copolymers.** *Biotechnology and Bioengineering* 2010, **105:**161-171.
179. Covert MW, Palsson BO: **Transcriptional regulation in constraints-based metabolic models of Escherichia coli.** *The Journal of biological chemistry* 2002, **277:**28058-28064.
180. Shlomi T, Eisenberg Y, Sharan R, Ruppin E: **A genome-scale computational study of the interplay between transcriptional regulation and metabolism.** *Mol Syst Biol* 2007, **3**.
181. Tomar N, De RK: **Comparing methods for metabolic network analysis and an application to metabolic engineering.** *Gene* 2013, **521:**1-14.
182. Terzer M, Stelling J: **Large-scale computation of elementary flux modes with bit pattern trees.** *Bioinformatics* 2008, **24:**2229-2235.
183. Jol SJ, Kümmel A, Terzer M, Stelling J, Heinemann M: **System-Level Insights into Yeast Metabolism by Thermodynamic Analysis of Elementary Flux Modes.** *PLoS Comput Biol* 2012, **8:**e1002415.
184. Mahadevan R, Schilling CH: **The effects of alternate optimal solutions in constraint-based genome-scale metabolic models.** *Metabolic Engineering* 2003, **5:**264-276.
185. Lovley DR: **Bug juice: harvesting electricity with microorganisms.** *Nature reviews Microbiology* 2006, **4:**497-508.
186. Raghavulu SV, Goud RK, Sarma PN, Mohan SV: **Saccharomyces cerevisiae as anodic biocatalyst for power generation in biofuel cell: Influence of redox condition and substrate load.** *Bioresource Technology* 2011, **102:**2751-2757.
187. Chang RL, Ghamsari L, Manichaikul A, Hom EFY, Balaji S, Fu W, Shen Y, Hao T, Palsson BO, Salehi-Ashtiani K, Papin JA: **Metabolic network reconstruction of**

Chlamydomonas offers insight into light-driven algal metabolism. *Mol Syst Biol* 2011, **7**.
188. Yoshikawa K, Kojima Y, Nakajima T, Furusawa C, Hirasawa T, Shimizu H: **Reconstruction and verification of a genome-scale metabolic model for Synechocystis sp. PCC6803.** *Appl Microbiol Biotechnol* 2011, **92:**347-358.
189. Sun J, Sayyar B, Butler JE, Pharkya P, Fahland TR, Famili I, Schilling CH, Lovley DR, Mahadevan R: **Genome-scale constraint-based modeling of Geobacter metallireducens.** *BMC systems biology* 2009, **3:**15.
190. Heavner BD, Smallbone K, Barker B, Mendes P, Walker LP: **Yeast 5 - an expanded reconstruction of the *Saccharomyces cerevisiae* metabolic network.** *BMC Syst Biol* 2012, **6:**55.
191. Novere NL, Finney A, Hucka M, Bhalla US, Campagne F, Collado-Vides J, Crampin EJ, Halstead M, Klipp E, Mendes P, et al: **Minimum information requested in the annotation of biochemical models (MIRIAM).** *Nat Biotech* 2005, **23:**1509-1515.
192. Trinh N, Park J, Kim B-W: **Increased generation of electricity in a microbial fuel cell using Geobacter sulfurreducens.** *Korean Journal of Chemical Engineering* 2009, **26:**748-753.
193. [http://nutmeg.easternct.edu/~adams/ChlamyTeach/growingchlamy.html]
194. Sheng J, Kim HW, Badalamenti JP, Zhou C, Sridharakrishnan S, Krajmalnik-Brown R, Rittmann BE, Vannela R: **Effects of temperature shifts on growth rate and lipid characteristics of Synechocystis sp. PCC6803 in a bench-top photobioreactor.** *Bioresource Technology* 2011, **102:**11218-11225.
195. Watson K: **Temperature relations.** In *The Yeasts. Volume* 2. Edited by Rose AH, Harrison JS. London: Academic Press; 1987: 41-71: *Yeasts and the Environment*].
196. Yoon HS, Hackett JD, Ciniglia C, Pinto G, Bhattacharya D: **A molecular timeline for the origin of photosynthetic eukaryotes.** *Mol Biol Evol* 2004, **21:**809-818.
197. Merchant SS, Prochnik SE, Vallon O, Harris EH, Karpowicz SJ, Witman GB, Terry A, Salamov A, Fritz-Laylin LK, Marécchal-Drouard L, et al: **The Chlamydomonas Genome Reveals the Evolution of Key Animal and Plant Functions.** *Science* 2007, **318:**245-250.
198. Harris EH: **Chlamydomonas as a model organism.** *Annual Review of Plant Physiology and Plant Molecular Biology* 2001, **52:**363-406.
199. Manichaikul A, Ghamsari L, Hom EF, Lin C, Murray RR, Chang RL, Balaji S, Hao T, Shen Y, Chavali AK, et al: **Metabolic network analysis integrated with transcript verification for sequenced genomes.** *Nat Methods* 2009, **6:**589-592.
200. Keller LC, Romijn EP, Zamora I, Yates JR, 3rd, Marshall WF: **Proteomic analysis of isolated chlamydomonas centrioles reveals orthologs of ciliary-disease genes.** *Curr Biol* 2005, **15:**1090-1098.
201. Pazour GJ, Agrin N, Walker BL, Witman GB: **Identification of predicted human outer dynein arm genes: candidates for primary ciliary dyskinesia genes.** *J Med Genet* 2006, **43:**62-73.
202. Vilchez C, Garbayo I, Markvicheva E, Galvan F, Leon R: **Studies on the suitability of alginate-entrapped Chlamydomonas reinhardtii cells for sustaining nitrate consumption processes.** *Bioresource Technology* 2001, **78:**55-61.
203. Ghirardi ML, Posewitz MC, Maness PC, Dubini A, Yu J, Seibert M: **Hydrogenases and hydrogen photoproduction in oxygenic photosynthetic organisms.** *Annu Rev Plant Biol* 2007, **58:**71-91.
204. Kosourov SN, Seibert M: **Hydrogen photoproduction by nutrient-deprived Chlamydomonas reinhardtii cells immobilized within thin alginate films under aerobic and anaerobic conditions.** *Biotechnology and Bioengineering* 2009, **102:**50-58.

205. [http://www.chlamy.org]
206. Chen P, Min M, Chen Y, Wang L, Li Y, Chen Q, Wang C, Wan Y, Wang X, Cheng Y, et al: **Review of biological and engineering aspects of algae to fuels approach.** *International Journal of Agricultural and Biological Engineering* 2009, **2:**1-30.
207. Pienkos PT, Darzins A: **The promise and challenges of microalgal-derived biofuels.** *Biofpr* 2009, **3:**431-440.
208. Campbell MN: **Biodiesel: Algae as a Renewable Source for Liquid Fuel.** *Guelph Engineering Journal* 2008, **1:**207.
209. Velasquez-Orta SB, Curtis TP, Logan BE: **Energy from algae using microbial fuel cells.** *Biotechnology and Bioengineering* 2009, **103:**1068-1076.
210. Rosenbaum M, Schröder U, Scholz F: **Utilizing the green alga Chlamydomonas reinhardtii for microbial electricity generation: a living solar cell.** *Appl Microbiol Biotechnol* 2005, **68:**753-756.
211. Strik DPBTB, Hamelers HVM, Buisman CJN: **Solar Energy Powered Microbial Fuel Cell with a Reversible Bioelectrode.** *Environmental Science & Technology* 2009, **44:**532-537.
212. Harnisch F, Schröder U: **Selectivity versus Mobility: Separation of Anode and Cathode in Microbial Bioelectrochemical Systems.** *ChemSusChem* 2009, **2:**921-926.
213. Melis A, Happe T: **Hydrogen Production. Green Algae as a Source of Energy.** *Plant Physiol* 2001, **127:**740-748.
214. Rupprecht J, Hankamer B, Mussgnug JH, Ananyev G, Dismukes C, Kruse O: **Perspectives and advances of biological H₂ production in microorganisms.** *Appl Microbiol Biotechnol* 2006, **72:**442-449.
215. Hankamer B, Lehr F, Rupprecht J, Mussgnug JH, Posten C, Kruse O: **Photosynthetic biomass and H2 production by green algae: from bioengineering to bioreactor scale-up.** *Physiologia Plantarum* 2007, **131:**10-21.
216. Gaffron H, Rubin J: **FERMENTATIVE AND PHOTOCHEMICAL PRODUCTION OF HYDROGEN IN ALGAE.** *The Journal of General Physiology* 1942, **26:**219-240.
217. Kruse O, Rupprecht J, Mussgnug JH, Dismukes GC, Hankamer B: **Photosynthesis: a blueprint for solar energy capture and biohydrogen production technologies.** *Photochem Photobiol Sci* 2005, **4:**957-970.
218. Melis A, Zhang L, Forestier M, Ghirardi ML, Seibert M: **Sustained Photobiological Hydrogen Gas Production upon Reversible Inactivation of Oxygen Evolution in the Green AlgaChlamydomonas reinhardtii.** *Plant Physiol* 2000, **122:**127-136.
219. Ghirardi ML, Zhang L, Lee JW, Flynn T, Seibert M, Greenbaum E, Melis A: **Microalgae: a green source of renewable H2.** *Trends in Biotechnology* 2000, **18:**506-511.
220. Esquìvel MG, Amaro HM, Pinto TS, Fevereiro PS, Malcata FX: **Efficient H2 production via Chlamydomonas reinhardtii.** *Trends in Biotechnology* 2011, **In Press, Corrected Proof**.
221. Mus F, Dubini A, Seibert M, Posewitz MC, Grossman AR: **Anaerobic Acclimation in Chlamydomonas reinhardtii.** *Journal of Biological Chemistry* 2007, **282:**25475-25486.
222. Dubini A, Mus F, Seibert M, Grossman AR, Posewitz MC: **Flexibility in Anaerobic Metabolism as Revealed in a Mutant of Chlamydomonas reinhardtii Lacking Hydrogenase Activity.** *Journal of Biological Chemistry* 2009, **284:**7201-7213.
223. Posewitz MC, Dubini A, Meuser JE, Seibert M, Ghirardi ML: **Hydrogenases, Hydrogen Production, and Anoxia.** In *The Chlamydomonas Sourcebook (Second*

Edition). Edited by Elizabeth HH, Ph.D, David BS, George BW. London: Academic Press; 2009: 217-255
224. Timmins M, Thomas-Hall SR, Darling A, Zhang E, Hankamer B, Marx UC, Schenk PM: **Phylogenetic and molecular analysis of hydrogen-producing green algae.** *Journal of Experimental Botany* 2009, **60:**1691-1702.
225. Doebbe A, Keck M, La Russa M, Mussgnug JH, Hankamer B, Tek√ße E, Niehaus K, Kruse O: **The Interplay of Proton, Electron, and Metabolite Supply for Photosynthetic H2 Production in Chlamydomonas reinhardtii.** *Journal of Biological Chemistry* 2010, **285:**30247-30260.
226. Grossman AR, Catalanotti C, Yang W, Dubini A, Magneschi L, Subramanian V, Posewitz MC, Seibert M: **Multiple facets of anoxic metabolism and hydrogen production in the unicellular green alga Chlamydomonas reinhardtii.** *New Phytologist* 2011, **190:**279-288.
227. Markov SA, Eivazova ER, Greenwood J: **Photostimulation of H2 production in the green alga Chlamydomonas reinhardtii upon photoinhibition of its O2-evolving system.** *International Journal of Hydrogen Energy* 2006, **31:**1314-1317.
228. Seibert M, King PW, Posewitz MC, Melis A, Ghirardi ML: **Chapter 22: photosynthetic water-splitting for hydrogen production.** In *Bioenergy.* Edited by Wall JD, Harwood CS, Demain A. Washington D.C: ASM Press; 2008: 273-291
229. Zorina A, Mironov K, Stepanchenko N, Sinetova M, Koroban N, Zinchenko V, Kupriyanova E, Allakhverdiev S, Los D: **Regulation systems for stress responses in cyanobacteria.** *Russian Journal of Plant Physiology* 2011, **58:**749-767.
230. Waterbury JB, Watson SW, Guillard RRL, Brand LE: **Widespread occurrence of a unicellular, marine, planktonic, cyanobacterium.** *Nature* 1979, **277:**293-294.
231. Carr NG, Whitton BA: *The Biology of cyanobacteria* Berkeley and Los Angeles: Unviersity of california press; 1982.
232. Martin W, Rujan T, Richly E, Hansen A, Cornelsen S, Lins T, Leister D, Stoebe B, Hasegawa M, Penny D: **Evolutionary analysis of Arabidopsis, cyanobacterial, and chloroplast genomes reveals plastid phylogeny and thousands of cyanobacterial genes in the nucleus.** *Proc Natl Acad Sci U S A* 2002, **99:**12246-12251.
233. Dutta D, De D, Chaudhuri S, Bhattacharya SK: **Hydrogen production by Cyanobacteria.** *Microb Cell Fact* 2005, **4:**36.
234. Kaneko T, Sato S, Kotani H, Tanaka A, Asamizu E, Nakamura Y, Miyajima N, Hirosawa M, Sugiura M, Sasamoto S, et al: **Sequence Analysis of the Genome of the Unicellular Cyanobacterium Synechocystis sp. Strain PCC6803. II. Sequence Determination of the Entire Genome and Assignment of Potential Protein-coding Regions.** *DNA Research* 1996, **3:**109-136.
235. Nakamura Y, Kaneko T, Hirosawa M, Miyajima N, Tabata S: **CyanoBase, a www database containing the complete nucleotide sequence of the genome of Synechocystis sp. strain PCC6803.** *Nucleic Acids Research* 1998, **26:**63-67.
236. Atsumi S, Higashide W, Liao JC: **Direct photosynthetic recycling of carbon dioxide to isobutyraldehyde.** *Nature Biotechnology* 2009, **27:**1177-1180.
237. Johnson CH, Stewart PL, Egli M: **The cyanobacterial circadian system: from biophysics to bioevolution.** *Annu Rev Biophys* 2011, **40:**143-167.
238. Lovley DR: **The microbe electric: conversion of organic matter to electricity.** *Current Opinion in Biotechnology* 2008, **19:**564-571.
239. Pisciotta JM, Zou Y, Baskakov IV: **Role of the photosynthetic electron transfer chain in electrogenic activity of cyanobacteria.** *Appl Microbiol Biotechnol* 2011, **91:**377-385.
240. Pisciotta JM, Zou Y, Baskakov IV: **Light-dependent electrogenic activity of cyanobacteria.** *PLoS ONE* 2010, **5:**e10821.

241. Madiraju KS, Lyew D, Kok R, Raghavan V: **Carbon neutral electricity production by *Synechocystis sp.* PCC6803 in a microbial fuel cell.** *Bioresource Technology* 2012, **110:**214-218.
242. McCormick AJ, Bombelli P, Scott AM, Philips AJ, Smith AG, Fisher AC, Howe CJ: **Photosynthetic biofilms in pure culture harness solar energy in a mediatorless bio-photovoltaic cell (BPV) system.** *Energy & Environmental Science* 2011, **4:**4699-4709.
243. Dequin S, Casaregola S: **The genomes of fermentative *Saccharomyces*.** *Comptes Rendus Biologies* 2011, **334:**687-693.
244. Kurtzman CP: **Phylogenetic circumscription of Saccharomyces, Kluyveromyces and other members of the Saccharomycetaceae, and the proposal of the new genera Lachancea, Nakaseomyces, Naumovia, Vanderwaltozyma and Zygotorulaspora.** *FEMS Yeast Res* 2003, **4:**233-245.
245. Vaughan-Martini A, Martini A: **Facts, myths and legends on the prime industrial microorganism.** *J Ind Microbiol* 1995, **14:**514-522.
246. Fan Y, Sharbrough E, Liu H: **Quantification of the Internal Resistance Distribution of Microbial Fuel Cells.** *Environmental Science & Technology* 2008, **42:**8101-8107.
247. Peralta-Yahya PP, Keasling JD: **Advanced biofuel production in microbes.** *Biotechnology Journal* 2010, **5:**147-162.
248. Haslett ND, Rawson FJ, Barriere F, Kunze G, Pasco N, Gooneratne R, Baronian KHR: **Characterisation of yeast microbial fuel cell with the yeast Arxula adeninivorans as the biocatalyst.** *Biosens Bioelectron* 2011, **26:**3742-3747.
249. Gunawardena A, Fernando S, To F: **Performance of a yeast-mediated biological fuel cell.** *Int J Mol Sci* 2008, **9:**1893-1907.
250. Feldmann H: **Yeast Molecular Biology – A Short Compendium on Basic Features and Novel Aspects.** In *Book Yeast Molecular Biology – A Short Compendium on Basic Features and Novel Aspects* (Editor ed.^eds.). City: Adolf-Butenandt-Institute, University of Munich; 2005.
251. Ganguli R, Dunn BS: **Kinetics of Anode Reactions for a Yeast-Catalysed Microbial Fuel Cell.** *Fuel Cells* 2009, **9:**44-52.
252. Powell EE, Evitts RW, Hill GA, Bolster JC: **A Microbial Fuel Cell with a Photosynthetic Microalgae Cathodic Half Cell Coupled to a Yeast Anodic Half Cell.** *Energy Sources Part A-Recovery Util Environ Eff* 2011, **33:**440-448.
253. Sayed ET, Tsujiguchi T, Nakagawa N: **Catalytic activity of baker's yeast in a mediatorless microbial fuel cell.** *Bioelectrochemistry* 2012, **86:**97-101.
254. Anderson RT, Vrionis HA, Ortiz-Bernad I, Resch CT, Long PE, Dayvault R, Karp K, Marutzky S, Metzler DR, Peacock A, et al: **Stimulating the in situ activity of Geobacter species to remove uranium from the groundwater of a uranium-contaminated aquifer.** *Appl Environ Microbiol* 2003, **69:**5884-5891.
255. Holmes DE, Finneran KT, O'Neil RA, Lovley DR: **Enrichment of members of the family Geobacteraceae associated with stimulation of dissimilatory metal reduction in uranium-contaminated aquifer sediments.** *Appl Environ Microbiol* 2002, **68:**2300-2306.
256. Lovley DR, Anderson RT: **Influence of dissimilatory metal reduction on fate of organic and metal contaminants in the subsurface.** *Hydrogeology Journal* 2000, **8:**77-88.
257. Coppi MV, Leang C, Sandler SJ, Lovley DR: **Development of a Genetic System for Geobacter sulfurreducens.** *Appl Environ Microbiol* 2001, **67:**3180-3187.
258. Caccavo F, Jr., Lonergan DJ, Lovley DR, Davis M, Stolz JF, McInerney MJ: **Geobacter sulfurreducens sp. nov., a hydrogen- and acetate-oxidizing**

dissimilatory metal-reducing microorganism. *Appl Environ Microbiol* 1994, **60:**3752-3759.
259. Holmes DE, Chaudhuri SK, Nevin KP, Mehta T, Methe BA, Liu A, Ward JE, Woodard TL, Webster J, Lovley DR: **Microarray and genetic analysis of electron transfer to electrodes in Geobacter sulfurreducens.** *Environ Microbiol* 2006, **8:**1805-1815.
260. Yi H, Nevin KP, Kim BC, Franks AE, Klimes A, Tender LM, Lovley DR: **Selection of a variant of Geobacter sulfurreducens with enhanced capacity for current production in microbial fuel cells.** *Biosens Bioelectron* 2009, **24:**3498-3503.
261. Salgado CA: **Microbial fuel cells powered by Geobacter sulfurreducens.** *MMG 445 Basic Biotechnology eJournal* 2009, **5:**96-101.
262. Lin WC, Coppi MV, Lovley DR: **Geobacter sulfurreducens Can Grow with Oxygen as a Terminal Electron Acceptor.** *Appl Environ Microbiol* 2004, **70:**2525-2528.
263. Bond DR, Holmes DE, Tender LM, Lovley DR: **Electrode-Reducing Microorganisms That Harvest Energy from Marine Sediments.** *Science* 2002, **295:**483-485.
264. Nevin KP, Richter H, Covalla SF, Johnson JP, Woodard TL, Orloff AL, Jia H, Zhang M, Lovley DR: **Power output and columbic efficiencies from biofilms of Geobacter sulfurreducens comparable to mixed community microbial fuel cells.** *Environmental Microbiology* 2008, **10:**2505-2514.
265. Gregory KB, Bond DR, Lovley DR: **Graphite electrodes as electron donors for anaerobic respiration.** *Environmental Microbiology* 2004, **6:**596-604.
266. Holmes DE, Bond DR, O'Neil RA, Reimers CE, Tender LR, Lovley DR: **Microbial communities associated with electrodes harvesting electricity from a variety of aquatic sediments.** *Microb Ecol* 2004, **48:**178-190.
267. Tender LM, Reimers CE, Stecher Iii HA, Holmes DE, Bond DR, Lowy DA, Pilobello K, Fertig SJ, Lovley DR: **Harnessing microbially generated power on the seafloor.** *Nature Biotechnology* 2002, **20:**821-825.
268. Mahadevan R, Bond DR, Butler JE, Esteve-Nunez A, Coppi MV, Palsson BO, Schilling CH, Lovley DR: **Characterization of metabolism in the Fe(III)-reducing organism Geobacter sulfurreducens by constraint-based modeling.** *Appl Environ Microbiol* 2006, **72:**1558-1568.
269. Champine JE, Underhill B, Johnston JM, Lilly WW, Goodwin S: **Electron Transfer in the Dissimilatory Iron-reducing Bacterium Geobacter metallireducens.** *Anaerobe* 2000, **6:**187-196.
270. Galushko AS, Schink B: **Oxidation of acetate through reactions of the citric acid cycle by Geobacter sulfurreducens in pure culture and in syntrophic coculture.** *Arch Microbiol* 2000, **174:**314-321.
271. Reguera G, McCarthy KD, Mehta T, Nicoll JS, Tuominen MT, Lovley DR: **Extracellular electron transfer via microbial nanowires.** *Nature* 2005, **435:**1098-1101.
272. Fredrickson JK, Romine MF, Beliaev AS, Auchtung JM, Driscoll ME, Gardner TS, Nealson KH, Osterman AL, Pinchuk G, Reed JL, et al: **Towards environmental systems biology of Shewanella.** *Nature reviews Microbiology* 2008, **6:**592-603.
273. Call DF, Wagner RC, Logan BE: **Hydrogen production by geobacter species and a mixed consortium in a microbial electrolysis cell.** *Appl Environ Microbiol* 2009, **75:**7579-7587.
274. El-Naggar MY, Gorby YA, Xia W, Nealson KH: **The molecular density of states in bacterial nanowires.** *Biophys J* 2008, **95:**L10-12.

275. Marsili E, Baron DB, Shikhare ID, Coursolle D, Gralnick JA, Bond DR: **Shewanella secretes flavins that mediate extracellular electron transfer.** *Proceedings of the National Academy of Sciences* 2008, **105:**3968-3973.
276. Newton GJ, Mori S, Nakamura R, Hashimoto K, Watanabe K: **Analyses of current-generating mechanisms of Shewanella loihica PV-4 and Shewanella oneidensis MR-1 in microbial fuel cells.** *Appl Environ Microbiol* 2009, **75:**7674-7681.
277. Ringeisen BR, Henderson E, Wu PK, Pietron J, Ray R, Little B, Biffinger JC, Jones-Meehan JM: **High Power Density from a Miniature Microbial Fuel Cell Using Shewanella oneidensis DSP10.** *Environmental Science & Technology* 2006, **40:**2629-2634.
278. Nevin KP, Zhang P, Franks AE, Woodard TL, Lovley DR: **Anaerobes unleashed: Aerobic fuel cells of Geobacter sulfurreducens.** *Journal of Power Sources* 2011, **196:**7514-7518.
279. Verwoerd WS, Mao L: **The Problem of Futile Cycles in Metabolic Flux Modeling: Flux Space Characterisation and Practical Approaches to its Solution.** In *Simulation Foundations, Methods and Applications: Modeling and Simulation Methods and Applications.* Edited by Basu SK, Kumar N: Springer, (In Press); 2013
280. Mao L, Verwoerd WS: **Model-driven elucidation of the inherent capacity of *Geobacter sulfurreducens* for electricity generation.** *Journal of Biological Engineering* 2013, **7:**14.
281. Mao L, Verwoerd WS: **MFCoT - a computational toolbox to study the metabolism of MFC biocatalysts.** In *4th international microbial fuel cell conference; Cairns, Australia*. 2013: 82-83.
282. Verwoerd W: **A new computational method to split large biochemical networks into coherent subnets.** *BMC systems biology* 2011, **5:**25.
283. Schuster S, Fell DA, Dandekar T: **A general definition of metabolic pathways useful for systematic organization and analysis of complex metabolic networks.** *Nature Biotechnology* 2000, **18:**326-332.
284. Pey J, Prada J, Beasley JE, Planes FJ: **Path finding methods accounting for stoichiometry in metabolic networks.** *Genome Biol* 2011, **12:**R49.
285. Stephanopoulos G, Aristidou AA, Nielsen JH, Nielsen J: *Metabolic engineering: principles and methodologies* San Diego: Academic Press; 1998.
286. Palsson BO: *Systems biology: Properties of reconstructed networks.* Cambridge university press; 2006.
287. Santos F, Boele J, Teusink B: **Chapter twenty-four - A Practical Guide to Genome-Scale Metabolic Models and Their Analysis.** In *Methods Enzymol. Volume* Volume 500. Edited by Daniel Jameson MV, Hans VW: Academic Press; 2011: 509-532
288. Lee K, Berthiaume F, Stephanopoulos GN, Yarmush DM, Yarmush ML: **Metabolic flux analysis of postburn hepatic hypermetabolism.** *Metab Eng* 2000, **2:**312-327.
289. Reed JL, Palsson BØ: **Genome-Scale In Silico Models of E. coli Have Multiple Equivalent Phenotypic States: Assessment of Correlated Reaction Subsets That Comprise Network States.** *Genome Research* 2004, **14:**1797-1805.
290. Thiele I, Fleming RMT, Bordbar A, Schellenberger J, Palsson BØ: **Functional Characterization of Alternate Optimal Solutions of Escherichia coli's Transcriptional and Translational Machinery.** *Biophys J* 2010, **98:**2072-2081.
291. Price ND, Famili I, Beard DA, Palsson BO: **Extreme pathways and Kirchhoff's second law.** *Biophys J* 2002, **83:**2879-2882.
292. Schuster S, Hilgetag C: **On elementary flux modes in biochemical reaction systems at steady state.** *Journal of Biological Systems* 1994, **2:**165-182.

293. Duarte N, Herrgard M, Palsson B: **Reconstruction and Validation of Saccharomyces cerevisiae iND750, a Fully Compartmentalized Genome-Scale Metabolic Model.** *Genome Res* 2004, **14:**1298 - 1309.
294. Beard DA, Liang SD, Qian H: **Energy balance for analysis of complex metabolic networks.** *Biophys J* 2002, **83:**79-86.
295. Qian H, Beard DA: **Metabolic futile cycles and their functions: a systems analysis of energy and control.** *Systems Biology, IEE Proceedings* 2006, **153:**192-200.
296. Ibarguren I, Diaz-Enrich MJ, Cao J, Fernandez M, Barcia R, Villamarin JA, Ramos-Martinez JI: **Regulation of the futile cycle of fructose phosphate in sea mussel.** *Comparative Biochemistry and Physiology Part B: Biochemistry and Molecular Biology* 2000, **126:**495-501.
297. Samoilov M, Plyasunov S, Arkin AP: **Stochastic amplification and signaling in enzymatic futile cycles through noise-induced bistability with oscillations.** *Proc Natl Acad Sci U S A* 2005, **102:**2310-2315.
298. Dauner M, Storni T, Sauer U: **Bacillus subtilis metabolism and energetics in carbon-limited and excess-carbon chemostat culture.** *J Bacteriol* 2001, **183:**7308-7317.
299. Tang YJ, Chakraborty R, Mart ń HG, Chu J, Hazen TC, Keasling JD: **Flux Analysis of Central Metabolic Pathways in Geobacter metallireducens during Reduction of Soluble Fe(III)-Nitrilotriacetic Acid.** *Appl Environ Microbiol* 2007, **73:**3859-3864.
300. Varma A, Palsson BO: **Metabolic capabilities of Escherichia coli: I. synthesis of biosynthetic precursors and cofactors.** *Journal of Theoretical Biology* 1993, **165:**477-502.
301. Holzh ütter HG: **The principle of flux minimization and its application to estimate stationary fluxes in metabolic networks.** *Eur J Biochem* 2004, **271:**2905-2922.
302. Henry CS, Broadbelt LJ, Hatzimanikatis V: **Thermodynamics-based metabolic flux analysis.** *Biophys J* 2007, **92:**1792-1805.
303. Fleming RMT, Thiele I, Provan G, Nasheuer HP: **Integrated stoichiometric, thermodynamic and kinetic modelling of steady state metabolism.** *Journal of Theoretical Biology* 2010, **264:**683-692.
304. Fleming RMT, Thiele I: **von Bertalanffy 1.0: a COBRA toolbox extension to thermodynamically constrain metabolic models.** *Bioinformatics* 2011, **27:**142-143.
305. Cogne G, R ügen M, Bockmayr A, Titica M, Dussap C-G, Cornet J-F, Legrand J: **A model-based method for investigating bioenergetic processes in autotrophically growing eukaryotic microalgae: Application to the green algae Chlamydomonas reinhardtii.** *Biotechnology Progress* 2011, **27:**631-640.
306. Noor E, Bar-Even A, Flamholz A, Lubling Y, Davidi D, Milo R: **An integrated open framework for thermodynamics of reactions that combines accuracy and coverage.** *Bioinformatics* 2012, **28:**2037-2044.
307. De Martino D, Figliuzzi M, De Martino A, Marinari E: **A Scalable Algorithm to Explore the Gibbs Energy Landscape of Genome-Scale Metabolic Networks.** *PLoS Comput Biol* 2012, **8:**e1002562.
308. Beard DA, Qian H: **Thermodynamic-based computational profiling of cellular regulatory control in hepatocyte metabolism.** *American journal of physiology Endocrinology and metabolism* 2005, **288:**E633-644.
309. Schellenberger J, Lewis NE, Palsson BO: **Elimination of thermodynamically infeasible loops in steady-state metabolic models.** *Biophys J* 2011, **100:**544-553.
310. Noor E, Lewis NE, Milo R: **A proof for loop-law constraints in stoichiometric metabolic networks.** *BMC Syst Biol* 2012, **6:**140.

311. Schuetz R, Zamboni N, Zampieri M, Heinemann M, Sauer U: **Multidimensional optimality of microbial metabolism.** *Science* 2012, **336:**601-604.
312. Klitgord N, Segrè D: **The importance of compartmentalization in metabolic flux models: yeast as an ecosystem of organelles.** *Genome Informatics* 2010, **22:**41-55.
313. Kelk SM, Olivier BG, Stougie L, Bruggeman FJ: **Optimal flux spaces of genome-scale stoichiometric models are determined by a few subnetworks.** *Scientific reports* 2012, **2:**580.
314. Park DH, Kim SK, Shin IH, Jeong YJ: **Electricity production in biofuel cell using modified graphite electrode with Neutral Red.** *Biotechnology Letters* 2000, **22:**1301-1304.
315. Boyle NR, Morgan JA: **Flux balance analysis of primary metabolism in Chlamydomonas reinhardtii.** *BMC systems biology* 2009, **3:**4.
316. Shastri AA, Morgan JA: **Flux Balance Analysis of Photoautotrophic Metabolism.** *Biotechnology Progress* 2005, **21:**1617-1626.
317. Pereyra V, Saunders M, Castillo J: **Equispaced Pareto front construction for constrained bi-objective optimization.** *Mathematical and Computer Modelling* 2013, **57:**2122-2131.
318. Virdis B, Freguia S, Rozendal RA, Rabaey K, Yuan Z, Keller J: **4.18 - Microbial Fuel Cells.** In *Treatise on Water Science.* Edited by Editor-in-Chief: Peter W. Oxford: Elsevier; 2011: 641-665
319. Cheng S, Liu H, Logan BE: **Increased Power Generation in a Continuous Flow MFC with Advective Flow through the Porous Anode and Reduced Electrode Spacing.** *Environmental Science & Technology* 2006, **40:**2426-2432.
320. Zhao F, Harnisch F, Schröder U, Scholz F, Bogdanoff P, Herrmann I: **Challenges and Constraints of Using Oxygen Cathodes in Microbial Fuel Cells.** *Environmental Science & Technology* 2006, **40:**5193-5199.
321. Suthers PF, Zomorrodi A, Maranas CD: **Genome-scale gene/reaction essentiality and synthetic lethality analysis.** *Mol Syst Biol* 2009, **5:**301.
322. Zomorrodi A, Maranas C: **Improving the iMM904 *S. cerevisiae* metabolic model using essentiality and synthetic lethality data.** *BMC systems biology* 2010, **4:**178.
323. Rocha I, Maia P, Evangelista P, Vilaca P, Soares S, Pinto JP, Nielsen J, Patil KR, Ferreira EC, Rocha M: **OptFlux: an open-source software platform for in silico metabolic engineering.** *BMC Syst Biol* 2010, **4:**45.
324. Schellenberger J, Que R, Fleming RM, Thiele I, Orth JD, Feist AM, Zielinski DC, Bordbar A, Lewis NE, Rahmanian S, et al: **Quantitative prediction of cellular metabolism with constraint-based models: the COBRA Toolbox v2.0.** *Nat Protoc* 2011, **6:**1290-1307.
325. Bornstein BJ, Keating SM, Jouraku A, Hucka M: **LibSBML: an API library for SBML.** *Bioinformatics* 2008, **24:**880-881.
326. Bond DR, Lovley DR: **Electricity Production by Geobacter sulfurreducens Attached to Electrodes.** *Appl Environ Microbiol* 2003, **69:**1548-1555.
327. Nevin KP, Lovley DR: **Mechanisms for accessing insoluble Fe(III) oxide during dissimilatory Fe(III) reduction by Geothrix fermentans.** *Appl Environ Microbiol* 2002, **68:**2294-2299.
328. Straub KL, Schink B: **Evaluation of electron-shuttling compounds in microbial ferric iron reduction.** *FEMS Microbiol Lett* 2003, **220:**229-233.
329. Aklujkar M, Coppi MV, Leang C, Kim BC, Chavan MA, Perpetua LA, Giloteaux L, Liu A, Holmes D: **Proteins involved in electron transfer to Fe(III) and Mn(IV) oxides by Geobacter sulfurreducens and Geobacter uraniireducens.** *Microbiology* 2013.

330. Kim K-Y, Chae K-J, Choi M-J, Ajayi FF, Jang A, Kim C-W, Kim IS: **Enhanced Coulombic efficiency in glucose-fed microbial fuel cells by reducing metabolite electron losses using dual-anode electrodes.** *Bioresource Technology* 2011, **102:**4144-4149.
331. Yeung M, Thiele I, Palsson B: **Estimation of the number of extreme pathways for metabolic networks.** *BMC Bioinformatics* 2007, **8:**363.
332. Esteve-Nunez A, Rothermich M, Sharma M, Lovley D: **Growth of Geobacter sulfurreducens under nutrient-limiting conditions in continuous culture.** *Environ Microbiol* 2005, **7:**641-648.
333. Rabaey K, Lissens G, Siciliano SD, Verstraete W: **A microbial fuel cell capable of converting glucose to electricity at high rate and efficiency.** *Biotechnology Letters* 2003, **25:**1531-1535.
334. Stewart PS, Franklin MJ: **Physiological heterogeneity in biofilms.** *Nat Rev Micro* 2008, **6:**199-210.
335. Lovley DR: **Electromicrobiology.** *Annual Review of Microbiology* 2012, **66:**391-409.
336. Kato S, Hashimoto K, Watanabe K: **Microbial interspecies electron transfer via electric currents through conductive minerals.** *Proceedings of the National Academy of Sciences* 2012.
337. Mao L, Verwoerd WS: **Computational comparison of mediated MFC current generation capacity of *Chlamydomonas reinhardtii* in photosynthetic and respiratory growth modes.** *Manuscript submitted for publication*.
338. Cheetham NWH: *Introducing Biological Energetics: How Energy and Information Control the Living World* New York: Oxford University Press; 2011.
339. Dal'Molin CG, Quek LE, Palfreyman RW, Nielsen LK: **AlgaGEM--a genome-scale metabolic reconstruction of algae based on the Chlamydomonas reinhardtii genome.** *BMC Genomics* 2011, **12 Suppl 4:**S5.
340. Takahashi H, Uchimiya H, Hihara Y: **Difference in metabolite levels between photoautotrophic and photomixotrophic cultures of Synechocystis sp. PCC 6803 examined by capillary electrophoresis electrospray ionization mass spectrometry.** *Journal of Experimental Botany* 2008, **59:**3009-3018.
341. Chen F, Johns MR: **Heterotrophic growth of Chlamydomonas reinhardtii on acetate in chemostat culture.** *Process Biochemistry* 1996, **31:**601-604.
342. Chandra R, Venkata Subhash G, Venkata Mohan S: **Mixotrophic operation of photo-bioelectrocatalytic fuel cell under anoxygenic microenvironment enhances the light dependent bioelectrogenic activity.** *Bioresour Technol* 2012, **109:**46-56.
343. Venkata Subhash G, Chandra R, Venkata Mohan S: **Microalgae mediated bio-electrocatalytic fuel cell facilitates bioelectricity generation through oxygenic photomixotrophic mechanism.** *Bioresource Technology* 2013.
344. Tanaka K, Kashiwagi N, Ogawa T: **Effects of light on the electrical output of bioelectrochemical fuel-cells containing Anabaena variabilis M-2: Mechanism of the post-illumination burst.** *Journal of Chemical Technology & Biotechnology* 1988, **42:**235-240.
345. Justin G, Zhang Y, Cui XT, Bradberry C, Sun M, Sclabassi R: **A Metabolic Biofuel Cell: Conversion of Human Leukocyte Metabolic Activity to Electrical Currents.** *Journal of biological engineering* 2011, **5:**5.
346. Kitano H: **Systems biology: a brief overview.** *Science* 2002, **295:**1662-1664.
347. Ying W: **NAD+/NADH and NADP+/NADPH in Cellular Functions and Cell Death: Regulation and Biological Consequences.** *Antioxidants & Redox Signaling* 2008, **10:**179-206.
348. van Hoek M, Merks R: **Redox balance is key to explaining full vs. partial switching to low-yield metabolism.** *BMC systems biology* 2012, **6:**22.

349. Mao L, Verwoerd WS: **Genome-scale stoichiometry analysis to elucidate the innate capability of the cyanobacterium *Synechocystis* for electricity generation.** *Journal of Industrial Microbiology & Biotechnology* 2013, **40:**1161-1180.
350. Okamoto A, Nakamura R, Hashimoto K: **In-vivo identification of direct electron transfer from Shewanella oneidensis MR-1 to electrodes via outer-membrane OmcA–MtrCAB protein complexes.** *Electrochimica Acta* 2011, **56:**5526-5531.
351. Kruk J, Jemioła-Rzemińska M, Strzałka K: **Cytochrome c is reduced mainly by plastoquinol and not by superoxide in thylakoid membranes at low and medium light intensities: its specific interaction with thylakoid membrane lipids.** *Biochem J* 2003, **375:**215-220.
352. Yang C, Hua Q, Shimizu K: **Metabolic Flux Analysis in Synechocystis Using Isotope Distribution from 13C-Labeled Glucose.** *Metabolic Engineering* 2002, **4:**202-216.
353. Loferer-Krossbacher M, Klima J, Psenner R: **Determination of bacterial cell dry mass by transmission electron microscopy and densitometric image analysis.** *Appl Environ Microbiol* 1998, **64:**688-694.
354. Lawrence BA, Suarez C, DePina A, Click E, Kolodny NH, Allen MM: **Two internal pools of soluble polyphosphate in the cyanobacterium Synechocystis sp. strain PCC 6308: an in vivo 31P NMR spectroscopic study.** *Arch Microbiol* 1998, **169:**195-200.
355. Vermaas WFJ: **Photosynthesis and Respiration in Cyanobacteria.** In *eLS.* John Wiley & Sons, Ltd; 2001
356. Gorby YA, Yanina S, McLean JS, Rosso KM, Moyles D, Dohnalkova A, Beveridge TJ, Chang IS, Kim BH, Kim KS, et al: **Electrically conductive bacterial nanowires produced by Shewanella oneidensis strain MR-1 and other microorganisms.** *Proc Natl Acad Sci U S A* 2006, **103:**11358-11363.
357. Bhaya D: **Light matters: phototaxis and signal transduction in unicellular cyanobacteria.** *Mol Microbiol* 2004, **53:**745-754.
358. Whitman WB, Coleman DC, Wiebe WJ: **Prokaryotes: The unseen majority.** *Proceedings of the National Academy of Sciences* 1998, **95:**6578-6583.
359. Navarro E, Montagud A, Fernández de Córdoba P, Urchueguía JF: **Metabolic flux analysis of the hydrogen production potential in Synechocystis sp. PCC6803.** *International Journal of Hydrogen Energy* 2009, **34:**8828-8838.
360. Mao L, Verwoerd WS: **Exploration and comparison of inborn microbial capacity of aerobic and anaerobic metabolisms of *Saccharomyces cerevisiae* for current production.** *Bioengineered* 2013, **4:**23-22.
361. Heiskanen A, Spégel C, Kostesha N, Lindahl S, Ruzgas T, Emnéus J: **Mediator-assisted simultaneous probing of cytosolic and mitochondrial redox activity in living cells.** *Anal Biochem* 2009, **384:**11-19.
362. Mo ML, Palsson BO, Herrgard MJ: **Connecting extracellular metabolomic measurements to intracellular flux states in yeast.** *BMC systems biology* 2009, **3:**37.
363. Videla HA, Arvía AJ: **The response of a bioelectrochemical cell with Saccharomyces cerevisiae metabolizing glucose under various fermentation conditions.** *Biotechnology and Bioengineering* 1975, **17:**1529-1543.
364. Sun M, Sheng G-P, Mu Z-X, Liu X-W, Chen Y-Z, Wang H-L, Yu H-Q: **Manipulating the hydrogen production from acetate in a microbial electrolysis cell–microbial fuel cell-coupled system.** *Journal of Power Sources* 2009, **191:**338-343.

365. Pharkya P, Burgard AP, Maranas CD: **Exploring the overproduction of amino acids using the bilevel optimization framework OptKnock.** *Biotechnology and Bioengineering* 2003, **84:**887-899.
366. Rocha M, Maia P, Mendes R, Pinto JP, Ferreira EC, Nielsen J, Patil KR, Rocha I: **Natural computation meta-heuristics for the in silico optimization of microbial strains.** *BMC Bioinformatics* 2008, **9:**499.
367. Huffer S, Roche CM, Blanch HW, Clark DS: **Escherichia coli for biofuel production: bridging the gap from promise to practice.** *Trends Biotechnol* 2012.
368. Lee CY, Antonsson EK: **Variable Length Genomes for Evolutionary Algorithms.** In *In Proceedings of the Genetic and Evolutionary Computation Conference, ; Las Vegas*. Morgan Kaufmann; 2000
369. Segrè D, Vitkup D, Church GM: **Analysis of optimality in natural and perturbed metabolic networks.** *Proceedings of the National Academy of Sciences* 2002, **99:**15112-15117.
370. Tännler S, Fischer E, Le Coq D, Doan T, Jamet E, Sauer U, Aymerich S: **CcpN Controls Central Carbon Fluxes in Bacillus subtilis.** *Journal of Bacteriology* 2008, **190:**6178-6187.
371. Pharkya P, Burgard AP, Maranas CD: **OptStrain: a computational framework for redesign of microbial production systems.** *Genome Research* 2004, **14:**2367-2376.
372. Feist AM, Zielinski DC, Orth JD, Schellenberger J, Herrgard MJ, Palsson BO: **Model-driven evaluation of the production potential for growth-coupled products of Escherichia coli.** *Metab Eng* 2010, **12:**173-186.
373. Fong S, Burgard A, Herring C, Knight E, Blattner F, Maranas C, Palsson B: **In silico design and adaptive evolution of Escherichia coli for production of lactic acid.** *Biotechnol Bioeng* 2005, **91:**643 - 648.
374. Steuer R, Knoop H, Machné R: **Modelling cyanobacteria: from metabolism to integrative models of phototrophic growth.** *Journal of Experimental Botany* 2012, **63:**2259-2274.
375. Dekel E, Alon U: **Optimality and evolutionary tuning of the expression level of a protein.** *Nature* 2005, **436:**588-592.
376. Beard DA, Babson E, Curtis E, Qian H: **Thermodynamic constraints for biochemical networks.** *J Theor Biol* 2004, **228:**327-333.
377. Papin JA, Stelling J, Price ND, Klamt S, Schuster S, Palsson BO: **Comparison of network-based pathway analysis methods.** *Trends in Biotechnology* 2004, **22:**400-405.
378. Kummel A, Panke S, Heinemann M: **Systematic assignment of thermodynamic constraints in metabolic network models.** *BMC Bioinformatics* 2006, **7:**512.
379. Kim HU, Kim TY, Lee SY: **Metabolic flux analysis and metabolic engineering of microorganisms.** *Molecular bioSystems* 2008, **4:**113-120.
380. Klumpp S, Zhang Z, Hwa T: **Growth Rate-Dependent Global Effects on Gene Expression in Bacteria.** *Cell* 2009, **139:**1366-1375.
381. Vogel U, Jensen KF: **The RNA chain elongation rate in Escherichia coli depends on the growth rate.** *Journal of Bacteriology* 1994, **176:**2807-2813.
382. Fuhrer T, Sauer U: **Different biochemical mechanisms ensure network-wide balancing of reducing equivalents in microbial metabolism.** *J Bacteriol* 2009, **191:**2112-2121.
383. Malaisse WJ, Zhang Y, Jijakli H, Courtois P, Sener A: **Enzyme-to-enzyme channelling in the early steps of glycolysis in rat pancreatic islets.** *Int J Biochem Cell Biol* 2004, **36:**1510-1520.
384. Zamboni N, Fendt SM, Ruhl M, Sauer U: **(13)C-based metabolic flux analysis.** *Nat Protoc* 2009, **4:**878-892.

385. Faria JP, Overbeek R, Xia F, Rocha M, Rocha I, Henry CS: **Genome-scale bacterial transcriptional regulatory networks: reconstruction and integrated analysis with metabolic models.** *Briefings in Bioinformatics* 2013.
386. Pfeffer C, Larsen S, Song J, Dong M, Besenbacher F, Meyer RL, Kjeldsen KU, Schreiber L, Gorby YA, El-Naggar MY, et al: **Filamentous bacteria transport electrons over centimetre distances.** *Nature* 2012, **491:**218-221.
387. Kostromins A, Stalidzans E: **Paint4Net: COBRA Toolbox extension for visualization of stoichiometric models of metabolism.** *Biosystems* 2012, **109:**233-239.

Appendices

Appendix 1. Identified reaction knockouts

Reaction and metabolite abbreviations are detailed in the Appendix 3.

Table 10-1: Identified reaction deletions for improving the electron transfer rate in the cases of *Geobacter sulferreducens*

Reaction ID	Enzyme	EC.	Reaction	Subsystem
DET				
ASPT	L-aspartase	4.3.1.1	[c] : asp-L --> fum + nh4	Amino Acid Metabolism
HIBD	3-hydroxyisobutyrate dehydrogenase	1.1.1.31	[c] : 3hmp + nad --> h + mmalsa-R + nadh	Amino Acid Metabolism
URAt2	uracil transport in via proton symport	N/A	h[e] + ura[e] --> h[c] + ura[c]	Transport
MET				
RBZP	alpha-ribazole-5-phosphatase	3.1.3.73	[c] : 5prdmbz + h2o --> pi + rdmbzi	Vitamins & Cofactor Biosynthesis
EX_h(e)	H+ exchange	N/A	N/A	N/A
Mixed mode				
CITt6	citrate transport in/out via proton symport	N/A	cit[e] + h[e] <==> cit[c] + h[c]	Transport
FACOAL150(ISO)	fatty-acid--CoA ligase (Iso-C15:0)	6.2.1.3	[c] : atp + coa + fa3 <==> amp + fa3coa + ppi	Fatty Acid Metabolism
NIT2	nitrogenase	1.18.6.1	[c] : (16) atp + (4) fdxr-4:2 + (16) h2o + n2 --> (16) adp + (4) fdxo-4:2 + (6) h + h2 + (2) nh4 + (16) pi	Nitrogen Metabolism

Table 10-2: Identified reaction deletions for improving the electron transfer rate in the cases of *Chlamydomonas reinhardtii*

Reaction ID	Enzyme	EC.	Reaction	Subsystem
Mixotrophic				
R_TAGAH1801819Z1835Z9Z12Z	triacylglycerol acylhydrolase (18:0/18:1(9Z)/18:3(5Z,9Z,12Z))	3.1.1.3	[c] : tag1801819Z1835Z9Z12Z + h2o --> 12dgr1801819Z + pa + h	Glycerolipid metabolism
Autotrophic				
R_EX_rib_DASH_D_LPAREN_e_RPAREN_	D-ribose exchange	N/A	[e] : rib-D <==>	Exchange
R_GLYCLTtx	glycolate transport, glyoxysome	N/A	glyclt[c] <==> glyclt[x]	Transport, glyoxysome
R_CTINBL	cystathionine beta-lyase, cystine	4.4.1.8	[h] : Lcystin + h2o --> pyr + nh4 + thcys	Cysteine metabolism
R_GLUTL	glutamate---tRNA ligase	6.1.1.17	[c] : atp + glu-L + trnaglu --> amp + ppi + glutrna	Glutamate metabolism
R_PGKf	phosphoglycerate kinase, flagellar	2.7.2.3	[f] : 13dpg + adp <==> 3pg + atp	Glycolysis / Gluconeogenesis; Carbon fixation
R_ITCY	ITP:cytidine 5'-phosphotransferase	2.7.1.48	[c] : itp + cytd --> idp + cmp + h	Pyrimidine metabolism
Heterotrophic				
R_AHCYStg	S-Adenosylhomocysteine transport, Golgi	N/A	ahcys[c] <==> ahcys[g]	Transport, Golgi
R_MDHC(nadp)hr	malate dehydrogenase (oxaloacetate decarboxylating) (NADP+)	1.1.1.40	[h] : mal-L + nadp <==> co2 + nadph + pyr	Carbon fixation;Pyruvate metabolism
R_RIBFS	riboflavin synthase	2.5.1.9	[h] : (2) dmlz + h --> ribflv + 4r5au	Riboflavin metabolism
R_DHRT(2mbcoa)	dihydrolipoyllysine-residue (2-methylpropanoyl)transferase, 2-Methylbutanoyl-CoA forming	2.3.1.168	[m] : coa + 2mbdhl --> 2mbcoa + dhlam	Valine, leucine and isoleucine degradation

Table 10-3: Identified reaction deletions for improving the electron transfer rate in the cases of *Synechocystis* sp. PCC6083

Reaction ID	Enzyme	EC.	Reaction	Subsystem
Autotrophic QH2				
315	alkaline phosphatase	EC:3.1.3.5	damp + h2o <=> dad-2 + pi	Purine metabolism
475		N/A	h2o <=> h2o[e]	Transport reaction
Autotrophic Ferred				
175	isocitrate lyase	EC:4.1.3.1	icit -> gox + succ	Glyoxylate shunt
251	homoserine dehydrogenase	EC:1.1.1.3	hom-L + nad <=> aspsa + nadh + H	Methionine biosynthesis
448	acetolactate synthase	EC:2.2.1.6	2ahtpp + pyr -> alac-S + thpp	Valine, leucine, isoleucine biosynthesis
529	exchange reaction	N/A	val-L[e] <=>	Exchange reaction
Autotrophic				
160	phosphopyruvate hydratase	EC:4.2.1.11	2pg <=> pep + h2o	Glycolysis
300	alkaline phosphatase	EC:3.1.3.5	amp + h2o <=> adn + pi	Purine metabolism
514	exchange reaction	N/A	leu-L[e] <=>	Exchange reaction
Heterotrophic				
286	NADH dehydrogenase	EC:1.6.99.3,1.6.5.3	nadh + 5 H + q -> 4 H[t] + nad + qh2	Photosynthesis and electron transport chain
520	exchange reaction	N/A	phe-L[e] <=>	Exchange reaction
Mixotrophic				
501	exchange reaction	N/A	co2[e] <=>	Exchange reaction
506	exchange reaction	N/A	gln-L[e] <=>	Exchange reaction

Table 10-4: Identified reaction deletions for improving the electron transfer rate in the cases of *S. cerevisiae*

Reaction ID	Enzyme	EC.	Reaction	Subsystem
Aerobic				
r_0380	fatty acid oxidation	N/A	8 s_0534 + 8 s_0809 + 8 s_1202 + s_1215 + s_1245 + 7 s_1279 <=> 9 s_0378 + 7 s_0801 + 7 s_0840 + 8 s_1206 + s_1211	Exchange reaction
r_1868	isobutyl alcohol transport	N/A	s_0932 <=> s_0933	Exchange reaction
r_2065	thiaminase	2.7.1.49	s_0803 + s_1489 <=> s_0270 + s_0310 + s_0794	Thiamin biosynthesis
Anaerobic				
r_0450	fructose-bisphosphate aldolase	4.1.2.13	s_0555 <=> s_0629 + s_0764	gluconeogenesis , glycolysis
r_1054	triose-phosphate isomerase	5.3.1.1	s_0629 <=> s_0764	glycolysis
r_1179	iron (II) transport	N/A	s_0924 <=> s_0926	Exchange reaction
r_1489	isa M(IP)2C	2.7.1.-	s_0861 -> 0.968 s_0858	sphingolipid synthesis [endoplasmic reticulum]
r_1537	isa MIPC	2.7.1.-	s_1142 -> 0.964 s_1115	sphingolipid synthesis [mitochondrion]
r_1760	ergosterol transport	N/A	s_0666 <=> s_0665	Exchange reaction
r_1795	formate transport	N/A	s_0723 <=> s_0722	Exchange reaction

Appendix 2. The metabolic network in the Matlab formats (*mat) and SBML formats (*.xml)

Download hyperlink: http://www.longfei.info

Appendix 3. Flux profiles, FATMIN/FVA results and lists of metabolite and reaction abbreviations for the four microorganisms (*.xlsx)

Download hyperlink: http://www.longfei.info

Appendix 4. MFCoT– a computational toolbox to study the metabolism of MFC biocatalysts.

The MFCoT was presented at 4th International Microbial Fuel Cell Conference [281].

Summary of key findings

MFCoT functionality can be used to 1) Compute the fundamental metabolic potential of a biocatalyst for current output; 2) Identify the pertinent metabolic mechanisms supporting the diversion of electrons to the anode; and 3) Visualize the identified pathways graphically.

Background and relevance

Current MFC research focusses on engineering improvements (electrochemistry, membranes, electrode configurations, etc.) and macroscopic biological aspects like candidate microbes and operating conditions. That leaves a gap of evaluating the inherent electrochemical capabilities of microbes on an intracellular scale, in the light of their complex network of thousands of intertwined metabolic pathways. Recent systems biology work is making genome-scale metabolic networks (GEMs) available for an increasing numbers of microbes, to serve as the framework for *in silico* modelling. Constraint-based modelling such as FBA is already well established in bioengineering, as implemented in general purpose software systems such as COBRA [324]. It is an ideal tool to investigate how microbial metabolism is perturbed by extracting current and energy, and establish quantitative limits on the capabilities of various organisms.

Results

To facilitate this emerging direction in MFC research, we have developed a computational systems metabolic engineering tool, MFC optimization toolbox (MFCoT). MFCoT is a COBRA extension, implemented as a Matlab package that comprises two functions:

Function One: *MFC-optimization*

This function employs flux balance analysis (FBA) to examine the amperage output of metabolic-driven electricity generation. The user can specify any desirable intracellular reducing metabolites (such as NADH, quinol, ferredoxin etc.). Also, different cultivation conditions (such as heterotrophic, photoautotrophic, and mixotrophic) can be chosen. Custom

designed modes (such as nutritionally scare) can be implemented if additional nutrient uptake data from batch growth are available.

Working from these inputs, the software automates calculation of 1) Maximal amperage allowed by physical constraints such as mass balance 2) Theoretical trade-offs between amperage yield and the biomass production (growth) rate, implemented by multi-objective optimization 3) Robustness analysis to study the effect of varying substrate uptake rate on the growth rate and the amperage output in any desirable cultivation conditions.

Function Two: *FATMIN*

This function implements our previously published algorithm Flux variability analysis with target flux minimization (FATMIN) [280] FATMIN is devised to eliminate futile loops in a metabolic network and characterize all the alternate optimal solutions (AOS) or equivalent phenotypic states in a metabolism. It is used to elucidate the metabolic strategies for sustaining any desirable reducing shuttle flux inside the cell for electricity generation in DET or MET mode. In MFCoT, the software can automatically identify dominant fluxes and display the different metabolic mechanisms chosen by the cell to generate the required surplus of the reducing shuttle, subject to stoichiometric balance and substrate uptake. The resultant lists of reactions from FATMIN can be visualized in a context of pathways and part of network by calling a recently published COBRA extension Paint4Net [387].

Download hyperlink: http://www.longfei.info